

**COPPER(I) COMPLEXES OF VERY BULKY PHOSPHINES AND
DEVELOPMENT OF NEW ASYMMETRIC THIA TRIAZINYLS FOR
MOLECULAR MAGNETS**

MUKAILA ABIODUN IBRAHIM
Master of Science, King Fahd University of Petroleum and Mineral, 2019

A thesis submitted
in partial fulfilment of the requirements for the degree of

MASTER OF SCIENCE

in

CHEMISTRY

Department of Chemistry and Biochemistry
University of Lethbridge
LETHBRIDGE, ALBERTA, CANADA

© Mukaila Abiodun Ibrahim, 2021

COPPER(I) COMPLEXES OF VERY BULKY PHOSPHINES AND DEVELOPMENT OF
NEW ASYMMETRIC THIA TRIAZINYLS FOR MOLECULAR MAGNETS

MUKAILA ABIODUN IBRAHIM

Date of Defence: August 26, 2021

Dr. R. Boéré Supervisor	Professor	Ph.D.
Dr. P. Hazendonk Examination Committee Member	Associate Professor	Ph.D.
Dr. P. Hayes Examination Committee Member	Professor	Ph.D.
Dr. M. Gerken Chair, Thesis Examination Committee	Professor	Ph.D.

DEDICATION

To Allah, the creator of heaven and earth and all it entails as well as my fellow students who have been supportive during the project.

ABSTRACT

The coordination of copper(I) halides by bulky triarylphosphines DippPh₂P and Dipp₂PhP (Dipp=2,6-diisopropylphenyl), and the synthesis of a stable radical dimer of 3-trichloromethyl-5-(2-pyridyl)-1-thia-2,4,6-triazinyl are described in this thesis. Copper(I) with DippPh₂P forms either trigonal-planar mononuclear [CuX(DippPh₂P)₂], or dinuclear dimeric [CuX(DippPh₂P)]₂ complexes (X = Cl, Br) depending on solvent; Dipp₂PhP afforded [CuX(Dipp₂PhP)]₂ irrespective of stoichiometry.

On the thiatriazinyl radical synthesis, free-base 2-pyridyl- and 2-pyrimidylamidines were synthesized and used to prepare *N'*-(2,2,2-trichloroethanimidoyl)-pyrid-2-yl-carboximidamide and *N'*-(2,2,2-trichloroethanimidoyl)-pyrimid-2-yl-carboximidamide. Condensation of HCl salts of the former with S₂Cl₂ or (better) SCl₂ formed the required 1-chloro-3-trichloromethyl-5-(2-pyridyl)-1-thia-2,4,6-triazine, but the preparation was inhibited by full or partial protonation at the 2-pyridyl N atom. Removal of HCl under pyrolysis conditions has been partly successful and allowed for the preparation of a first sample of the target 3-trichloromethyl-5-(2-pyridyl)-1-thia-2,4,6-triazinyl radical dimer. The products reported have been fully characterized by chemical, spectroscopic and single-crystal, X-ray diffraction.

ACKNOWLEDGEMENTS

It is my pleasure to express my deep feelings on my success in this project.

First, I really appreciate the effort and support of my supervisor, Prof. René T. Boéré for his significant contributions and support throughout this project. I also acknowledge his technical, scientific, and financial support. Also, special thanks to my committee members Prof. Paul Hayes and Prof. Paul Hazendonk for their guidance.

I also want to recognise the chairman of Chemistry Department and the members of staff including the academic and non-academic. Particularly, the immense technical know-how and inputs of Mr. Tony Montana, Mr. Michael Opyr, and Mr. Kris Fisher greatly assisted my achievements.

It also worth mentioning the contribution and immeasurable support of my lab members including Nathan, Nolan, Eric, Flavia among others who helped me succeed.

Lastly, I thank my father, Mr. Ibrahim Olaitan Titilope, my mother Mrs. Ibrahim Tawakalt, my sister, Mrs. Halimat Ibrahim as well as my lovely wife; Mrs. Rasheedat Opeyemi Adebayo and daughter, Mazeedatulkhayr for their support and prayers.

TABLE OF CONTENTS

DEDICATION	iii
ABSTRACT	iv
ACKNOWLEDGEMENTS	v
TABLE OF CONTENTS	vi
LIST OF TABLES	xi
LIST OF FIGURES.....	xiii
LIST OF SCHEMES.....	xviii
ABBREVIATIONS AND SYMBOLS	xix
LIST OF COMPOUNDS	xxii
Chapter 1 Introduction	1
1.1 Chemistry of sterically bulky tertiary aryl phosphines and their applications	1
1.2 Molecular magnets and their versatility	6
1.3 Closed shell and open shell thiazines.....	12
1.3.1 Thiazine complexes and their viability as building blocks for molecular magnets.....	15
1.3.2 Redox non-innocence of TTA radical	19
1.4 Goals of the thesis	22
1.5 References	24
Chapter 2 Copper (I) halide-phosphine complexes of highly sterically demanding phosphines bearing 2,6-diisopropylphenyl groups	36

2.1 Introduction	36
2.2 Synthesis and Characterization of [CuXDipp _(n-1) Ph _n P] Complexes.....	38
2.3 Computational studies.....	46
2.4 X-Ray Crystal Structure Analyses of the Complexes	49
2.5 Conclusions	69
2.6 References	70
Chapter 3 Preparation and isolation of 2-amidinopyridine and 2-amidinopyrimidine	75
3.1 Introduction	75
3.2 Results and discussion.....	79
3.2.1 Optimized synthesis of 2-amidinopyridine and isolation of its salts and mixtures	79
3.2.2 2-Pyrimidylamidine and its hydrochloride salt	82
3.3 X-ray crystal structures of amidine salts and the free amidines.....	84
3.3.1 Crystal structures of amidinium chlorides 7, 9 and 9.H ₂ O	85
3.3.2 Crystal structures of 8 and its hemi-amidinium chloride (8a) and carbonate (8b) salts.....	94
3.4 Conclusions	104
3.5 References	105
Chapter 4 Preparation of functionalized imidoamidines	108
4.1 Introduction	108
4.2 Results and discussion.....	115
4.2.1 Synthesis of PyCCl ₃ Imidoamidine and PmCCl ₃ Imidoamidine and the HCl salts.....	115

4.3 Crystal structures.....	119
4.4 Conclusions.....	125
4.5 References.....	126
Chapter 5 Progress towards the preparation of asymmetric 3-trichloromethyl-5-(2-pyridyl)-1-thia-2,4,6-triazinyl.....	132
5.1 Introduction.....	132
5.2 Preparation of 1-chloro-3-trichloromethyl-5-(2-pyridyl)-1-thia-2,4,6-triazine via S ₂ Cl ₂ condensation reaction.....	134
5.3 Crystallographic analysis of structures.....	139
5.3.1 Structure of 15–15.HCl and 15.HCl.....	140
5.3.2 Structure of 16.....	146
5.3.3 Crystal structure of 17.....	150
5.4 Conclusions.....	153
5.5 Future work.....	154
5.6 References.....	155
Chapter 6 Experimental procedures.....	157
6.1 General procedures.....	157
6.2 Synthetic procedures.....	158
6.2.1 [CuCl(DippPh ₂ P)] ₂ (1).....	158
6.2.2 [CuBr(DippPh ₂ P)] ₂ (2).....	159

6.2.3 [CuCl(Dipp ₂ PhP)] ₂ (3).....	159
6.2.4 [CuBr(Dipp ₂ PhP)] ₂ (4)	160
6.2.5 [CuCl(DippPh ₂ P)] ₂ (5).....	161
6.2.6 [CuBr(DippPh ₂ P)] ₂ (6)	162
6.2.7 Synthesis of 2-amidinopyridine hydrochloride (7).....	162
6.2.8 Preparation of 2-amidinopyridine (8).....	163
6.2.9 Synthesis of 2-amidinopyrimidine hydrochloride (9)	164
6.2.10 Preparation of 2-amidinopyrimidine (10).....	165
6.2.11 Synthesis of trichloromethyl-2-pyridylimidoylamidine (11)	165
6.2.12 Generation of trichloromethyl-2-pyridylimidoylamidine hydrochloride (12).....	166
6.2.13 Synthesis of trichloromethyl-2-pyrimidylimidoylamidine (13)	167
6.2.14 Generation of trichloromethyl-2-pyrimidylimidoylamidinehydrochloride (14)	167
6.2.15 Synthesis of asymmetric 1-chloro-3-trichloromethyl-5-(2-pyridyl)-1-thia-2,4,6- triazine, PyCCl ₃ TTACl (15).....	168
6.2.16 Preparation of asymmetric 1-oxo-3-trichloromethyl-2-pyridyl thiatriazine, PyCCl ₃ TTA=O (16) from the hydrolysis of PyCCl ₃ TTACl	169
6.2.17 Synthesis of 3-trichloromethyl-5-(2-pyridyl)-1-thia-2,4,6-triazinyl, PyCCl ₃ TTA' (17)	169
6.2.18 X-ray crystal structure data collection and refinement.....	170
6.2.19 Computational studies	171

6.3 References 180

Appendix 181

LIST OF TABLES

Table 2.1. ^{31}P NMR data for ligands and complexes.	40
Table 2.2. The results of the computational study	47
Table 2.3. Selected interatomic distances and angles in the crystal structures.	50
Table 2.4. Structural deformation parameters in 1 to 4	51
Table 2.5. Selected bond lengths and bond angles of complexes 1 and 2 compared to less bulky previously studied analogs	52
Table 2.6. Selected bond lengths and bond angles of 3 and 4 compared to previously studied analogs with bulky phosphines.....	60
Table 2.7. Selected bond lengths and bond angles of 5 and 6 compared to previously studied analogues	68
Table 3.1. Selected bond parameters in 7 , 9 and 9.H₂O (using atomic the numbering scheme in Figure 3.5a).	86
Table 3.2. Hydrogen bonds of 7	89
Table 3.3. Hydrogen bonds of 9	92
Table 3.4. Hydrogen bonds of 9.H₂O	92
Table 3.5. Selected bond parameters of 8 , 8a and 8b (using atomic numbering scheme in the Figures).....	96
Table 3.6. Hydrogen Bonds of 8	98
Table 3.7. Hydrogen Bonds for 8a	101
Table 3.8. Hydrogen Bonds for 8b	103
Table 4.1. ^1H NMR chemical shift comparison of 11 and 13 with corresponding amidines.....	118
Table 4.2. Selected bond lengths (Å) and angles (°) of 11 and 13 in comparison with the average parameters of the aryl analogs.....	120
Table 4.3. Hydrogen bonds of 11	122
Table 4.4. Hydrogen bonds of 13	122
Table 5.1. ^1H NMR data of 15–15.HCl and 16	136

Table 5.2. Selected bond distances (Å) and bond angles (°) of thiatriazines and the thiatriazinyl dimer.....	141
Table 5.3. Hydrogen bonds of 15.HCl	144
Table 5.4. Hydrogen bonds of 15–15.HCl	144
Table 5.6. Comparison of bond distances and angles of 16 with previously reported analogs.	149
Table 5.6. Hydrogen bonds of 16b	149
Table 6.1. X-ray crystal structure and refinement data of compounds	172
Table 6.1, continued. X-ray crystal structure and refinement data of compounds	173
Table 6.1, continued. X-ray crystal structure and refinement data of compounds	174
Table 6.1, continued. X-ray crystal structure and refinement data of compounds	175
Table 6.1, continued. X-ray crystal structure and refinement data of compounds	176
Table 6.1, continued. X-ray crystal structure and refinement data of compounds	177
Table 6.1, continued. X-ray crystal structure and refinement data of compounds	178
Table 6.1, continued. X-ray crystal structure and refinement data of compounds	179

LIST OF FIGURES

Figure 1.1. Classification of phosphines (view down P atom)	1
Figure 1.2. structure of triphenyl phosphine (Ph_3P).....	1
Figure 1.3. Structure of Mes_3P and Tripp_3P	2
Figure 1.4. Structures of $\text{Dipp}_n\text{Ph}_{(3-n)}\text{P}$	3
Figure 1.5. Illustration of steric pressure arrangement of endo and exo in 2- and 6-position substituted Ar_3P	4
Figure 1.6. coordination of phosphines with transition metals.	5
Figure 1.7. Two kinds of ligand-metal unpaired spin interactions	7
Figure 1.8. Radical ligands previously explored as building blocks for SMMs.....	8
Figure 1.9. Different nodal properties of DTDA^\bullet and TTA^\bullet	10
Figure 1.10. DTDA radical coordination to metals via only N-atoms.....	11
Figure 1.11. The π MOs surfaces of benzene and TTA radical obtained from DFT computations using $\text{ROB3LYP}/6\text{-}31\text{+G(d,p)}$. The surfaces are rendered using an isovalue of 0.02.	13
Figure 1.12. Solid-state structure of TTA^\bullet dimer.....	15
Figure 1.13. The 4-phenyldithiadiazolyl complexes of (a) Fe and (b) Ni^+	16
Figure 1.14. The dithiadiazolyl complexes formed from $\text{M}(\text{PPh}_3)_3$ reactions	17
Figure 1.15. Complex of DTDA^\bullet of reaction with $[\text{CpCr}(\text{CO})_3]_2$	17
Figure 1.16. Metallocene complexes of TTA^\bullet	18
Figure 1.17. Iron (Fe) complex of Py_2TTA	19
Figure 1.18. Mechanisms of innocent and non-innocent ligands.	20
Figure 1.19. The π SOMO surfaces of PyCCl_3TTA radical and dimer obtained from DFT computations using $\text{ROB3LYP}/6\text{-}31\text{+G(d,p)}$. The surfaces are rendered using an isovalue of 0.02.	21
Figure 2.1. ^1H NMR spectrum of 5 in CDCl_3 (300 MHz) for the H nuclei attached to the labeled C atoms.	42

Figure 2.2. ^1H NMR spectrum of 6 in CDCl_3 (300 MHz) for the H nuclei attached to the labeled C atoms.	42
Figure 2.3. ^1H NMR spectrum of 1 in CDCl_3 (300 MHz) for the H nuclei attached to the labeled C atoms.	44
Figure 2.4. ^1H NMR spectrum of 2 in CDCl_3 (300 MHz) for the H nuclei attached to the labeled C atoms.	44
Figure 2.5. ^1H NMR spectrum of 3 in CDCl_3 (300 MHz) for the H nuclei attached to the labeled C atoms.	45
Figure 2.6. ^1H NMR spectrum of 4 in CDCl_3 (300 MHz) for the H nuclei attached to the labeled C atoms.	45
Figure 2.7. Displacement ellipsoid plots (50%) showing the complexes and solvent molecules as found in the crystal structures of (a) 1 and (b) 1a . Hydrogen atoms have been omitted for clarity.	53
Figure 2.8. Displacement ellipsoid plots (50%) showing only the Cu_2Cl_2 core of (a) 1 and (b) 1a	54
Figure 2.9. Displacement ellipsoid plots (50%) showing (a) the complexes 2a and solvent molecules as found in the crystal structures. Hydrogen atoms have been omitted for clarity. (b) A similar plot showing only the Cu_2Cl_2 core in 2a	56
Figure 2.10. Displacement ellipsoid plots (50%) showing the complexes and solvent molecules as found in the crystal structures of (a) 3 and (b) 3a . Hydrogen atoms have been omitted for clarity.	58
Figure 2.11. Displacement ellipsoid plots (50%) showing just the Cu_2Cl_2 core of (a) 3 and (b) 3a	61
Figure 2.12. Displacement ellipsoid plots (50%) showing the complexes and solvent molecules as found in the crystal structures of (a) 4a and (b) 4b . Hydrogen atoms and some labels in 4b have been omitted for clarity.	63
Figure 2.13. Displacement ellipsoid plots (50%) showing the (a) eclipsed phosphine aryl rings conformation and (b) only the Cu_2Br_2 core center of 4b'	64
Figure 2.14. Crystal structure of (a) 5 and (b) 6 drawn at 50% probability level. Hydrogen atoms are omitted for clarity.	66
Figure 3.1. The ^1H NMR spectrum of sublimed 8 . * and # are impurities.	80
Figure 3.2. The ^1H NMR spectra of (a) 0.5 g and (b) 1.0 g scale of 7 for feasible neutralization with KOH in MeOH-DCM.	81

- Figure 3.3.** The ^1H NMR spectrum of **8** obtained by DCM extraction from MeOH neutralization of 10 g scale of **7**. * is solvent and # is TMS and silicone grease. 83
- Figure 3.4.** The ^1H NMR spectrum of **10**. (The signals label * belong to residual solvents.) 83
- Figure 3.5.** The asymmetric units of (a) **7** and (b) **9** showing the atom-labelling schemes and hydrogen bonding indicated with dashed lines. Displacement ellipsoids are drawn at 50% probability level and H atoms are shown as small spheres of arbitrary radii. In **9**, both C11 and C12 atoms have 50% occupancies. 87
- Figure 3.6.** The asymmetric unit of **9.H₂O** showing the atom-labelling scheme and hydrogen bonding indicated with dashed lines. Displacement ellipsoids are drawn at 50% probability level and H atoms are shown as small spheres of arbitrary radii. 88
- Figure 3.7.** The crystal packing tube structure of **7** projected down c axis. Hydrogen bonding is indicated by green dashed lines. Cl are shown as green balls; N is blue; C is ash; and H is grey. 89
- Figure 3.8.** The crystal packing structure of **9** projected down b. Displacement ellipsoids drawn at the 50% probability level. Hydrogen bonding is indicated by blue dashed lines. 91
- Figure 3.9.** The (a) H-bond motif and (b) crystal packing structure of **9.H₂O** projected down b. Displacement ellipsoids drawn at the 50% probability level. Hydrogen bonding is indicated by green dashed lines. 93
- Figure 3.10.** The asymmetric unit of **8** showing the atom-labelling scheme and with hydrogen bonding indicated with dashed lines. Displacement ellipsoids are drawn at 50% probability level and H atoms are shown as small spheres of arbitrary radii. 96
- Figure 3.11.** The H-bond motif (a) and crystal packing structure (b) of **8** projected down b. Displacement ellipsoids drawn at the 50% probability level. Hydrogen bonding is indicated by green dashed lines. 97
- Figure 3.12.** The asymmetric unit of **8a** showing the atom-labelling scheme and hydrogen bonding indicated with dashed lines. Displacement ellipsoids are drawn at 50% probability level and H atoms are shown as small spheres of arbitrary radii. 98
- Figure 3.13.** The crystal packing structure of **8a** displaying $\pi - \pi$ interaction approximately down b axis. Displacement ellipsoids drawn at the 50% probability level. 100
- Figure 3.14.** The crystal packing structure of **8a** projected down b. Displacement ellipsoids drawn at the 50% probability level. Hydrogen bonding is indicated by green dashed lines. 100
- Figure 3.15.** The asymmetric unit of **8b** showing the atom-labelling scheme and with hydrogen bonding indicated with dashed lines. Displacement ellipsoids are drawn at 50% probability level and H atoms are shown as small spheres of arbitrary radii. 101

Figure 3.16. The (a) H-bond motif and (b) crystal packing structure of 8b projected down c axis. Displacement ellipsoids drawn at the 50% probability level. Hydrogen bonding is indicated by green dashed lines.	102
Figure 4.1. Coordination mode of bridged complexes of imidoamidines.	111
Figure 4.2. The synthetic routes to 11 , 12 , 13 , and 14	116
Figure 4.3. ¹ H NMR spectra of 11 (* are solvent peaks and # is TMS).	117
Figure 4.4. ¹ H NMR spectra of 13 (* are tautomer peaks and # is TMS and silicone grease). .	118
Figure 4.5. Displacement ellipsoid plots of (a) 11 and (b) 13 drawn at the 50% probability level showing the atom-labelling scheme and intramolecular hydrogen bonding (indicated with dashed lines). The H atoms are shown as small spheres of arbitrary radii.	121
Figure 4.6. Structure of 11 showing hydrogen bonding (indicated by dashed lines). Displacement ellipsoids drawn at the 50% probability level. Key atoms involved in H-bonding are labelled.	123
Figure 4.7. Structure of 13 showing hydrogen bonding (indicated by dashed lines). Displacement ellipsoids drawn at the 50% probability level. Key atoms involved in H-bonding are labelled.	124
Figure 5.1. Setup for reduction of 15 to corresponding radical dimer 17	139
Figure 5.2. Displacement ellipsoid plot of 15.HCl drawn at the 50% probability level showing the atom-labelling scheme and with short contacts indicated with dashed lines. The H atoms are shown as small spheres of arbitrary radii.	142
Figure 5.3. Displacement ellipsoid plot of 15–15.HCl solvated with CH ₃ CN drawn at the 50% probability level showing the atom-labelling scheme with short contacts indicated with dashed lines. The H atoms are shown as small spheres of arbitrary radii. The two H ⁺ atoms have half occupancy each.	142
Figure 5.4. Displacement ellipsoid plot of (a) 16a (space group P2 ₁ /c) and (b) 16b (space group P1 with minor disorder O component omitted for clarity) drawn at the 50% probability level showing the atom-labelling schemes and with short contacts indicated with dashed lines. The H atoms are shown as small spheres of arbitrary radii.	143
Figure 5.5. A crystal packing diagram of 15–15.HCl projected almost down the b axis. Displacement ellipsoids are drawn at the 50% probability level. Hydrogen bonding and short contacts are indicated by green dashed lines.	144
Figure 5.6. The crystal packing structure of 15.HCl projected down the c axis (a) without and (b) with short contacts. Displacement ellipsoids are drawn at the 50% probability level. Hydrogen bonding and short contacts are indicated by green dashed lines.	145

- Figure 5.7.** A crystal packing diagram of **16a** projected down c axis (a) without and (b) with short contacts. Displacement ellipsoids are drawn at the 50% probability level. Short contacts are indicated by blue dashed lines. 147
- Figure 5.8.** A crystal packing diagram of **16b** (a) projected down the a axis with displacement ellipsoids drawn at the 50% probability level. Hydrogen bonding is indicated by green dashed lines (b) capped sticks projected almost down the b axis, short contacts are indicated by green dashed lines. O is red; S is yellow; N is purple; C is ash; and H is grey..... 148
- Figure 5.9.** Displacement ellipsoid plot of the monomer which is the asymmetric unit of **17** (the true structure is the dimer) drawn at the 50% probability level showing the atom-labelling scheme. The H atoms are shown as small spheres of arbitrary radii. 151
- Figure 5.10.** (a) The crystal packing Displacement ellipsoid plot drawn at the 50% probability level. Short contacts are indicated by green dashed lines. (b) Space filling structure of **17**. Cl is green; S is yellow; N is purple; C is charcoal; and H is grey. 152
- Figure 5.11.** The crystal packing structure of **17** shown as capped sticks. Short contacts are indicated by green dashed lines with a chain running along a axis. Cl is green; S is yellow; N is blue; C is ash; and H is grey. 153

LIST OF SCHEMES

Scheme 1.1. Preparation of bulky phosphine from organometal reaction with halophosphines.....	3
Scheme 1.2. Preparation of TTA [•] from TTACl.....	12
Scheme 1.3. Synthesis of VII using S ₃ N ₃ Cl ₃	14
Scheme 2.1. The observed types of structures known for R ₃ P–CuX complexes.....	38
Scheme 2.2. Reaction of IV and V with CuX in CH ₃ CN and CHCl ₃	39
Scheme 2.3. Proposed exchange mechanism pathways of complexes in solution (CH ₃ CN or CHCl ₃).....	41
Scheme 2.4. Change in free energies of gas phase model of complexes and their equilibria reactions.....	46
Scheme 3.1. Classification of amidines.....	76
Scheme 3.2. Pinner reaction pathway for the synthesis of unsubstituted amidines.....	77
Scheme 3.3. Synthesis of amidines via lithiated silylated amidine route.....	78
Scheme 3.4. Synthetic procedure for 8 and 10.....	79
Scheme 3.5. Structures of amidines and salts as found in crystal structures.....	84
Scheme 4.1. Structure of imidoamidines and analogous unsaturated chelates.....	109
Scheme 4.2. Tautomers and conformers of imidoamidine.....	112
Scheme 4.3. Pinner method.....	113
Scheme 4.4. Ley and Muller method.....	113
Scheme 4.5. Primary imidoamidine synthesis from nitriles and amidines.....	114
Scheme 4.6. Synthesis of symmetric pyridine/pyrimidine-substituted primary imidoamidines.....	115
Scheme 5.1. Asymmetric TTACl and TTA radical synthesis route.....	133
Scheme 5.2. Synthesis of XXIV using S ₂ Cl ₂	134
Scheme 5.3. Synthesis of 15 by S ₂ Cl ₂ condensation.....	137
Scheme 5.4. Reduction of 15 to corresponding radical dimer 17.....	138

ABBREVIATIONS AND SYMBOLS

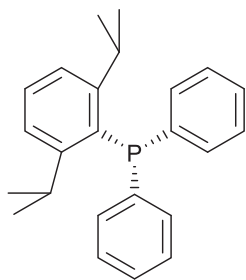
2D	Two dimension
3D	Three dimension
Å	Angstrom
ACN	Acetonitrile
Acac	β-diketonate
B3LYP	Becke, three-parameter, Lee-Yang-Parr
Br	Bromine
C	Carbon
CCl ₄	Carbon tetrachloride
CF ₃	Trifluoromethyl
CH ₂ Cl ₂	Dichloromethane
CH ₃	Methyl
cm ⁻¹	Wavenumber
C-N	Carbon-nitrogen
CN	Cyanide
CO	Carbonyl
Co	Cobalt
Cp	Cyclopentadienyl
C-P	Carbon-phosphorus bond
Cr	Chromium
Cu	Copper
CuX	Copper(I)halide
CV	Cyclic voltammogram
DCM	Dichloromethane
DFT	Density functional theory
Dipp	2,6-diisopropylphenylphosphine
Dipp ₃ P	Tris(2,6-diisopropylphenyl)phosphine
DippCu	2,6-diisopropylphenyl-copper
DippPh ₂ P	2,6-diisopropylphenyl-biphenyl phosphine
DTDA [•]	Dithiadiazinyl radical
DTDACl	Dithiadiazine chloride
e ⁻	Electron
EPR	Electron Paramagnetic Resonance
Fe	Iron
HCl	Hydrochloric acid
Hfac	Hexafluoroacetylacetone
IR	Infrared
IUPAC	International Union of Pure and Applied Chemistry
KCl	Potassium chloride
M	Molar
Me	Methyl
MeCN	Acetonitrile
Mes ₃ P	Trimesitylphosphine
Mg	Magnesium

MHz	Megahertz
Mn	Manganese
N	Nitrogen
Nacnac	β -diimidinate
Nacac	β -iminoketonate
N-H	Nitrogen-hydrogen
Ni	Nickel
NIL	Non-innocent ligand
NMe ₂	Dimethylamino
N-S-N	Nitrogen-Sulfur-Nitrogen group
°C	Degree Celsius
P	Phosphorus
PCl ₃	Phosphorus trichloride
Pd	Palladium
Ph	Phenyl
Ph ₂ PCl	Diarylchlorophosphine
Ph ₃	Phosphine
Ph ₃ P	Triphenylphosphine
Ph ₃ Sb	Triphenyl antimony
ppm	Parts per million
Pt	Platinum
Py	Pyridyl
R	Alkyl/Aryl
r.h.s.	Right hand side
R ₂ HP	Secondary phosphines
R ₃ P	Tertiary phosphines
R ₃ P	Triarylphosphine
RH ₂ P	Primary phosphines
S	Sulfur
S	Spin
S...S	Sulfur-sulfur contact
S ₂ Cl ₂	Sulfur monochloride
S ₃ N ₃ Cl ₃	3,5-dichlorothiazine chloride
S ₄ N ₄	Tetrasulfur tetranitride
SCL ₂	Sulfur monochloride
SCMs	Single chain magnets
SMMs	Single-molecule magnets
S-N	Sulphur-nitrogen
SOMO	Singly occupied molecular orbital
S-S	Sulfur-sulfur bond
T _C	Curie temperature
Tripp	Triisopropylphenylphosphine
Tripp ₃ P	Tris(2,4,6-triisopropylphenyl)phosphine
T _N	Néel temperature
tphz	Tetrapyridophenazine
TTA·	Thiaziazinyl radical

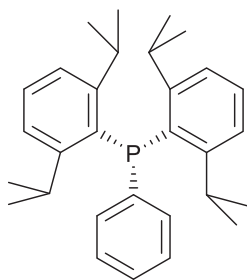
TTACl
 α
 π

Thiatriazine chloride
Alpha
Pi bonding

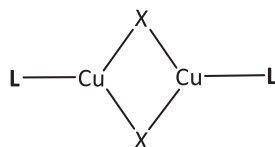
LIST OF COMPOUNDS



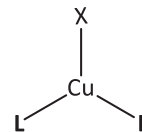
IV



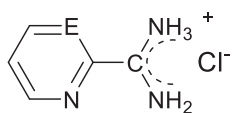
V



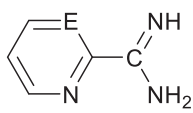
- 1, L = DippPh₂P, X = Cl
 2, L = DippPh₂P, X = Br
 3, L = Dipp₂PhP, X = Cl
 4, L = Dipp₂PhP, X = Br



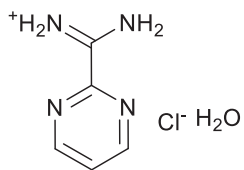
- 5, L = DippPh₂P, X = Cl
 6, L = DippPh₂P, X = Br



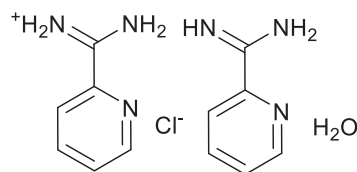
- 7 - E = CH
 9 - E = N



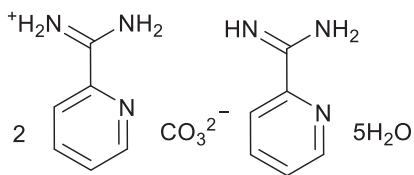
- 8 - E = CH
 10 - E = N



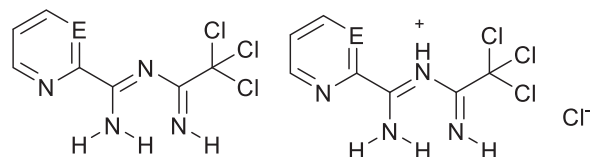
9.H₂O



8a

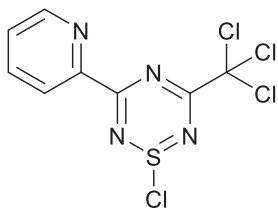


8b



- 11, E = C
 13, E = N

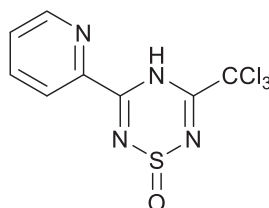
- 12, E = C
 14, E = N



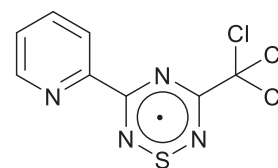
15



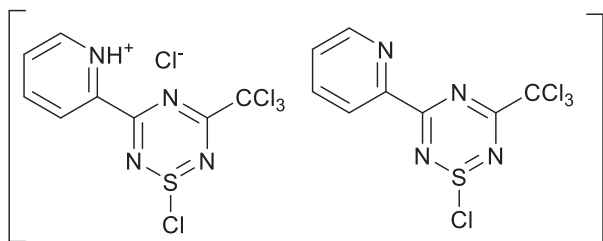
15.HCl



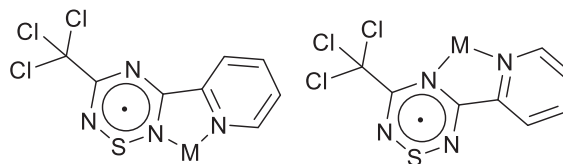
16



17



15-15.HCl



XXVII

Chapter 1 Introduction

1.1 Chemistry of sterically bulky tertiary aryl phosphines and their applications

Phosphines are ubiquitous Lewis bases that are known for their distinct electronic and chemical properties with numerous derivatives. Organophosphines are derivatives of PH_3 , which itself is rarely used as a ligand. They are structurally similar to ammonia with characteristic pyramidal shape and a lone pair. Based on their general formula ($\text{R}_n\text{H}_{(3-n)}\text{P}$), they are classified as primary (RH_2P), secondary (R_2HP) and tertiary (R_3P) where the n value is 1, 2, and 3 respectively (Figure 1.1).¹

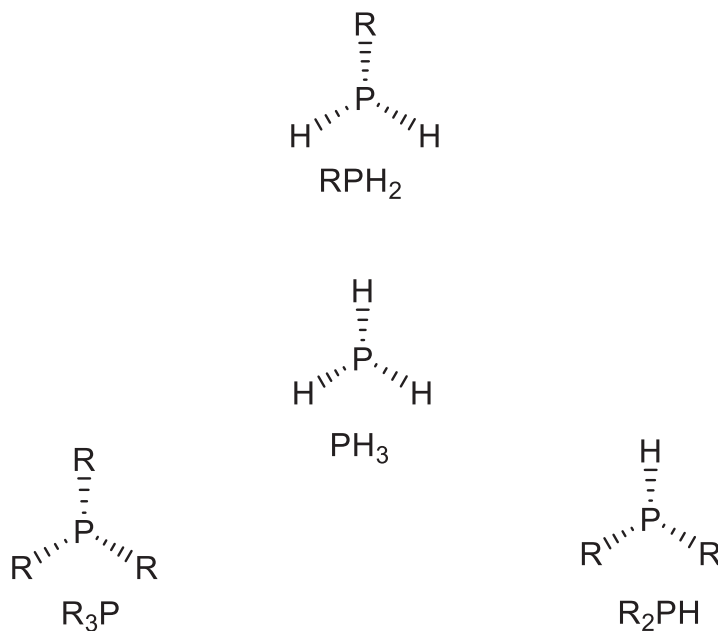


Figure 1.1. Classification of phosphines (view down P atom)

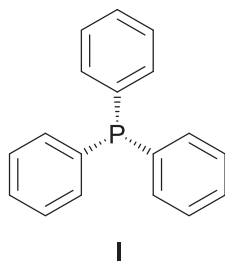


Figure 1.2. Structure of triphenyl phosphine (Ph_3P)

Tertiary triarylphosphines (Ar_3P) such as triphenylphosphine (**I**, Figure 1.2) and its derivatives, are important L-type ligands in organometallic and coordination chemistry.² Ar_3P form complexes with metals in various oxidation states which are quite soluble in a variety of organic solvents due to their high lipophilicity. Their steric and electronic properties like donor strength towards metals can be manipulated by varying the Ar group in a predictable and systematic way that may fine-tune transition metal catalytic properties.³⁻⁴ The steric capacities of Ar_3P are generally used to determine the extent of bulkiness, most commonly via Tolman's cone angle.⁵ An interesting aspect of bulky phosphines is their ability to exhibit outstanding properties to stabilize radical cations and their propensity as prominent supporting ligands in transition metal catalyst development.⁶⁻⁷ Trimesitylphosphine (Mes_3P), **II** (Figure 1.3) is the first popular highly crowded triaryl phosphine synthesized with Tolman's cone angle of 212° which was still able to form copper(I)⁸⁻⁹ and gold(I)⁹⁻¹¹ two coordinate complexes of the type Mes_3PMCl where M is Cu or Au in a linear geometry.

Traditionally, triarylphosphines are formed using metal-aryl compounds such as organolithiums reacting with phosphorus halides such as phosphorus trichloride (PCl_3) or reaction of its aryl derivatives such as diarylchlorophosphine (Ph_2PCl) with Grignard reagents (Scheme 1.1).

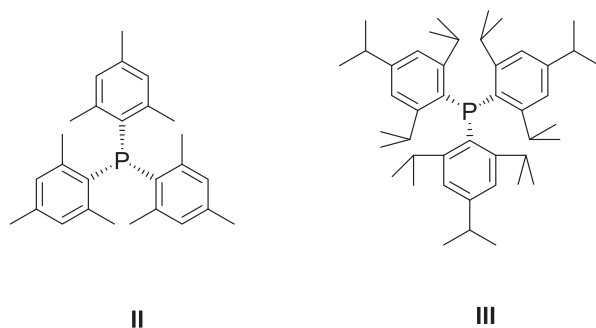
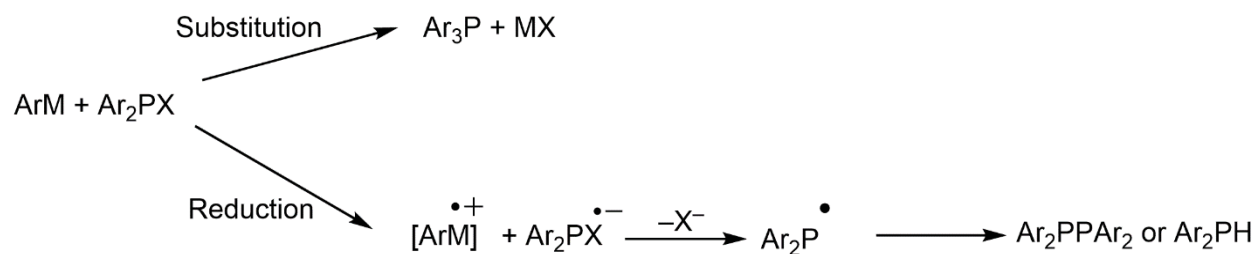


Figure 1.3. Structure of Mes_3P and Tripp_3P



Scheme 1.1. Preparation of bulky phosphine from organometal reaction with halophosphines.

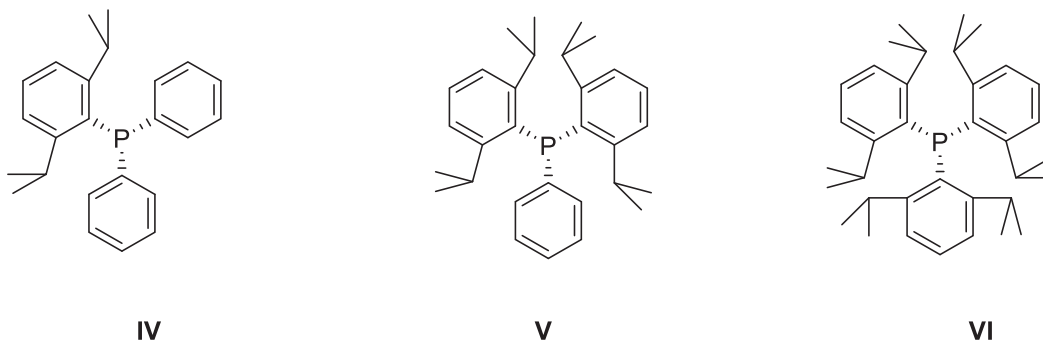


Figure 1.4. Structures of $\text{Dipp}_n\text{Ph}_{(3-n)}\text{P}$

Addition of the last aryl group in sterically hindered triarylphosphines is the main barrier towards their synthesis. As shown in the lower branch of Scheme 1.1, a redox reaction that results in either P-P coupling or R_2PH products becomes more competitive when the size of the R groups makes the three-fold substitution too difficult. Many of the bulkiest triarylphosphines including Mes_3P and 2,4,6-triisopropylphenylphosphine (Tripp_3P , **III**, Figure 1.3) have been prepared by Sasaki and co-workers.^{3-4, 12-16} The Grignard reagent route has been found unfavorable for the preparation of congested phosphines like **III**. An alternative method using arylcopper organometallic compounds have been found excellent for its synthesis and other related analogs such as Mes_3P . The reaction usually requires 24 h on reflux in tetrahydrofuran (THF) for effective transformation of the intermediate $\text{Tripp}_2\text{PCl}_2$ into the formation of product. Our group has also demonstrated the formation of (2,6-diisopropylphenyl)-diphenylphosphine (DippPh_2P , **IV**), bis(2,6-diisopropylphenyl)-phenylphosphine (Dipp_2PhP , **V**), and tris(2,6-diisopropylphenyl)-

phosphine (Dipp₃P, VI) via a similar method utilising tetrameric Dipp₄Cu₄. The study pointed out that Dipp₃P has almost identical steric properties at the phosphorus atom as Tripp₃P and that the extreme bulky nature of the aryl groups in both architectures make them flat with wider bond angles and enhancement of radical cation stability and also have very low oxidation potentials.^{6, 17} In such systems, it has been concluded that the isopropyl (*iPr*) substituents at positions 2 and 6 of the aryl rings instigates flattening associated with local steric congestion around the phosphorus atom with consequent steric pressure as presented in Figure 1.5. There are endo (En) and exo (Ex) sets of *iPr* groups in the structure. The steric pressure is associated with steric repulsion of the endo groups with consequent twisting of the exo group above the phosphorus atom to protect the lone pair.

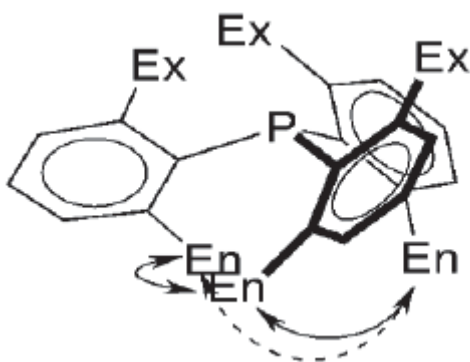


Figure 1.5. Illustration of steric pressure arrangement of endo and exo in 2- and 6-position substituted Ar₃P

Thus, the sums of angles of 334.4° and 335.6° were recorded for Tripp₃P and Dipp₃P respectively which are greater than the average value of 308.1° reported for Ph₃P.¹⁸ On this note, the effect of the steric pressure leads to dynamic intramolecular rotation along the C–P bonds that force the *exo* substituents on the aryl rings to move to a position where it encloses the phosphorus lone pair for protection from reaction.¹⁹

The coordination chemistry of phosphines (R_3P) has been extensively investigated. Based on the electronic structure around the phosphorus atom, they can coordinate with transition metals through sigma donation or pi (π) back bonding (Figure 1.6). They can coordinate to empty σ -orbitals of transition metals mostly via donation of their lone pairs to form sigma bonds (σ). The interaction is dependent on the electronic property of the R-substituent. Electron donating groups such as alkyl increase the donating ability of the phosphorus atom lone pair electron by raising the energy of the highest occupied molecular orbital (HOMO). However, electron withdrawing groups like phenyl (Ph) reduce the donating ability of the lone pair electron by lowering the energy of the HOMO. Moreover, phosphines can undergo backbonding somewhat analogously to carbon monoxide. This involves interaction of filled d orbitals of metals with an empty antibonding (σ^*) orbital of the phosphine molecule. Such an interaction is much greater with strongly electron withdrawing R groups on the phosphorous atom which lower the energies of the σ^* orbitals. Of much greater significance, however, is that for any given R_3P , backbonding is correspondingly more important for the lowest oxidation states of the metal, and less important for higher oxidation states. This is vital to many reaction and catalytic processes in which the oxidation state of the metals change (usually by two units, like 0/II or II/IV; or I/III, depending on group number).

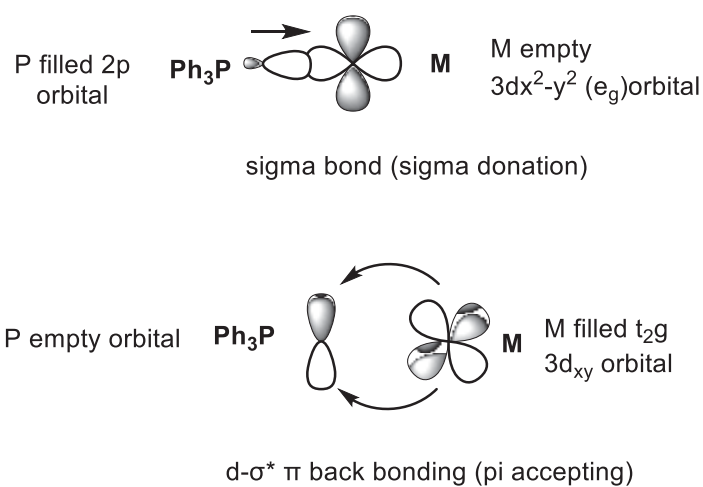


Figure 1.6. coordination of phosphines with transition metals.

1.2 Molecular magnets and their versatility

There is strong interest currently in a molecular-based chemistry of materials. The performance of inorganic materials like metals and semiconductors (e.g., boron- or phosphorus-doped silicon chips) in electronics are based on the entire material. On the other hand, for molecular-based compounds like metal-organic frameworks, the function of materials depends on synergy between properties of the organic component and the metal.²⁰⁻²⁵

The flexibility, low cost, and minimum energy requirements, coupled with the influence of individual components, makes the molecular tailoring of materials more appealing than their purely inorganic counterparts. The combination of inorganic character and organic traits have led to the isolation of materials with excellent optical, electronic, catalytic, and magnetic properties.^{17, 22, 26-42} Recent studies have led to the syntheses and isolation of these substances via solution chemistry. The designing of novel ligands suitable for metal coordination to construct materials with inherent useful properties is one of the main challenges of chemists in the field of materials engineering and various investigations are being considered to overcome the hurdles.

One active area of molecular materials research is the production of single molecule magnets (SMMs). SMMs are molecules (organic compounds or metal complexes) that display zero-field slow magnetic relaxation at low temperature.^{40, 43} A molecule must exhibit magnetic bistability in order to act as an SMM.^{41, 44-46} Also, the relaxation time must be long enough to observe hysteresis with consequent magnetic memory retention effects. Such systems must have a high electronic ground state spin, blocking temperature (T_B) and energy barrier. This gives them capacity for high density information storage and processing at the nanoscale, thus making them rich candidates for quantum computer devices and spintronics.²²

In addition to zero-field splitting and high spin ground states, strong exchange interactions have been found to enhance slow relaxation in SMMs. A significant approach to introduce such efficient magnetic coupling is to design complexes that contain stable radical ligands. This kind of system will result in strong magnetic interactions between the paramagnetic centers on the ligand and metal ions due to direct orbital overlap (Figure 1.7). The radical ligands that have been investigated include nitronyl nitroxide (NITN),^{35, 47-51} imino nitroxide (IMN),^{35, 52} nitroxide (N),⁵³⁻⁵⁶ verdazyl (VDZ),^{38, 57-65} and thiazyl such as 1,2,3,5-dithiadiazolyl (DTDA)⁶⁶⁻⁷⁰, as presented in Figure 1.8. The NITN, IMN and N are the most widely studied radicals for SMM development due to their stability in air. The stability is based on the delocalization of the unpaired electron over the oxygen atoms. A main setback to this system is the weak basicity which minimizes its coordination to metal centers. However, using heterocyclic derivatives with chelating nitrogen atoms enhances coordination to metals with poor electrophilicity.^{35, 47, 51}

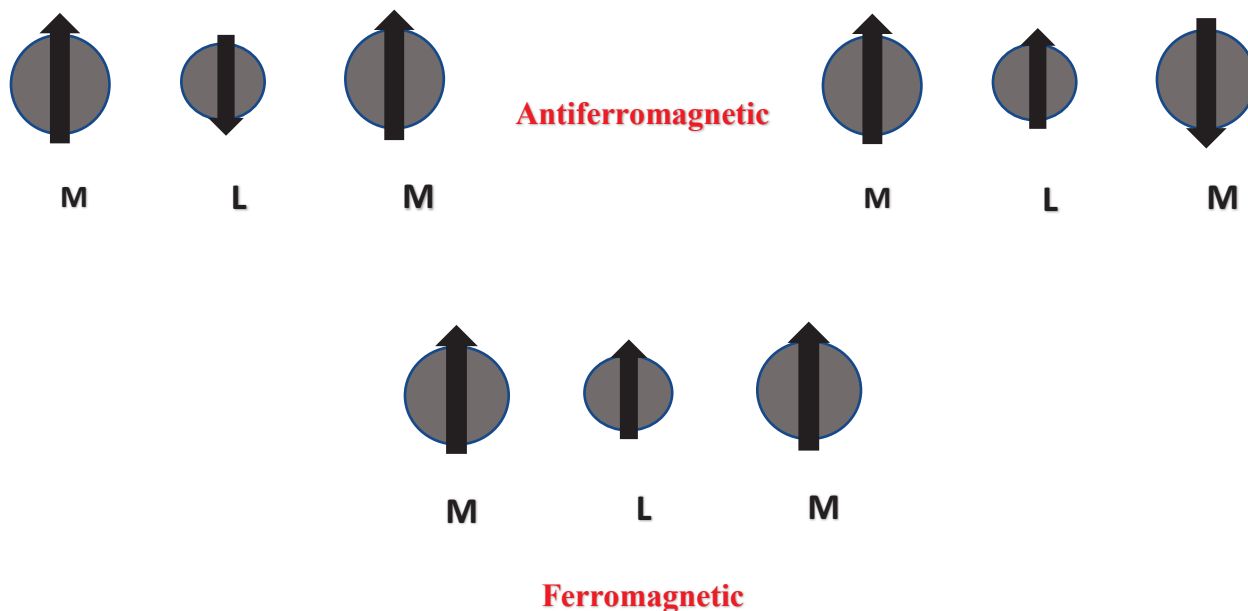


Figure 1.7. Two kinds of ligand-metal unpaired spin interactions

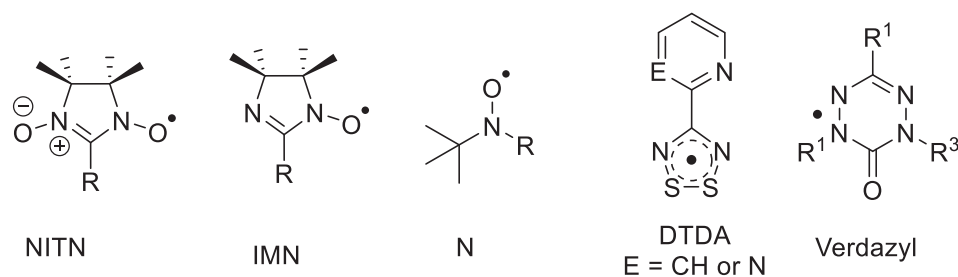


Figure 1.8. Radical ligands previously explored as building blocks for SMMs.

The metal complexes of the first-row transition metals Cu, Mn, Ni, Fe and Co for all radicals listed in Figure 1.8 have been reported. Most of these radical-metal complexes display SMM behaviour with ferromagnetic or antiferromagnetic coupling magnetic susceptibility.^{35, 38, 51, 55, 58, 61, 63, 71} Magnetic ordering in these complexes inherently depends on the strong magnetic interaction between the metal and ligand spin.⁷²⁻⁷⁵ Moreover, strong electron delocalization in the whole system usually results in remarkable magnetic and conduction properties. Using spin bearing ligands to bridge metal centers helps to promote delocalization of electrons in the material with consequent improvement in electronic and magnetic properties.⁷⁶

Heterocyclic DTDA derivatives are a class of thiazyl radical which have identical coordination behaviour with verdazyl, which is relatively stable to moisture and air like nitronyl nitroxide.⁶⁹ The nitrogen atoms in these congeners are σ -donors which chelate metal centers in a bidentate fashion.⁷⁷⁻⁷⁸ Moreover, the unpaired spin which is localized within the heterocyclic ring in both ligands helps in strengthening their magnetic coupling with metal ions.⁷¹ However, the symmetry of the interacting orbitals determines the magnetic behaviour. For instance, pyridyl (Py)- and pyrimidyl (Pm)-substituted verdazyls have been reported to form mononuclear, (VDZ)M(hfac)₂ and dinuclear, (hfac)₂M (VDZ)M(hfac)₂ complexes, respectively, with M = Mn, Ni (here *hfac* represents hexafluoroacetoacetato, a mononegative chelating supporting ligand that fills the additional coordination sites at the metals).⁶⁴ The Mn^{II} complexes results in

antiferromagnetic coupling, while those of the Ni^{II} analogues afford ferromagnetic interactions.³⁸ Similar mono- and di-nuclear complexes of Mn^{II}, Ni^{II}, including Fe^{II}, Cu^{II} and Co^{II} have been reported for PyDTDA^{67, 70, 77} and PmDTDA^{69, 79}. It was discovered that both mononuclear (Py/PmDTDA) and dinuclear (PmDTDA) complexes displayed identical magnetic susceptibilities as found in the structurally and electronically related verdazyl heterocycle derivatives. The Mn^{II} and Fe^{II} complexes exhibited antiferromagnetic magnetic coupling with the DTDA type radical ligands^{69-70, 80} while Ni^{II}, Cu^{II} and Co^{II} complexes revealed ferromagnetic interactions.^{67, 78, 80}

Strong coupling of paramagnetic centers on the ligand and on the metal has been found to contribute significantly to the overall magnetic moment through direct exchange interactions which can be achieved by strong delocalization of electrons in the radical ligand.^{40-41, 81} PyDTDA and PmDTDA, which are a class of thiazyl radical ligands, have shown potential properties of SMMs. However, the restriction of the unpaired electron spin within the DTDA[•] heterocyclic ring influences their magnetic interactions based on orbital overlap between the metal and the ligand. 1,2,4,6-thiatriazinyl (TTA[•]) is another class of thiazyl radical with a similar 7e π electronic system to DTDA[•]. However, it has received limited attention due to the difficulties in its synthesis compared to the corresponding DTDA[•]. Nonetheless, the absence of a perpendicular node in the single occupied molecular orbital (SOMO) in TTA[•] facilitates the delocalization of the electron throughout the whole system including the substituents (R) as shown in Figure 1.9. In the figure, R is hydrogen (H) for simplicity, but the same applies for other groups. Since the C atom is not centred on a node but has a finite contribution to the SOMO, delocalization of electron (or spin) density into the substituents R at C occurs. By contrast, the CR moiety in DTDA radicals is nodal in the SOMO, so that only inductive influences of the substituents R occurs. Therefore, it is

proposed that replacing TTA[•] could be a more versatile ligand for the development of complexes with SMM properties that may improve over the DTDA[•] systems.

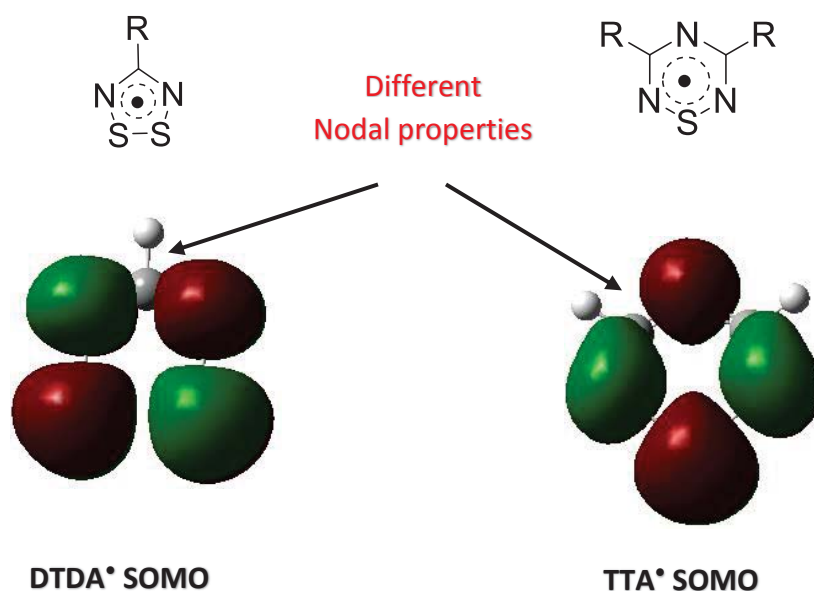


Figure 1.9. Different nodal properties of DTDA[•] and TTA[•]

The use of chelating X congeners with heterocyclic substituents have also been found promising in the design of excellent SMM and conducting materials.^{66-68, 70-71, 82-85} This is typically achieved through magnetic coupling mediation of the ligand and high-spin transition metals.⁷⁰ Chelate coordination complexes of this kind help in ordering the magnetic orbital of both the chelating ligand and metal center.⁷⁷

Preuss and coworker investigated pyridine and pyrimidine functionalized dithiadiazolyl radical (DTDA[•]) complexes with metals of the first transition series as potential building blocks for SMM.^{67, 70, 78} Both derivatives displayed interesting electronic and magnetic properties.^{67, 77} The authors demonstrated the possibility of metal-ligand coordination at the electronegative hard N atom of DTDA[•] instead of the conventional electropositive soft S atoms. The complexes exhibited a variety of coordination modes with a common characteristic of perpendicular

coordination to the heterocyclic DTDA[•] ring via the σ -donation of nitrogen atoms as reflected in Figure 1.10. Mononuclear complexes of the type DTDA(M)(hfac)₂ (where M = Cu, Co, Ni, or Mn; R = 2'-Py, 4'-CN-Py, 5'-CN-Py, or 5'-Br-Py and hfac = 1,1,1,5,5,5-hexafluoroacetylacetonato) were isolated with pyridine substituent^{77, 80} The copper (II) complex (Figure 1.17a with M = Cu(II)) is formed by orthogonal correlation of the partially filled *d*-orbitals with the π SOMO of the ligand⁸⁰ while in the cobalt (II) and nickel (II) complexes, one of the three unpaired electrons of the *d*-orbital is non-orthogonal to the π system of the ligand.⁷⁷ Conversely, three out of five unpaired *d*-electrons of the metal are non-orthogonal to the π electrons of the ligand in the manganese (II) complex.⁸⁰ Binuclear complexes were obtained using the pyrimidine (Pym) analogue (Figure 1.17b).⁷⁹ All the complexes exhibit interesting magnetic interactions (vide supra).

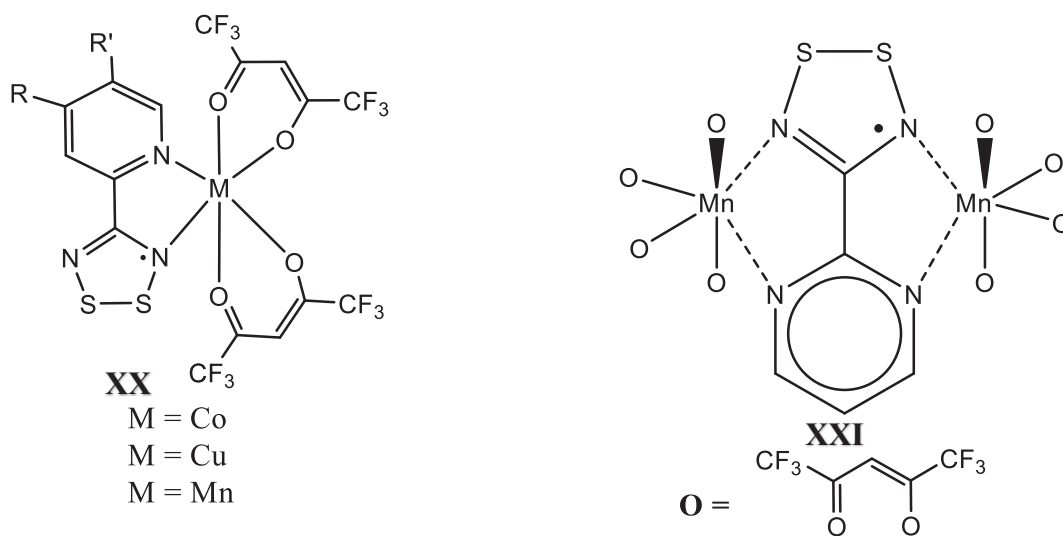
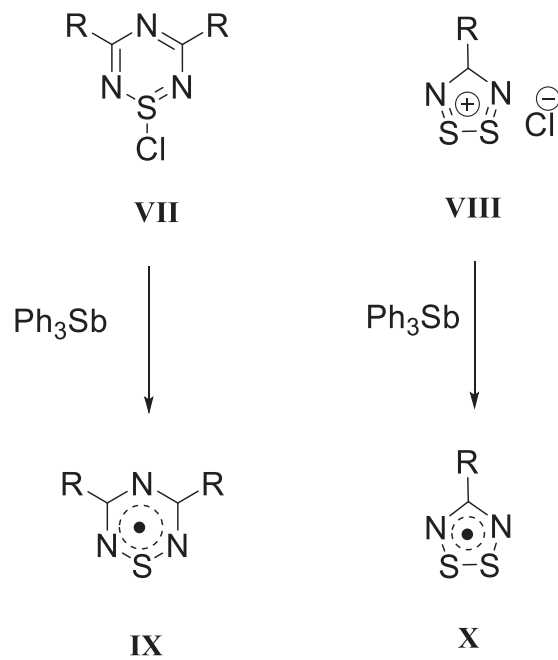


Figure 1.10. DTDA radical coordination to metals via only N-atoms.

1.3 Closed shell and open shell thiazines



Scheme 1.2. Preparation of TTA* from TTACl

The CNS framework thiazine heterocycles such as closed shell chlorothiazine, TTACl (**VII**) and dithiadiazolium chloride, DTDACl (**VIII**) are precursors to the stable neutral thiatriazinyl (TTA*) (**IX**) and dithiadiazolyl radicals DTDA*, **X**. **IX** is a six-membered ring radical of the type $\text{R}_2\text{C}_2\text{N}_3\text{S}^*$ with IUPAC nomenclature of 1-thia-2,4,6-triazinyl having R-groups at 3- and 5- positions. DTDA* have been found to be useful radical ligands for SMM development (Scheme 1.2).^{71-72, 86} The delocalization of the π -electron in the N–S–N fragment of **IX** is facilitated by overlap of N and S π electrons in conjunction with sulfur and nitrogen electronegativity. An energy level diagram of the π MOs of benzene and **IX** is presented in Figures 1.11. The SOMO (π^4) energy of **IX** is considerably lower than the LUMO energy of benzene due to the much higher electronegativities of N and S compared to C. This facilitates the stability of the TTA neutral radical.

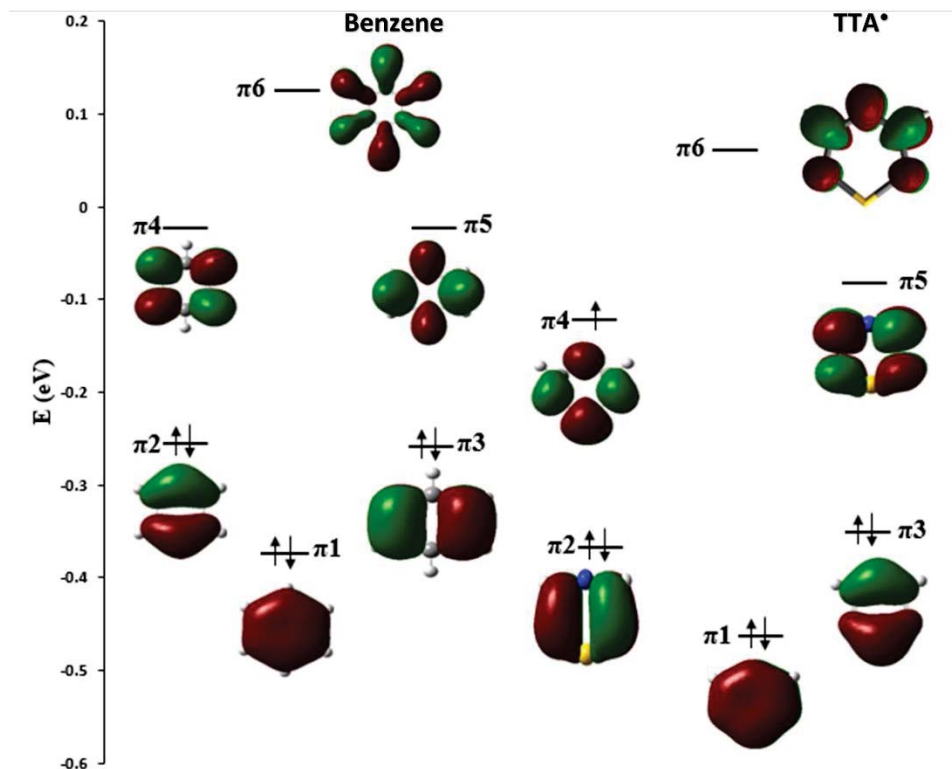
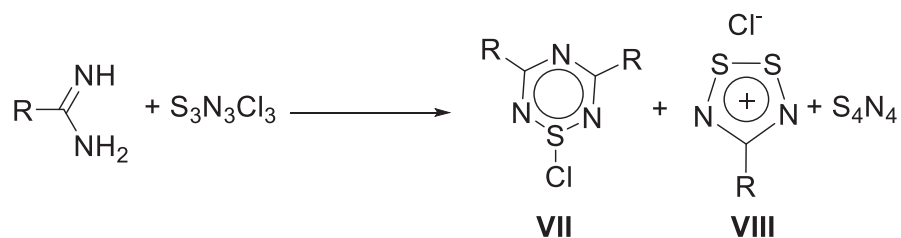


Figure 1.11. The π MOs surfaces of benzene and TTA radical obtained from DFT computations using ROB3LYP/6-31+G(d,p). The surfaces are rendered using an isovalue of 0.02.

The first discovery of a radical of type **IX** was demonstrated by Markovskii et al.⁸⁷ through EPR experiments. They are typically products of the reduction of the 1-chloro-1-thia-2,4,6-triazine (**VII**) with triphenylantimony (Ph_3Sb) in suitably degassed solvents such as acetonitrile or dichloromethane.⁸⁸⁻⁹¹ Numerous symmetric **VII** (identical R) have been prepared by condensation of imidoamidine derivatives with sulfur monochloride (SCl_2), by the reaction of trichlorothiazine ($\text{N}_3\text{S}_3\text{Cl}_3$) with amidine, or via substitution reactions with other reagents (Scheme 1.3). For instance, Ramakrishna et al.⁹² reported that 1-chloro-3,5-bis(dimethylamino)-1,2,4,6-thiazine can be generated via reaction of trichlorothiazine with tetramethylmethylenediamine in which the two chlorine atoms on the carbon are substituted with dimethyl amine.

The amidine-trichlorothiazine pathway is not an efficient route as its results in low yields. This can be attributed to side products like dithiadiazolium chloride, **VIII** and tetrasulfur tetranitride (S_4N_4).⁹¹ The majority of the publications on symmetric TTACl and TTA \cdot were published by Oakley and co-workers^{88, 91, 93-94} through the condensation reaction of imidolyamidines with SCl_2 . Other aryl derivatives ($p\text{-NO}_2C_6H_4$ and $p\text{-MeOC}_6H_4$)⁹⁵ and halogenated derivatives Cl_3 and CF_3 ⁹⁵⁻⁹⁶² have also been reported using a similar procedure.



Scheme 1.3. Synthesis of VII using $S_3N_3Cl_3$

Electrochemical studies of aryl substituted TTA \cdot have shown that it could exist in different ionic forms (neutral, cation and anion). As compared to the neutral radical or salts of the cation, the anionic TTA has not been isolated but was trapped with H^+ as the NH imine reduced compound.⁸⁸ However, the reversible closed-shell one-electron reduction of the neutral radical species using solution cyclic voltammetry (CV) has been reported.⁹⁷ Recently, a pyridine (Py) derivative was attempted using sulfur monochloride (S_2Cl_2) in place of SCl_2 .⁹⁸ The TTA \cdot heterocyclic systems have been known around four decades, but less work has been done on its transition metal complexes compared to DTDA \cdot (**X**).^{36, 86, 99}

Cordes and co-workers have investigated **X** and its selenium analogs as building blocks in the development of organic conductors.¹⁰⁰ Its derivatives have also been utilized as building blocks in organic magnet construction by Rawson and co-workers.¹⁰¹ The electrochemistry of many derivatives of **X** have been compiled by Boéré et al.¹⁰⁸

The heterocyclic ring of **IX** has been shown to be redox active and even have non-innocent behavior when the 3,5-substituents are pyridine (Py).⁹⁸ The S···S distances are shorter than the inter ligand distances of atoms within the dimer, indicating high spin density concentration on the S (i.e. in the SOMO, the π_4 orbital in Figure 1.9)⁹¹. This feature has also been exhibited by the selenathiaziazinyl radical dimer analogues.⁹⁴ Such behaviour has also been observed in structure **IX** where α - spin density is distributed on the N and S atoms with the largest density of the SOMO on the S atom resulting to the formation of a co-facial reversible π - π intermolecular dimer in the solid state (Figure 1.12).

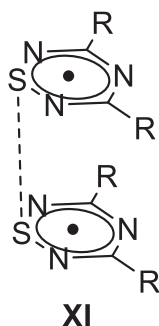


Figure 1.12. Solid-state structure of TTA[•] dimer

EPR investigations for symmetric **X** with 3,5-electron donating substituents towards the TTA radical ring, where R = Ph, H or *p*-MeOC₆H₄^{91,95} revealed a septet hyperfine coupling to three equivalent N atoms. However, with electron withdrawing analogues R = CF₃, Cl, *p*-CF₃C₆H₄, or *p*-NO₂C₆H₄,⁹⁵ the spectra show two different couplings i.e. one to the central N atom and the two N atoms next to S atom.

1.3.1 Thiazine complexes and their viability as building blocks for molecular magnets

Development of new radical-metal cation conductors using spin-bearing stable neutral radicals is a major focus of new research in materials design.⁷⁷ This strategy will ultimately leads

to interesting tunable magnetic and conducting properties for electronic applications. Extensive studies have been done on 1,2,3,5-dithiadiazolyl radical **X** coordination chemistry exploring their magnetic and electronic properties. The first reported transition metal complexes of **X** were those in which it coordinated through the two S atoms as shown in Figure 1.13.

The complex of $(\mu^1\text{-CO})_3\text{Fe} - \text{Fe}(\mu^1\text{-CO})_3(\mu - \text{RDTDA})$, **XII** (Figure 1.13a) was reported in 1989 by Banister et al.¹⁰², where R = Ph. The complex was generated from the reaction of $\text{Fe}_2(\text{CO})_9$ or $\text{Fe}_3(\text{CO})_{12}$ with DTDA^\bullet where the oxidation state of Fe is zero. The metallocene analogue (**XI**, Figure 1.13b) was also made via the same route,¹⁰³ by reacting DTDA^\bullet with $[\text{Ni}(\text{Cp})(\text{CO})]_2$ to generate a binuclear nickel (I) complex dimer bridged by the S...S bond. An EPR study of both complexes revealed the presence of unpaired electron in **XI** which is delocalized among S, C and the Ni atom and no spin density was observed on the N atoms, but **XII** was shown to be diamagnetic.¹⁰³

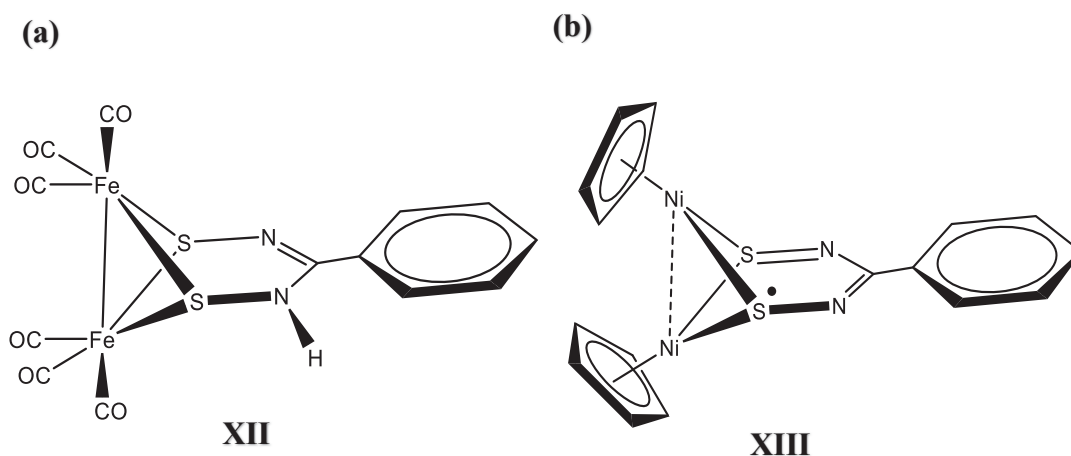


Figure 1.13. The 4-phenyldithiadiazolyl complexes of (a) Fe and (b) Ni^+

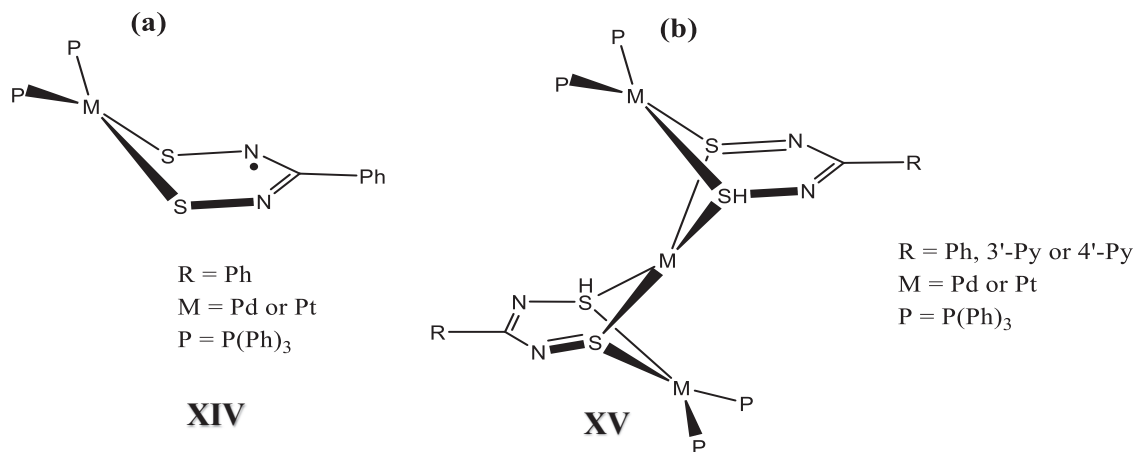


Figure 1.14. The dithiadiazolyl complexes formed from M(PPh₃)₃ reactions

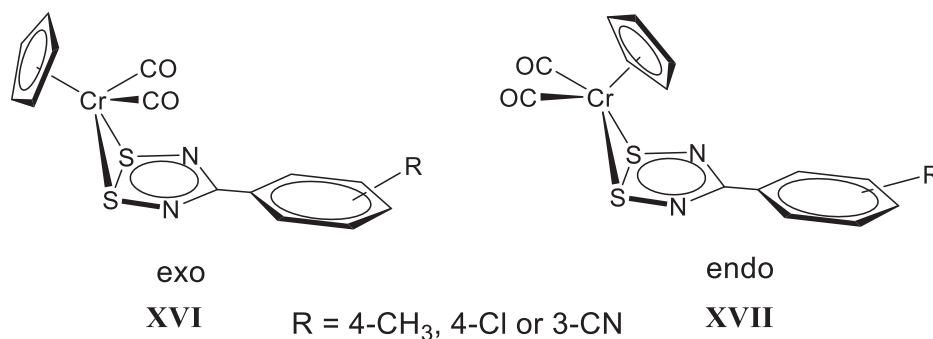


Figure 1.15. Complex of DTDA[·] of reaction with [CpCr(CO)₃]₂.

An extension from the first transition series are the sets of platinum (Pt) and palladium (Pd) complexes of the type DTDA(M)(PPh₃)₂ Figure 1.14a¹⁰⁴ and (DTDA)₂(M)₃(PPh₃)₄ Figure 1.14b¹⁰⁵⁻¹⁰⁶ where R = Ph, 3'-pyridine (3'-Py) or 4'-pyridine (4'-Py); M = Pt or Pd; and P = PPh₃ from the reaction of DTDA[·] with M(PPh₃)₃. All these compounds were proved by EPR experiments to be paramagnetic showing coupling with P, N and Pt nuclei. In general, the coordination to the S atoms usually leads to S–S bond cleavage, or significant elongation, in all the complexes that have been structurally characterized. A recent report has shown the coordination of **X** with the retention of the S–S bond when reacted with [CpCr(CO)₃]₂.¹⁰⁷ The complexes obtained are diamagnetic in

which **X** coordinated to the chromium(I) center in either *endo* or *exo* form where R = CH₃, 4-Cl or 3-CN (Figure 1.15).

Limited work has been done on the coordination chemistry of TTA[•] compared to DTDA[•]. The first reported complexes of TTA[•] were the metallocene carbonyl complexes, **XVIII** and **XIX** (Figure 1.16) which were obtained from the reaction of symmetric and asymmetric derivatives with [CpCr(CO)₃]₂.⁹⁶ Both adducts are diamagnetic. **XVIII** was formed by one-electron (η^1) coordination to the chromium ion via a sulfur p-orbital. It was isolated by reaction of symmetric 3,5-diphenyl-1-thia-2,4,6-triazinyl radical with the 17 electron [CpCr(CO)₃] moiety reflecting an *exo* conformation in which the cyclopentadienyl ring is located opposite to the TTA heterocyclic ring. The η^1 bond length corresponds to the S-S bond distance of the diamagnetic TTA[•] dimer (TTA₂) in the solid state. On the other hand, the asymmetric 3-trifluoromethyl, 5-phenyl-1,2,4,6-thiatiazinyl radical (R = CF₃ and Ph) was reacted with 17 electron [CpCr(CO)₃] to generate complex **XIX** through three-electron (η^2) bonding to the 15 electron CpCr(CO)₂ complex formed by elimination of a CO molecule. The coordination occurred via interaction of the σ -orbitals of both S and one of the adjacent N atoms having the largest spin density. The complex also shows an *exo* coordination mode (Figure 1.16).

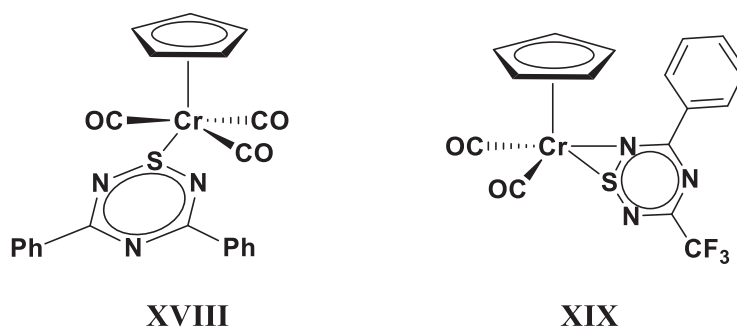


Figure 1.16. Metallocene complexes of TTA[•]

A recent report by Brusso and co-workers led to the isolation of a redox active iron pincer complex of heterocycle substituted TTA* (Figure 1.17).^{98, 108} The complex was achieved via the reaction of 3,5-bis(2-pyridyl)-1-thia-2,4,6-triazine hydride (**XXII**) or its anionic derivative (Py₂TTA⁻) with FeCl₂ and FeCl₃ respectively. The reactions led to the formation of the same product, [FePy₂TTA]Cl₂, **XXIII** which demonstrated redox non-innocent properties. This material exhibited a ferromagnetic electronic interaction between the ligand and iron center, resulting in a high spin S = 5/2 electronic ground state based on delocalization of electron density between the two redox active centers.

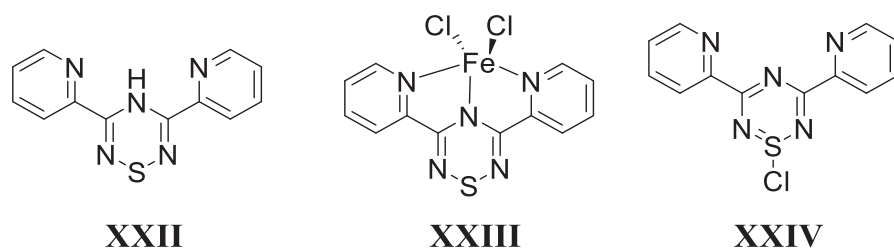


Figure 1.17. Iron (Fe) complex of Py₂TTA

1.3.2 Redox non-innocence of TTA radical

The term non-innocent applied to a ligand is commonly used in coordination chemistry of transition metals as the ability of a ligand to participate in redox activities in the presence of the metal.^{25, 109-125} An ideal ligand behaves as a spectator in coordination compounds. This resulted in the classification by Jorgensen in 1966 as “innocent” and “non-innocent” ligands.¹²⁶ Redox active compounds are a recent important topic of discussion due to their versatility in various fields, particularly catalysis^{124, 127-129} and superconducting materials applications^{118, 124}.

“Redox-active” and “non-innocent” ligands are two words that are being used interchangeably in some articles. However, this had been proved wrong as a ligand might be redox

active but still innocent. Properties of metal coordination complexes are based on the overall contribution of the ligands and the metal involved.¹³⁰⁻¹³¹ Redox active ligands are the kinds that partially or fully participate in the redox-chemistry in metal-ligand complexes in which acceptance and removal of electrons in the system can involve the ligand and/or the metal (Figure 1.18).¹³²⁻¹³³ In cases where the oxidation state of a metal cannot be unambiguously determined in the presence of redox active ligands, the ligand is said to be “non-innocent”. Based on this, Kaim¹³⁴ defined non-innocent as uncertainty in assigning oxidation state to ligand and metal in a complex such that the experimental oxidation state is different from that determined from coordination chemistry rules. Diverse attempts had been made by various authors to elucidate the electronic configurations and/or oxidation states of most non-innocent ligand (NILs) complexes using spectroscopy, electrochemistry, computational calculations and crystallographic analyses.¹³⁵⁻¹³⁸ This had been identified as a special challenge associated to NIL complexes and had been proclaimed as their intrinsic character as compared to their innocent counterparts in which the central metal oxidation state is easily determined due to their spectator nature.¹³⁹⁻¹⁴⁰

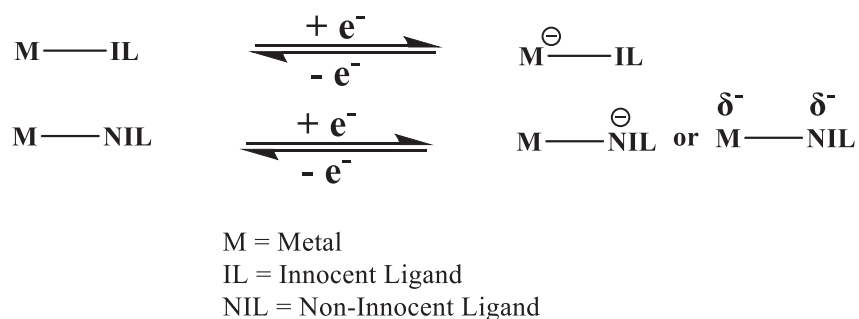


Figure 1.18. Mechanisms of innocent and non-innocent ligands.

There is a rapid growth in investigation of redox-active and non-innocent ligands. They were even discussion forums in some journals such as *Inorganic Chemistry*¹⁴⁰ and *Coordination Chemistry Reviews*.¹²⁷ Their ability to undergo electron transfer by involving in electrochemical electron transfer or chemical reactions in the presence of metals with potential to a variation in the

metal oxidation state, is an interesting topic. The performance of some naturally existing molecules has been recognized for relying upon redox activity of the participating ligands. These include metalloenzymes (like galactose oxidase and cytochrome P450) and chlorophyll, for which their mechanism of action is based on synergistic collaboration of the center metal (such as Mg in chlorophyll and Fe in P450) that have limited oxidation events and the surrounding ligands (like the porphyrin in chlorophyll and the non-innocent oxo and heme thiolate ligand in P450). For instance, Green et al.¹⁴¹ reported Fe (IV) d^4 as the oxidation state in P450 based upon the kinetic and spectroscopic investigation which contradicts the formal Fe(V) calculated theoretically. This revealed the true non-innocence of the ligands in the complex.

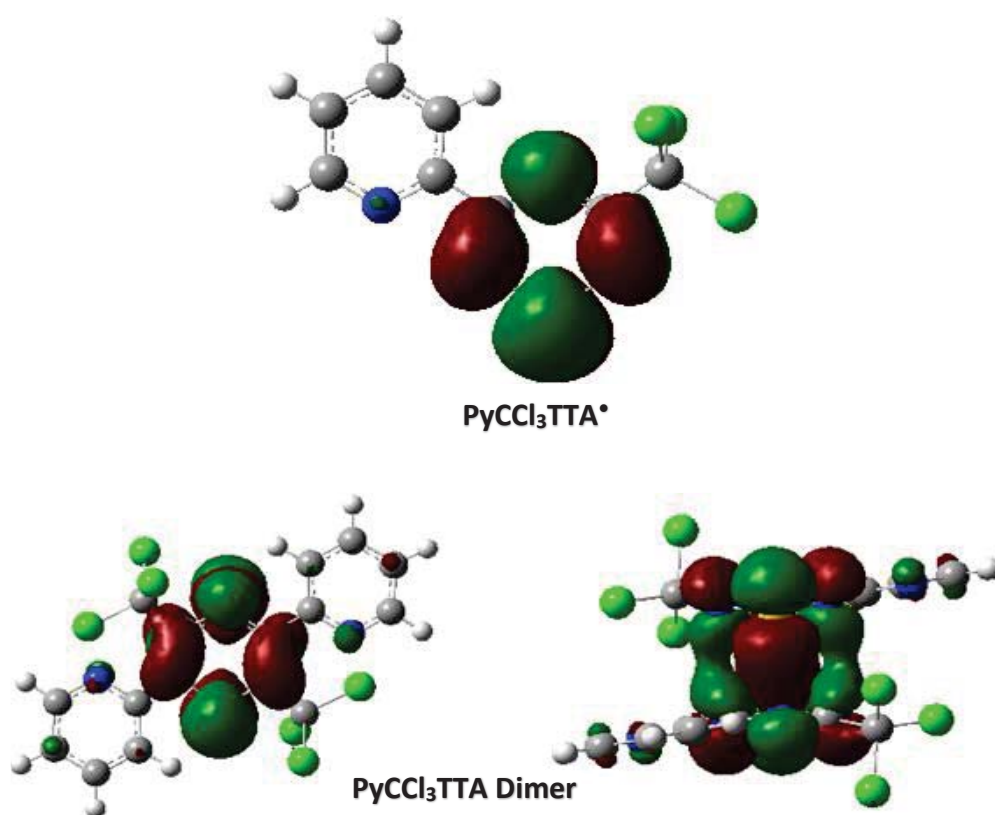
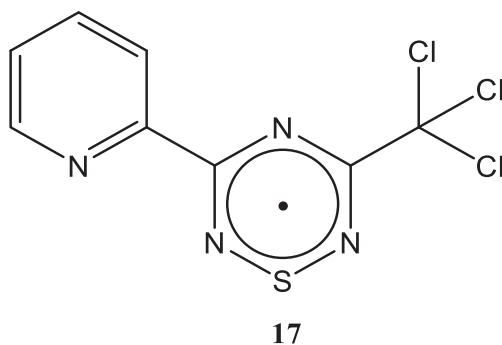


Figure 1.19. The π SOMO surfaces of PyCCl₃TTA radical and dimer obtained from DFT computations using ROB3LYP/6-31+G(d,p). The surfaces are rendered using an isovalue of 0.02.

Thus, DFT calculation of 3-trichloromethyl-5-(2-pyridyl)-1-thia-2,4,6-triazinyl (PyCCl₃TTA[•]) and its dimer were undertaken to show their possibility as redox non-innocent ligands. The π SOMO of the radical shows a partial overlap of the π orbital of C=N with the *ipso* carbon (C) of the substituent and there is no nodal plane cutting across the C atoms (Figure 1.19). This shows potential delocalization of an additional electron that may be added to the system across the substituents.

1.4 Goals of the thesis

Contemporary studies of spin-bearing ligands as well as their metal coordination complex aim to enhance the paramagnetic behavior of the metal centers through exchange or magnetic coupling and the tendency of the radical to undergo one-electron intramolecular reversible redox reactions.⁷¹ One of the recent options to eliminate antiferromagnetic interactions in molecular materials, which usually occur below the critical temperature (T_N , Néel temperature), is to manipulate the magnetic ordering. The natural strategic way of achieving this is the use of bridging ligands or chelating substituents which tend to transmit magnetism through polarization of antiparallel spin such as utilizing a bridging ligand.^{41, 50} The most robust option is to use substituents possessing sigma donor heteroatoms with the option of pyridine (Py) or pyrimidine (Pym) on the central TTA[•] ring.



In this thesis report, asymmetric 1-thia-2,4,6-triazinyl radicals with 2-pyridyl and trichloromethyl groups at the 5- and 3-positions as in **17**, along with an N-pyridyl protonated salt, are synthesized and fully characterized by NMR (^1H and ^{13}C), IR spectroscopy and X-ray diffraction experiments. Also, the synthesis of molecular synthons such as 2-pyridylcarboximidamide and the precursor 2-amidinoimidoyl amidine and their pyrimidine analogs are also reported, as well as a variety of encountered compounds in the process of achieving the aim and objective of the project.

1.5 References

1. Berchadsky, Y.; Tordo, P.; Gronchi, G.; Culcasi, M., Anodic behavior of crowded triarylphosphines. ESR study of triarylphosphoniumyl radicals, $\text{Ar}_3\text{P}^{\bullet+}$. *J. Org. Chem.* **1991**, *56*, 3537-3542.
2. Aslanidis, P.; Divanidis, S.; Cox, P. J.; Karagiannidis, P., Polymer and cage-type structures in silver(I) complexes with heterocyclic thiones and bridging diphosphine ligands. Crystal structures of $[\text{Ag}(\mu\text{-dppent})(\text{tHpymtH})(\text{ONO}_2)]_n$ and $[\text{Ag}_2(\mu\text{-trans-dppen})_3(\text{pymtH})_2](\text{NO}_3)_2 \cdot \text{CH}_3\text{CN}$. *Polyhedron* **2005**, *24*, 853-863.
3. Araki, H.; Tsuge, K.; Sasaki, Y.; Ishizaka, S.; Kitamura, N., Synthesis, structure and emissive properties of Copper(I) complexes $[\text{Cu}^{\text{I}}_2(\mu\text{-X})_2(\mu\text{-1,8-naphthyridine})(\text{PPh}_3)_2]$ (X = I, Br) with a butterfly-shaped dinuclear core having a short Cu–Cu distance. *Inorg. Chem.* **2007**, *46*, 10032-10034.
4. Sasaki, S.; Murakami, F.; Murakami, M.; Watanabe, M.; Kato, K.; Sutoh, K.; Yoshifuji, M., Synthesis of crowded triarylphosphines carrying functional sites. *J. Organomet. Chem.* **2005**, *690*, 2664-2672.
5. Tolman, C. A., Steric effects of phosphorus ligands in organometallic chemistry and homogeneous catalysis. *Chem. Rev.* **1977**, *77*, 313-348.
6. Bullock, J. P.; Bond, A. M.; Boeré, R. T.; Gietz, T. M.; Roemmele, T. L.; Seagrave, S. D.; Masuda, J. D.; Parvez, M., Synthesis, characterization, and electrochemical studies of $\text{PPh}_3\text{-}_n(\text{dipp})_n$ (dipp = 2,6-Diisopropylphenyl): Steric and electronic effects on the chemical and electrochemical oxidation of a homologous series of triarylphosphines and the reactivities of the corresponding phosphoniumyl radical cations. *J. Am. Chem. Soc.* **2013**, *135*, 11205-11215.
7. Zagumennov, V. A.; Nikitin, E. V., Reactivity of radical cations of trimesitylphosphine. *Russ. J. Electrochem.* **2003**, *39*, 1236-1239.
8. Alyea, E. C.; Ferguson, G.; Malito, J.; Ruhl, B., Monomeric (trimesitylphosphine)copper(I) bromide. X-ray crystallographic evidence for the first two-coordinate copper(I) phosphine halide complex. *Inorg. Chem.* **1985**, *24*, 3719-3720.
9. Bayler, A.; Bowmaker, G. A.; Schmidbaur, H., Propeller isomerism in bis(trimesitylphosphine)gold(i), -silver(i), and -copper(i) tetrafluoroborates. *Inorg. Chem.* **1996**, *35*, 5959-5960.
10. Bayler, A.; Schier, A.; Bowmaker, G. A.; Schmidbaur, H., Gold is smaller than silver. Crystal structures of $[\text{bis}(\text{trimesitylphosphine})\text{gold}(\text{I})]$ and $[\text{bis}(\text{trimesitylphosphine})\text{silver}(\text{I})]$ tetrafluoroborate. *J. Am. Chem. Soc.* **1996**, *118*, 7006-7007.
11. Alyea, E. C.; Ferguson, G.; Gallagher, J. F.; Malito, J., Chloro(trimesitylphosphine)gold(I). *Acta Crystallogr., Sect. C* **1993**, *49*, 1473-1476.

12. Sasaki, S.; Yoshifuji, M., Synthesis, structure and properties of crowded triarylphosphines. *Curr. Org. Chem.* **2007**, *11*, 17-31.
13. Ogawa, S.; Kikuchi, M.; Kawai, Y.; Niizuma, S.; Sato, R., Synthesis, structure and redox reactions of a new crowded benzodithiolium salt: first isolation and characterization of a stable dithioly radical with a 7 pi electron framework. *Chem. Commun.* **1999**, 1891-1892.
14. Sasaki, S.; Aoki, H.; Sutoh, K.; Hakiri, S.; Tsuji, K.; Yoshifuji, M., Synthesis and redox properties of bis[4-[bis(4-methoxyphenyl)amino]-2,6-bis(2,4,6-triisopropylphenyl)phenyl diphosphene). *Helv. Chim. Acta* **2002**, *85*, 3842-3847.
15. Sasaki, S.; Chowdhury, R.; Yoshifuji, M., Synthesis, structure, and redox properties of crowded triarylphosphines carrying 2,6-diarylphenyl substituents. *Tetrahedron Lett.* **2004**, *45*, 9193-9196.
16. Sasaki, S.; Murakami, F.; Yoshifuji, M., Synthesis and redox properties of (3-phenothiazinomesityl)- and (4-phenothiazinoduryl)dimesitylphosphines and the corresponding arsines. *Organometallics* **2006**, *25*, 140-147.
17. Boéré, R. T.; Bond, A. M.; Cronin, S.; Duffy, N. W.; Hazendonk, P.; Masuda, J. D.; Pollard, K.; Roemmele, T. L.; Tran, P.; Zhang, Y., Photophysical, dynamic and redox behavior of tris(2,6-diisopropylphenyl)phosphine. *New J. Chem.* **2008**, *32*, 214-231.
18. Howell, J. A. S.; Lovatt, J. D.; McArdle, P.; Cunningham, D.; Maimone, E.; Gottlieb, H. E.; Goldschmidt, Z., The effect of fluorine, trifluoromethyl and related substitution on the donor properties of triarylphosphines towards [Fe(CO)₄]. *Inorg. Chem. Commun.* **1998**, *1*, 118-120.
19. Laleu, B.; Bernardinelli, G.; Chauvin, R.; Lacour, J., Trimesitylmethylphosphonium cation. Supramolecular stereocontrol and simple enantiomerization mechanism determination. *J. Org. Chem.* **2006**, *71*, 7412-7416.
20. Priimagi, A.; Cavallo, G.; Metrangolo, P.; Resnati, G., The halogen bond in the design of functional supramolecular materials: Recent advances. *Acc. Chem. Res.* **2013**, *46*, 2686-2695.
21. Ratera, I.; Veciana, J., Playing with organic radicals as building blocks for functional molecular materials. *Chem. Soc. Rev.* **2012**, *41*, 303-349.
22. Coronado, E., Molecular magnetism: from chemical design to spin control in molecules, materials and devices. *Nat. Rev. Mater.* **2020**, *5*, 87-104.
23. Feng, D.; Xia, Y., Comparisons of glyphosate adsorption properties of different functional Cr-based metal-organic frameworks. *J. Sep. Sci.* **2018**, *41*, 732-739.
24. Kim, H.; Nguyen, Y.; Yen, C. P.-H.; Chagal, L.; Lough, A. J.; Kim, B. M.; Chin, J., Stereospecific synthesis of C₂ symmetric diamines from the mother diamine by resonance-

- assisted hydrogen-bond directed diaza-Cope rearrangement. *J. Am. Chem. Soc.* **2008**, *130*, 12184-12191.
25. Kitagawa, S.; Kawata, S., Coordination compounds of 1,4-dihydroxybenzoquinone and its homologues. Structures and properties. *Coord. Chem. Rev.* **2002**, *224*, 11-34.
 26. Bond, A. M.; Fletcher, S.; Symons, P. G., The relationship between the electrochemistry and the crystallography of microcrystals. The case of TCNQ (7,7,8,8-tetracyanoquinodimethane). *Analyst* **1998**, *123*, 1891-1904.
 27. Katz, T. J.; Sudhakar, A.; Teasley, M. F.; Gilbert, A. M.; Geiger, W. E.; Robben, M. P.; Wuensch, M.; Ward, M. D., Synthesis and properties of optically-active helical metallocene oligomers. *J. Am. Chem. Soc.* **1993**, *115*, 3182-3198.
 28. Kuznik, W.; Kityk, I. V.; Kopylovich, M. N.; Mahmudov, K. T.; Ozga, K.; Lakshminarayana, G.; Pombeiro, A. J. L., Quantum chemical simulations of solvent influence on UV-vis spectra and orbital shapes of azoderivatives of diphenylpropane-1,3-dione. *Spectrochim. Acta, Part A* **2011**, *78*, 1287-1294.
 29. Malandrino, G.; Bettinelli, M.; Speghini, A.; Fragala, I., Europium "second generation" precursors for metal-organic chemical vapor deposition: Characterization and optical spectroscopy. *Eur. J. Inorg. Chem.* **2001**, 1039-1044.
 30. Moore, G. F.; Hambourger, M.; Kodis, G.; Michl, W.; Gust, D.; Moore, T. A.; Moore, A. L., Effects of protonation state on a tyrosine-histidine bioinspired redox mediator. *J. Phys. Chem. B* **2010**, *114*, 14450-14457.
 31. Schauer, P. A.; Low, P. J., Ligand redox non-innocence in transition-metal sigma-alkynyl and related complexes. *Eur. J. Inorg. Chem.* **2012**, 390-411.
 32. Turkoglu, G.; Berber, H.; Kani, I., Synthesis, crystal structure, optical and electrochemical properties of novel diphenylether-based formazan derivatives. *New J. Chem.* **2015**, *39*, 2728-2740.
 33. Vigato, P. A.; Peruzzo, V.; Tamburini, S., The evolution of β -diketone or β -diketophenol ligands and related complexes. *Coord. Chem. Rev.* **2009**, *253*, 1099-1201.
 34. Alberola, A.; Less, R. J.; Pask, C. M.; Rawson, J. M.; Palacio, F.; Oliete, P.; Paulsen, C.; Yamaguchi, A.; Farley, R. D.; Murphy, D. M., A thiazyl-based organic ferromagnet. *Angew. Chem., Int. Ed.* **2003**, *42*, 4782-4785.
 35. Aoki, C.; Ishida, T.; Nogami, T., Molecular metamagnet $\text{Ni}(\text{4ImNNH})_2(\text{NO}_3)_2$ (4ImNNH=4-imidazolyl nitronyl nitroxide) and the related compounds showing supramolecular H-bonding interactions. *Inorg. Chem.* **2003**, *42*, 7616-7625.
 36. Banister, A. J.; Bricklebank, N.; Lavender, I.; Rawson, J. M.; Gregory, C. I.; Tanner, B. K.; Clegg, W.; Elsegood, M. R. J.; Palacio, F., Spontaneous magnetization in a sulfur-nitrogen radical at 36 K. *Angew. Chem., Int. Ed.* **1996**, *35*, 2533-2535.

37. Barclay, T. M.; Beer, L.; Cordes, A. W.; Haddon, R. C.; Itkis, M. I.; Oakley, R. T.; Preuss, K. E.; Reed, R. W., trans-4,4'-dichloro-1,1',2,2',3,3'-tetrathiadiazafulvalene (DC-TAF) and its 1 : 1 radical cation salts DC-TAF X : Preparation and solid-state properties of BF₄⁻, ClO₄⁻, and FSO₃⁻ derivatives. *J. Am. Chem. Soc.* **1999**, *121*, 6657-6663.
38. Barclay, T. M.; Hicks, R. G.; Lemaire, M. T.; Thompson, L. K., Verdazyl radicals as oligopyridine mimics: Structures and magnetic properties of M(II) complexes of 1,5-dimethyl-3-(2,2'-bipyridin-6-yl)-6-oxoverdazyl (M = Mn, Ni, Cu, Zn). *Inorg. Chem.* **2003**, *42*, 2261-2267.
39. Beekman, R. A.; Boere, R. T.; Moock, K. H.; Parvez, M., Synthesis, electrochemistry, structure, and magnetic susceptibility of 5-tert-butyl-1,3-bis-(1,2,3,5-dithiadiazolyl)benzene. Structural effect of the bulky substituent. *Can. J. Chem.* **1998**, *76*, 85-93.
40. Bogani, L.; Vindigni, A.; Sessoli, R.; Gatteschi, D., Single chain magnets: where to from here? *J. Mater. Chem.* **2008**, *18*, 4750-4758.
41. Caneschi, A.; Gatteschi, D.; Sessoli, R.; Rey, P., Toward molecular magnets - the metal-radical approach. *Acc. Chem. Res.* **1989**, *22*, 392-398.
42. Chi, X.; Itkis, M. E.; Patrick, B. O.; Barclay, T. M.; Reed, R. W.; Oakley, R. T.; Cordes, A. W.; Haddon, R. C., The first phenalenyl-based neutral radical molecular conductor. *J. Am. Chem. Soc.* **1999**, *121*, 10395-10402.
43. Demir, S.; Jeon, I. R.; Long, J. R.; Harris, T. D., Radical ligand-containing single-molecule magnets. *Coord. Chem. Rev.* **2015**, *289*, 149.
44. Alkorta, I.; Elguero, J.; Mo, O.; Yanez, M.; Del Bene, J. E., Do coupling constants and chemical shifts provide evidence for the existence of resonance-assisted hydrogen bonds? *Mol. Phys.* **2004**, *102*, 2563-2574.
45. Ghosh, P.; Bill, E.; Weyhermuller, T.; Wieghardt, K., Molecular and electronic structures of iron complexes containing N,S-coordinated, open-shell o-iminothionebenzosemiquinonate(1-), pi radicals. *J. Am. Chem. Soc.* **2003**, *125*, 3967-3979.
46. Iwamura, H.; Koga, N., Molecular approaches to photomagnetic materials. Metal-dependent regiospecificity in the exchange coupling of magnetic metal ions with free radical substituents on pyridine base ligands. *Pure Appl. Chem.* **1999**, *71*, 231.
47. Tamura, M.; Nakazawa, Y.; Shiomi, D.; Nozawa, K.; Hosokoshi, Y.; Ishikawa, M.; Takahashi, M.; Kinoshita, M., Bulk ferromagnetism in the β-phase crystal of the p-nitrophenyl nitronyl nitroxide radical. *Chem. Phys. Lett.* **1991**, *186*, 401-404.
48. Caneschi, A.; Gatteschi, D.; Lalioti, N.; Sangregorio, C.; Sessoli, R.; Venturi, G.; Vindigni, A.; Rettori, A.; Pini, M. G.; Novak, M. A., Cobalt(II)-nitronyl nitroxide chains as molecular magnetic nanowires. *Angew. Chem., Int. Ed.* **2001**, *40*, 1760-1763.

49. Benelli, C.; Caneschi, A.; Gatteschi, D.; Pardi, L., Gadolinium(iii) complexes with pyridine-substituted nitronyl nitroxide radicals. *Inorg. Chem.* **1992**, *31*, 741-746.
50. Caneschi, A.; Gatteschi, D.; Lalioti, N.; Sessoli, R.; Sorace, L.; Tangoulis, V.; Vindigni, A., Ising-type magnetic anisotropy in a cobalt(II) nitronyl nitroxide compound: A key to understanding the formation of molecular magnetic nanowires. *Chem. - Eur. J.* **2002**, *8*, 286-292.
51. Wang, J.; Li, J. N.; Zhang, S. L.; Zhao, X. H.; Shao, D.; Wang, X. Y., Syntheses and magnetic properties of a pyrimidyl-substituted nitronyl nitroxide radical and its cobalt(II) complexes. *Chem. Commun.* **2016**, *52*, 5033.
52. Herebian, D.; Wieghardt, K. E.; Neese, F., Analysis and interpretation of metal-radical coupling in a series of square planar nickel complexes: Correlated Ab initio and density functional investigation of [Ni(LISQ)₂] (LISQ=3,5-di-tert-butyl-o-diiminobenzosemiquinonate(1-)). *J. Am. Chem. Soc.* **2003**, *125*, 10997-11005.
53. Kaizaki, S., Coordination effects of nitroxide radicals in transition metal and lanthanide complexes. *Coord. Chem. Rev.* **2006**, *250*, 1804-1818.
54. Chiarelli, R.; Novak, M. A.; Rassat, A.; Tholence, J. L., A ferromagnetic transition at 1.48 K in an organic nitroxide. *Nat.* **1993**, *363*, 147-149.
55. Iwamura, H.; Inoue, K.; Hayamizu, T., High-spin polynitroxide radicals as versatile bridging ligands for transition metal complexes with high ferri/ferromagnetic TC. *Pure Appl. Chem.* **1996**, *68*, 243.
56. Kaizaki, S., Spectroscopic implications for magnetic interactions in metal complexes with nitroxide radicals. *Bull. Chem. Soc. Jpn.* **2003**, *76*, 673-688.
57. Johnston, C. W.; McKinnon, S. D. J.; Patrick, B. O.; Hicks, R. G., The first "Kuhn verdazyl" ligand and comparative studies of its PdCl₂ complex with analogous 6-oxoverdazyl ligands. *Dalton Trans.* **2013**, *42*, 16829-16836.
58. Koivisto, B. D.; Hicks, R. G., The magnetochemistry of verdazyl radical-based materials. *Coord. Chem. Rev.* **2005**, *249*, 2612-2630.
59. Jankowiak, A.; Pocięcha, D.; Szczytko, J.; Monobe, H.; Kaszynski, P., Photoconductive liquid-crystalline derivatives of 6-oxoverdazyl. *J. Am. Chem. Soc.* **2012**, *134*, 2465-2468.
60. Brook, D. J. R.; Lynch, V.; Conklin, B.; Fox, M. A., Spin delocalization in the copper(I) complexes of bis(verdazyl) diradicals. *J. Am. Chem. Soc.* **1997**, *119*, 5155-5162.
61. Hicks, R. G.; Lemaire, M. T.; Thompson, L. K.; Barclay, T. M., Strong ferromagnetic and antiferromagnetic exchange coupling between transition metals and coordinated verdazyl radicals. *J. Am. Chem. Soc.* **2000**, *122*, 8077-8078.

62. Barclay, T. M.; Hicks, R. G.; Lemaire, M. T.; Thompson, L. K., Structure and magnetic properties of a nickel(II) complex of a tridentate verdazyl radical: strong ferromagnetic metal-radical exchange coupling. *Chem. Commun.* **2000**, 2141-2142.
63. Gilroy, J. B.; Lemaire, M. T.; Patrick, B. O.; Hicks, R. G., Structure and magnetism of a verdazyl radical clathrate hydrate. Strong intermolecular magnetic interactions derived from π -stacking within ice-like channels. *Cryst. Eng. Comm.* **2009**, *11*, 2180-2184.
64. Barclay, T. M.; Hicks, R. G.; Lemaire, M. T.; Thompson, L. K., Synthesis, structure, and magnetism of bimetallic manganese or nickel complexes of a bridging verdazyl radical. *Inorg. Chem.* **2001**, *40*, 5581-5584.
65. McKinnon, S. D. J.; Patrick, B. O.; Lever, A. B. P.; Hicks, R. G., Verdazyl radicals as redox-active, non-innocent, ligands: Contrasting electronic structures as a function of electron-poor and electron-rich ruthenium bis(β -diketonate) co-ligands. *Chem. Commun.* **2010**, *46*, 773-775.
66. Fatila, E. M.; Clerac, R.; Rouziers, M.; Soldatov, D. V.; Jennings, M.; Preuss, K. E., Ferromagnetic superexchange in a 1D- La-III-radical -coordination polymer. *Chem. Commun.* **2013**, *49*, 6271-6273.
67. Hearn, N. G. R.; Clerac, R.; Jennings, M.; Preuss, K. E., Manipulating the crystal packing of pyDTDA radical ligand coordination complexes with Mn(II) and Ni(II). *Dalton Trans.* **2009**, 3193-3203.
68. Fatila, E. M.; Clerac, R.; Jennings, M.; Preuss, K. E., McConnell I, Mechanism promotes ferromagnetic interactions between π -stacked Ni(II)-thiazyl complexes. *Chem. Commun.* **2013**, *49*, 9431-9433.
69. Wu, J.; MacDonald, D. J.; Clerac, R.; Jeon, I.-R.; Jennings, M.; Lough, A. J.; Britten, J.; Robertson, C.; Dube, P. A.; Preuss, K. E., Metal complexes of bridging neutral radical ligands: PymDTDA and pymDSDA. *Inorg. Chem.* **2012**, *51*, 3827-3839.
70. Hearn, N. G. R.; Fatila, E. M.; Clerac, R.; Jennings, M.; Preuss, K. E., Ni(II) and hs-Fe(II) complexes of a paramagnetic thiazyl ligand, and decomposition products of the iron complex, including an Fe(III) tetramer. *Inorg. Chem.* **2008**, *47*, 10330-10341.
71. Preuss, K. E., Metal-radical coordination complexes of thiazyl and selenazyl ligands. *Coord. Chem. Rev.* **2015**, *289-290*, 49-61.
72. Barclay, T. M.; Cordes, A. W.; Haddon, R. C.; Itkis, M. E.; Oakley, R. T.; Reed, R. W.; Zhang, H., Preparation and characterization of a neutral π -radical molecular conductor. *J. Am. Chem. Soc.* **1999**, *121*, 969-976.
73. Perlepe, P.; Oyarzabal, I.; Pedersen, K. S.; Negrier, P.; Mondieig, D.; Rouzières, M.; Hillard, E. A.; Wilhelm, F.; Rogalev, A.; Suturina, E. A.; Mathonière, C.; Clérac, R., Cr(pyrazine)₂(OSO₂CH₃)₂: a two-dimensional coordination polymer with an antiferromagnetic ground state. *Polyhedron* **2018**, *153*, 248.

74. Bryan, C. D.; Cordes, A. W.; Fleming, R. M.; George, N. A.; Glarum, S. H.; Haddon, R. C.; Oakley, R. T.; Palstra, T. T. M.; Perel, A. S.; Schneemeyer, L. F.; Waszczak, J. V., Conducting charge-transfer salts based on neutral π -radicals. *Nat.* **1993**, *365*, XI-823.
75. Bryan, C. D.; Cordes, A. W.; Haddon, R. C.; Palstra, T. T. M.; Perel, A. S.; Schneemeyer, L. F.; Waszczak, J. V.; Hicks, R. G.; Kennepohl, D. K.; MacKinnon, C. D.; Oakley, R. T.; Scott, S. R., Molecular conductors from neutral-radical charge-transfer salts: Preparation and characterization of an i doped hexagonal phase of 1, 2, 3, 5-dithiadiazolyl ([HCN₂S₂]). *J. Am. Chem. Soc.* **1994**, *116*, 1205-1210.
76. Pedersen, K. S.; Perlepe, P.; Aubrey, M. L.; Woodruff, D. N.; Reyes-Lillo, S. E.; Reinholdt, A.; Voigt, L.; Li, Z.; Borup, K.; Rouzières, M.; Samohvalov, D.; Wilhelm, F.; Rogalev, A.; Neaton, J. B.; Long, J. R.; Clérac, R., Formation of the layered conductive magnet CrCl₂(pyrazine)₂ through redox-active coordination chemistry. *Nat. Chem.* **2018**, *10*, 1056.
77. Hearn, N. G. R.; Preuss, K. E.; Richardson, J. F.; Bin-Salamon, S., Design and synthesis of a 4-(2'-pyridyl)-1,2,3,5-dithiadiazolyl cobalt complex. *J. Am. Chem. Soc.* **2004**, *126*, 9942-9943.
78. Hearn, N. G. R.; Hesp, K. D.; Jennings, M.; Korcok, J. L.; Preuss, K. E.; Smithson, C. S., Monodentate N-coordination of a 1,2,3,5-dithiadiazolyl to Mn(II), Co(II) and Ni(II): A new coordination mode. *Polyhedron* **2007**, *26*, 2047-2053.
79. Jennings, M.; Preuss, K. E.; Wu, J., Synthesis and magnetic properties of a 4-(2'-pyrimidyl)-1,2,3,5-dithiadiazolyl dimanganese complex. *Chem. Commun.* **2006**, 341-343.
80. Britten, J.; Hearn, N. G. R.; Preuss, K. E.; Richardson, J. F.; Bin-Salamon, S., Mn(II) and Cu(II) complexes of a dithiadiazolyl radical ligand: Monomer/dimer equilibria in solution. *Inorg. Chem.* **2007**, *46*, 3934-3945.
81. Gatteschi, D.; Sessoli, R.; Villain, J., Molecular nanomagnets. *Oxford University Press* 2007; Vol. 9780198567530, p 1-408.
82. Jennings, M.; Preuss, K. E.; Wu, J., Synthesis and magnetic properties of a 4-(2'-pyrimidyl)-1,2,3,5-dithiadiazolyl dimanganese complex. *Chem. Commun.* **2006**, 341.
83. Fatila, E. M.; Rouzières, M.; Jennings, M. C.; Lough, A. J.; Clerac, R.; Preuss, K. E., Fine-Tuning the single-molecule magnet properties of a [Dy(III)-radical]₂ pair. *J. Am. Chem. Soc.* **2013**, *135*, 9596-9599.
84. Fatila, E. M.; Clérac, R.; Rouzières, M.; Soldatov, D. V.; Jennings, M.; Preuss, K. E., High-spin ribbons and antiferromagnetic ordering of a Mn II-biradical-MnII complex. *J. Am. Chem. Soc.* **2013**, *135*, 13298-13301.
85. Fatila, E. M.; Goodreid, J.; Clerac, R.; Jennings, M.; Assoud, J.; Preuss, K. E., High-spin supramolecular pair of Mn(II)/thiazyl radical complexes. *Chem. Commun.* **2010**, *46*, 6569-6571.

86. Preuss, K. E., Metal complexes of thiazyl radicals. *Dalton Trans.* **2007**, 2357-2369.
87. Markovskii, L.; Kornuta, P.; Kachkovskaya, L., 1,2,4,6-thiatriazinyls - A new class of nitrogen- and sulfur-containing free radicals. *Sulphur Lett* **1983**, *1*, 143.
88. Boere, R. T.; Cordes, A. W.; Hayes, P. J.; Oakley, R. T.; Reed, R. W.; Pennington, W. T., Redox chemistry of 1,2,4,6-thiatriazinyls - preparation and crystal-structures of "3,5-diphenyl-1,2,4,6-thiatriazinium hexafluorophosphate, $\text{Ph}_2\text{C}_2\text{N}_3\text{S}^+ \text{PF}_6^-$, and 3,5-diphenyl-4-hydro-1,2,4,6-thiatriazine, $\text{Ph}_2\text{C}_2\text{N}_3\text{SH}$. *Inorg. Chem.* **1986**, *25*, 2445-2450.
89. Chen, S. J.; Mews, R.; Behrens, U.; Fischer, E.; Pauer, F.; Sheldrick, G. M.; Stalke, D.; Stohrer, W. D., Chlorthiatriazine. *Chem. Ber.* **1993**, *126*, 2601-2607.
90. Cordes, A. W.; Hayes, P. J.; Josephy, P. D.; Koenig, H.; Oakley, R. T.; Pennington, W. T., Preparation and molecular structure of 1-chloro-3,5-diphenyl-1,2,4,6-thiatriazine; reduction of $\text{Ph}_2\text{C}_2\text{N}_3\text{SCI}$ and the E.S.R. spectrum of the $\text{Ph}_2\text{C}_2\text{N}_3\text{S}$ ·radical. *J. Chem. Soc., Chem. Commun.* **1984**, 1021-1022.
91. Hayes, P. J.; Oakley, R. T.; Cordes, A. W.; Pennington, W. T., Preparation and dimerization of 1,2,4,6-thiatriazinyl radicals - crystal and molecular-structure of bis(3,5-diphenyl-1,2,4,6-thiatriazine). *J. Am. Chem. Soc.* **1985**, *107*, 1346-1351.
92. Ramakrishna, T. V. V.; Elias, A. J.; Vij, A., Dealkylation reactions of trialkylamines with 1,3,5-trichloro-1,2,4,6-cyclothiatriazine: A novel route to regiospecific dialkylamino substitution on cyclocarbathiazines. *Inorg. Chem.* **1999**, *38*, 3022-3026.
93. Cordes, A. W.; Bryan, C. D.; Davis, W. M.; de Laat, R. H.; Glarum, S. H.; Goddard, J. D.; Haddon, R. C.; Hicks, R. G.; Kennepohl, D. K., Prototypal 1,2,3,5-dithia- and -diselenadiazolyl [HCN_2E_2].bul. (E = sulfur, selenium): Molecular and electronic structures of the radicals and their dimers, by theory and experiment. *J. Am. Chem. Soc.* **1993**, *115*, 7232-7239.
94. Oakley, R. T.; Reed, R. W.; Cordes, A. W.; Craig, S. L.; Graham, J. B., 1,2,4,6-selenatriazinyl radicals and dimers - preparation and structural characterization of 1-chloro-3,5-diphenyl-1,2,4,6-selenatriazine ($\text{Ph}_2\text{C}_2\text{N}_3\text{SeCl}$) and bis(3,5-diphenyl-1,2,4,6-selenatriazine) ($(\text{Ph}_2\text{C}_2\text{N}_3\text{Se})_2$). *J. Am. Chem. Soc.* **1987**, *109*, 7745-7749.
95. Boere, R. T.; Oakley, R. T.; Reed, R. W.; Westwood, N. P. C., Ultraviolet photoelectron and ESR studies of 1,2,4,6-thiatriazinyl and 1,2,3,5-dithiadiazolyl radicals. *J. Am. Chem. Soc.* **1989**, *111*, 1180-1185.
96. Ang, C. Y.; Boeré, R. T.; Goh, L. Y.; Koh, L. L.; Kuan, S. L.; Tan, G. K.; Yu, X., η^1 and η^2 complexes of λ^3 -1,2,4,6-thiatriazinyls with $\text{CpCr}(\text{CO})_x$. *Chem. Commun.* **2006**, 4735-4737.
97. Boere, R. T.; Roemmele, T. L.; Yu, X., Unsymmetrical 1 λ^3 -1,2,4,6-thiatriazinyls with aryl and trifluoromethyl substituents: synthesis, crystal structures, EPR spectroscopy, and voltammetry. *Inorg. Chem.* **2011**, *50*, 5123-5136.

98. Harriman, K. L. M.; Leitch, A. A.; Stoian, S. A.; Habib, F.; Kneebone, J. L.; Gorelsky, S. I.; Korobkov, I.; Desgreniers, S.; Neidig, M. L.; Hill, S.; Murugesu, M.; Brusso, J. L., Ambivalent binding between a radical-based pincer ligand and iron. *Dalton Trans.* **2015**, *44*, 10516-10523.
99. Sullivan, D. J.; Clerac, R.; Jennings, M.; Lough, A. J.; Preuss, K. E., Trinuclear Mn(II) complex with paramagnetic bridging 1,2,3-dithiazolyl ligands. *Chem. Commun.* **2012**, *48*, 10963-10965.
100. Cordes, A. W.; Hayes, P. J.; Josephy, P. D.; Koenig, H.; Oakley, R. T.; Pennington, W. T., Preparation and molecular-structure of 1-chloro-3,5-diphenyl-1,2,4,6-thiatiazine - reduction of Ph₂C₂N₃SCl and the electron-spin-resonance spectrum of the Ph₂C₂N₃S radical. *J. Chem. Soc., Chem. Commun.* **1984**, 1021-1022.
101. Rawson, J. M.; McManus, G. D., Benzo-fused dithiazolyl radicals: from chemical curiosities to materials chemistry. *Coord. Chem. Rev.* **1999**, *189*, 135-168.
102. Banister, A. J.; Hansford, M. I.; Hauptman, Z. V.; Wait, S. T.; Clegg, W., Direct insertion of a nitrogen atom into the S-S bond of a 1,2,3,5-dithiadiazole ring in a direct-current nitrogen glow-discharge, and X-ray crystal-structure of 4-methyl-1,2,3,5-dithiadiazole. *Dalton Trans.* **1989**, 1705-1713.
103. Banister, A. J.; Gorrell, I. B.; Clegg, W.; Jørgensen, K. A., Preparation, crystal structure and extended-Hückel molecular-orbital study of the free-radical complex [Ni₂(Cp)₂(PhCN₂S₂)]. *Dalton Trans.* **1991**, 1105-1109.
104. Banister, A. J.; Gorrell, I. B.; Howard, J. A. K.; Lawrence, S. E.; Lehman, C. W.; May, I.; Rawson, J. M.; Tanner, B. K.; Gregory, C. I.; Blake, A. J.; Fricker, S. P., Synthesis and characterisation of three Group 10 metal dithiadiazolyl complexes. *Dalton Trans.* **1997**, 377-384.
105. Banister, A. J.; Howard, J. A. K.; May, I.; Rawson, J. M., Preparation and characterisation of a dithiadiazolyline complex: X-ray crystal structure of [Pd₂{μ-SNC(Ph)N(H)S-S,S'}(dppe)₂][BF₄]₂·3CDCl₃. *Chem. Commun.* **1997**, 1763-1764.
106. Wong, W. K.; Sun, C.; Wong, W. Y.; Kwong, D. W. J.; Wong, W. T., Synthesis and chemistry of dithiadiazole free radicals 4-(4'-C₅H₄N)CN₂S₂ and 4-(3'-C₅H₄N)CN₂S₂; X-ray crystal structures of [Pd₃{μ-SNC(Ar')NS-S,S'}₂(PPh₃)₄] (Ar' = 4'-C₅H₄N, 4'-C₅H₄NBET₃ and 3'-C₅H₄NBET₃). *Eur. J. Inorg. Chem.* **2000**, 1045-1054.
107. Lau, H. F.; Ng, V. W. L.; Koh, L. L.; Tan, G. K.; Goh, L. Y.; Roemmele, T. L.; Seagrave, S. D.; Boere, R. T., Cyclopentadienylchromium complexes of 1,2,3,5-dithiadiazolyls: η² π complexes of cyclic sulfur-nitrogen compounds. *Angew. Chem., Int. Ed.* **2006**, *45*, 4498-4501.
108. Harriman, K. L. M.; Kühne, I. A.; Leitch, A. A.; Korobkov, I.; Clérac, R.; Murugesu, M.; Brusso, J. L., Halide influence on molecular and supramolecular arrangements of iron

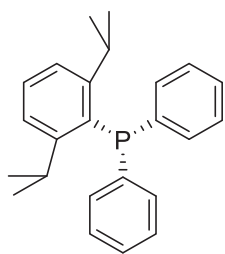
- complexes with a 3,5-bis(2-pyridyl)-1,2,4,6-thiatriazine ligand. *Inorg. Chem.* **2016**, *55*, 5375-5383.
109. Scheuermann, S.; Kretz, T.; Vitze, H.; Bats, J. W.; Bolte, M.; Lerner, H.-W.; Wagner, M., Redox-active p-quinone-based bis(pyrazol-1-yl)methane ligands: Synthesis and coordination behaviour. *Chem. - Eur. J.* **2008**, *14*, 2590-2601.
 110. Tejel, C.; del Rio, M. P.; Asensio, L.; van den Bruele, F. J.; Ciriano, M. A.; Spithas, N. T. i.; Hettterscheid, D. G. H.; de Bruin, B., Cooperative double deprotonation of bis(2-picolyl)amine leading to unexpected bimetallic mixed valence (M-1, M-1) rhodium and iridium complexes. *Inorg. Chem.* **2011**, *50*, 7524-7534.
 111. Weisser, F.; Huebner, R.; Schweinfurth, D.; Sarkar, B., Energy-level tailoring in a series of redox-rich quinonoid-bridged diruthenium complexes containing tris(2-pyridylmethyl)amine as a Co-ligand. *Chem. - Eur. J.* **2011**, *17*, 5727-5736.
 112. Tejel, C.; Ciriano, M. A.; Del Rio, M. P.; Van den Bruele, F. J.; Hettterscheid, D. G. H.; Spithas, N. T. I.; De Bruin, B., Deprotonation induced ligand-to-metal electron transfer: Synthesis of a mixed-valence Rh(-I,I) dinuclear compound and its reaction with dioxygen. *J. Am. Chem. Soc.* **2008**, *130*, 5844-+.
 113. Schweinfurth, D.; Rechkemmer, Y.; Hohloch, S.; Deibel, N.; Peremykin, I.; Fiedler, J.; Marx, R.; Neugebauer, P.; van Slageren, J.; Sarkar, B., Redox-induced spin-state switching and mixed valency in quinonoid-bridged dicobalt complexes. *Chem. - Eur. J.* **2014**, *20*, 3475-3486.
 114. Ringenberg, M. R.; Kokatam, S. L.; Heiden, Z. M.; Rauchfuss, T. B., Redox-switched oxidation of dihydrogen using a non-innocent ligand. *J. Am. Chem. Soc.* **2008**, *130*, 788-789.
 115. Peters, J. C.; Harkins, S. B.; Brown, S. D.; Day, M. W., Pincer-like amido complexes of platinum, palladium, and nickel. *Inorg. Chem.* **2001**, *40*, 5083-5091.
 116. Nguyen, A. I.; Blackmore, K. J.; Carter, S. M.; Zarkesh, R. A.; Heyduk, A. F., One- and two-electron reactivity of a tantalum(V) complex with a redox-active tris(amido) ligand. *J. Am. Chem. Soc.* **2009**, *131*, 3307-3316.
 117. Miller, J. S.; Min, K. S., Oxidation leading to reduction: redox-induced electron transfer (RIET). *Angew. Chem., Int. Ed.* **2009**, *48*, 262-272.
 118. Lyaskovskyy, V.; de Bruin, B., Redox non-innocent ligands: Versatile new tools to control catalytic reactions. *ACS Catal.* **2012**, *2*, 270-279.
 119. Luca, O. R.; Crabtree, R. H., Redox-active ligands in catalysis. *Chem. Soc. Rev.* **2013**, *42*, 1440-1459.
 120. Leschke, M.; Melter, M.; Lang, H., Mono- and bimetallic silver(I) complexes with bridging and terminal-bound organic chelating ligands. *Inorg. Chim. Acta* **2003**, *350*, 114-120.

121. Kar, S.; Sarkar, B.; Ghumaan, S.; Janardanan, D.; van Slageren, J.; Fiedler, J.; Puranik, V. G.; Sunoj, R. B.; Kaim, W.; Lahiri, G. K., 2,5-dioxido-1,4-benzoquinonediimine (H_2L^{2-}), a hydrogen-bonding noninnocent bridging ligand related to aminated topaquinone: Different oxidation state distributions in complexes $[\{(bpy)_2Ru\}_2(\mu-H_2L)^n]$ ($n=0,+2+,3+,4+$) and $[\{(acac)_2Ru\}_2(\mu-H_2L)^m]$ ($m=2-,-,0,+,2+$). *Chem. - Eur. J.* **2005**, *11*, 4901-4911.
122. Deibel, N.; Schweinfurth, D.; Hohloch, S.; Delor, M.; Sazanovich, I. V.; Towrie, M.; Weinstein, J. A.; Sarkar, B., Electrochemistry, chemical reactivity, and time-resolved infrared spectroscopy of donor-acceptor systems $[Q_xPt(pap)_y]$ (Q = substituted o-quinone or o-Iminoquinone; pap = phenylazopyridine). *Inorg. Chem.* **2014**, *53*, 1021-1031.
123. Chirik, P. J.; Wieghardt, K., Radical ligands confer nobility on base-metal catalysts. *Sci.* **2010**, *327*, 794-795.
124. Chaudhuri, P.; Verani, C. N.; Bill, E.; Bothe, E.; Weyhermuller, T.; Wieghardt, K., Electronic structure of bis(o-iminobenzosemiquinonato)metal complexes (Cu, Ni, Pd). The art of establishing physical oxidation states in transition-metal complexes containing radical ligands. *J. Am. Chem. Soc.* **2001**, *123*, 2213-2223.
125. Boyer, J. L.; Cundari, T. R.; DeYonker, N. J.; Rauchfuss, T. B.; Wilson, S. R., Redox activation of alkene ligands in platinum complexes with non-innocent ligands. *Inorg. Chem.* **2009**, *48*, 638-645.
126. Jørgensen, C. K., Recent progress in ligand field theory. In *Structure and bonding*, Springer: 1966; pp 3-31.
127. Vlcek, A., Dithiolenes and non-innocent redox-active ligands. *Coord. Chem. Rev.* **2010**, *254*, 1357.
128. Blanchard, S.; Derat, E.; Desage-El Murr, M.; Fensterbank, L.; Malacria, M.; Mouries-Mansuy, V., Non-innocent ligands: New opportunities in iron catalysis. *Eur. J. Inorg. Chem.* **2012**, 376-389.
129. Chen, Y.; Ruppel, J. V.; Zhang, X. P., Cobalt-catalyzed asymmetric cyclopropanation of electron-deficient olefins. *J. Am. Chem. Soc.* **2007**, *129*, 12074-+.
130. Dzik, W. I.; Calvo, S. E.; Reek, J. N. H.; Lutz, M.; Ciriano, M. A.; Tejel, C.; Hettler, D. G. H.; de Bruin, B., Binuclear $[(cod)(Cl)Ir(bpi)Ir(cod)]^+$ for catalytic water oxidation. *Organometallics* **2011**, *30*, 372-374.
131. Griitzmacher, H., Cooperating ligands in catalysis. *Angew. Chem., Int. Ed.* **2008**, *47*, 1814-1818.
132. Heyduk, A. F.; Zarkesh, R. A.; Nguyen, A. I., Designing catalysts for nitrene transfer using early transition metals and redox-active ligands. *Inorg. Chem.* **2011**, *50*, 9849-9863.
133. Lu, F.; Zarkesh, R. A.; Heyduk, A. F., A Redox-active ligand as a reservoir for protons and electrons: O_2 reduction at zirconium(IV). *Eur. J. Inorg. Chem.* **2012**, 467-470.

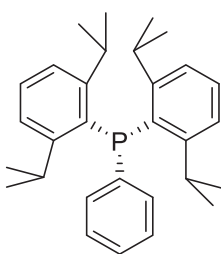
134. Kaim, W.; Schwederski, B., Non-innocent ligands in bioinorganic chemistry-An overview. *Coord. Chem. Rev.* **2010**, *254*, 1580-1588.
135. Otten, E.; Meetsma, A.; Hessen, B., Structure and reactivity of the β -agostic [ansa-Cp-arene] Ta(ⁿPr) cation: Ambivalent behavior induced by intramolecular arene coordination. *J. Am. Chem. Soc.* **2007**, *129*, 10100-10101.
136. Smith, A. L.; Clapp, L. A.; Hardcastle, K. I.; Soper, J. D., Redox-active ligand-mediated Co-Cl bond-forming reactions at reducing square planar cobalt(III) centers. *Polyhedron* **2010**, *29*, 164-169.
137. Yamaguchi, K.; Tsunekawa, T.; Toyoda, Y.; Fueno, T., Ab initio molecular orbital calculations of effective exchange integrals between transition metal ions. *Chem. Phys. Lett.* **1988**, *143*, 371-376.
138. Zhu, D.; Thapa, I.; Korobkov, I.; Gambarotta, S.; Budzelaar, P. H. M., Redox-active ligands and organic radical chemistry. *Inorg. Chem.* **2011**, *50*, 9879-9887.
139. van der Vlugt, J. I.; Reek, J. N. H., Neutral tridentate PNP ligands and their hybrid analogues: versatile non-innocent scaffolds for homogeneous catalysis. *Angew. Chem., Int. Ed.* **2009**, *48*, 8832-8846.
140. Chirik, P. J., Preface: Forum on redox-active ligands. *Inorg. Chem.* **2011**, *50*, 9737-9740.
141. Green, M. L. H., A new approach to the formal classification of covalent compounds of the elements. *J. Organomet. Chem.* **1995**, *500*, 127-148.

Chapter 2 Copper (I) halide-phosphine complexes of highly sterically demanding phosphines bearing 2,6-diisopropylphenyl groups

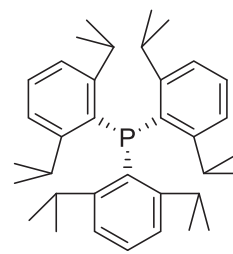
This chapter presents about half of the total work in this thesis. The topic is the synthesis, structure and understanding of copper(I) halo complexes with two bulky triaryl phosphines, 2,6-diisopropylphenyl(diphenylphosphine), **IV**, and bis(2,6-diisopropylphenyl)(phenyl)phosphine, **V**. The relationship of these phosphines to tris(2,6-diisopropylphenyl)phosphine, **VI**, will be considered.



IV



V



VI

2.1 Introduction

A large number of air-stable coinage metal complexes of triphenylphosphine and its derivatives have been synthesized and isolated, ranging from copper(I) halides (CuX) to other silver and gold halides and their chemistry has been widely studied.¹⁻¹⁴ Many CuX (X = Cl, Br, or I) complexes have been prepared and their crystal structures reported for less and more sterically hindered triaryl phosphines in the literature.¹⁵⁻¹⁸ The bulkiness of the R group usually influences the basicity and the donating strength of these Lewis bases.^{6, 9, 19-20} For instance, trimesitylphosphine (Mes₃P, $\Sigma \angle CPC = 318^\circ$)²¹ was able to form a linear complex with CuBr despite its bulkiness.²² However, the even larger tris(2,6-diisopropylphenyl)phosphine (Dipp₃P,

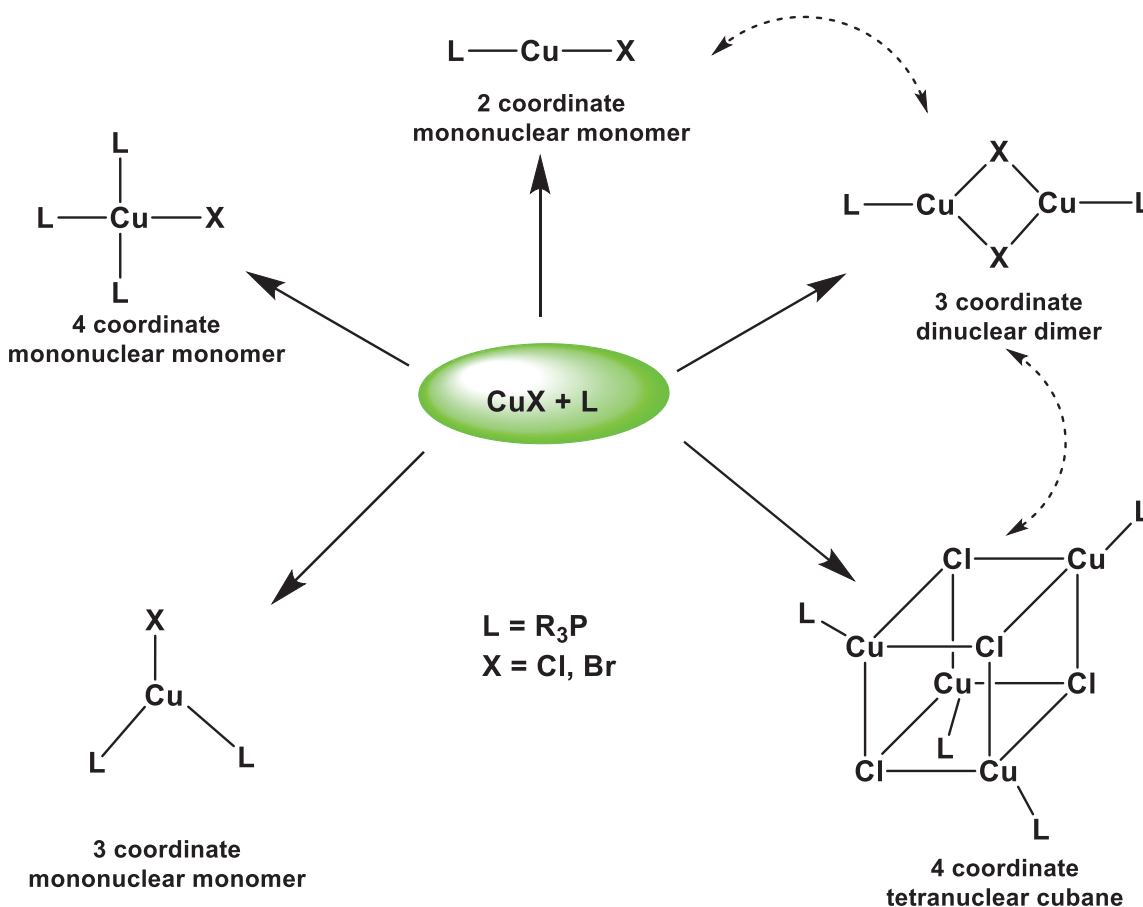
VI, $\Sigma <CPC = 335.6^\circ$)²³ and tris(2,4,6-triisopropylphenyl)phosphine (Tripp₃P, $\Sigma <CPC = 334.4^\circ$)²⁴⁻²⁵ completely prevent metal coordination.

The route to the synthesis of bulky 2,6-diisopropylphenyl(diphenylphosphine) (**IV**) ($\Sigma <CPC = 314.7^\circ$), bis(2,6-diisopropylphenyl)(phenyl)phosphine (**V**) ($\Sigma <CPC = 324.6^\circ$), and tris(2,6-diisopropylphenyl)phosphine (**VI**) has been developed by the Boéré group and their chemical and electrochemical characteristics have been published.²⁶ They discovered that the overall steric congestion of **V** around the P atom appears to be similar to that of Mes₃P. The synthetic route for the preparation of Dipp₃P necessitated the use of organocopper reagents, specifically [DippCu]₄.²³ This reagent was also found essential for the synthesis of **V** and was also tried but found detrimental to the preparation of **IV**, which is better prepared via traditional organolithium chemistry. In the course of working out the synthetic method, several copper(I) chloro complexes of these phosphines were isolated, including one that was crystallographically characterized as a tricoordinate dimer [CuCl(**IV**)]₂.

IV and **V** are amongst the most sterically demanding triarylphosphines (Ar₃P) known. Complexes of these two ligands have not been thoroughly investigated, but it has been established that Dipp₃P is too bulky to coordinate to any metal.²³ Factors such as reaction solvent, type of the halide counter ion, procedure of synthesis and the crystallization technique significantly determines the physical and chemical behaviour of the phosphine complexes generated, including the coordination mode at copper.¹⁹

The categories of the geometries that have been published include the mononuclear systems of coordination numbers 2-, 3- or 4- at the Cu center i.e. [(R₃P)CuX], [(R₃P)₂CuX] and [(R₃P)₃CuX];⁶ the halide-bridged dimers with 3- [(R₃P)CuX₂Cu(PR₃)] or 4- [(R₃P)₂CuX₂Cu(PR₃)₂] coordinate metal centers, mixed dimers like [(R₃P)₂CuX₂Cu(PR₃)]^{17, 20, 27}

and the tetranuclear cubanes $[(R_3P)CuX]_4$ (Scheme 2.1).^{2, 12, 28-29} Dimeric $[R_3PCuX]_2$ and tetrameric $[R_3PCuX]_4$ are related because they both have monomer, $[R_3PCuX]$ in common. The focus of my work is to examine which structure class or classes are feasible in the CuX coordination chemistry of **IV** and **V**. Chloride and bromide complexes are considered for comparison because they are the most reported. The influences of different non-aqueous solvents and variable CuX/phosphine stoichiometric ratios have been investigated.

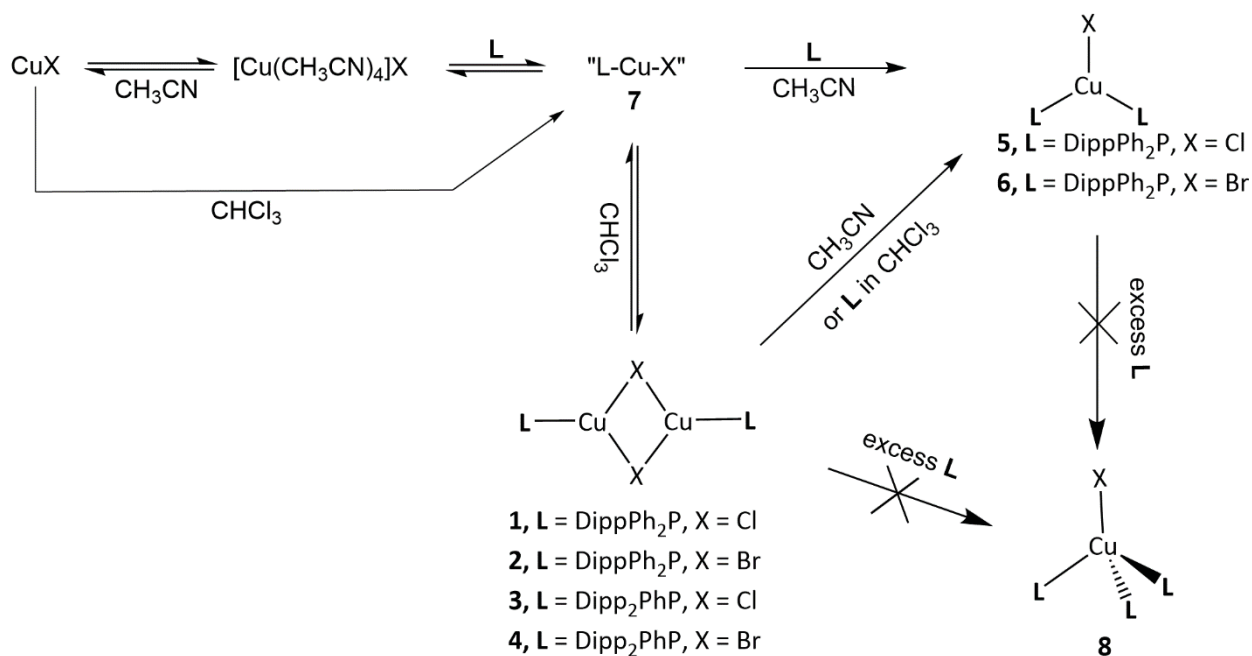


Scheme 2.1. The observed types of structures known for R_3P-CuX complexes.

2.2 Synthesis and Characterization of $[CuXDipp_{(n-1)}Ph_nP]$ Complexes

As presented in Scheme 2.2, tricoordinate L_2CuX (**5** and **6**) complexes were formed by precipitating out of solution when 1 or 2 equivalents of **IV** were reacted with CuX in acetonitrile

(CH₃CN). However, in chloroform (CHCl₃), the reaction of CuX with 1 equivalent of **IV** gave the dinuclear dimers (**1** and **2**), while the tricoordinate L₂CuX (**5** and **6**) were also formed with 2 equivalents of **IV**. Moreover, **1** and **2** were converted into **5** and **6**, respectively, simply by attempting to dissolve them in CH₃CN. Phosphine **V** led to the formation of only the dinuclear dimers (**3** and **4**) in both CH₃CN and CHCl₃ irrespective of the equivalents of the ligand reacted per CuX. An attempt to form **8** with either ligand was not successful. Single crystals of all compounds suitable for X-ray crystallography were grown by two general methods: layering heptane on, or slow evaporation, of the CHCl₃ solutions of the complexes.



Scheme 2.2. Reaction of **IV** and **V** with CuX in CH₃CN and CHCl₃.

The ¹H, ¹³C and ³¹P NMR spectra were obtained for all the materials in CDCl₃. 2D NMR (Figures A. 7 – 21, Appendix) experiments were also carried out on all the samples on a Bruker 700 MHz NMR instrument to further interpret the ¹³C spectra. Line broadened ³¹P NMR peaks were observed for all the complexes compared to the ligand due to the quadrupolar relaxation

effect of copper (Table 2.1). Generally, all the complexes that have the same structural morphology have almost similar NMR spectra features except **1** where smaller J_{PH} is observed relative to **2**.

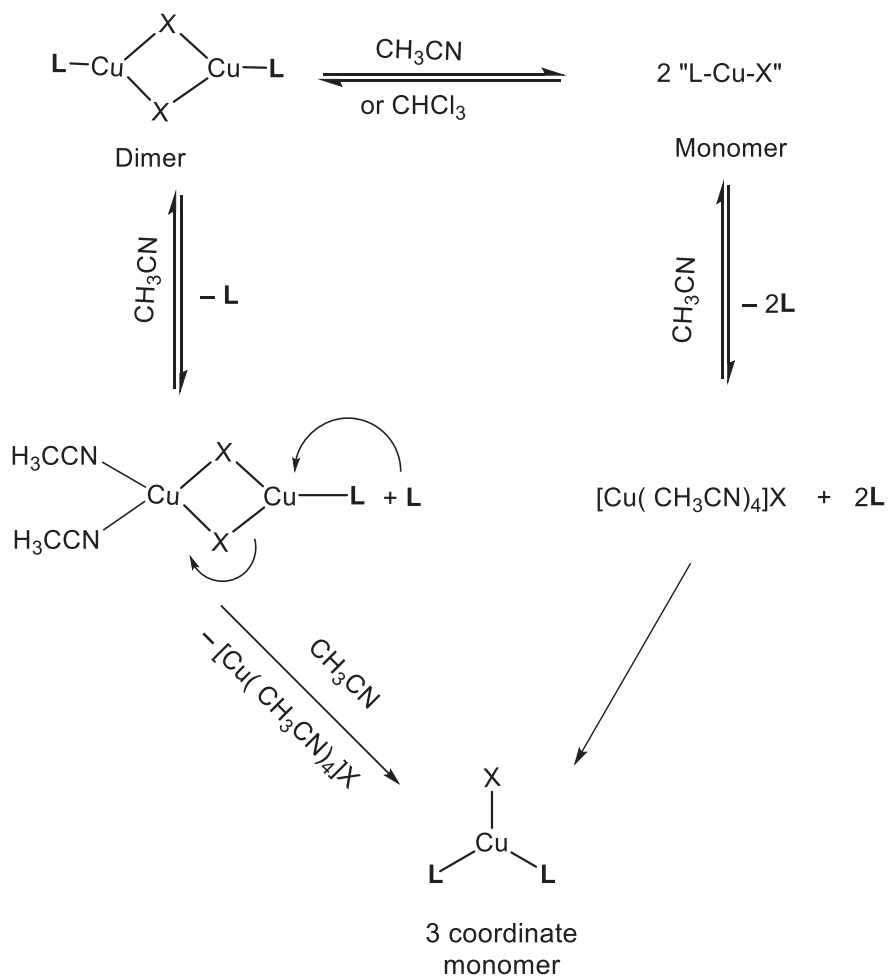
Table 2.1. ^{31}P NMR data for ligands and complexes.

Compound	^{31}P δ (ppm)	$\Delta\delta$ (ppm)	LWHH (Hz)	1H δ (ppm) ³	J_{PH} (Hz) ³
DippPh ₂ P, IV	-20.9	—	15.2	3.7	6.9
Dipp ₂ PhP, V	-28.4	—	17.1	3.6	6.7
[CuCl(IV) ₂], 1	-13.7	+7.2	106.7	3.7	< 1
[CuBr(IV) ₂], 2	-16.7	+4.2	96.0	3.7	4.2
[CuCl(V) ₂], 3	-17.3 ¹	+11.1	84.2	3.5	3.7
[CuBr(V) ₂], 4	-17.5 ²	+10.9	79.1	3.6	3.9
[CuCl(IV) ₂], 5	-17.9	+3.0	74.7	3.6	5.4
[CuBr(IV) ₂], 6	-18.7	+2.2	69.3	3.6	6.1

¹ An additional small signal with $\delta = 31.2$ ppm found for IV=O. ² $\delta = 34.8$ ppm for V=O. ³ Isopropyl methine proton NMR chemical shift and its proton – phosphorus coupling (J_{PH}); LWHH = line width at half height

Figures 2.1 to 2.4 show 1H NMR for complex **5**, **6**, **1** and **2**. Signal **a** is for the isopropyl methyl protons; signal **b** is for the isopropyl methine proton; and **c – g** are signals of the aromatic **Dipp** and phenyl ring protons. Both **5** and **6** 1H NMR spectra revealed coupling of the Dipp meta protons (Figures 2.1 and 2.2) through-bond, and the isopropyl methine protons through-space with J_{PH} of 5.4 Hz and 6.1 Hz respectively (Table 2.1) to phosphorus. Large through-space coupling of the isopropyl methine H atoms in **5** and **6** with the P atom in solution indicates close proximity in their structural conformation involving two phosphine ligands.³⁰ Their ^{31}P NMR spectra display a single broadened peak (Figure A.1 and A.2, appendix) with small positive coordination shifts of 3.0 ppm (**5**) and 2.2 ppm (**6**) (Table 2.1) from the free ligand (**IV**).

The ^1H NMR spectral features of **1** and **2** (Figures 2.3 and 2.4) are almost similar to those of **5** and **6**, but their chemical shifts move a bit to higher frequencies. Notwithstanding, the isopropyl methine proton through space coupling to P is less in **1** (< 1 Hz) than in **2** (4.2 Hz).



Scheme 2.3. Proposed exchange mechanism pathways of complexes in solution (CH₃CN or CHCl₃).

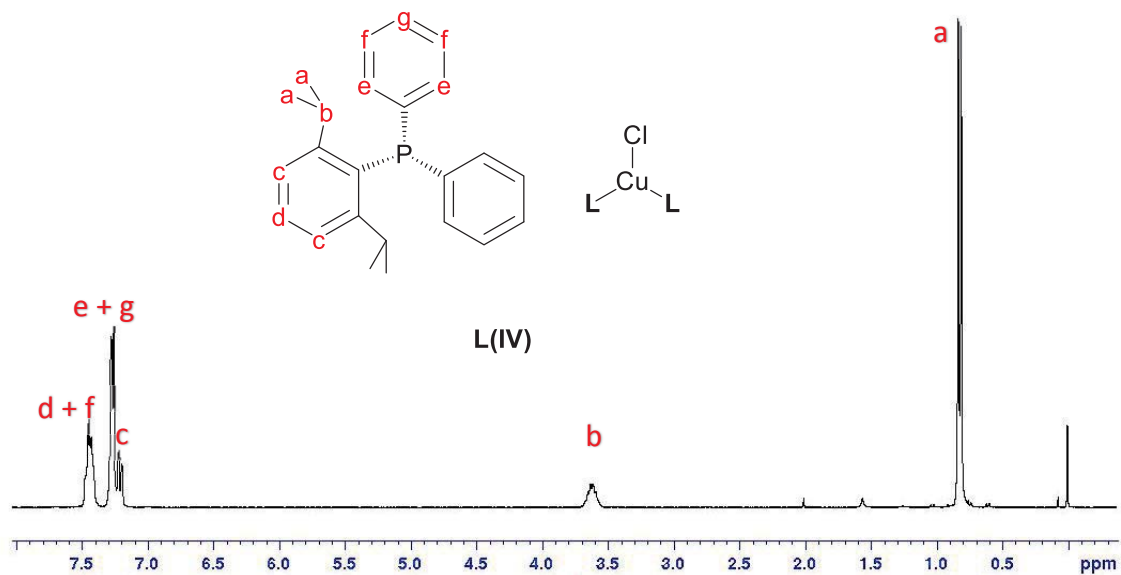


Figure 2.1. ^1H NMR spectrum of **5** in CDCl_3 (300 MHz) for the H nuclei attached to the labeled C atoms.

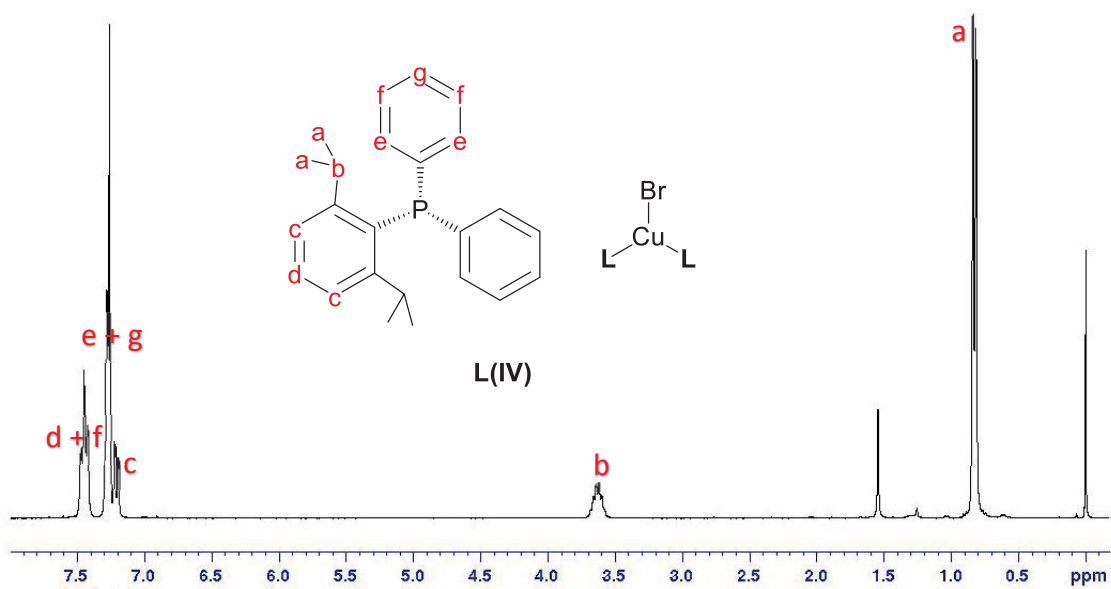


Figure 2.2. ^1H NMR spectrum of **6** in CDCl_3 (300 MHz) for the H nuclei attached to the labeled C atoms.

This suggests less dynamic effect of $[\text{CuBr(IV)}]_2$ (**2**) in solution which could also be ascribed to the isolation of its solvated crystals in spite of using different crystal growing

techniques (vide infra) compared to $[\text{CuCl}(\text{IV})]_2$ (**1**). Their ^{31}P chemical shifts are more positive than those of the mononuclear complexes (Table 2.1; Figures A.3 and A.4, appendix) with values of 7.2 ppm for **1** and 4.2 ppm for **2** deviations from that of **IV** (Table 2.1). The two possible exchange mechanism pathways of the dimer complexes in solvents (CH_3CN or CHCl_3) are depicted in Scheme 2.3. The conversion of the dimer $[\text{LCuX}]_2$ to the tricoordinate mononuclear $[\text{L}_2\text{CuX}]$ complex may either proceed via equilibrium between the dimer and the monomer or through equilibrium dissociation of one of the ligands (**L**). Both routes could possibly contribute to averaging proton NMR signals between the interconverting equilibrium species due to fast exchange. This, in addition to the copper quadrupolar relaxation may account for less isopropyl methine J_{PH} coupling recorded for complex **1**.

The complexes **3** and **4** possess almost identical NMR characteristics (Figures 2.5 and 2.6) with little variation. The ^1H spectra of **3** and **4** show coupling of the isopropyl methine protons to phosphorus with J_{PH} of 3.7 Hz and 3.9 Hz with chemical shift of 3.5 ppm and 3.6 ppm respectively (Table 2.1). They have analogous Dipp signals in similar locations in the aromatic region to the complexes of **IV**, but their Ph *para* and *ortho* proton peaks are slightly moved to higher frequency (7.18 ppm to 7.22 ppm) such that the *ortho* and the *meta* signals overlap, while the *para* protons show up at higher chemical shift of 8.4 ppm. The ^{31}P chemical shifts of **3** and **4** (Figures A.5 and A.6, appendix) are relatively the same with approximately 11.0 ppm positive coordination shifts from that of **V** (Table 2.1). This shows that **V** has identical coordination interaction with CuCl in **3** and CuBr in **4**. In addition, the isopropyl methyl group protons show two separate doublet signals similar to the free phosphine as reported by Bullock et al.²⁶ wherein those that are close to the aromatic ring shielding current of phenyl and Dipp rings on neighbouring groups cause shift to higher frequency whilst the two sets away from the ring surface are a bit shifted to lower frequency.

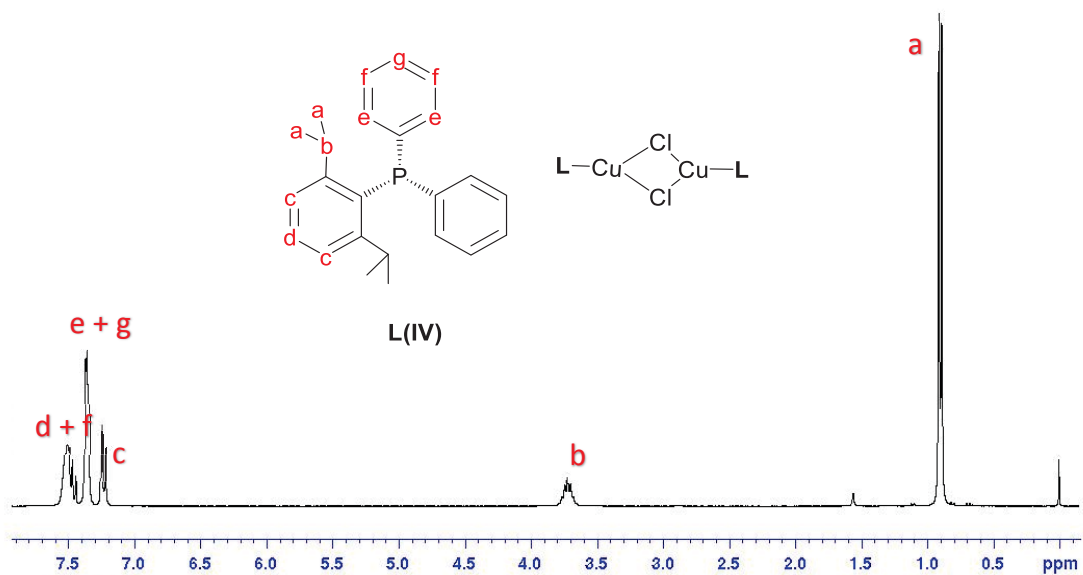


Figure 2.3. ^1H NMR spectrum of **1** in CDCl_3 (300 MHz) for the H nuclei attached to the labeled C atoms.

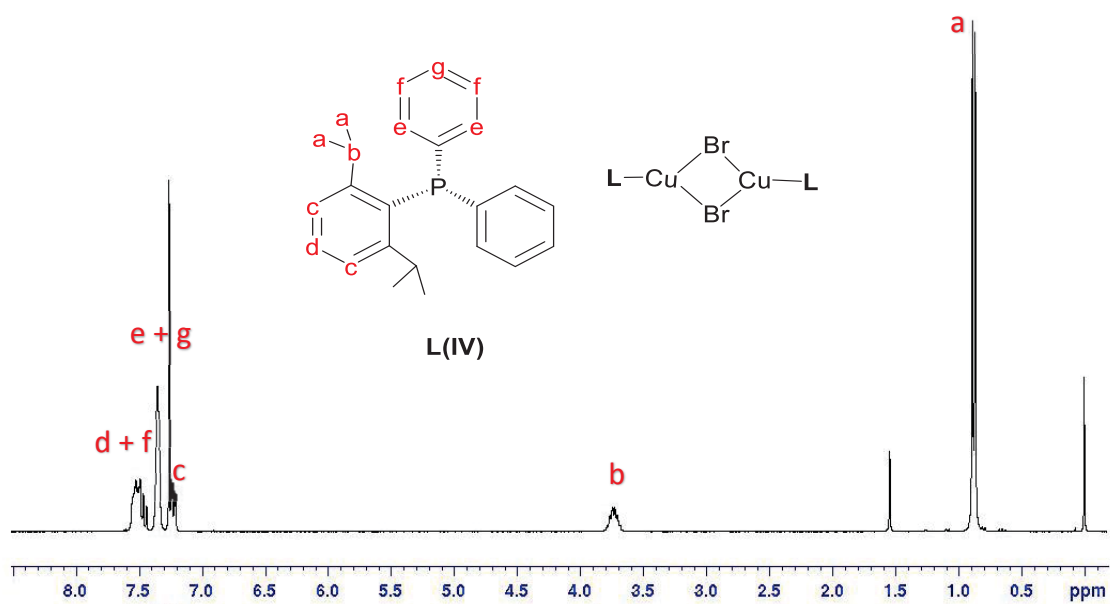


Figure 2.4. ^1H NMR spectrum of **2** in CDCl_3 (300 MHz) for the H nuclei attached to the labeled C atoms.

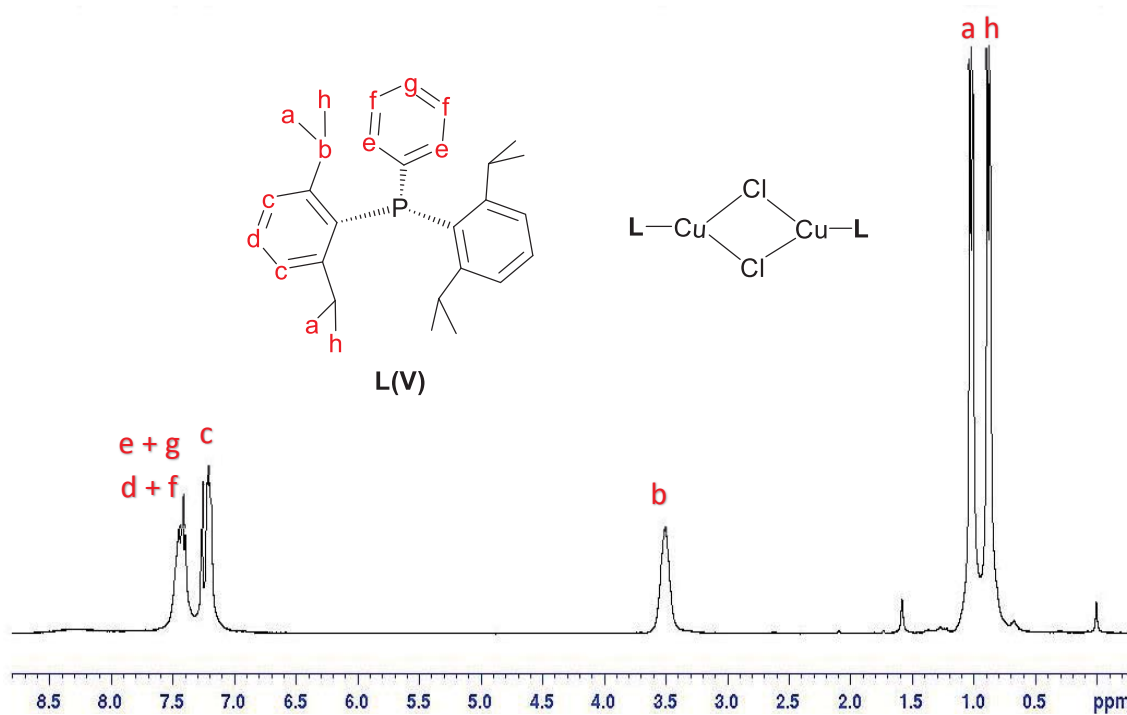


Figure 2.5. ^1H NMR spectrum of **3** in CDCl_3 (300 MHz) for the H nuclei attached to the labeled C atoms.

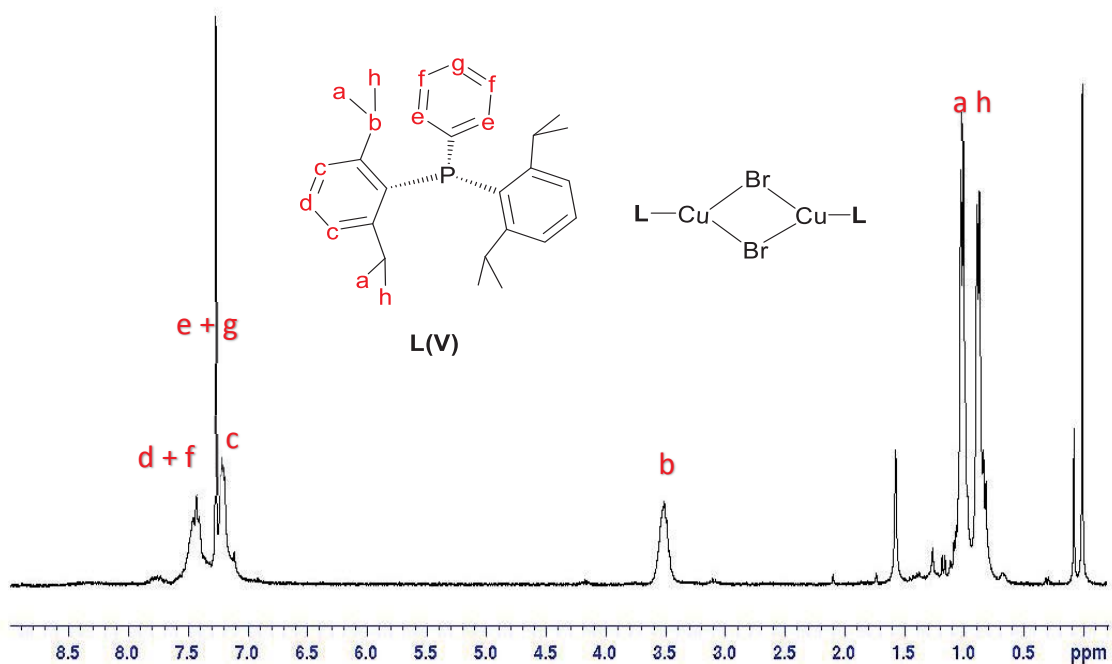
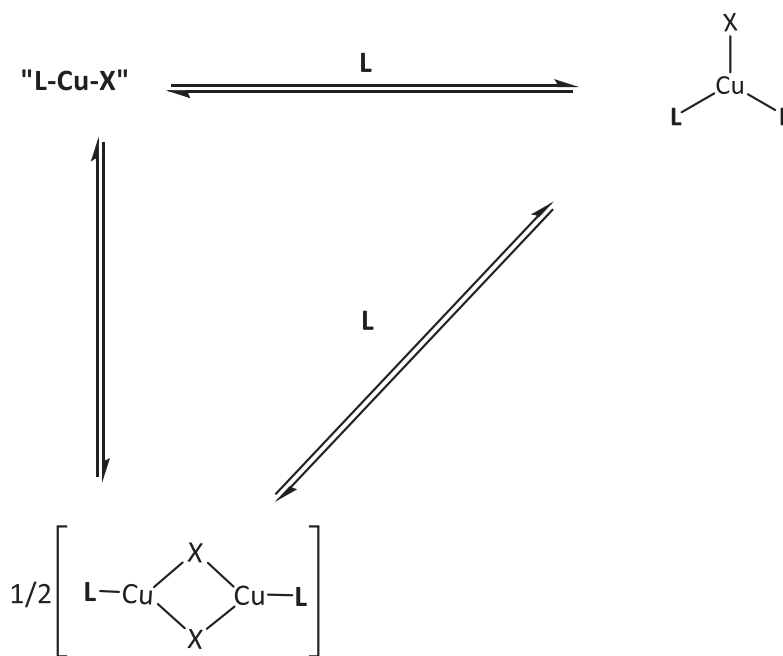


Figure 2.6. ^1H NMR spectrum of **4** in CDCl_3 (300 MHz) for the H nuclei attached to the labeled C atoms.

2.3 Computational studies

The electronic energy and frequency calculations of the complexes, their monomers, and the free phosphines were computed on gas phase models to obtain the change in free energies (ΔG) of the equilibrium species at 298.15 K and 1.0 atm. Their electronic energies EE and the zero-point corrected values EE^{ZPC} were also determined. The calculations were performed with density function theory (DFT) using Becke, 3-parameter, Lee–Yang–Parr with Pople-type Gaussian composite wavefunctions that are ‘double zeta’ as the basis set [B3LYP/6-31+G(d, p)] and the Cartesian coordinates obtained from the crystal structures as the inputs to full geometry optimizations.



Scheme 2.4. Change in free energies of gas phase model of complexes and their equilibria reactions.

Table 2.2. The results of the computational study

Reaction	ΔG_r (kJ/mol)	ΔEE (kJ/mol)	ΔEE with ZPC (kJ/mol)
[c] \rightarrow $\frac{1}{2}$ [1]	-6.2	-24.9	-27.0
[d] \rightarrow $\frac{1}{2}$ [2]	-26.4	-55.7	-56.4
[e] \rightarrow $\frac{1}{2}$ [3]	+4.4	-17.7	-19.6
[f] \rightarrow $\frac{1}{2}$ [4]	-23.4	-50.9	-52.4
[a] + [c] \rightarrow [5]	+48.3	-13.4	-15.3
[a] + [d] \rightarrow [6]	+15.3	-44.2	-46.5
[a] + $\frac{1}{2}$ [1] \rightarrow [5]	+54.5	+11.5	+11.7
[a] + $\frac{1}{2}$ [3] \rightarrow [6]	+41.7	+11.5	+10.0

a = DippPh₂P, b = Dipp₂PhP, c = DippPh₂PCuCl, d = DippPh₂PCuBr, e = Dipp₂PhPCuCl, f = Dipp₂PhPCuBr, R = reactant, P = product.

The results of free energy changes of reaction (Δ_rG) in the gas phase models of possible reaction equilibria of the copper complexes are shown in Scheme 2.4 (with full data in the Appendix, Table A.1) and in Table 2.2 with ΔEE and ΔEE^{ZPC} . The Δ_rG s were calculated using the following equation.

$$\Delta_rG = \sum(E + G_{\text{corr}})_{\text{products}} - \sum(E + G_{\text{corr}})_{\text{reactants}}$$

Where Δ_rG = free energy of reaction; E = electronic energy; and G_{corr} = thermal free energy correction.

In order to account for the formation and behavior of the molecules as observed during reaction and ¹H NMR experiment, the Δ_rG , ΔEE and ΔEE^{ZPC} of going from reactant to product were compared. The CuBr adducts generally have lower Δ_rG , ΔEE and ΔEE^{ZPC} than their CuCl analogues. The negative Δ_rG for adducts **1** (-6.2 kJ/mol), **2** (-26.4 kJ/mol) and **4** (-23.4 kJ/mol) suggests that the the dinuclear dimers are more stable than the monomers (i.e., the combined energy of two monomers (L–Cu–X) or a monomer and the free ligand, L) in gas phase as expected.

These are also supported by negative ΔEE (exothermic) and lower ΔEE^{ZPC} recorded for **1** (–24.9 and –27.0 kJ/mol), **2** (–55.7 and –56.4 kJ/mol) and **4** (–50.9 and –52.4 kJ/mol).

The positive $\Delta_r G$ (4.4 kJ/mol) value for **3**, implies that its monomer is more favoured than the dimer. However, its electronic energy of formation is exothermic (ΔEE , –17.7 kJ/mol) and has a lower ΔEE^{ZPC} (–19.6 kJ/mol). A reasonable explanation for this observation is that the high steric repulsion of Dipp₂PhP in the presence of small atomic size Cl bridging atoms in **3** might be responsible for destabilization of its formation with consequent positive $\Delta_r G$. Such experience is absent in **4** because the larger Br bridging atoms provides adequate space that relieves the ligand bulky substituents repulsion. Despite the steric influence, **3** could be generated by its removal from solution by crystallization as observed.

To provide further insights into the above results, the minimum energies of CuX monomer and dimer complexes of tri-*ortho*xylylphosphine, Xyl₃P, were attempted as a simplified computational model for complexes of Mes₃P.²⁶ The Mes₃PCuBr has been reported to crystallize as its monomer in the solid-state by Alyea *et al.*²² The Xyl₃PCuBr model compound, starting from the published crystal structure of Mes₃PCuBr, was optimized successfully including its Cl derivative. In contrast, the dimer was very difficult to optimize with various bending of the Cu–X bond. The most stable conformations found are centrosymmetric dimers with a weak propensity to bend their Cu–X bond that have electronic energies that lie only slightly lower than the monomers (ΔEE of 2.5 and 0.5 kJ/mol). The apparent explanation of why Mes₃PCuX fails to dimerize and Dipp₂PhPCuX does is the presence of the single phenyl group which lacks ortho substituents. This reduces the local steric interaction that could hinder dimerization in *o*-Xyl₃P.

Interestingly, complex **5** and **6** are not energetically favourable, with both having high $\Delta_r G$ s in the two possible routes of reactions considered. Considering addition of two ligands to the

copper center via intermediate monomer formation (in the reaction of CuX with two equivalent phosphine), Δ_rG of **5** lying higher at 48.3 kJ/mol above 15.3 kJ/mol recorded for **6**. But they have exothermic ΔEEs (-13.4 and -44.2 kJ/mol) and lower ΔEE^{ZPCs} (-15.3 and -46.5 kJ/mol) respectively. On the other hand, the Δ_rGs 54.4 kJ/mol and 41.7 kJ/mol for **5** and **6** respectively were calculated in the pathway involving reaction of dimers **1** or **2** with an additional ligand, **L**. Contrary to the first route, the ΔEEs are exothermic (-11.5 and -11.5 kJ/mol) and ΔEE^{ZPCs} (-11.7 and -10.0 kJ/mol) are positive. Thus, formation of **5** and **6** are not spontaneously promising with reference to their high positive Δ_rGs for both reaction protocols. This lends credence to the proposal that **5** and **6** production in CH₃CN is due to the lattice energy gained by crystallizing the 2:1 complex (**5** and **6**). Acetonitrile may simply be too polar a solvent to be able to dissolve the large, globular and low polarity 2:1 complexes. Finally, the tricoordinate 2:1 analogs with phosphine **V** experienced dissociation in all computational attempts at geometry optimization. The steric demands are too high for fitting two phosphines around a single CuX, and the lattice energy is apparently not sufficient to overcome this energetic cost.

2.4 X-Ray Crystal Structure Analyses of the Complexes

Single crystals of complexes **1** – **6** suitable for X-ray diffraction were grown from suitable solvent combinations by either layering or slow evaporation. To be specific, crystals of **5** and **6** were grown from saturated chloroform solution by slow evaporation while structures **1** – **4** were crystallized by layering heptane on the saturated chloroform solutions except **4b** which crystallized from acetonitrile via slow evaporation. Descriptions of the crystallography experiments and tabulated crystal and refinement parameters are provided in Chapter 6.

Selected bond distances and angles of all the complexes are presented in Table 2.3 while Table 2.4 illustrates position of P atoms relative to the dimer core plane. Pure crystal structure, **1** and its

Table 2.3. Selected interatomic distances and angles in the crystal structures.

Complex	Cu–P (Å)	Cu–X (Å)	Cu–X' (Å)	Cu···Cu (Å)	Cu···Cu (Å) < vdW	X···X (Å) < vdW	X···X (Å) < vdW	P–Cu–P (°)
1	2.1930(6)	2.2556(6)	2.3459(5)	3.1341(4)	1.63	3.3705(7)	0.270	NA
1a	2.1940(1)	2.270(1)	2.330(2)	3.0261(7)	1.73	3.465(2)	0.175	NA
2a	2.2122(8)	2.4030(4)	2.4374(4)	2.9966(5)	1.76	3.8015(4)	–0.08	NA
3	2.208(1)	2.253(1)	2.377(1)	2.9813(8)	1.78	3.545(2)	0.095	NA
3a	2.2235(5)	2.2451(5)	2.4465(6)	3.1660(6)	1.59	3.4681(6)	0.172	NA
4a	2.2326(5)	2.3702(4)	2.5415(6)	3.2301(5)	1.53	3.7041(4)	0.016	NA
4b	2.246(3)	2.400(3)	2.447(2)	3.249(3)	1.51	3.611(3)	–0.109	NA
	2.237(3)	2.435(3)	2.434(3)	“	“	“	“	NA
4b'	2.221(3)	2.374(2)	2.471(2)	2.940(2)	1.82	3.852(2)	–0.132	NA
5	2.2460(1)	2.2427(1)	NA	NA	NA	NA	NA	125.62(1)
6	2.2481(1)	2.3750(1)	NA	NA	NA	NA	NA	126.80(1)

NA: Not applicable; **4b**: Symmetric dimer crystal structure; **4b'**: Non symmetric second dimer crystal structure in **4b**. The distances Cu···Cu and X···X refer to separation of the metal and the halogen centers in Cu₂X₂ ‘dimer’ moieties.

co-crystallized solvent crystal, **1a** ($1 \cdot 4\text{CHCl}_3$) were isolated depending on the crystallization condition. Rapid crystallization results in the incorporation of solvent molecules within the lattice. The presence of the solvent molecules in the lattice is proven by location and refinement of their atoms but is also evident from the 40.1% increase in unit cell volume observed in **1a**. Figures 2.7a and 2.7b depict the displacement ellipsoid plots of **1** and **1a** respectively. Both display centrosymmetric staggered conformations to accommodate the Dipp rings with a $\bar{1}$ site symmetry at the center of the Cu_2Cl_2 ring.

Table 2.4. Structural deformation parameters in **1** to **4**

Compound	P–Cu–X (°)	P–Cu–X – 180 (°)	P–Cu–Cu (°)	Cu_2X_2 plane – P (Å)
1	143.69(2)	– 36.31	166.96(2)	0.174
1a	134.94(4)	– 45.06	175.14(4)	0.049
2a	130.44(2)	– 49.56	176.38(2)	0.091
3	146.08(4)	– 33.92	161.96(4)	0.085
3a	153.30(2)	– 26.7	156.37(2)	0.026
4a	150.60(2)	– 29.4	157.96(2)	0.033
4b, P1	142.93(1)	– 37.07	162.84(1)	0.051
4b', P2	148.89(1)	– 31.11	166.47(1)	0.123
4b', P3	145.89(1)	– 34.11	162.87(1)	0.038

P–Cu–X – 180: Deviation from linear; P–Cu–Cu: Alignment of P in line with Cu_2X_2 core; **4b, P1**: Centrosymmetric structure in **4b** crystal structure and its P atoms; **4b', P2, P3**: Noncentrosymmetric structure in **4b** crystal structure and its P atoms.

Table 2.5. Selected bond lengths and bond angles of complexes **1** and **2** compared to less bulky previously studied analogs

Complex	Cu–P (Å)	Cu–X (Å)	Cu–X' (Å)	Cu...Cu (Å)	X...X (Å)	Cu–X–Cu (°)	X–Cu–X (°)	Ref. codes
1	2.1930(6)	2.2556(6)	2.3459(5)	3.1341(4)	3.3705(7)	85.84(2)	94.16(2)	
1a	2.194(1)	2.270(1)	2.330(2)	3.0261(7)	3.465(2)	82.26(5)	97.74(5)	
[CuCl(IV)] ₂	2.209(3)	2.247(4)	2.340(3)	3.132(2)	3.354(4)	86.1(1)	93.9(1)	GUQSAO ²⁶
[CuCl(mes)Ph ₂ P] ₂	2.186(2)	2.272(2)	2.330(3)	3.063(2)	3.435(3)	83.45(7)	96.55(8)	VUHYEC ³¹
[CuCl(dpbb)Ph ₂ P] ₂	2.1719(4)	2.2702(4)	2.3265(5)	2.9585(4)	3.5186(7)	80.11(1)	99.89(2)	CEFKUW ³²
[CuCl(quinap)Ph ₂ P] ₂	2.173(1)	2.268(1)	2.305(2)	3.0496(8)	3.407(2)	83.66(6)	96.34(6)	SUQGAN ³³
[CuCl(dpa)Ph ₂ P] ₂	2.174(1)	2.291(1)	2.3069(9)	2.862(1)	3.599(1)	76.98(2)	103.02(2)	CELHUZ ³⁴
[CuCl(carb)Ph ₂ P] ₂	2.1847(9)	2.2690(8)	2.3614(9)	2.9876(9)	3.523(1)	78.60(2)	99.07(3)	DOFDIO ³⁵
2a	2.2122(8)	2.4030(4)	2.4374(4)	2.9966(5)	3.8015(4)	76.49(1)	103.51(2)	
[CuBr(dpbb)Ph ₂ P] ₂	2.1918(8)	2.3909(5)	2.4168(6)	2.8771(7)	3.8780(6)	73.14(1)	106.86(1)	CEFKOQ ³²
[CuBr(dpa)Ph ₂ P] ₂	2.1918(8)	2.3909(5)	2.4168(6)	2.9201(6)	3.8194(6)	74.80(2)	105.20(2)	CELKUC ³⁴
[CuBr(carb)Ph ₂ P] ₂ .CHCl ₃	2.201(1)	2.4954(6)	2.3810(6)	2.9352(7)	3.8777(5)	72.44(2)	105.33(2)	DOFDOU ³⁵
[BrCu(Quinap)] ₂	2.199(1)	2.4308(9)	2.4728(9)	3.026(1)	3.8125(9)	76.45(3)	102.06(3)	OFUTEO ³⁶
[CuBr(mes)Ph ₂ P] ₂	2.198(3)	2.440(2)	2.397(2)	3.083(2)	3.728(2)	79.19(5)	100.81(5)	VUHYIG ³¹

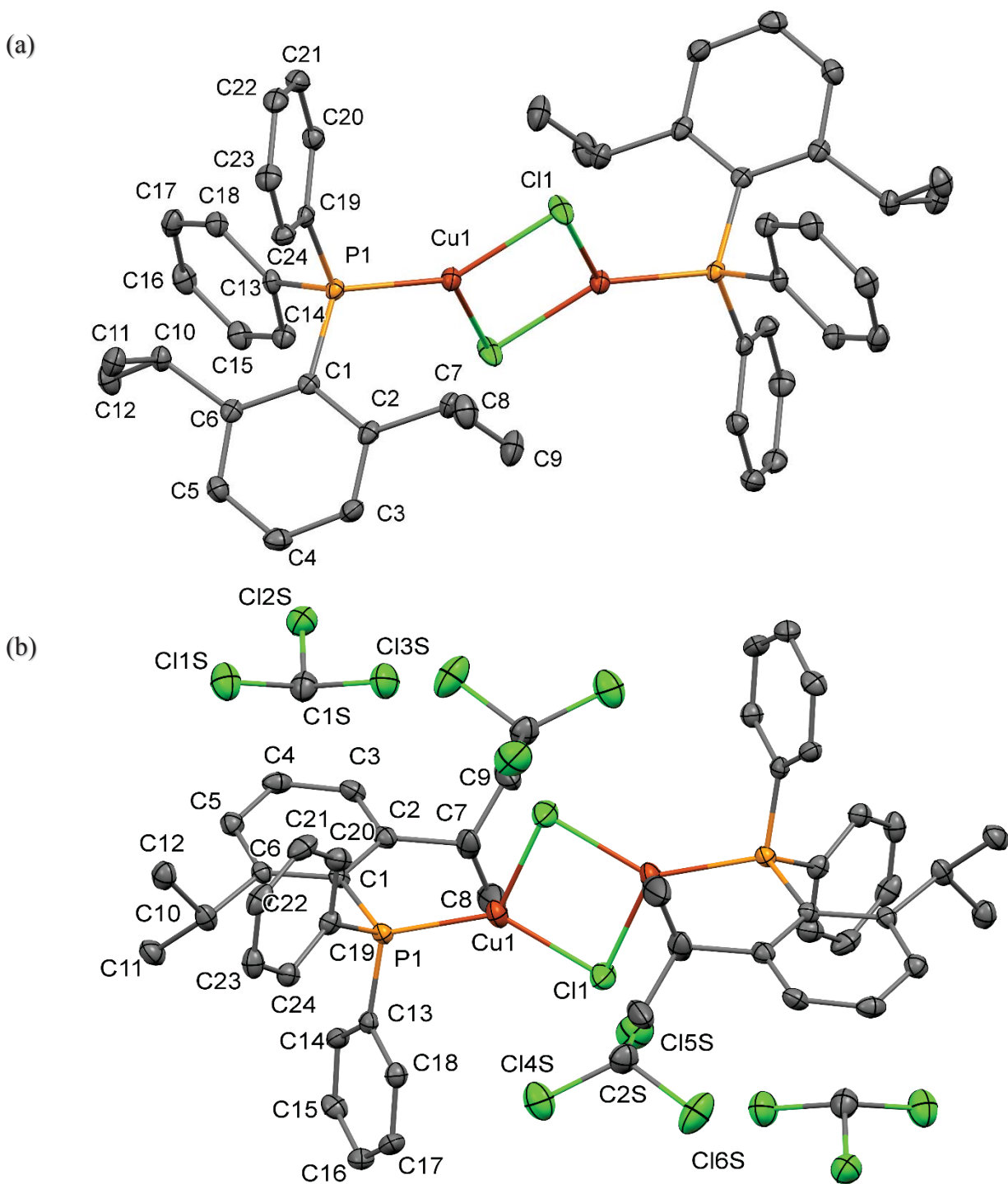


Figure 2.7. Displacement ellipsoid plots (50%) showing the complexes and solvent molecules as found in the crystal structures of (a) **1** and (b) **1a**. Hydrogen atoms have been omitted for clarity.

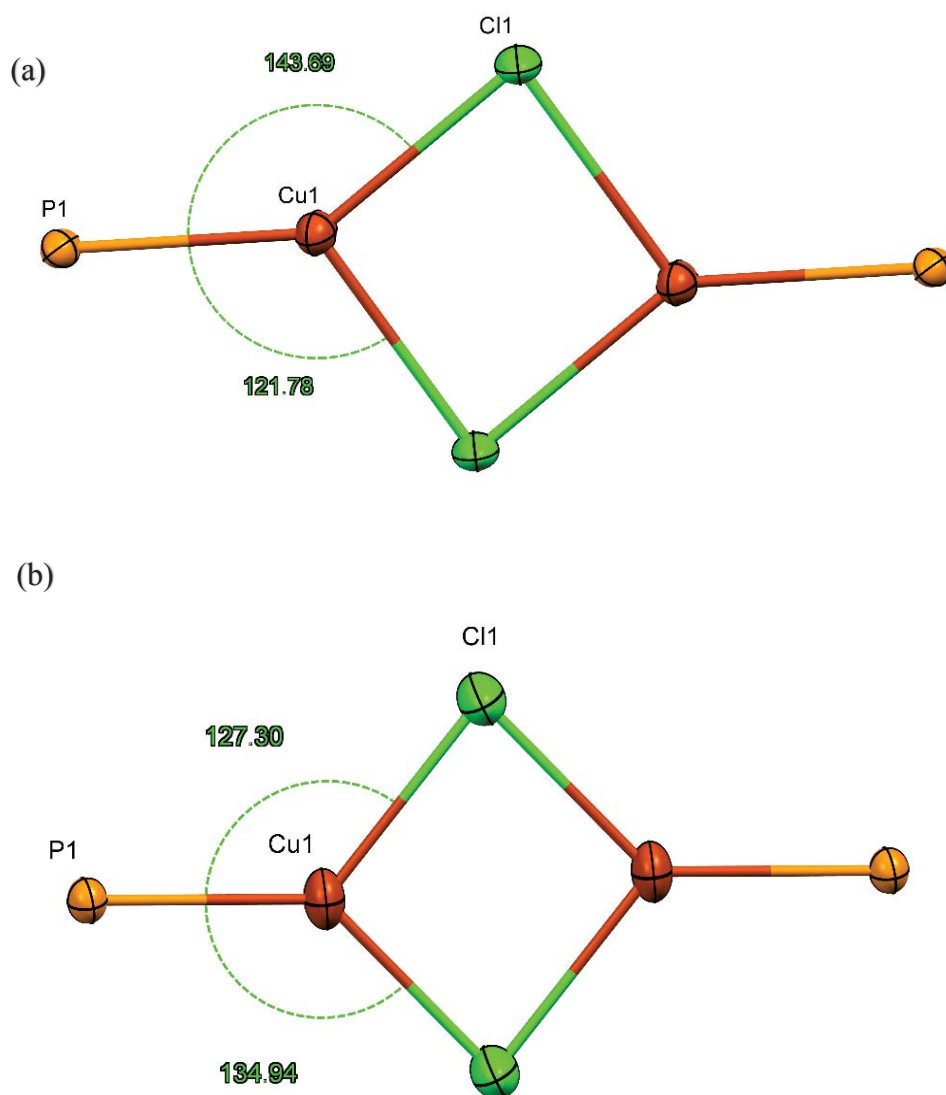


Figure 2.8. Displacement ellipsoid plots (50%) showing only the Cu_2Cl_2 core of (a) **1** and (b) **1a**.

The unit cell parameters are quite different but with little variations in the structural geometries, especially the Cu_2Cl_2 rings. In the packing arrangement, the phosphine of one dimer lies over the Cu_2Cl_2 plane of another molecule in **1** (Figure A. 23a, appendix) while in **2a**, there is an offset of the phosphine moiety by width of the Cu_2Cl_2 plane because the space is being occupied by a solvent molecule (Figure A. 23b, appendix). The Cu–P bond of **1a**, 2.1940(1) Å is not

significantly different from that of **1**, 2.1930(6) Å (Table 2.5). However, $d(\text{Cu}\cdots\text{Cu})$ is slightly larger in **1** than **1a** which are respectively 3.1341(4) Å and 3.0261(7) Å. The two solvent molecules per monomer in **1a** are oriented toward the electron rich Dipp ring and the bridging chloride (Figure A. 22a, appendix) with short contacts less than the sum of van der Waals radii ascribed to dipole–dipole interactions. Figure A.22b (Appendix) displays the solvent voids packing diagram which account for 29.7% of the unit cell volume, computed by deliberately removing the solvent molecules from the model. The phosphorus atoms are lying at 0.049 Å above or below the Cu_2X_2 plane in **1a**, and they are more aligned with the plane at $175.14(4)^\circ$ than in **1** at 0.174 Å and $166.96(2)^\circ$ respectively (Table A. 2, Appendix). This corresponds to more distortion in **1**. Intramolecular interactions are practically equal in **1** and **1a** in arrangements of the isopropyl groups. Interestingly, both structures possess short contacts of the Dipp methine hydrogen and Cu atom, with 2.098 Å for **1a** shorter than 2.429 Å for **1**, as well as with the phosphorus atoms. In context, the geometric parameters of **1** and **1a** are very close to data reported for related structures (Table 2.4). The largest Cu–P–Cl angle of $143.69(2)^\circ$ for **1** shows that it is more close to linear than **1a** having $134.94(4)^\circ$ (Figure 2.8).

As shown in Figure 2.9a, compound **2** only crystallized as a solvate, **2a** (2.2CHCl_3) in the centrosymmetric triclinic space group $P\bar{1}$ employing a slow crystallization technique. However, the Cu–P bond, 2.2122(8) Å in **2a** is considerably longer, and the $\text{Cu}\cdots\text{Cu}$ distance, 2.9966(5) Å is remarkably shorter, than the analogue **1** and **1a**. Looking closely the structural architectures of **2a**, it has staggered conformation of the phosphines as found in **1** and **1a**. Although the molecular packing in the lattice is similar to **1a**, the phosphine is much further offset away from the Cu_2Br_2 core (Figure A. 24, appendix). The solvent molecules occupy 21.0% of the unit cell volume (Figure A. 25, appendix), and the short contacts observed except that between the Br atoms and the solvent

molecules are related to those seen in **1a**. However, the largest Cu–P–X angle of $130.44(2)^\circ$ shows that it is less linear than **1a**.

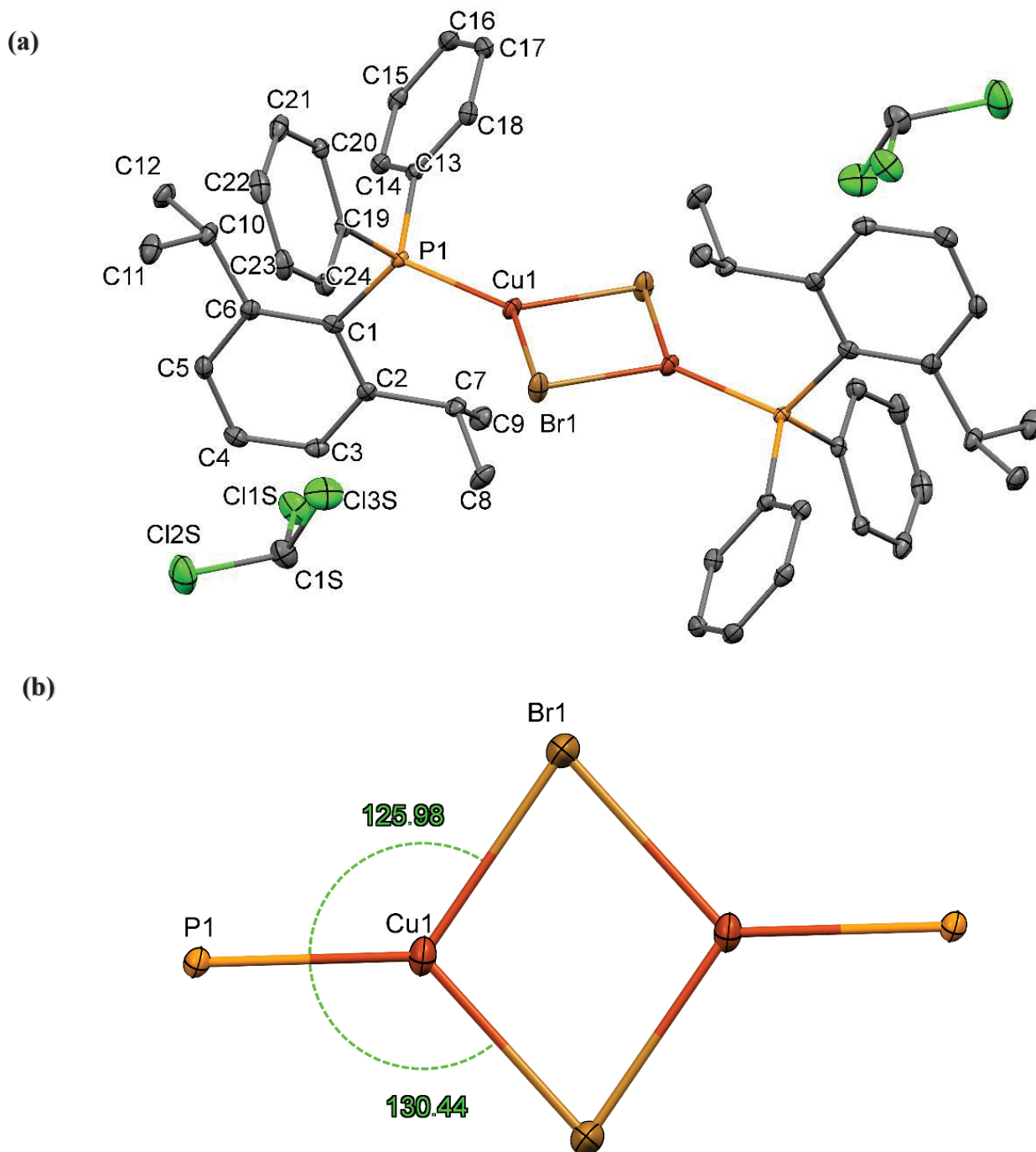


Figure 2.9. Displacement ellipsoid plots (50%) showing (a) the complexes **2a** and solvent molecules as found in the crystal structures. Hydrogen atoms have been omitted for clarity. (b) A similar plot showing only the Cu_2Cl_2 core in **2a**.

Less distortion is experienced in **2a** with the P atoms making an angle of $176.38(2)^\circ$ against Cu_2Br_2 and a distance 0.091 \AA above or below the Cu_2Br_2 plane. The Cu–P bond is slightly longer in **2a** than those recorded for related reported structures (Table 2.5).

Attractive forces of the Cu atoms and the X atoms which surpasses the repulsive forces of the ligands facilitates dimer formation in the solid state. The slightly shorter $d(\text{Cu}\cdots\text{Cu})$ observed on switching from Cl to Br may indicate a stronger metallophilic $\text{M}\cdots\text{M}$ interaction.³⁷ It has been suggested that, since Br is less electronegative than Cl which tends to lower the metal positive charges.³⁸ However, since the $d(\text{Cu}\cdots\text{Cu})$ are much shorter than the sums of their v.d.Waals radii, there is a strong metallophilic interaction which is caused by dispersion (London) forces. It therefore seems more likely that the less electronegative, and more polarizable, bromide allows the copper centres to also be more polarizable – a key contribution to dispersion interactions.

Intriguingly, two crystal structures were recorded for compound **3**, similar to what was obtained for **1**. Both pure **3** and the solvated form **3a** (3.2CHCl_3) crystallize as centrosymmetric monoclinic dimers (Figure 2.10) in space group $P2_1/n$ having trigonal planar coordination at the copper atom and a staggered conformation arrangement of the two bulky ligands **V** as established in **1** and **2**. The Cu–P bond and $\text{Cu}\cdots\text{Cu}$ distance of $2.2235(5) \text{ \AA}$ and $3.1660(6) \text{ \AA}$ **3a** are markedly longer than $2.2080(1) \text{ \AA}$ and $2.9813(8) \text{ \AA}$ of **3**.

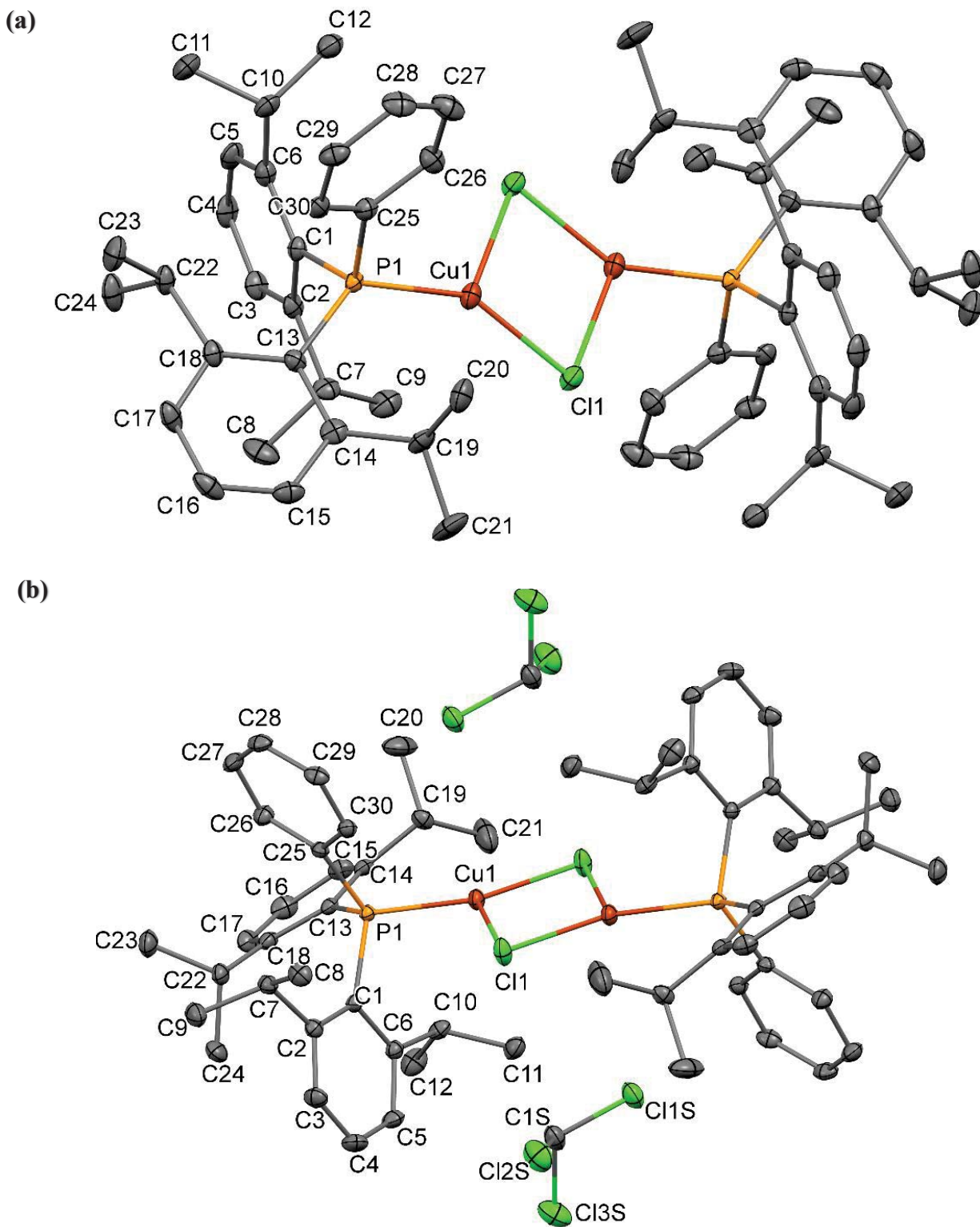


Figure 2.10. Displacement ellipsoid plots (50%) showing the complexes and solvent molecules as found in the crystal structures of (a) **3** and (b) **3a**. Hydrogen atoms have been omitted for clarity.

The changes in the Cu···Cu distances are contrary to the observation in the **1** and **1a** pair where Cu···Cu distances diminished in the solvated **1a**, because only two solvents with no direct contact with Cl atoms or orientation towards the Dipp ring are accommodated in the lattice of **3a** occupying 12.9% voids of the unit cell volume (Figure A. 26, appendix), compared to **1a**. Also, the two offset monomers participating in the dimer contribute to the larger Cu···Cu due to high steric repulsion from the two Dipp rings. The structure of **3** (146.08(2)°) and **3a** (153.30(2)°) are more close to linear than **1** and **1a** (Figure 2.11)

The observation that **3a** accommodates solvent more readily than **1a** could be ascribed to the larger volume of ligand **V** compared to ligand **IV**. One of the methine protons of the ligand orients towards the Cu₂Cl₂ core with intramolecular contacts of 2.456 Å for Cu···H and 2.844 Å Cl···H in **3**, and 2.564 Å for Cu···H in **3a**. The overall geometry of the dimer core is comparable with previously reported structures for inherently congested copper-phosphine dimers (Table 2.6).^{11, 39-40} The solvent-free structure, **3** is similar to **1** and **3a** at the P-CuCl₂-P unit with the two phosphines having the same orientation. However, they are different in the degree of twist of the aromatic rings as well as the Cu-P bond and Cu···Cu distances. Clear structural changes for this pair include the Cu-P bond 2.2080(1) Å for **3** which is longer than 2.1930(6) Å in **1** as expected for a highly sterically hindered phosphine ligand, and the Cu···Cu distance which notably decreases by approximately 5% in **3** (2.9813(8) Å) compared to 3.1341(4) Å recorded for **1** though the phosphine conformations remain almost identical. As seen in Table 2.6, the Cu-P and Cu···Cu distances in **3** are not different from those reported for [CuBr(mes)₂PhP]₂ [(CSD refcode: VUHYUS)³¹ with related steric capacity in the *ortho* position.

Table 2.6. Selected bond lengths and bond angles of **3** and **4** compared to previously studied analogs with bulky phosphines

Complex	Cu-P (Å)	Cu-X (Å)	Cu-X' (Å)	Cu...Cu (Å)	X...X (Å)	Cu-X-Cu (°)	X-Cu-X (°)	Ref.
3	2.208(1)	2.253(1)	2.377(1)	2.9813(8)	3.545(2)	80.11(4)	99.89(4)	
3a	2.2235(5)	2.2451(5)	2.4465(6)	3.1660(6)	3.4681(6)	84.77(2)	95.23(2)	
[CuCl(mes) ₂ PhP] ₂	2.206(1)	2.284(2)	2.330(2)	3.091(2)	3.426(2)	84.10(5)	95.90(5)	VUHYUS ³¹
[CuCl(<i>o</i> -tol) ₃ P] ₂	2.192(2)	2.289(2)	2.316(2)	3.103(1)	3.403(2)	84.73(5)	95.27(6)	PECHOU02 ¹⁹
CuCl(<i>o</i> -tol) ₃ P] ₂	2.1961(8)	2.2922(8)	2.3169(8)	3.1072(6)	3.4045(9)	84.77(3)	95.23(3)	PECHOU01 ⁴⁰
[CuCl(<i>o</i> -tol) ₃ P] ₂	2.183(3)	2.281(2)	2.342(3)	3.130(2)	3.404(3)	85.20(8)	94.80(9)	PECHOU ¹¹
[CuCl(<i>o</i> -tol) ₃ P] ₂	2.1942(4)	2.3230(4)	2.2876(4)	3.0905(3)	3.4217(5)	84.18(1)	95.82(1)	PECHOU04 ¹⁷
[CuCl(<i>o</i> -tol) ₃ P] ₂	2.1935(4)	2.3022(5)	2.3099(4)	3.0441(4)	3.4648(6)	82.60(1)	97.40(1)	PECHOU03 ¹⁷
[CuCl(bp) ₃ P] ₂	2.170(1)	2.269(2)	2.304(2)	2.844(1)	3.505(2)	77.31(5)	100.04(5)	XUNXAG ³⁹
4a	2.2326(5)	2.3702(4)	2.5415(6)	3.2301(5)	3.7041(4)	82.16(1)	97.84(1)	
[CuBr(<i>o</i> -tol) ₃ P] ₂	2.198(2)	2.416(1)	2.428(1)	3.112(1)	3.711(2)	79.95(4)	100.05(5)	PECHUA ¹¹
[CuBr(<i>o</i> -tol) ₃ P] ₂	2.206(1)	2.4157(9)	2.4318(9)	3.1123(8)	3.7165(9)	79.89(3)	100.11(3)	PECHUA01 ⁴⁰
[CuBr(<i>o</i> -tol) ₃ P] ₂	2.208(2)	2.414(1)	2.431(1)	3.109(1)	3.716(1)	79.83(4)	100.17(4)	PECHUA02 ¹⁹
[CuBr(<i>o</i> -MeO-tol) ₃ P] ₂	2.194(1)	2.356(1)	2.5406(9)	3.0850(9)	3.807(1)	78.01(3)	101.99(3)	QABZUO
[CuBr(mes) ₂ PhP] ₂	2.198(3)	2.393(3)	2.415(2)	3.052(3)	3.685(3)	78.79(5)	100.06(5)	VUHZA ³¹

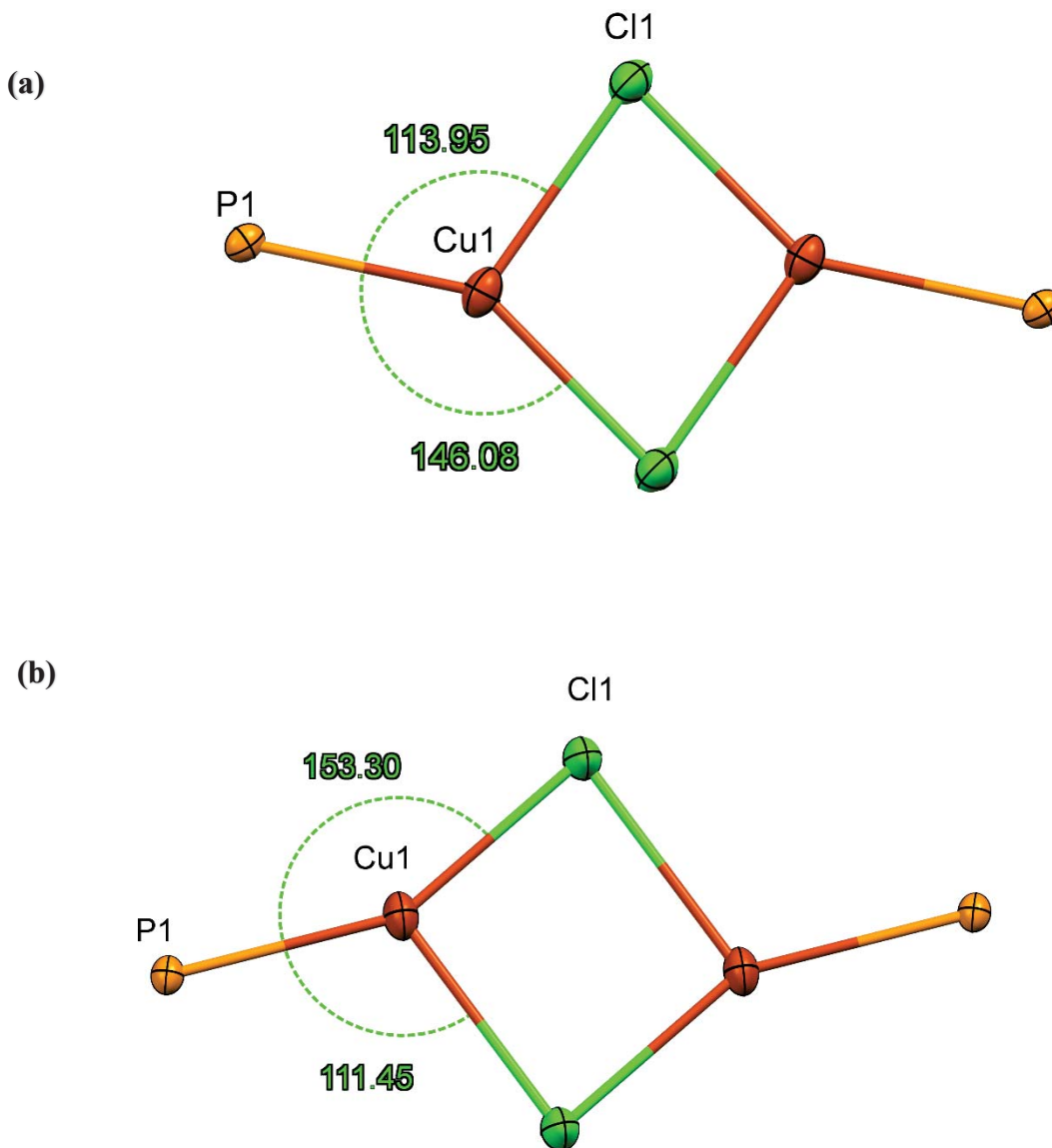


Figure 2.11. Displacement ellipsoid plots (50%) showing just the Cu_2Cl_2 core of (a) **3** and (b) **3a**. The packing arrangement that exists in structures **3** and **3a** ((Figures A. 27a and b, Appendix) correspond to those found in **1** and **1a** respectively.

The solvate **4a** (4.2CHCl_3) is the only confirmed structure for compound **4** when crystallized in chloroform (Figure 2.12a), and it is isostructural to **3a** with a similar unit cell volume. The two solvent molecules occupy corresponding voids associated with 12.9% of the unit cell volume exhibited by **4a** (Figure A. 28a, appendix). But **4b** crystallizes in the orthorhombic space group *Pbca* **4b** ($4.\text{CH}_3\text{CN}$) when recrystallized in acetonitrile (Figure 2.12b). The structure of **4b** contains two dimer structures: a centrosymmetric (**4b'**) and non centrosymmetric (**4b**) with Cu_1Cu_1 and Cu_2Cu_3 cores, respectively. The asymmetric unit contains one solvent molecule which is consistent with overall 2% solvent void of the unit cell volume found in the structure (Figure A. 28b, Appendix). The core copper-halide rings within the crystal packing are almost planar. The Cu_2Cu_2 dimer in **4b** is a bit less distorted than **4a**, with P2 and P3 making an angle of $162.87(1)^\circ$ and $166.47(1)^\circ$ with the linear $\text{Cu}_2\cdots\text{Cu}_3$ atoms and P2 and P3 lying 0.038 \AA and 0.123 \AA out of $\text{Cu}_2\text{Cu}_3\text{Br}_2$ plane. The Cu_1Cu_1 dimer with its P atom $162.84(1)^\circ$ to the $\text{Cu}_1\cdots\text{Cu}_1$ plane and lying 0.051 \AA out of Cu_2Br_2 plane compare to $157.96(2)^\circ$ and P located at 0.033 \AA to the Cu_2Br_2 plane observed in **4a** (Table A. 2, appendix). The $\text{Cu}\cdots\text{Cu}$ distance of $2.940(2) \text{ \AA}$ for the symmetric $\text{Cu}_1\cdots\text{Cu}_1$ in **4b'** is shorter than the analogues value $3.2301(5) \text{ \AA}$ for **4a**. Surprisingly, structure **4b** shows an eclipsed conformation of the two phosphine ligands (Figure 2.13a) and the core ring is bent outward with the largest Cu-P-Br angle of $148.89(1)^\circ$ and $145.89(1)^\circ$ respectively for Cu_2 and Cu_3 (Figure 2.13b). This leads to enclosure of half of the co-crystallized acetonitrile as depicted in Figure 2.12b. The structural packing in **4a** (Figure A. 29, Appendix) conforms with that of **3a** such that two dimer molecules are aligned on top of another.

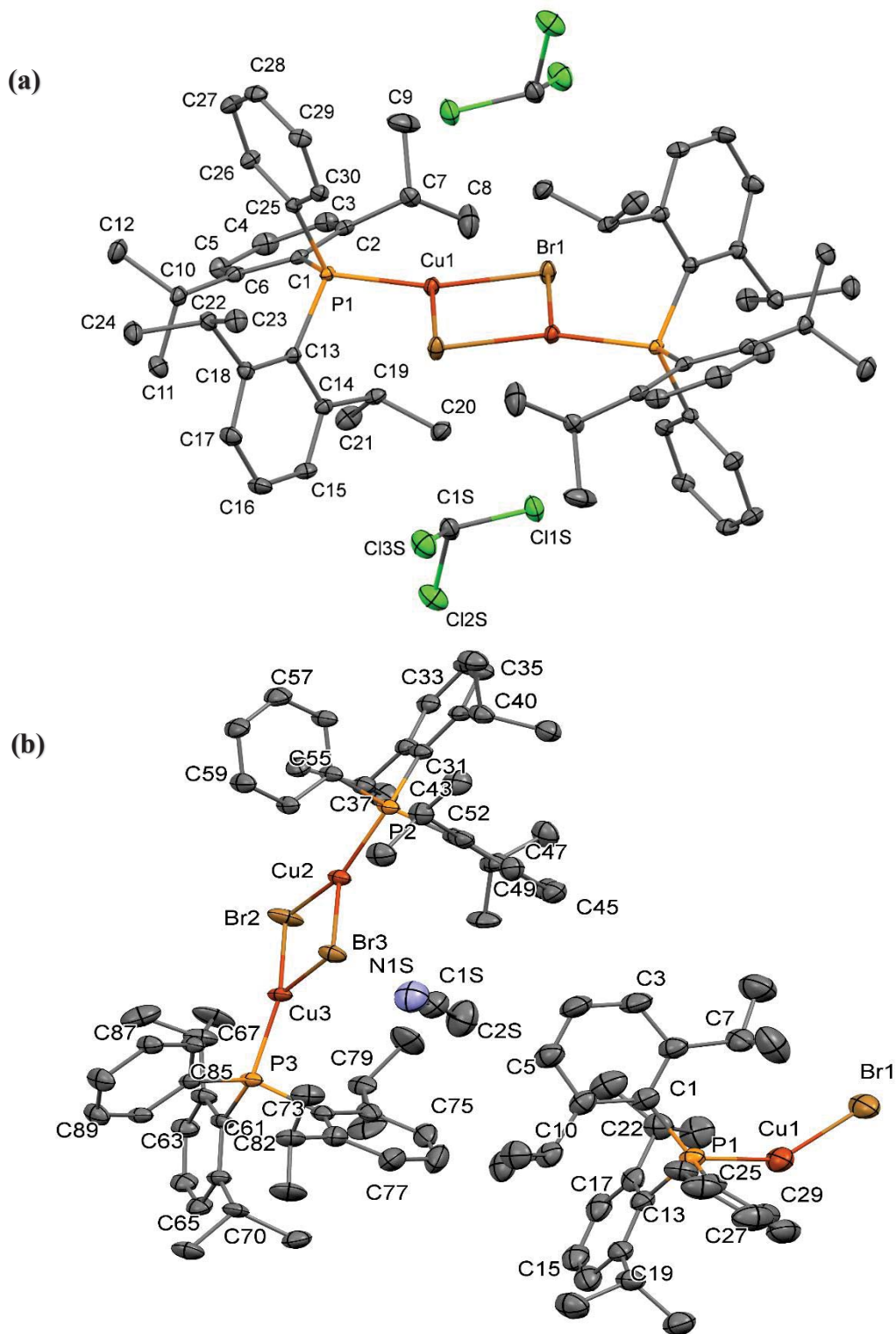


Figure 2.12. Displacement ellipsoid plots (50%) showing the complexes and solvent molecules as found in the crystal structures of (a) **4a** and (b) **4b**. Hydrogen atoms and some labels in **4b** have been omitted for clarity.

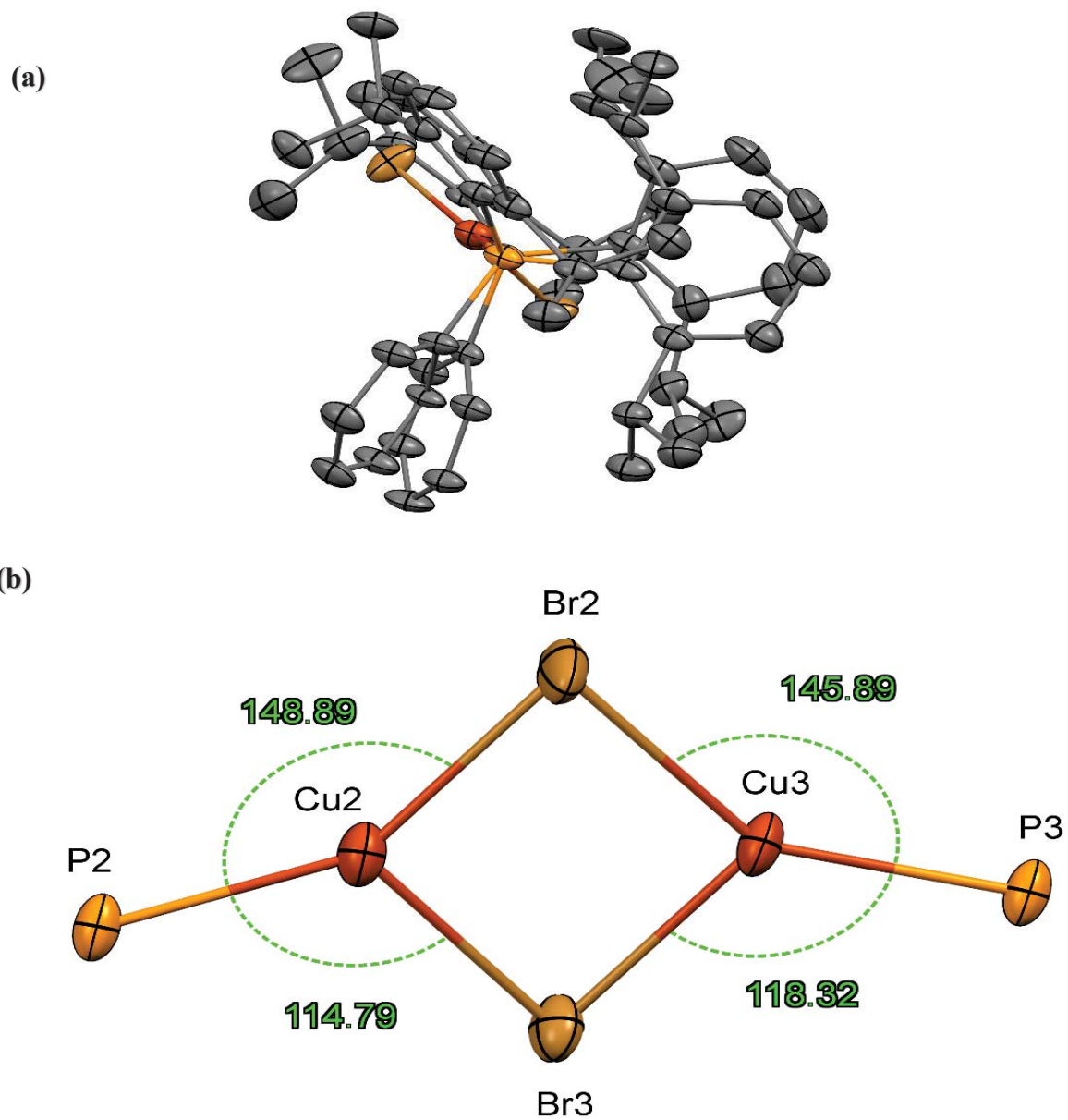


Figure 2.13. Displacement ellipsoid plots (50%) showing the (a) eclipsed phosphine aryl rings conformation and (b) only the Cu_2Br_2 core center of **4b**.

The crystal structures of **5** (Figure 2.14a) and **6** (Figure 2.14b) are isomorphous and show tricoordinate mononuclear complexes having 2-fold rotational site symmetry and crystallize in monoclinic space groups *I2/a* and *C2/c* respectively. The *I2/a* and *C2/c* are different settings of the same space group, but the β angles are different enough to keep them in the two forms. They have trigonal planar coordination at the copper atoms and their geometries are consistent with previously reported CuL_2X type complexes (Tables 2.7).

As expected, the Cu–P and Cu–X distances as well as the bond angles involving the central Cu atoms are different. The Cu–P and Cu–X bonds of 2.2481(1) Å and 2.3750(1) Å for **6** are statistically longer than 2.2460(1) Å and 2.2427(1) Å in **5** respectively which contributes to the increase in unit cell volume by 1.1% going from Cl to Br. Moreover, there is a small deviation of the L–Cu–L angle from an ideal trigonal planar (120°) which slightly increases in the Br complex **6**, $126.80(1)^\circ$ compared to the Cl complex **5**, $125.62(1)^\circ$. The Cu–P and Cu–X bond distances for **5** and **6** are very close to the average of previously reported analogous mononuclear copper-halide phosphine complexes. The Cu–P distance in **5** is quite similar to the mean value (2.2509 Å) and the P–Cu–P angle falls within a large range ($125.48 - 130.43^\circ$) in published structures in Table 2.7.

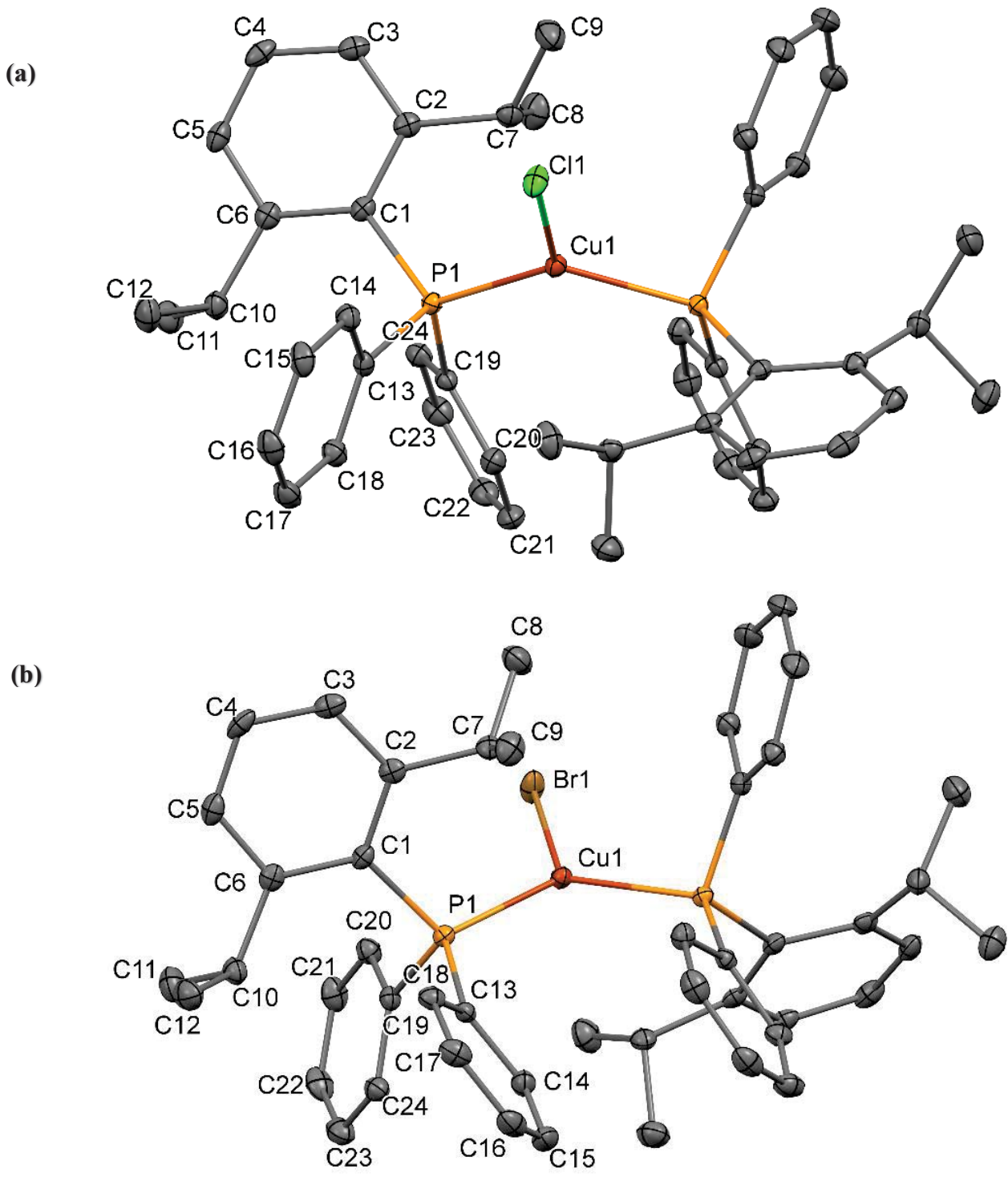


Figure 2.14. Crystal structure of (a) **5** and (b) **6** drawn at 50% probability level. Hydrogen atoms are omitted for clarity.

The parameters are apparently identical to [CuCl(PPh₂*o*-tol)₂] (refcod: FOXVIX)⁴¹ having average Cu–P bond lengths of 2.2460 Å and inter ligand angles of 125.62(1)°. On the other hand, the Cu–P distance of **6** is very close to the 2.2481 Å average value reported for related complexes (Table 2.7). Its P–Cu–P angle also fall within reported wide range (122.46 – 131.59°). The Cu–P bond distance and angle values (2.2481(1) Å and 126.80(1)°) recorded are comparable to that of [CuBr (Ph₂P *o*-tol)₂] (FOXVOD)⁴¹ with means Cu–P of 2.2475 and 127.88° angle. It should be noted that **5** and **6** possess indistinguishable features with *ortho* substituted triaryl phosphines with matching steric hindrance as reflected in the P–Cu–P angle expansion. The bulkier the *ortho* substituent, the wider the inter ligand angle at the copper center.

The substituents of tertiary aryl phosphines and the bulkiness of the whole metal complex generally contributes to the geometry of the Cu(I)X-PR₃ adducts. Overall, the reduction of the Cu···Cu distance is a noticeable trend in all the dimers going from the harder bridging ligand (Cl) to softer Br.⁴⁰ This might be associated with the metallophilic interaction between the two copper atoms because of dispersion forces which are enhanced when there is less electron withdrawal in the case of bromide versus chloride bridging ligands. Also, pronounced changes are observed in $d(\text{Cu-P})$, $d(\text{Cu}\cdots\text{Cu})$ and $\angle(\text{X-Cu-X})$ with increase in steric repulsion of the phosphine.

The results of the analyses of the crystal structures reveals the geometry of coordination at the copper environment to corroborate the spectroscopic results. The four-coordinate Cu(I) dimers are the most reported type of triaryl phosphine complexes, followed by the trigonal three-coordinate dimers while the less common trigonal mononuclear (L₂CuX) and the linear (LCuX) species are typically formed by bulky triaryl phosphines based on data mined from the Cambridge Structural Database (CSD).²⁰ Moreover, copper complexes of low steric size ligands like PPh₃ tends to aggregate in polynuclear configuration such as the cubane (Scheme 2.1).³⁹

The coordination environment at the copper centers in all the complexes reported here are approximately planar as the sum of angles is approximately 360°. However, the two phosphorus atoms in the dimers are not planar with the Cu₂X₂ ring with the degree of distortion influenced by the presence or absence of co-crystallized solvent, the type of halide involved and the bulkiness of ligand. The LCuX dimers usually crystallize as centrosymmetric halide bridges, with a center of symmetry ($\bar{1}$) located in the middle of the Cu₂X₂ core, except for the Cu₂Cu₃ dimer in **4b**. Similar three-coordinate monomeric 2:1 and dimeric 1:1 geometries have been reported for other bulky phosphine-copper (I) complexes.^{31, 34, 42-44}

Table 2.7. Selected bond lengths and bond angles of **5** and **6** compared to previously studied analogues

Complex	Cu–P (Å)	Cu–P' (Å)	Cu–Cl (Å)	P–Cu–P (°)	Ref.
5	2.2460(1)	2.2460(1)	2.2427(1)	125.62(1)	
[CuCl(Ph ₂ PC ₆ H ₄ (<i>o</i> -OMe)) ₂]	2.2327(7)	2.2387(7)	2.2241(7)	129.46(3)	BABNEZ ¹⁸
[CuCl(PPh ₂ CHO) ₂]	2.2265(5)	2.2486(5)	2.2448(6)	130.17(2)	CITFER ²⁰
[CuCl(PPh ₃) ₂]	2.260(2)	2.272(2)	2.208(2)	125.49(5)	FEYPEE ⁴
[CuCl(PPh ₂ <i>o</i> -tol) ₂]	2.241(2)	2.256(2)	2.204(2)	126.98(7)	FOXVIX ⁴¹
[CuCl(PPh ₂ dnpa) ₂]	2.2472(7)	2.2528(7)	2.2269(6)	130.41(2)	KESKUR ¹⁰
[CuCl(PPh ₂ <i>p</i> -tol) ₂]	2.257(1)	2.258(1)	2.233(1)	126.72(5)	NERSIN ¹²
[CuCl(PPh ₃) ₂]	2.2564(8)	2.2676(7)	2.214(1)	125.55(3)	TINRAJ ⁸
6	2.2481(1)	2.2481(1)	2.3750(1)	126.80(1)	
[CuBr(Ph ₃ P) ₂].C ₆ H ₆	2.263	2.282	2.345	126.04	BTPCUB ⁴⁵
[CuBr (Ph ₂ PC ₆ H ₄ <i>o</i> -CHO) ₂]	2.2367	2.2367	2.3364	123.53	CITFIV ²⁰
[CuBr (Ph ₂ PC ₆ H ₄ <i>o</i> -Cl) ₂]	2.255(1)	2.237(2)	2.3561(9)	122.46(5)	EVIBAO ⁴⁶
[CuBr (Ph ₂ PC ₆ H ₄ <i>o</i> -Br) ₂]	2.258(2)	2.242(2)	2.344(2)	127.12(6)	EVIBOC ⁴⁶
[CuBr (Ph ₂ P <i>o</i> -tol) ₂]	2.255(2)	2.240(2)	2.336(1)	127.88(7)	FOXVOD ⁴¹
[CuBr(Ph ₂ Pdnpa) ₂]	2.2478(7)	2.2535(7)	2.3566(5)	131.59(2)	KESLAY ¹⁰
[CuBr (Ph ₂ P <i>o</i> -ester) ₂]. tol	2.2277(9)	2.2391(9)	2.3464(4)	126.83(3)	LELZEI ⁴⁷

2.5 Conclusions

This work led to the synthesis, isolation and understanding of the coordination chemistry of trigonal geometry 1:1 and 2:1 $\text{Dipp}_{(n-1)}\text{Ph}_n\text{P}$ copper (I) halides. Factors like solvent, crystal growing condition and steric bulk have significant influences on the generated metal complexes. The less hindered **IV** preferentially forms single metal halide complexes in a polar aprotic solvent, and halide bridged dimers in a less-polar solvent, irrespective of the halide involved. The adducts of the bulkier phosphine **V** are solvent independent; it only resulted in dimer formation. Structural analyses show that all CuCl and CuBr adducts of the same ligand do not have significant structural differences.

2.6 References

1. Araki, H.; Tsuge, K.; Sasaki, Y.; Ishizaka, S.; Kitamura, N., Synthesis, structure and emissive properties of copper(I) complexes $[\text{Cu}_2(\text{I})-\mu\text{-}1,8\text{-naphthyridine})(\text{PPh}_3)_2]$ ($\text{X}=\text{I}, \text{Br}$) with a butterfly-shaped dinuclear core having a short Cu-Cu distance. *Inorg. Chem.* **2007**, *46*, 10032-10034.
2. Barron, P. F.; Dyason, J. C.; Engelhardt, L. M.; Healy, P. C.; White, A. H., Lewis base adducts of group-1B metal(I) compounds high-resolution solid-state P-31 nuclear magnetic-resonance spectra of tetrameric (triphenylphosphine)copper(I) halide-complexes and crystal-structure determination of cubane $\text{PPh}_3\text{CuBr}_4$. *Inorg. Chem.* **1984**, *23*, 3766-3769.
3. Bernersprice, S. J.; Johnson, R. K.; Mirabelli, C. K.; Faucette, L. F.; McCabe, F. L.; Sadler, P. J., Copper(I) complexes with bidentate tertiary phosphine-ligands - solution chemistry and antitumor-activity. *Inorg. Chem.* **1987**, *26*, 3383-3387.
4. Bowmaker, G. A.; Dyason, J. C.; Healy, P. C.; Engelhardt, L. M.; Pakawatchai, C.; White, A. H., Lewis-base adducts of group 11 metal(I) compounds solid-state phosphorus-31 cross-polarization magic-angle spinning nuclear magnetic resonance, far-infrared, and structural studies on the mononuclear 2 : 1 adducts of triphenylphosphine with copper(I) and gold(I) halides. *J. Chem. Soc., Dalton Trans.* **1987**, 1089-1097.
5. Darensbourg, D. J.; Holtcamp, M. W.; Klausmeyer, K. K.; Reibenspies, J. H., Crystal-structure of di- μ -chloro-tris(triphenylphosphine)dicopper(i)dichloromethane, $\text{C}_{55}\text{H}_{47}\text{Cl}_4\text{Cu}_2\text{P}_3$. *Z. Krystallog.* **1995**, *210*, 615-616.
6. Gill, J. T.; Mayerle, J. J.; Welcker, P. S.; Lewis, D. F.; Ucko, D. A.; Barton, D. J.; Stowens, D.; Lippard, S. J., Structural determinations of 4 mononuclear and binuclear tertiary phosphine and arsine complexes of copper(I) chloride. *Inorg. Chem.* **1976**, *15*, 1155-1168.
7. Hadjikakou, S. K.; Aslanidis, P.; Karagiannidis, P.; Hountas, A.; Terzis, A., Synthesis and photolysis of a new series of Cu(I) complexes with tri-meta-tolylphosphine and heterocyclic thiones - the crystal-structure of bis μ -iodo(pyridine-2-thione)(tri-meta-tolylphosphine)copper(I). *Inorg. Chim. Acta* **1991**, *184*, 161-166.
8. Kräuter, T.; Neumüller, B., Triphenylphosphane complexes of copper(I): Structural and ^{31}P NMR investigations. *Polyhedron* **1996**, *15*, 2851-2857.
9. Lazarou, K.; Bednarz, B.; Kubicki, M.; Verginadis, I. I.; Charalabopoulos, K.; Kourkoumelis, N.; Hadjikakou, S. K., Structural, photolysis and biological studies of the bis(μ -(2)-chloro)-tris(triphenylphosphine)-di-copper(I) and chloro-tris(triphenylphosphine)- copper(I) complexes. Study of copper(I)-copper(I) interactions. *Inorg. Chim. Acta* **2010**, *363*, 763-772.
10. Li, Q.; Liu, L.; Zhong, X. X.; Li, F. B.; Asiri, A. M.; Alamry, K. A.; Zhu, N. Y.; Wong, W. Y.; Qin, H. M., Synthesis, characterization and luminescent properties of copper(I) halide complexes containing 1-(diphenylphosphino) naphthalene. *J. Inorg. Organomet. Polym. Mater.* **2017**, *27*, S101-S109.

11. Ramaprabhu, S.; Amstutz, N.; Lucken, E. A. C.; Bernardinelli, G., Copper-63,65 nuclear-quadrupole resonance of complexes of copper(I) halides with phosphorus-containing ligands. *J. Chem. Soc., Dalton Trans.* **1993**, 871-875.
12. Steyl, G., Chlorobis diphenyl(p-tolyl)phosphine copper(I). *Acta Crystallogr., Sect. E: Crystallogr. Commun.* **2006**, 62, M3277-M3278.
13. Yeh, W. Y.; Lee, G. H.; Peng, S. M., Syntheses, characterization and crystal structures of [Cu(PCHO)₂(2,2'-bipy)][BF₄], [Cu₂(PCHO)₄(4,4'-bipy)][BF₄]₂ and [Cu₂(PCHO)₄(bptz)][BF₄]₂ (PCHO = o-(diphenylphosphino) benzaldehyde and bptz = 3,6-bis(2'-pyridyl)-1,2,4,5-tetrazine). *Inorg. Chim. Acta* **2006**, 359, 659-664.
14. Yeh, W. Y.; Lin, C. S.; Peng, S. M.; Lee, G. H., Syntheses and structures of tungsten o-(diphenylphosphino)benzaldehyde complexes bearing π-bonded aldehyde groups. *Organometallics* **2004**, 23, 917-920.
15. Bowmaker, G. A.; Hart, R. D.; Jones, B. E.; Skelton, B. W.; White, A. H., Structural and vibrational spectroscopic studies of complexes of trimethylphosphine with copper(I) and silver(I) halides. *J. Chem. Soc., Dalton Trans.* **1995**, 3063-3070.
16. Singh, S.; Wang, G.; Mao, J. X.; Flores, J. A.; Kou, X.; Campana, C.; Kroll, P.; Dias, H. V. R., Gold(I) complexes [N{(C₃F₇)C(Dipp)N}₂]AuL (L = ethylene, tert-butyl isocyanide, tetrahydrothiophene, triphenylphosphine) and different triazapentadienyl ligand coordination modes. *Eur. J. Inorg. Chem.* **2016**, 2016, 5435-5444.
17. Espinoza, S.; Arce, P.; San-Martin, E.; Lemus, L.; Costamagna, J.; Farias, L.; Rossi, M.; Caruso, F.; Guerrero, J., The crystal structure of mono- and di-nuclear copper(I) complexes with substituted triphenylphosphine ligands. *Polyhedron* **2015**, 85, 405-411.
18. Chuang, W. J.; Lin, I. J.; Chen, H. Y.; Chang, Y. L.; Hsu, S. C. N., Characterization of a new copper(I)-nitrito complex that evolves nitric oxide. *Inorg. Chem.* **2010**, 49, 5377-5384.
19. Bowmaker, G.; Hanna, J.; Hart, R.; Healy, P.; White, A., structural and spectroscopic studies on the dimeric complexes of tris(2-methylphenyl)phosphine with copper(I) halides. *Aust. J. Chem.* **1994**, 47, 25-45.
20. Mamais, M.; Cox, P. J.; Aslanidis, P., Three- and four-coordinate copper(I) halide complexes of 2-(diphenylphosphano)benzaldehyde: Dimerization induced by thione-S ligation. *Polyhedron* **2008**, 27, 175-180.
21. Blount, J. F.; Maryanoff, C. A.; Mislow, K., Molecular structure of trimesitylphosphine: An unprecedented enlargement of valence bond angles in a phosphine. *Tetrahedron Lett.* **1975**, 16, 913-916.
22. Alyea, E. C.; Ferguson, G.; Malito, J.; Ruhl, B., Monomeric (trimesitylphosphine)copper(I) bromide. X-ray crystallographic evidence for the first two-coordinate copper(I) phosphine halide complex. *Inorg. Chem.* **1985**, 24, 3719-3720.

23. Boéré, R. T.; Bond, A. M.; Cronin, S.; Duffy, N. W.; Hazendonk, P.; Masuda, J. D.; Pollard, K.; Roemmele, T. L.; Tran, P.; Zhang, Y., Photophysical, dynamic and redox behavior of tris(2,6-diisopropylphenyl)phosphine. *New J. Chem.* **2008**, *32*, 214-231.
24. Sasaki, S.; Sutoh, K.; Murakami, F.; Yoshifuji, M., Synthesis, structure, and redox properties of the extremely crowded triarylphosphines: Tris(2,4,6-triisopropylphenyl)phosphine, arsine, stibine, and bismuthine. *J. Am. Chem. Soc.* **2002**, *124*, 14830-14831.
25. Sasaki, S.; Yoshifuji, M., Synthesis, structure and properties of crowded triarylphosphines. *Curr. Org. Chem.* **2007**, *11*, 17-31.
26. Bullock, J. P.; Bond, A. M.; Boéré, R. T.; Gietz, T. M.; Roemmele, T. L.; Seagrave, S. D.; Masuda, J. D.; Parvez, M., Synthesis, characterization, and electrochemical studies of PPh₃-_n(dipp)_n (dipp = 2,6-diisopropylphenyl): steric and electronic effects on the chemical and electrochemical oxidation of a homologous series of triarylphosphines and the reactivities of the corresponding phosphoniumyl radical cations. *J. Am. Chem. Soc.* **2013**, *135*, 11205-11215.
27. Dyason, J. C.; Healy, P. C.; Engelhardt, L. M.; Pakawatchai, C.; Patrick, V. A.; Raston, C. L.; White, A. H., Lewis-base adducts of group-1b metal(I) compounds synthesis, structure, and solid-state P-31 nuclear magnetic-resonance spectra of some novel Cu₄X₄L₄ (X = halogen, L = N, P base) cubane clusters. *J. Chem. Soc., Dalton Trans.* **1985**, 831-838.
28. Churchill, M. R.; Deboer, B. G.; Donovan, D. J., Molecules with an M₄X₄ core crystallographic detection of a step configuration for Cu₄I₄ core in tetrameric triphenylphosphinecopper(I) iodide, PPh₃CuI₄. *Inorg. Chem.* **1975**, *14*, 617-623.
29. Hadjikakou, S. K.; Antoniadis, C. D.; Aslanidis, P.; Cox, P. J.; Tshipis, A. C., An exploration of the structural and bonding variability in mixed-ligand benzimidazole-2-thione(bromo)(triarylphosphane)dicopper(I) complexes with diamond-shaped Cu-2(μ-X)(2) core structures. *Eur. J. Inorg. Chem.* **2005**, 1442-1452.
30. Dračinský, M.; Buchta, M.; Buděšínský, M.; Vacek-Chocholoušová, J.; Stará, I. G.; Starý, I.; Malkina, O. L., Dihydrogen contacts observed by through-space indirect NMR coupling. *Chem. Sci.* **2018**, *9*, 7437-7446.
31. Bowmaker, G.; Camp, D.; Hart, R.; Healy, P.; Skelton, B.; White, A., Comparative structural studies on three-coordinate copper (I) halide complexes with tertiary phosphines. crystal structures of [(PPh₂Mes)CuX₂] and [(PPhMes₂)CuX₂] (Mes = Mesityl; X = Cl, Br, I). *Aust. J. of Chem.* **1992**, *45*, 1155-1166.
32. Qi, L.; Li, Q.; Hong, X.; Liu, L.; Zhong, X. X.; Chen, Q.; Li, F. B.; Liu, Q.; Qin, H. M.; Wong, W. Y., Synthesis, characterization and luminescent properties of three-coordinate copper(I) halide complexes containing 2-(diphenylphosphino)biphenyl. *J. Coord. Chem.* **2016**, *69*, 3692-3702.

33. Fleming, W. J.; Müller-Bunz, H.; Lillo, V.; Fernández, E.; Guiry, P. J., Axially chiral P-N ligands for the copper catalyzed β -borylation of α,β -unsaturated esters. *Org. Biomol. Chem.* **2009**, *7*, 2520-2524.
34. Chen, B.-L.; Liu, L.; Zhong, X.-X.; Asiri, A. M.; Alamry, K. A.; Li, F.-B.; Zhu, N.-Y.; Wong, W.-Y.; Qin, H.-M., Synthesis, characterization and luminescent properties of three-coordinate copper(I) halide complexes containing diphenylamino monodentate phosphine ligand. *J. Coord. Chem.* **2017**, *70*, 2916-2928.
35. Li, Q.; Wei, Q.; Xie, P.; Liu, L.; Zhong, X.-X.; Li, F.-B.; Zhu, N.-Y.; Wong, W.-Y.; Chan, W. T.-K.; Qin, H.-M.; Alharbi, N. S., Synthesis, characterization, and luminescent properties of three-coordinate copper(I) halide complexes containing a carbazolyl monodentate phosphine ligand. *J. Coord. Chem.* **2018**, *71*, 4072-4085.
36. Koradin, C.; Polborn, K.; Knochel, P., Enantioselective synthesis of propargylamines by copper-catalyzed addition of alkynes to enamines. *Angew. Chem., Int. Ed.* **2002**, *41*, 2535-2538.
37. Assadollahzadeh, B.; Schwerdtfeger, P., A comparison of metallophilic interactions in group 11[X-M-PH₃]_n (n=2-3) complex halides (M=Cu, Ag, Au; X=Cl, Br, I) from density functional theory. *Chem. Phys. Lett.* **2008**, *462*, 222-228.
38. Dem'yanov, P. I.; Polestshuk, P. M.; Kostin, V. V., The nature of metal-metal interactions in dimeric hydrides and halides of group 11 elements in the light of high level relativistic calculations. *Chem. - Eur. J.* **2017**, *23*, 3257-3261.
39. Fujihara, T.; Semba, K.; Terao, J.; Tsuji, Y., Copper-catalyzed hydrosilylation with a bowl-shaped phosphane ligand: Preferential reduction of a bulky ketone in the presence of an aldehyde. *Angew. Chem., Int. Ed.* **2010**, *49*, 1472-1476.
40. Hadjikakou, S. K.; Akrivos, P. D.; Karagiannidis, P.; Raptopoulou, E.; Terzis, A., Study of the geometric preferences of copper(I) halide coordination-compounds with triarylphosphines - crystal-structures of [CuCl(P(*o*-Tolyl)₃)]₂ and [CuBr(P(*o*-Tolyl)₃)]₂. *Inorg. Chim. Acta* **1993**, *210*, 27-31.
41. Bowmaker, G. A.; Engelhardt, L. M.; Healy, P. C.; Kildea, J. D.; Papasergio, R. I.; White, A. H., Lewis-base adducts of group-11 metal(I) compounds. 32. steric effects in the 2-1-adducts of (2-methylphenyl)diphenylphosphine with copper(I) halides. *Inorg. Chem.* **1987**, *26*, 3533-3538.
42. Hashimoto, M.; Igawa, S.; Yashima, M.; Kawata, I.; Hoshino, M.; Osawa, M., Highly efficient green organic light-emitting diodes containing luminescent three-coordinate copper(I) complexes. *J. Am. Chem. Soc.* **2011**, *133*, 10348-10351.
43. Chaudhuri, P.; Nazari Verani, C.; Bill, E.; Bothe, E.; Weyhermüller, T.; Wieghardt, K., Electronic structure of bis(*o*-iminobenzosemiquinonato)metal complexes (Cu, Ni, Pd). The art of establishing physical oxidation states in transition-metal complexes containing radical ligands. *J. Am. Chem. Soc.* **2001**, *123*, 2213-2223.

44. Yeh, W. Y.; Liu, Y. C.; Peng, S. M.; Lee, G. H., Syntheses, characterization and crystal structures of copper(I) o-(diphenylphosphino)benzaldehyde complexes. *Inorg. Chim. Acta* **2005**, *358*, 1987-1992.
45. Davis, P. H.; Belford, R. L.; Paul, I. C., Crystal and molecular-structure of bromobis(triphenylphosphine)copper(I) hemibenzenate. *Inorg. Chem.* **1973**, *12*, 213-218.
46. Williams, M. L., Boyd, S. E., Dunstan, S. P. C., Slade, D. L., Healy, P. C., Bromo[(diphenylphosphino-P)(diphenylphosphinoyl)methane]gold(I) acetonitrile solvate. *Acta Cryst.* **2003**, E59, m768-m770.
47. Demel, P.; Keller, M.; Breit, B., o-DPPB-directed copper-mediated and -catalyzed allylic substitution with grignard reagents. *Chem. - Eur. J.* **2006**, *12*, 6669-6683.

Chapter 3 Preparation and isolation of 2-amidinopyridine and 2-amidinopyrimidine

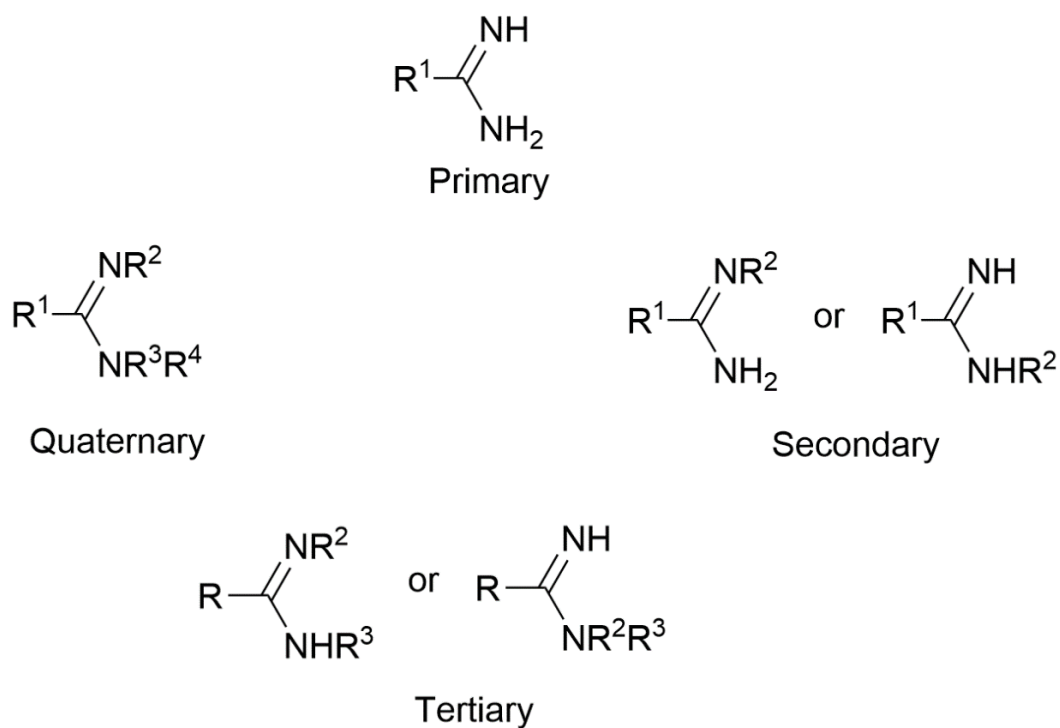
This chapter covers the synthesis and isolation of pyridine and pyrimidine substituted primary amidines (formally known as carboximidamides) via robust simple and convenient pathways. Herein, the syntheses and characterizations of the HCl salt and chloride and carbonate mixed salts of 2-amidinopyridine; the 2-amidinopyrimidine HCl salt as well as the isolation of the free primary amidine bases without sublimation is established which are important precursors to asymmetric imidoamidines (Chapter 4).

3.1 Introduction

Amidines are nitrogen containing strong bases that are isoelectronic to carboxylic acids. As classified in Scheme 3.1, they contain an imino and amino nitrogen with various substituent groups. The vast majority of primary amidine structures in the Cambridge Crystallographic Database (CSD) are salts or metal adducts while only ten free-base primary amidines have been reported. They are important intermediates in the synthesis of numerous heterocyclic molecules and materials with applications ranging from medicine¹⁻⁴ to molecular electronics⁵⁻⁶.

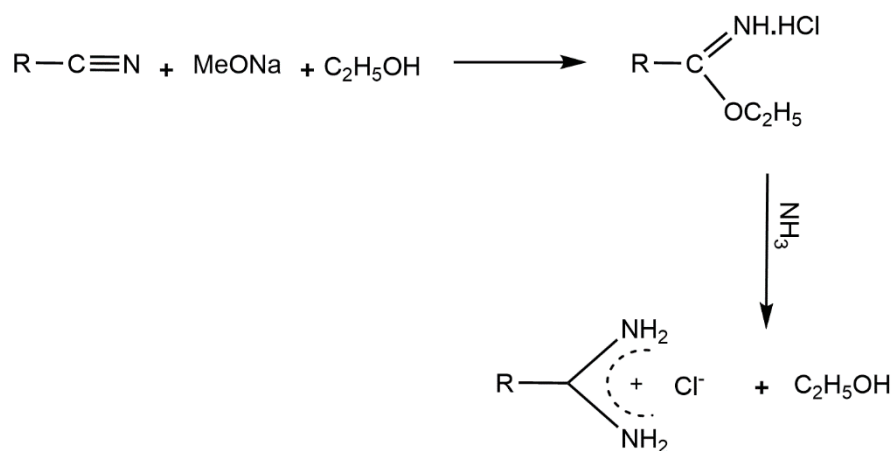
Various routes have been considered in the literature for the synthesis and isolation of substituted free-base primary amidines of alkyl⁷⁻⁸ and aryl⁹⁻¹⁰ including pyrimidine¹¹ and their structures have been reported. However, a 2-pyridine substituted primary amidine has not been published. Its hydrochloride salt¹² and those of the 3-¹³ and 4-pyridine¹⁴ analogs have been synthesized and characterized. Primary amidine synthesis usually starts with the nitrile (R-CN, where R = alkyl, aryl etc.) of the targeted unsubstituted amidines to be produced.

Primary amidines are often handled as hydrochloride salts due to instability of the free base towards hydrolysis. Preparation of primary alkyl- and aryl-substituted amidine hydrochlorides by the Pinner method¹⁵ is well known.^{8, 16-17} This involves the treatment of the nitrile with dry hydrogen chloride in anhydrous alcohol to form imidic ester hydrochloride which is then converted to the amidine hydrochloride on reaction with alcohol (ethanol or methanol) solutions of ammonia (Scheme 3.2). Aside from hydrogen chloride, which is the most common acid, hydrogen bromide also works perfectly. Many researchers have modified the Pinner method using sodium methoxide and ammonium chloride instead of using ammonia as a more convenient method for amidine hydrochloride synthesis.^{12, 14, 18}



$\text{R}^1\text{-R}^4$ = Alkyl, aryl, halogen or heterocycles

Scheme 3.1. Classification of amidines

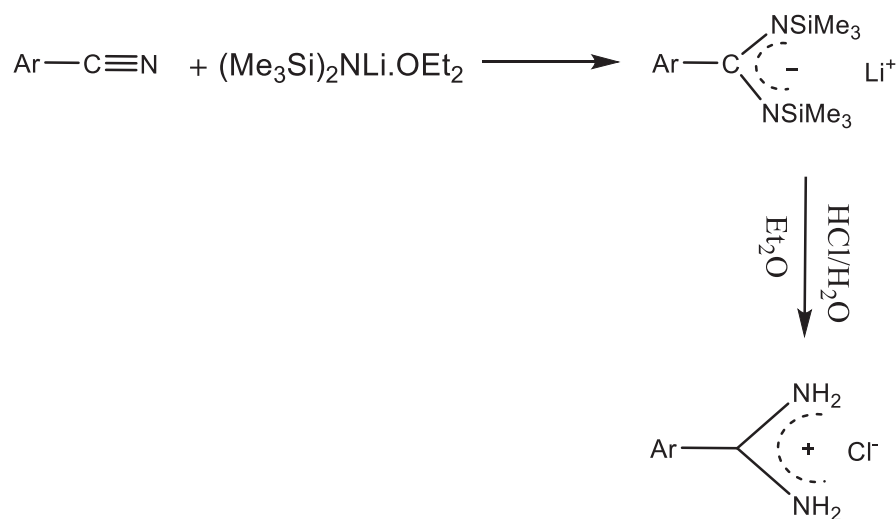


Scheme 3.2. Pinner reaction pathway for the synthesis of unsubstituted amidines

A series of amidine hydrochlorides have also been generated from lithium silylated amidine intermediates¹⁹⁻²¹. According to Boéré et al.¹⁹ as depicted in Scheme 3.3, hydrolysis of lithiated amidine $[\text{R}-\text{C}(\text{NSiMe}_3)_2^- \text{Li}^+]$ intermediate generated from the reaction of the proposed amidine nitrile with a crystalline ether adduct of lithium bis(trimethylsilyl)amide, $(\text{Me}_3\text{Si})_2\text{NLi}\cdot\text{OEt}_2$, or the persilylated amidine by reacting with ethanolic hydrochloric acid, produces the corresponding amidine hydrochlorides. Larger scales for this reaction tend to give higher yields. The method is applicable to nitriles having no chlorine or α -hydrogen atoms. This procedure has become a standard approach for many amidines but only works with aromatics (Ar) and some alkyls lacking alpha-protons like *tert*butyl.

Recently, pyrimidine-2-carboximidamide was inadvertently synthesized in an attempt to prepare bis(2-pyrimidine)imidolyamidine by reacting pyrimidine carbonitrile with ammonia gas under pressure at around 110 °C.^{11, 22} The method requires the use of dried solvent (acetonitrile) and longer reaction time (72 h) to give a moderate yield of crude product, around 78%. However, this process is peculiar to pyrimidine-2-carboximidamide as a similar procedure tested by the same group for pyridine-2-carboximidamide resulted in di(2-pyrididyl)imidolyamidine.²³

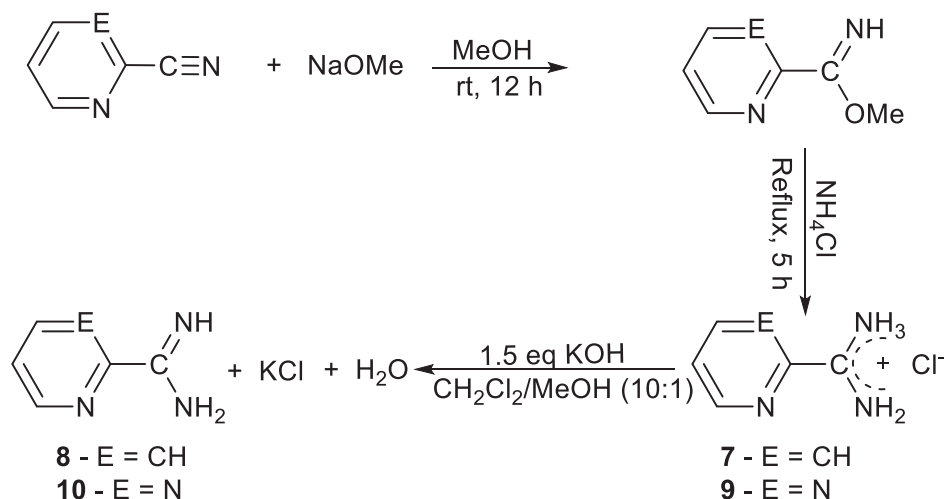
The free primary amidine bases are great synthons for production of essential organic molecules in pharmaceuticals and functional materials.^{8,24-25} By far the most common approach in the literature is *in situ* generation of the free amidine during reaction from its HCl salt in the presence of an inorganic base like K_2CO_3 in organic solvents.²⁶⁻²⁷ However, situations where a synthesis necessitates pure free amidine as a starting material, the route involves neutralization of the amidine.HCl salt hydrate with excess strong inorganic base (such as NaOH or KOH) in water; extraction in a suitable organic solvent; and the pure amidine is sublimed from an oily residue after removal of solvent. This method leads to low to moderate yields of amidine due to partial hydrolysis in the presence of water.²⁸ The production of imidoylamidines (Chapter 4) by direct condensation with nitriles requires the use of neutral primary amidines.¹⁷



Scheme 3.3. Synthesis of amidines via lithiated silylated amidine route

3.2 Results and discussion

3.2.1 Optimized synthesis of 2-amidinopyridine and isolation of its salts and mixtures



Scheme 3.4. Synthetic procedure for **8** and **10**

The 2-amidinopyridine hydrochloride (**7**) was prepared according to the synthetic route depicted in Scheme 3.4 with a slight modification of a previously published procedure for **8**. The method has been reported to result in a high yield of **7** (93%).¹² The 85% yield of **7** obtained by crystallization from the reaction solution by ether is close to those in literature even without switching reaction solvent from methanol to high boiling ethanol during synthesis as reported by Blumhoff et al.²⁹

Neutralization of **7** was undertaken to isolate 2-amidinopyridine (**8**) using a previously successful protocol of Boéré et al.²⁸ by employing 5 M of KOH in distilled water followed by extraction of **8** into dichloromethane. The bulk sublimation of a crude light-yellow oil for purification led to white crystalline material with a low yield. The limited yield is probably due to hydrolysis from excess water used to dissolve and force all the amidine hydrochloride into solution

as indicated by the yellow color of the final product reflecting a higher amount of impurities. The NMR analysis of the sublimed **8** (Figure 3.1) revealed traces of impurity suspected to be a mixture of 2-pyridine carbonitrile (annotated with *)^{19, 21, 30} and di(2-pyrididyl)imidolyamidine (#) (Chapter 4).¹¹ This issue might be due to partial thermal decomposition of **8** to nitrile and consequent reaction with amidine to produce di(2-pyrididyl)imidolyamidine. As a result, an alternative way was developed and optimized to avoid purification of **8** via sublimation which is leading to some decomposition. Various parameters including solvent, amount of KOH, reaction and workup steps were manipulated in the neutralization procedure. In the first approach, **7** was dissolved in a 1:10 ratio of methanol:dichloromethane and reacted with 2 equivalents solid KOH. The solution from the reaction, upon drying with MgSO₄ and filtering, and the removal of solvent, led to a white crystalline product with high yield (above 70%). This procedure works perfectly for small scales in the range of 0 – 0.5 g but failed for 1.0 g of **7** as confirmed by a ¹H NMR experiment (Figure 3.2) of the final product.

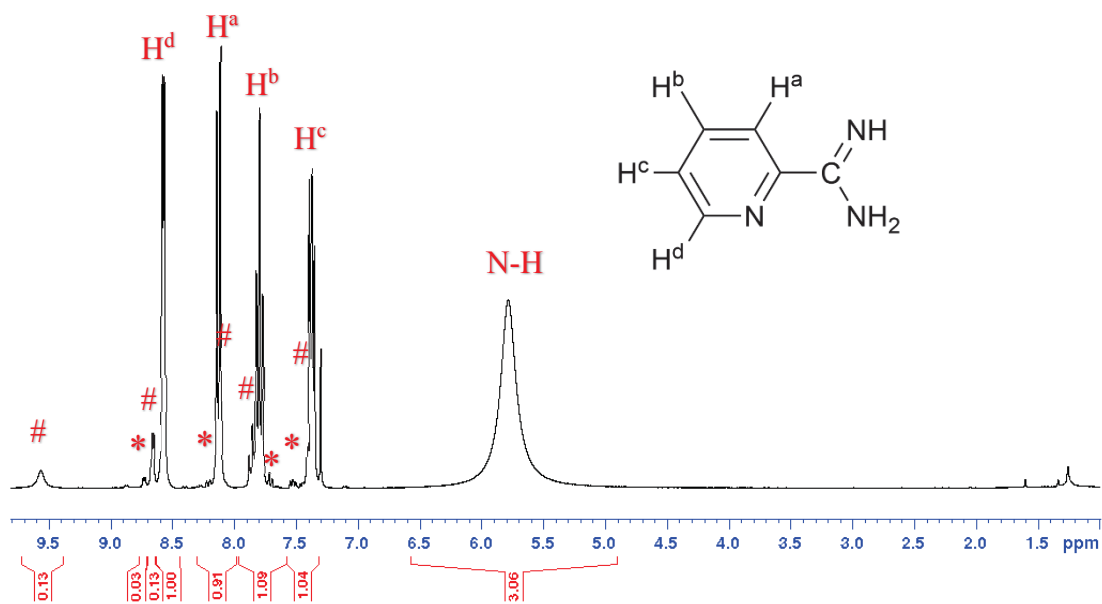
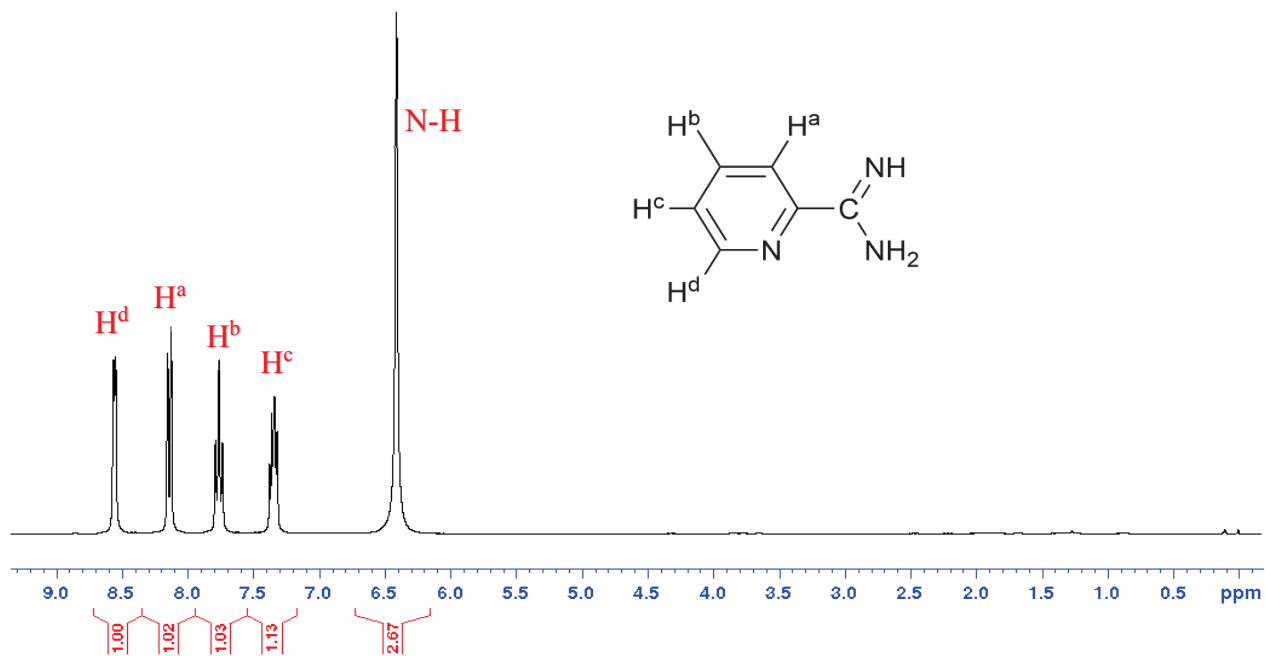


Figure 3.1. The ¹H NMR spectrum of sublimed **8**. * and # are impurities.

(a)



(b)

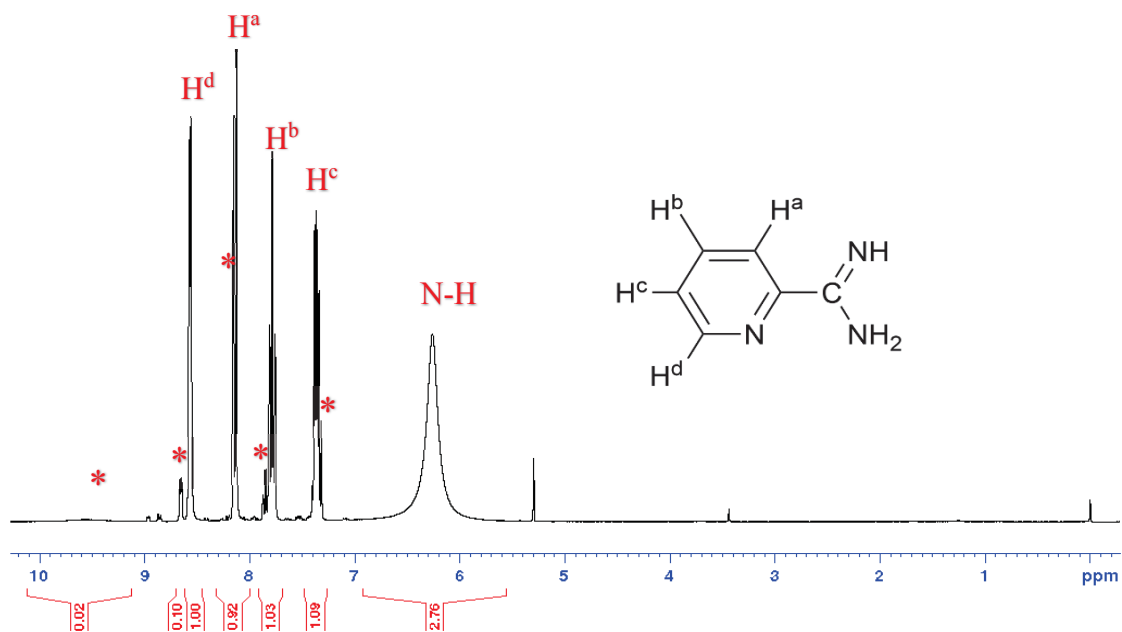


Figure 3.2. The ¹H NMR spectra of (a) 0.5 g and (b) 1.0 g scale of 7 for feasible neutralization with KOH in MeOH-DCM.

As shown in Figure 3.2a for the neutral product from 0.5 g amidine salt neutralization, there is no trace of any impurity in the aromatic region as only one set of peaks belong to a species, **8** is present in solution. However, switching to 1.0 g scale neutralization did not result to complete neutralization as small amount of amidine HCl salt (*) is still present with slight signals overlap with those of **8** (Figure 3.2b). This suggests the presence of 2-amidinopyridine hydrochloride salt–2-amidinopyridine (**7–8**) hemi–salt due to partial solubility of **7** in DCM which is also confirmed with single crystal X-ray structural determination (see section 3.3.2). After several trials, high purity **8** was finally produced by first executing the neutralization of **7** with 1.5 equivalent KOH in MeOH within 5 min to prevent hydrolysis of **8**³¹ by co-product water molecules through quick extraction into DCM. The entire process led to a colourless oil which gave off-white crystalline material when dried in frozen state. The procedure also performed excellently when used for large scale preparation of **8** which gave a clean NMR spectrum (Figure 3.3).

3.2.2 2-Pyrimidylamidine and its hydrochloride salt

The synthetic strategy and its optimization employed for **7** and **8** was also applied to the preparation of 2-pyrimidineamidine hydrochloride (**9**) and subsequent neutralization of the salt to liberate the 2-pyrimidineamidine (**10**). Indeed, the method gave the required outcome with high yield (86.1%) which is slightly lower than that of **7** which may be ascribed to likely side reactions associated with **9** that cause a brown color in the solution from which the colorless crystals of the salt were grown by adding ether. When **9** was neutralized as earlier described, a brownish material was obtained from which colorless crystals of **10** were grown by slow cooling from 1:10 MeOH–DCM since it is not quite soluble in DCM. The NMR analysis of the crystals gave clean spectra confirming high purity of its isolation as depicted in Figure 3.4 with residual solvent peaks annotated with *.

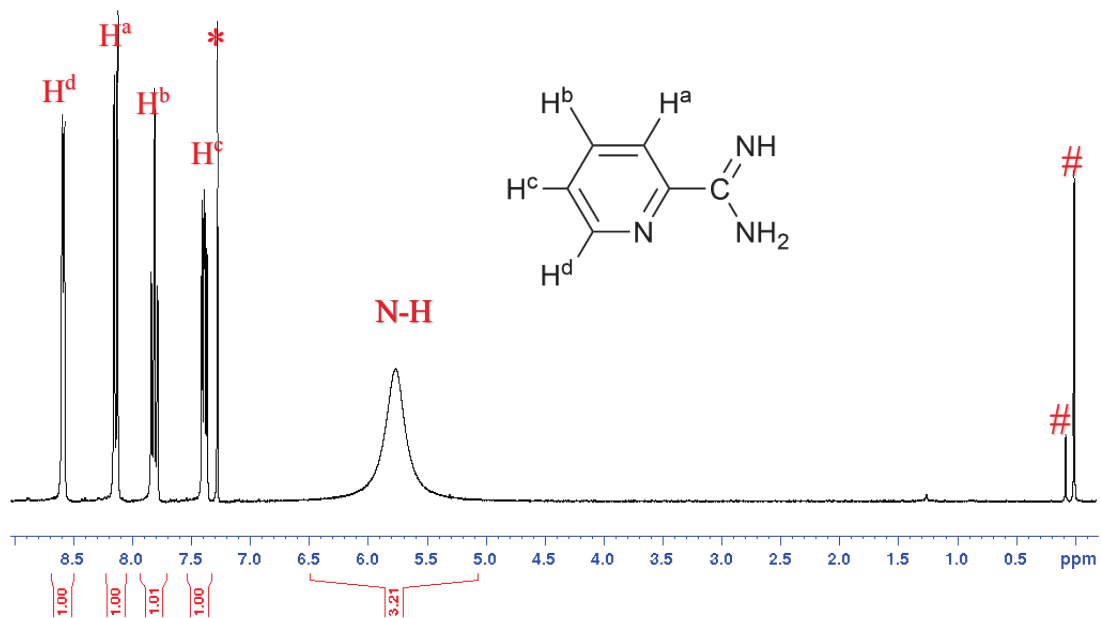


Figure 3.3. The ^1H NMR spectrum of **8** obtained by DCM extraction from MeOH neutralization of 10 g scale of **7**. * is solvent and # is TMS and silicone grease.

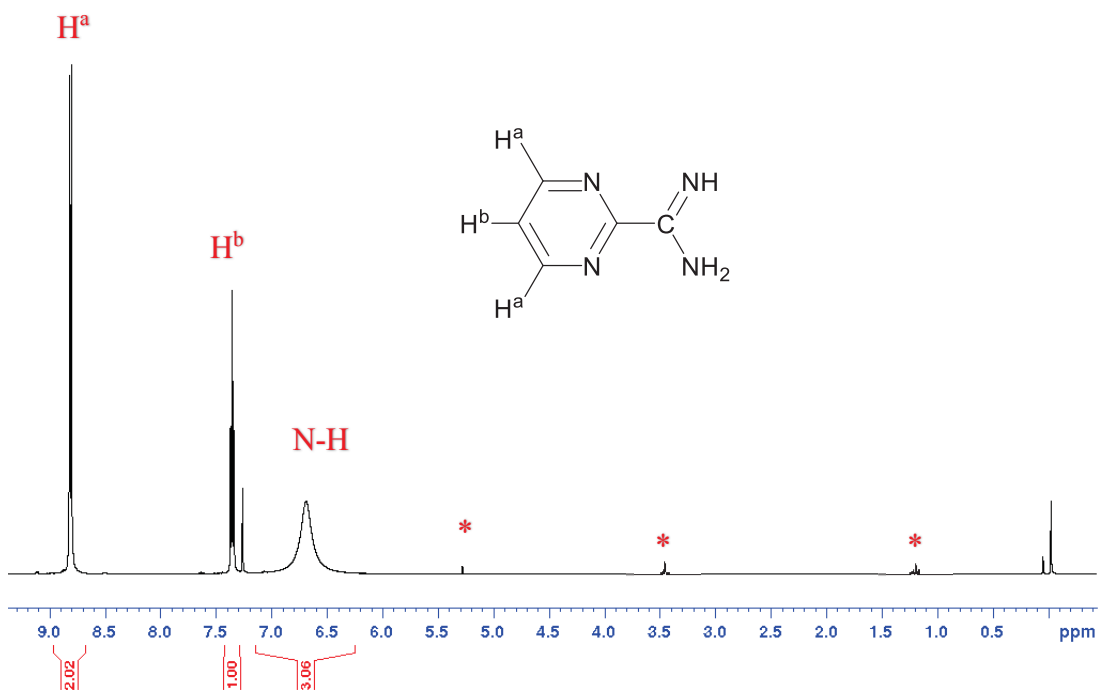
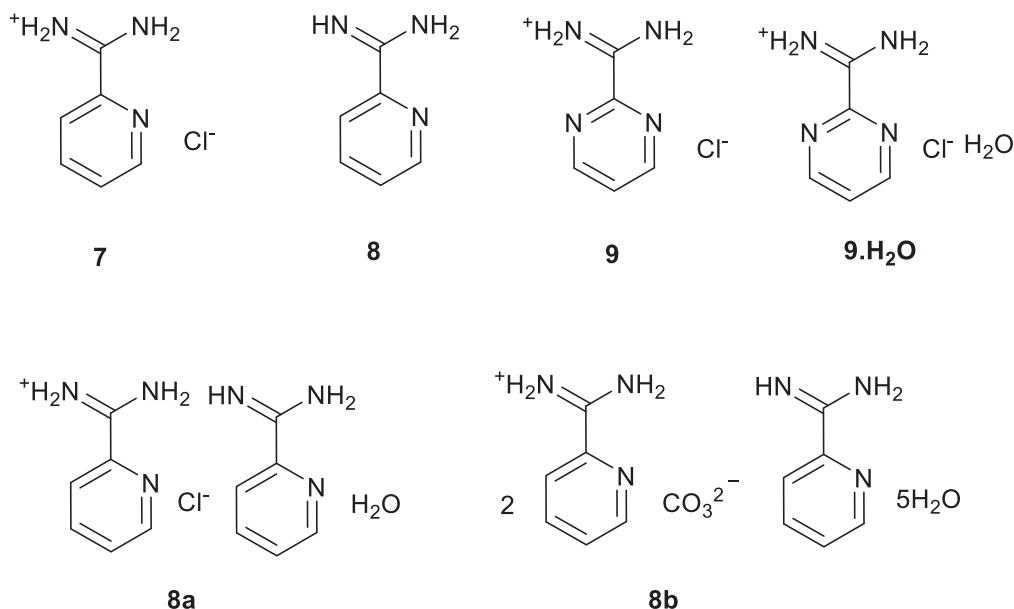


Figure 3.4. The ^1H NMR spectrum of **10**. (The signals label * belong to residual solvents.)

A broad amidine group proton signal with approximately 3H integration is observed which is at a bit higher frequency (δ 6.69) compared to **8** (δ 6.0) due to the additional N at *ortho* position in the ring. Interestingly, the colorless plate-crystals obtained are contrary to the beige needles obtained from acetonitrile by Safin *et al.*²²

3.3 X-ray crystal structures of amidine salts and the free amidines



Scheme 3.5. Structures of amidines and salts as found in crystal structures.

During the synthesis of the amidine hydrochlorides and the amidines, various crystals of good quality for X-ray analysis were recovered and analyzed to deduce their structures. Structures of the hemi-salts of 2-amidinopyridine–2-amidinopyridine hydrochloride dihydrate (**8a**) and 2-amidinopyridine–2-amidinopyridine cation dicarbonate pentahydrate (**8b**) were encountered during the optimization of the neutralization methodology (Scheme 1.5). It is important to note that amidines and their hydrochloride salts are not stable in air, with an intrinsic ability to rapidly abstract moisture and carbon dioxide from ambient environment thus forming hydrated and/or carbonated adducts.³² Moreover, the anhydrous structure of unreported **7** is first obtained but it

was observed that it converted to the known hydrate, $7 \cdot \text{H}_2\text{O}$ [WADPUO]¹² which was identified by screening the crystals that showed the same unit cell. The structure of **9** and its hydrated form ($9 \cdot \text{H}_2\text{O}$) were similarly obtained. Solid state recrystallization or transformation of **7** and **9** to their hydrates occur by picking up water on leaving the crystals at room temperature, and they are also generated by slow evaporation of their ethanol solutions in air. It is necessary to mention that a structure of **10** was previously reported²¹ from powder X-ray studies and is essentially identical to the one obtained in this work. The analysis of the structure as well as its supramolecular network had been extensively discussed by Safin et al.²²

3.3.1 Crystal structures of amidinium chlorides **7**, **9** and $9 \cdot \text{H}_2\text{O}$

Compound **7** crystalizes with one formula unit in the orthorhombic space group *Fdd2* with a total of sixteen formula (*Z*) units and one asymmetric formula (*Z'*) unit in its unit cell, while **9** and $9 \cdot \text{H}_2\text{O}$ crystalize with two formula units (with two of the Cl atoms having half occupancy each due to site symmetry occupancies) and one formula unit in the monoclinic space group *C2* with a *Z* = 8 (and *Z'* = 2) and *P2/n* with *Z* = 4 (and *Z'* = 1) in their unit cells, respectively (Chapter 6). The asymmetric units of **7** and **9** are presented in Figures 3.5 while that of $9 \cdot \text{H}_2\text{O}$ in Figure 3.6. Selected bond lengths and angles together with their standard uncertainties are given in Table 3.1. The $-\text{C}(\text{NH}_2)_2^+$ of **7** and **9** are twisted out of plane of the rings with average N1–C1–C2–N3 torsional angles of $13.0(5)^\circ$ and $11.7(4)^\circ$ respectively. These values are lower than the range of $17.8(2)^\circ$ – $33.2(2)^\circ$, $36.7(3)^\circ$ – $37.8(3)^\circ$ and 23.2° – 30.4° recorded in related structures of WADPUO¹², pyridine-3-carboxamidinium ion by Liu et al.¹³ and benzaminium salts³³ respectively. Amidinium cation systems possessing *ortho* protons on aromatic substituents are usually nonplanar as a result of steric repulsion of the amidine group and H atoms which overcome a low rotational barrier of the C–C bond (C1–C2, Table 3.1) connecting the two moieties. The

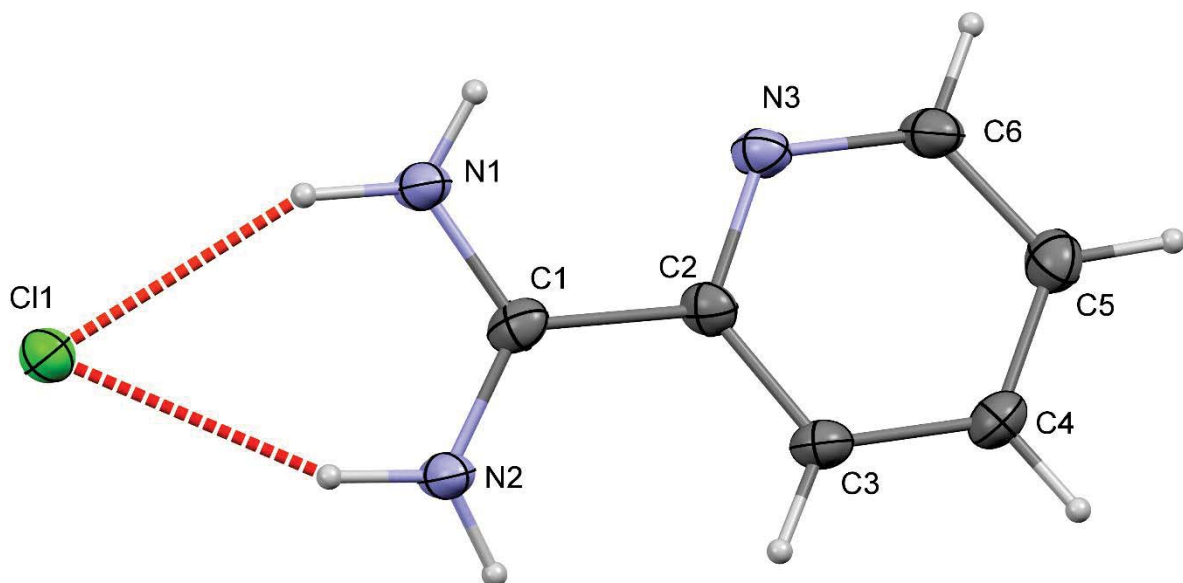
amidinium group in **9**.H₂O is approximately planar with N1–C1–C2–N3 and N1–C1–C2–N4 torsion angles of 0.3 (1) and 0.4 (1)°, respectively, which seems to be an unusual configuration for small molecules of protonated amidine cations but particular to amidiniums with larger substituents.³⁴ These values are comparable to the dihedral angles of 0.5(2)° and 0.7(2)° for N1–C1–C2–N3 and N1–C1–C2–N4 respectively found in benzamidium dilaurate by Portalone *et al.*³³ Overall, the C–N (N1–C1 and N2–C1) bond distances are the same in all three structures as expected which implies the delocalization of π electrons as well as sp² character in the N–C–N unit.

Table 3.1. Selected bond parameters in **7**, **9** and **9**.H₂O (using atomic the numbering scheme in Figure 3.5a).

Compound	7	9	9 .H ₂ O	WADPUO ¹²
N1–C1 (Å)	1.308(5)	1.303(4) ^a 1.300(4) ^b	1.307(1)	1.307(2) ^a 1.302(2) ^b 1.309(3) ^c
N2–C1 (Å)	1.319(4)	1.316(3) ^a 1.310(4) ^b	1.312(1)	1.311(2) ^d
C1–C2 (Å)	1.492(5)	1.495(3) ^a 1.504(4) ^b	1.498(1)	1.492(2) ^a 1.487(2) ^b 1.485(2) ^c
N1–C1–N2 (°)	120.5(3)	121.8(2) ^a 124.8(3) ^b	122.34(8)	122.6(2) ^a 122.0(2) ^b 122.8(2) ^c
N1–C1–C2–N3 (°)	13.0(5)	11.5(4) ^a 11.8(4) ^b	0.3(1)	17.8(2) ^a 29.8(2) ^b 33.2(2) ^c
N2–C1–C2–C3/N4 (°)	14.2(5)	21.4(4) ^a 20.0(4) ^b	0.4(1)	19.22(2) ^a 31.2(2) ^b 34.5(2) ^c

^a First molecule; ^b second molecule; ^c third molecule; ^d all molecules.

a



b

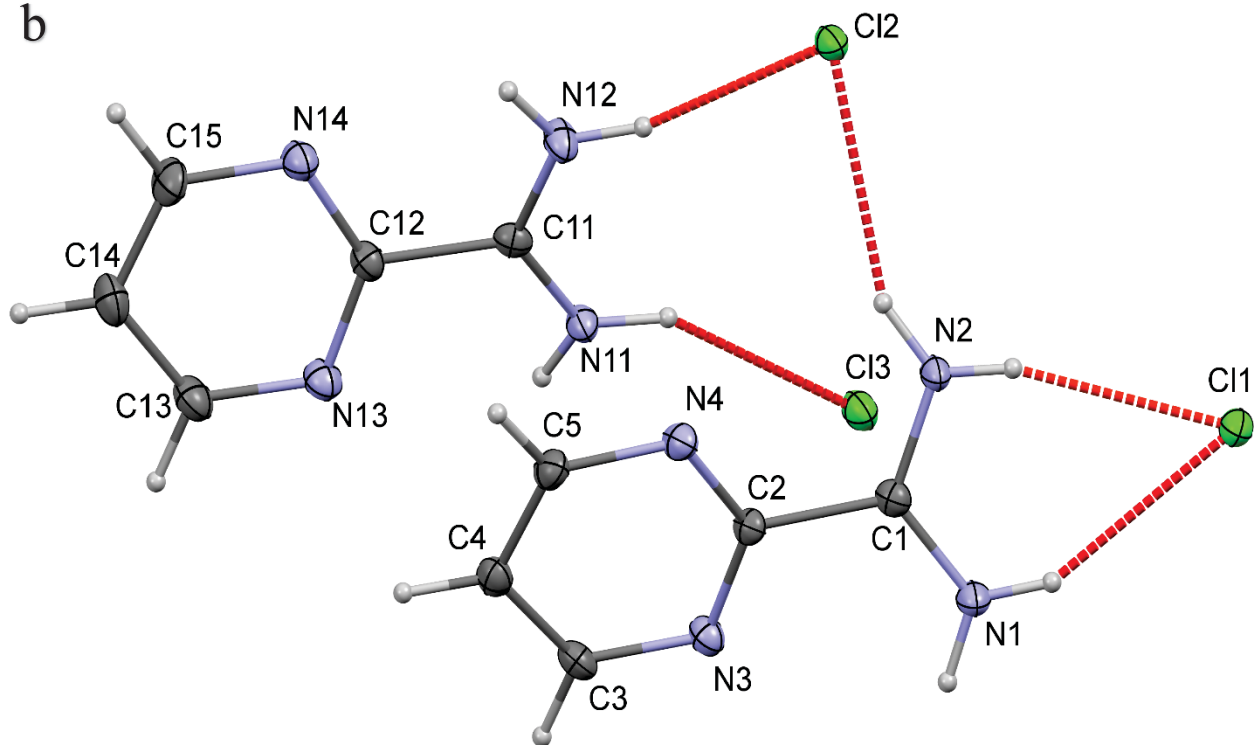


Figure 3.5. The asymmetric units of (a) **7** and (b) **9** showing the atom-labelling schemes and hydrogen bonding indicated with dashed lines. Displacement ellipsoids are drawn at 50% probability level and H atoms are shown as small spheres of arbitrary radii. In **9**, both Cl1 and Cl2 atoms have 50% occupancies.

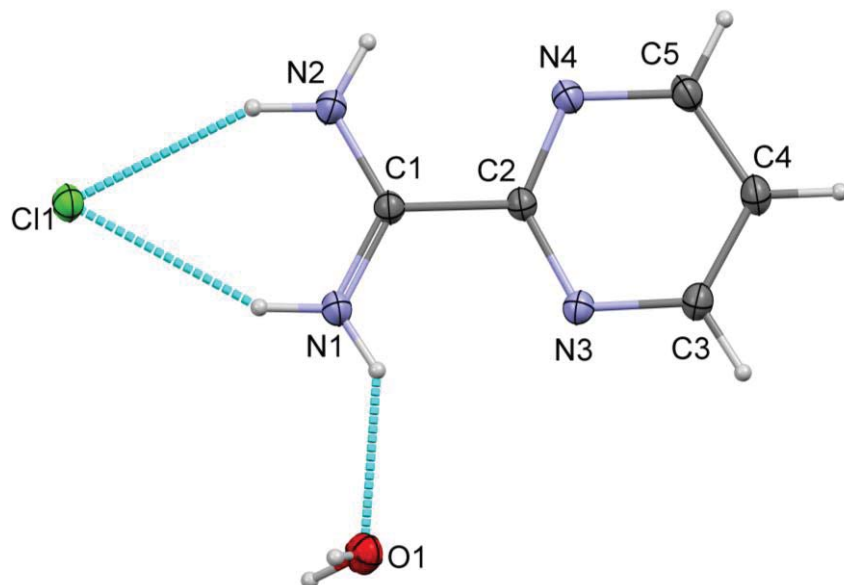


Figure 3.6. The asymmetric unit of **9**.H₂O showing the atom-labelling scheme and hydrogen bonding indicated with dashed lines. Displacement ellipsoids are drawn at 50% probability level and H atoms are shown as small spheres of arbitrary radii.

The amidinium N–H are well known hydrogen bond donors, and all three structures are linked together with charge-assisted hydrogen bond (CAHB) networks. As demonstrated in Figures 3.5, the asymmetric units of **7**, **9** and **9**.H₂O display one bifurcated (in which one Cl atom is connected to two N acceptor atoms) H–bond connecting the amidinium fragment of the molecules to acceptor chloride anion with two N⁺–H...Cl[−] CAHB generating a graph-set motif of $R_2^1(6)$. Besides, **9** contains additional 3 N⁺–H...Cl[−] H–bonds with graph set motifs of $D_2^1(5)$ and $D_1^1(3)$ and **9**.H₂O is further connected to O atom of water by N⁺–H...O.

The extensive supramolecular networks in the crystal packing of the structures were analyzed using a substructural approach within the unit cell. In the packing diagram of **7** (Figure 3.7), three distinctive N⁺–H...Cl[−] and one N⁺–H...N intermolecular charge-assisted hydrogen bonds (CAHB) link the amidinium ions together (Table 3.2). Each amidinium ion is attached to

two chloride ions by three moderate electrostatic N⁺–H...Cl⁻ [range of 3.145(3) – 3.216(3) Å] hydrogen bond interactions. One amidinium ion is connected to another via a moderate N⁺–H...N [2.912(4) Å] contact resulting in the formation of graph sets R₂¹(6) and R₂²(10). The two rings of [R₂¹(6) and R₂²(10)] result in the formation of a one dimensional (1D) supramolecular polymeric chain along the *a* axis with one chloride ion connection. The second chloride ion extends the chain into two-dimensional (2D) H-bond network running across the *b* axis of the unit cell.

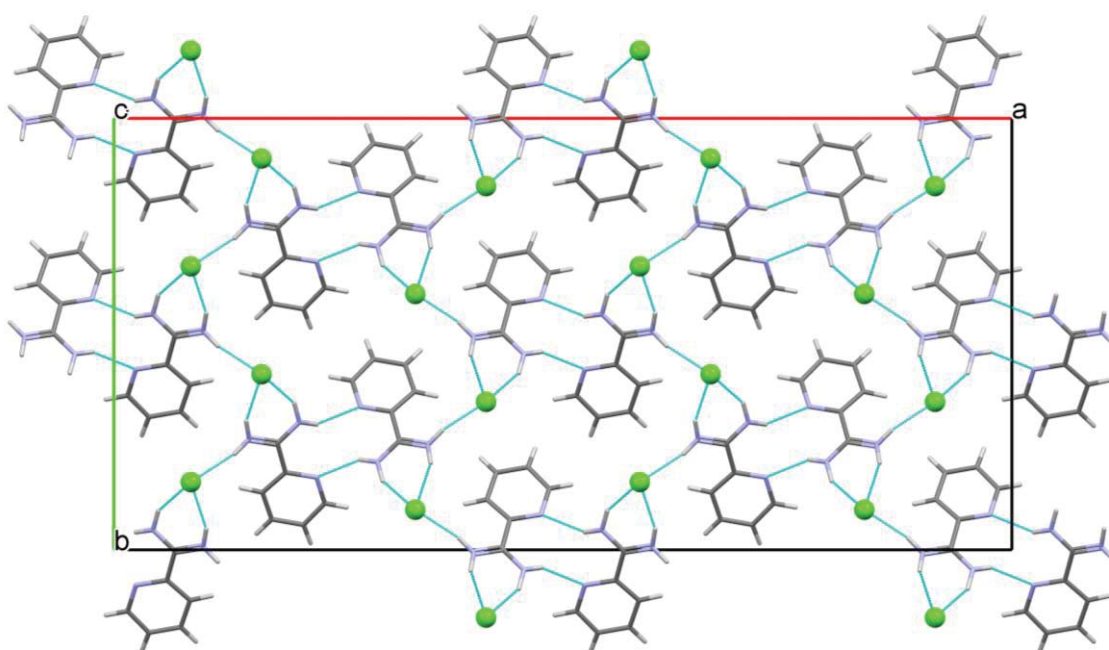


Figure 3.7. The crystal packing tube structure of **7** projected down *c* axis. Hydrogen bonding is indicated by green dashed lines. Cl are shown as green balls; N is blue; C is ash; and H is grey.

Table 3.2. Hydrogen bonds of **7**

D	H	A	d(D-H)/Å	d(H-A)/Å	d(D-A)/Å	D-H-A/°
N1	H1A	Cl1	0.93(4)	2.34(5)	3.185(3)	150(4)
N1	H1B	N3 ¹	0.84(5)	2.14(5)	2.912(4)	151(4)
N2	H2A	Cl1	0.90(5)	2.37(5)	3.216(3)	156(4)
N2	H2B	Cl1 ²	0.89(5)	2.28(5)	3.145(3)	166(4)

¹1-X,1-Y,+Z; ²5/4-X,1/4+Y,1/4+Z

The supramolecular framework of **9** demonstrates a complex H-bond arrangement involving combinations of seven $\text{N}^+-\text{H}\cdots\text{Cl}^-$ and three $\text{N}^+-\text{H}\cdots\text{N}$ donor–acceptor pairs as shown in Table 3.3 which produces a 2D network. There are two unique H-bond arrays relative to the two different amidinium ions in the structure as presented in Figure 3.8. These include the graph set motif $R_2^2(14)$ from four H-bonds formed by $\text{N}^+-\text{H}\cdots\text{N}$ intermolecular interactions in the amidinium group of the first independent ion and the N atoms of the aromatic ring in the second ion and the centrosymmetric subunit are organized with multiple $\text{N}^+-\text{H}\cdots\text{Cl}^-$ to form two bifurcated $R_2^1(6)$ and $R_4^2(8)$ graphs. The first generates infinite 1D chains of cations running parallel to *c* axis of the cell and the latter leads to the association of the chains into a 2D arrangement of H-bonds.

The molecules of **9**.H₂O are aggregated together with a combination of three $\text{N}^+-\text{H}\cdots\text{Cl}^-$, two $\text{O}-\text{H}\cdots\text{Cl}^-$, one $\text{N}^+-\text{H}\cdots\text{N}$ and one $\text{N}^+-\text{H}\cdots\text{O}$ CAHB (Table 3.4). Two centrosymmetric amidinium ions form a bifurcated ring motif [$R_2^1(6)$] with two $\text{N}^+-\text{H}\cdots\text{Cl}^-$ H-bonds connected to another via an $R_4^2(8)$ motif unit which is further linked to another subunit by an $R_5^3(10)$ motif (Figure 3.9b) involving water molecules and chloride ions with $\text{N}^+-\text{H}\cdots\text{O}$ and $\text{O}-\text{H}\cdots\text{Cl}^-$ CAHB. Both form a 1D chain ribbon propagating along the *c* axis which is further linked into a 2D sheet through a water molecule acting as an acceptor and a donor with $\text{O}-\text{H}\cdots\text{Cl}^-$ intermolecular interactions along the *b* axis. From this observation, the planarity of amidinium fragment in **9**.H₂O may be ascribed to the nature of H-bonding change in the presence of water molecule as compared to **9**. In the presence of water, the pyrimidine N atoms do not participate as an acceptor as seen in **9** which makes chloride ion a multiple H-bonds acceptor, whereas water acts as bifunctional donor-acceptor, forming larger $R_5^3(10)$ rings that stabilize the structure with consequent prevention of twisting in the amidinium group. This implies that the type of H-bonding framework might

contribute to the planarity of amidinium cation moiety in amidine salts in addition to the conventional theory of steric hindrance from *ortho* hydrogen atoms in the aromatic group.

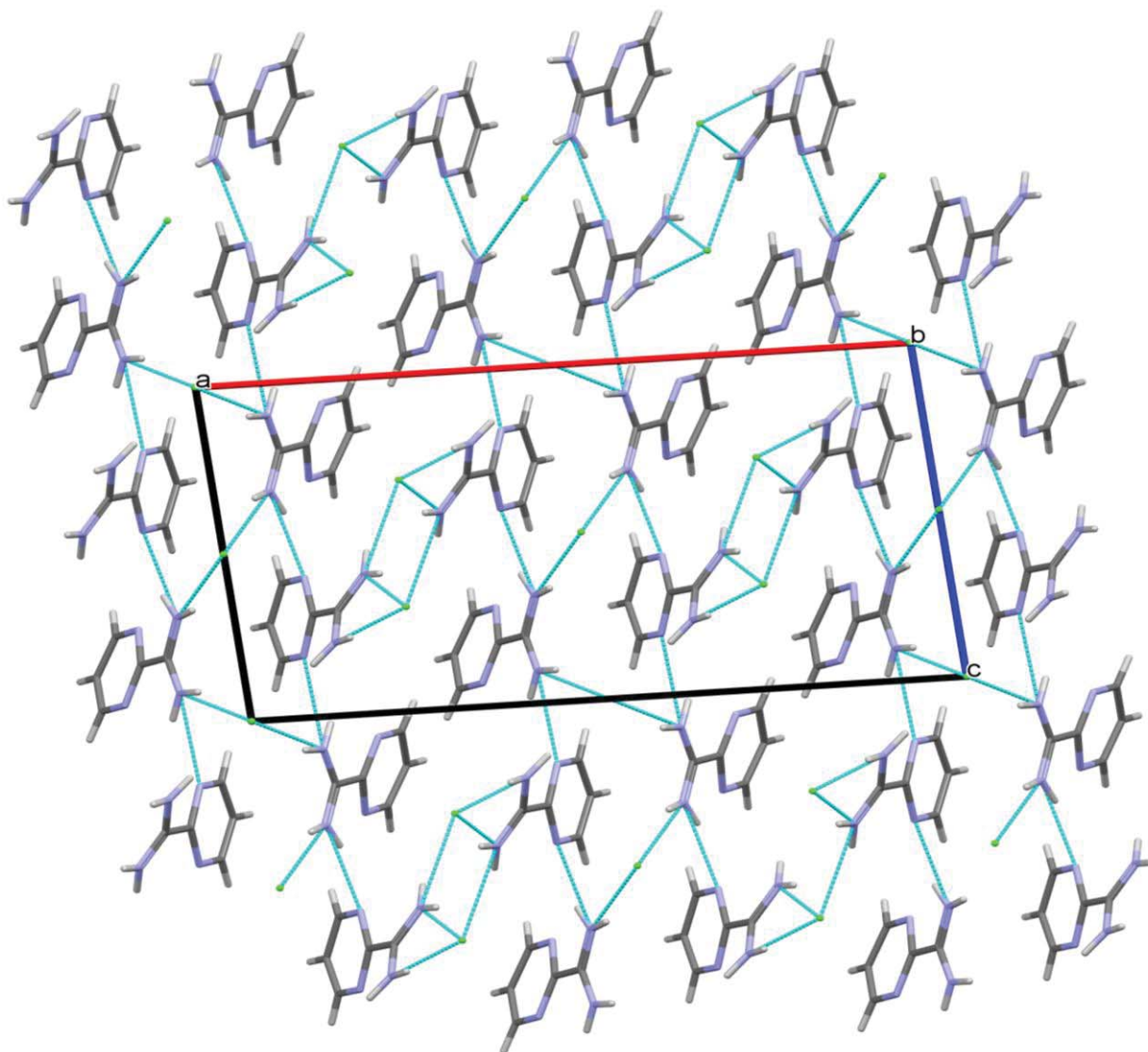


Figure 3.8. The crystal packing structure of **9** projected down *b*. Displacement ellipsoids drawn at the 50% probability level. Hydrogen bonding is indicated by blue dashed lines.

Table 3.3. Hydrogen bonds of **9**

D	H	A	d(D-H)/Å	d(H-A)/Å	d(D-A)/Å	D-H-A/°
N1	H1A	Cl1	0.82(4)	2.45(4)	3.198(3)	151(3)
N1	H1B	Cl1 ¹	0.87(4)	2.39(4)	3.155(2)	146(3)
N1	H1B	N11 ²	0.87(4)	3.24(3)	3.784(3)	123(3)
N2	H2A	Cl1	0.79(4)	2.36(4)	3.123(2)	163(3)
N2	H2B	Cl2	0.86(4)	2.53(4)	3.310(2)	151(3)
N2	H2B	N12 ³	0.86(4)	3.01(4)	3.642(3)	132(3)
N11	H11A	Cl3	0.88(4)	2.37(4)	3.158(2)	148(3)
N11	H11B	N3 ²	0.84(4)	2.17(4)	2.963(3)	158(3)
N12	H12A	Cl2	0.85(4)	2.35(4)	3.150(3)	155(3)
N12	H12B	N4 ³	0.87(4)	2.27(4)	3.047(3)	149(3)

¹1/2-X,1/2+Y,1-Z; ²1-X,+Y,1-Z; ³1-X,+Y,2-Z

Table 3.4. Hydrogen bonds of **9.H₂O**

D	H	A	d(D-H)/Å	d(H-A)/Å	d(D-A)/Å	D-H-A/°
O1	H1A	Cl1 ¹	0.800(16)	2.371(17)	3.1704(8)	177.5(14)
O1	H1B	Cl1 ²	0.850(16)	2.380(16)	3.2023(8)	162.8(14)
N3	H3A	Cl1	0.880(14)	2.439(14)	3.2358(8)	150.7(12)
N3	H3A	N3 ³	0.880(14)	3.224(14)	3.9433(16)	140.5(11)
N3	H3B	Cl1 ³	0.857(14)	2.593(14)	3.2294(8)	131.9(12)
N4	H4A	Cl1	0.871(13)	2.474(13)	3.2708(8)	152.3(12)
N4	H4B	O1	0.838(14)	2.108(14)	2.8205(11)	142.7(13)

¹3/2-X,-1/2+Y,1/2-Z; ²+X,-1+Y,+Z; ³2-X,2-Y,1-Z

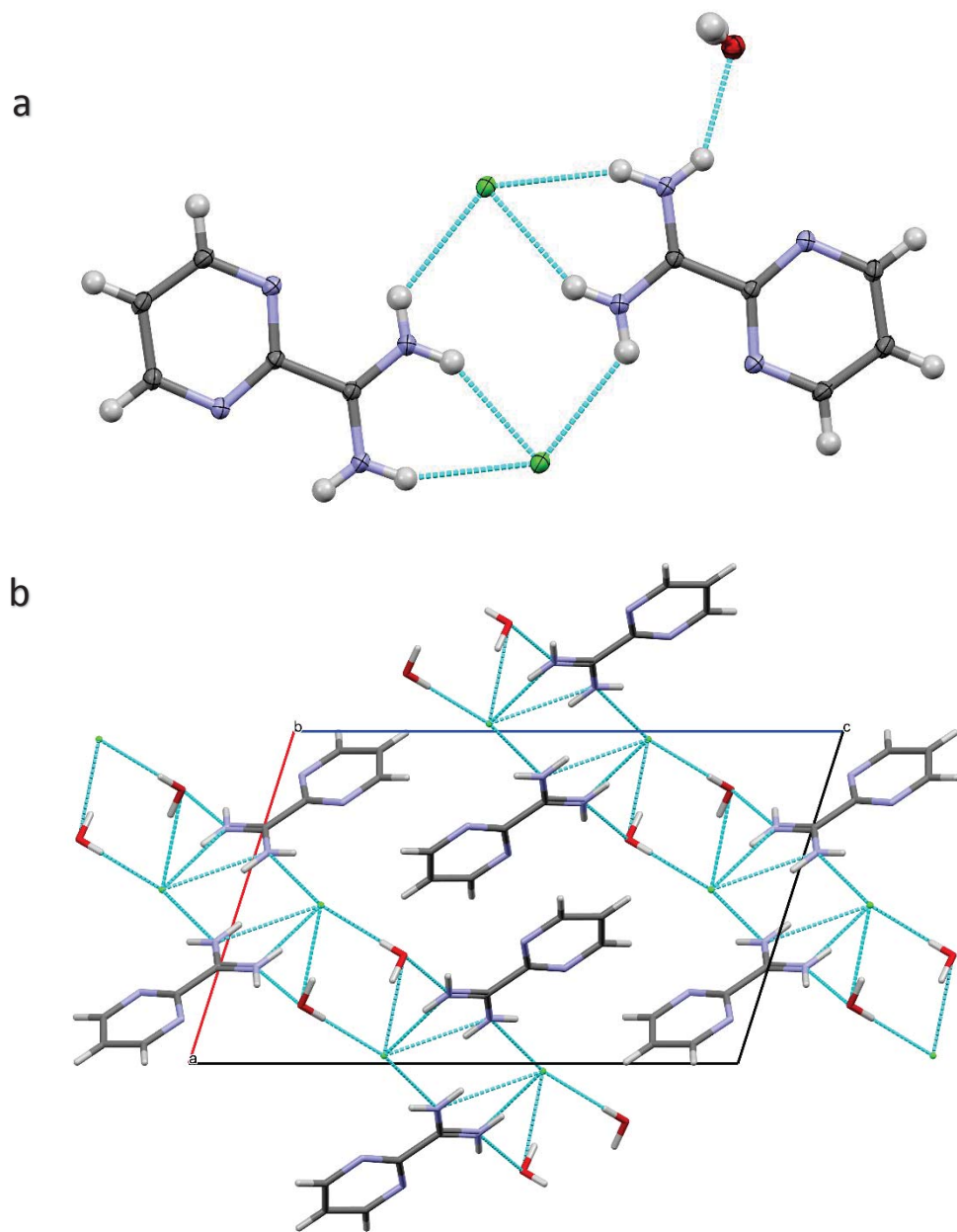


Figure 3.9. The (a) H-bond motif and (b) crystal packing structure of **9**.H₂O projected down *b*. Displacement ellipsoids drawn at the 50% probability level. Hydrogen bonding is indicated by green dashed lines.

3.3.2 Crystal structures of **8** and its hemi-amidinium chloride (**8a**) and carbonate (**8b**) salts

Compounds **8**, **8a** and **8b** crystalize in monoclinic space groups $I2/a$, $P2_1/n$ and $P2_1/c$, respectively (Chapter 6). Selected bond distances and angles of the molecules are presented in Table 3.5.

Selected bond parameters of **8**, **8a** and **8b** are highlighted in Table 3.5. The free amidines in all three structures demonstrate shorter $N1=C1$ and longer $N2-C1$ bond lengths as anticipated, and their amidinium ions have approximately the same $N2-C1$ distances due to π electron delocalization around the cationic fragments. The bond distances $C1-C2$ in all the compounds are not significantly different from one another. However, the average angle at $N1-C1-N2$ for **8**, $126.1(1)^\circ$ is larger than the one recorded for amidine [$121.00(9)^\circ$] and the cation [$122.10(9)^\circ$] as well as the average found in free amidine [$121.7(2)^\circ$] and in amidinium [$120.8(2)^\circ$] in **8b**. Likewise, significant discrepancies are observed in the degree of torsion of the amidine or amidinium cation moiety of identical molecules in the same crystal structure. For instance, in **8**, the average dihedral angles of $12.7(2)^\circ$, $5.7(2)^\circ$ and $3.0(2)^\circ$ recorded for the three independent molecules are substantially different from one another. Also, the two amidine molecules in **8b** exhibit $14.7(3)^\circ$ and $9.4(3)^\circ$ respectively differ from those in **8**. Of the four amidinium ions in **8b**, torsion of only two of them with average of $12.6(3)^\circ$ and $12.2(3)^\circ$ has some sort of similarity while the remaining two with average values of $19.0(3)^\circ$ and $24.2(3)^\circ$ are outliers. Some of the low torsion angle values, from $10.6(1)^\circ$ in **8a** to $12.6(3)^\circ$ in **8b**, recorded for the amidinium cations are somewhat unprecedented in protonated amidine salts (within $23.2 - 30.4^\circ$ or above).^{13,35} Thus, it implies that the claim of twisting in the $-C(HN-C=NH_2)$ group of protonated amidines associated with aromatic substituent having hydrogen atom next to the fragment is not hundred percent accurate. In the analyses of the H-bonding pattern in the crystal structures, it can be deduced that the packing

orientation of individual molecules as facilitated by the direction of hydrogen bonding play a key role in the rotation of $-\text{C}(\text{HN}=\text{C}=\text{NH}_2)$ parts of the compounds.

As illustrated in Figure 3.10, the asymmetric unit of **8** contains three independent 2-amidinopyridine molecules having discrete $\text{N}-\text{H}\cdots\text{N}$ H-bonds associating them together with $D_1^1(3)$ and $D_1^1(4)$ motifs which are one of the essential H-bonds found in **7** and other related analogs.⁹⁻¹⁰ However, the structure of **8a** demonstrates CAHB which is made up of an amidinium cation, a neutral amidine, a chloride ion and two water molecules (Figure 3.12). The two independent molecules are connected by $\text{N}^+-\text{H}\cdots\text{Cl}^-$, $\text{N}^+-\text{H}\cdots\text{N}$, $\text{N}-\text{H}\cdots\text{O}$ and $\text{N}^+-\text{H}\cdots\text{O}$ H-bonds forming two $R_3^2(8)$ graph set motifs in which the $\text{C}=\text{NH}$ of the free amidine participate as both donor and acceptor. The asymmetric component of **8b** consists of two sets of two amidinium ions, an amidine and a carbonate in addition to five molecules of water as shown in Figure 3.15. A closely related amidinium carbonate structure of acetamide has been reported by Norrestam³² which only contains amidinium ion, a carbonate and a water molecule. Meanwhile, protonated amidines practically form multiple H-bonds with oxygen-containing anions which are potential sites of accepting the charge donation. Each carbonate in the structure forms two $R_2^2(8)$ motifs with the two amidinium ions and a discrete connection with the free amidine as well as two water molecules via $\text{N}^+-\text{H}\cdots\text{O}$, $\text{N}-\text{H}\cdots\text{O}$ and $\text{O}-\text{H}\cdots\text{O}$ H-bonds. The two independent subunits are further linked together by two $\text{N}^+-\text{H}\cdots\text{N}$ H-bonds to form a web pattern with $R_2^2(10)$ motifs (Figure 3.16) as observed in **8**.

Table 3.5. Selected bond parameters of **8**, **8a** and **8b** (using atomic numbering scheme in the Figures).

Compound	8	8a	8b
N1–C1 (Å)	1.292(1) ^a	1.307(1) ^b	1.313(3) ^d
		1.288(1) ^c	1.283(3) ^a
N2–C1 (Å)	1.349(2) ^a	1.318(1) ^b	1.317(3) ^d
		1.347(1) ^c	1.359(3) ^a
C1–C2 (Å)	1.501(1) ^a	1.497(1) ^b	1.493(3) ^d
		1.504(1) ^c	1.511(3) ^a
N1–C1–N2 (°)	126.1(1) ^a	122.10(9) ^b	120.8(2) ^d
		121.00(9) ^c	121.7(2) ^a
$\frac{1}{2}$ [N1–C1–C2–N2 + N2–C1–C2–C3] (°)	12.7(2) ^a	10.6(1) ^d	19.0(3) ^d
	5.8(2) ^a	15.7(1) ^a	12.6(3) ^d
	3.0(2) ^a		24.2(3) ^d
			12.2(3) ^d
			14.7(3) ^a
			9.4(3) ^a

a = average amidine parameter; b = non-average amidinium parameter; c = non-average amidine parameter; and d = average amidinium parameter

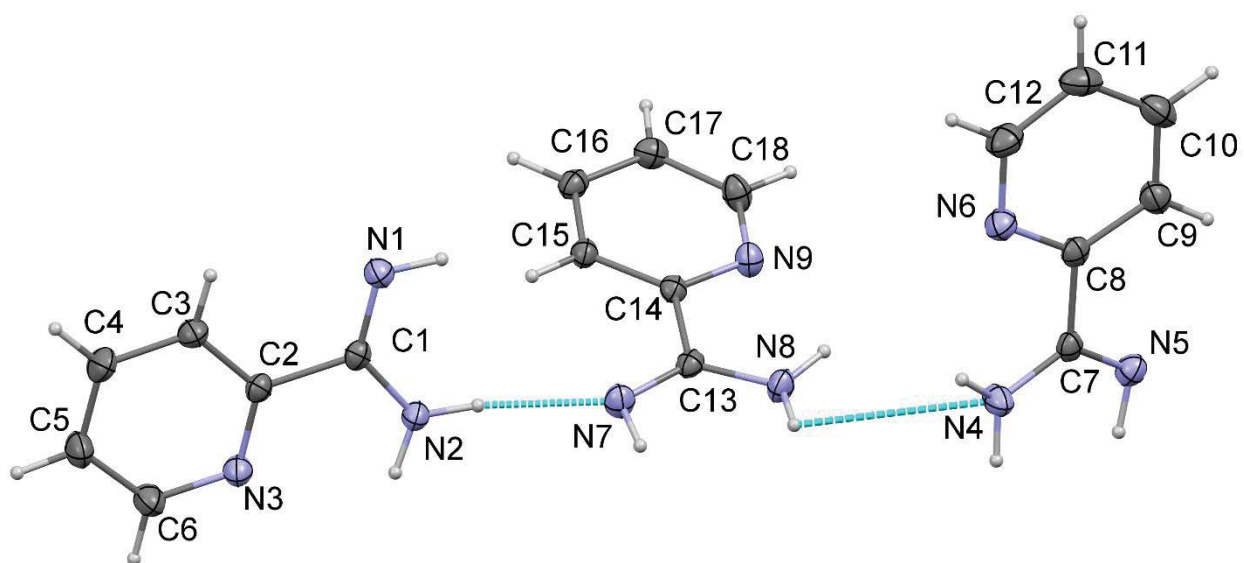


Figure 3.10. The asymmetric unit of **8** showing the atom-labelling scheme and with hydrogen bonding indicated with dashed lines. Displacement ellipsoids are drawn at 50% probability level and H atoms are shown as small spheres of arbitrary radii.

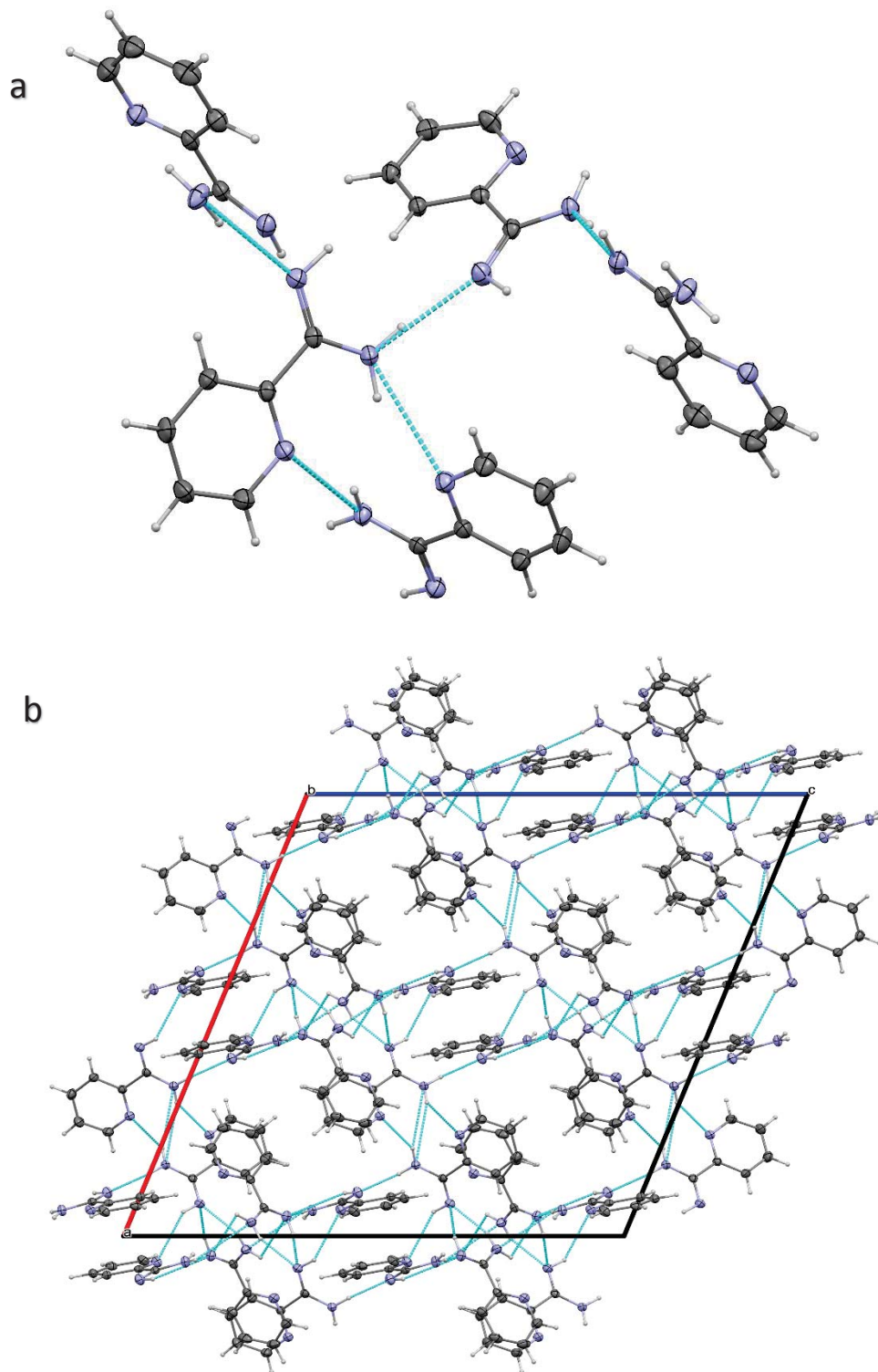


Figure 3.11. The H-bond motif (a) and crystal packing structure (b) of **8** projected down b. Displacement ellipsoids drawn at the 50% probability level. Hydrogen bonding is indicated by green dashed lines.

Table 3.6. Hydrogen Bonds of **8**

D	H	A	d(D-H)/Å	d(H-A)/Å	d(D-A)/Å	D-H-A/°
N2H2A	N1 ¹		0.913(15)	2.133(15)	3.0443(12)	174.8(12)
N2H2A	N2 ¹		0.913(15)	3.146(14)	3.8099(17)	131.2(10)
N2H2B	N3 ²		0.892(14)	3.087(13)	3.6660(13)	124.4(10)
N1H1	N2 ³		0.896(14)	2.836(13)	3.5159(12)	133.7(10)
N1H1	N3		0.896(14)	2.288(13)	2.7933(12)	115.5(10)

¹1-X,1-Y,2-Z; ²1+X,+Y,+Z; ³-1+X,+Y,+Z

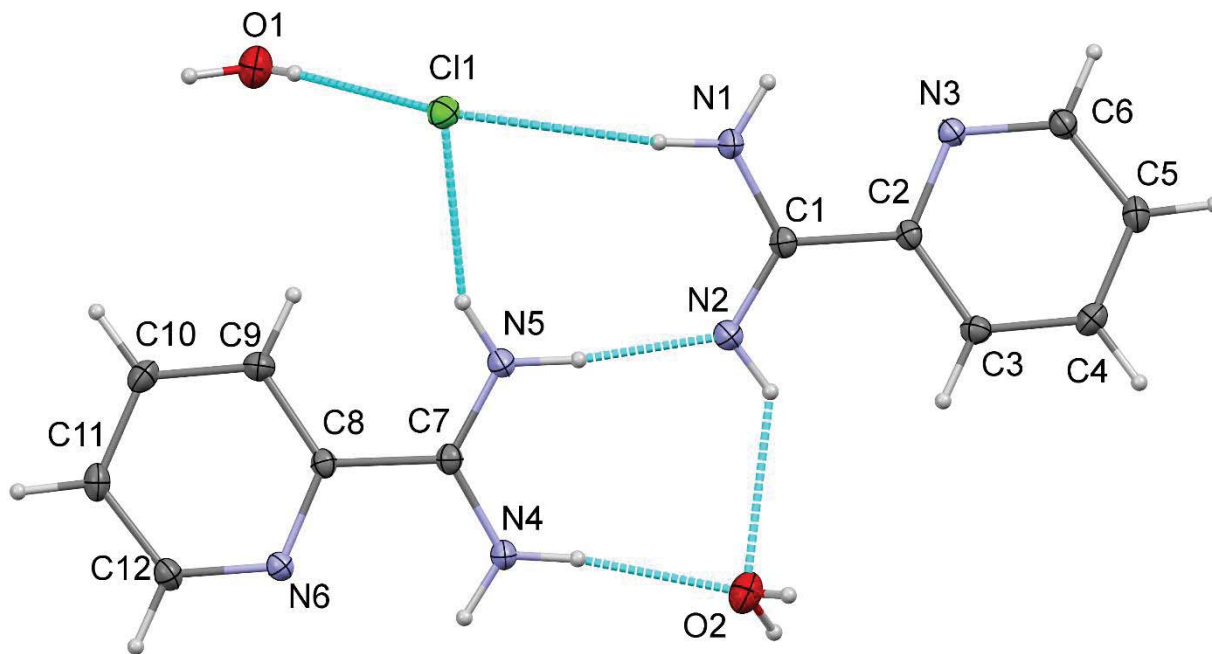


Figure 3.12. The asymmetric unit of **8a** showing the atom-labelling scheme and hydrogen bonding indicated with dashed lines. Displacement ellipsoids are drawn at 50% probability level and H atoms are shown as small spheres of arbitrary radii.

Both amidine and amidinium structures exhibit interesting hydrogen bonding that generate supramolecular networks. The H-bonds in a unit cell and crystal packing of **8** are depicted in Figures 3.11. A total of six N–H \cdots N H-bonds (Table 3.6) result in formation of a 2D pattern. The subunit with one $R_2^2(10)$ graph set motifs and a continuous intermolecular chain links the structures in 1D by 4 N–H \cdots N which translate along the *a* axis and while the other two N–H \cdots N further extend the chain in 2D across the *c* axis. In contrast, combinations of intermolecular $\pi - \pi$ stacking (Figure 3.13) and hydrogen bonding (Figure 3.14) are responsible for the packing structure in **8a**. The 3.447 Å stacking distance between offset carbon and the ring centroid indicates the existence of significant $\pi \cdots \pi$ interactions. A total of 11 hydrogen bonds (Table 3.7) including three N–H \cdots N, three O–H \cdots Cl, one O–H \cdots O, two N–H \cdots Cl and two N–H \cdots O are present within the crystal lattice which connect the molecules in a 3D pattern. The two N–H \cdots Cl and three N–H \cdots N form infinite chains along *a* while the three O–H \cdots Cl and two N–H \cdots O extended the chain into a 2D arrangement and the O–H \cdots O bridges the 2D plane to form a 3D network.

The hydrogen bonding connections in **8b** are extremely complex. The network consists of thirty-four H-bonds (Table 3.8) which include seventeen N–H \cdots O, eight O–H \cdots O, six N–H \cdots N, two O–H \cdots N and a C–H \cdots O. The ribbon formed by intermolecular H-bonds involving the asymmetric unit of the crystal structure to generate $5R_2^2(8)$ motifs (Figure 3.16a) is linked with a series of the same unit to form a chain running along the *a* axis. The individual chains are then aggregated into 2D and 3D networks with the interaction of water molecules.

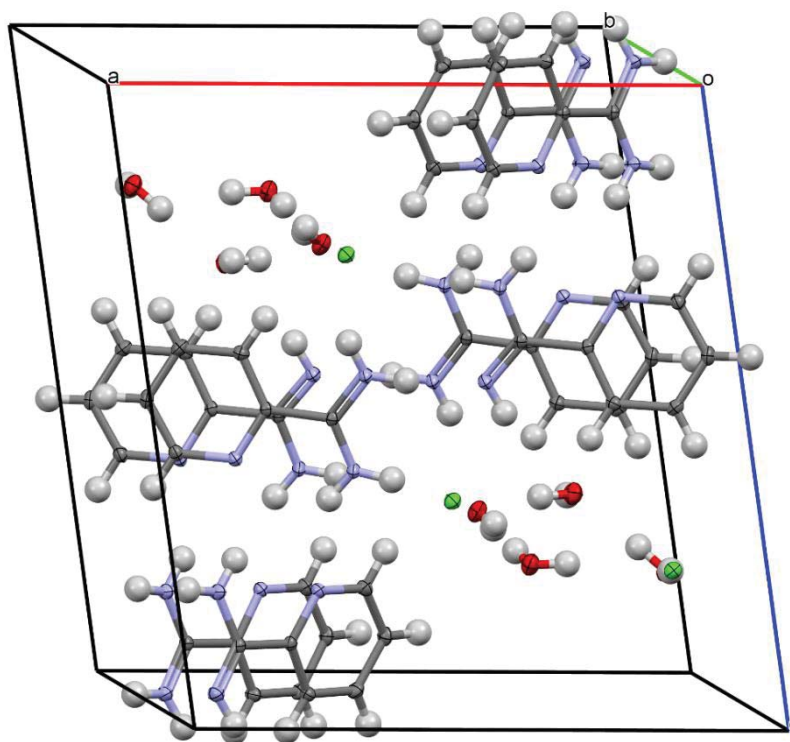


Figure 3.13. The crystal packing structure of **8a** displaying $\pi - \pi$ interaction approximately down *b* axis. Displacement ellipsoids drawn at the 50% probability level.

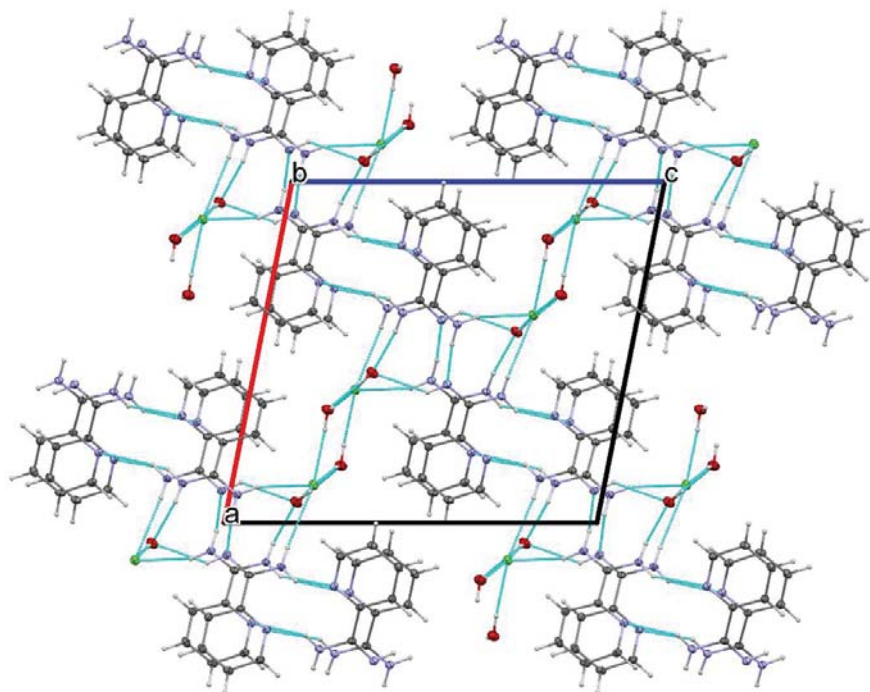


Figure 3.14. The crystal packing structure of **8a** projected down *b*. Displacement ellipsoids drawn at the 50% probability level. Hydrogen bonding is indicated by green dashed lines.

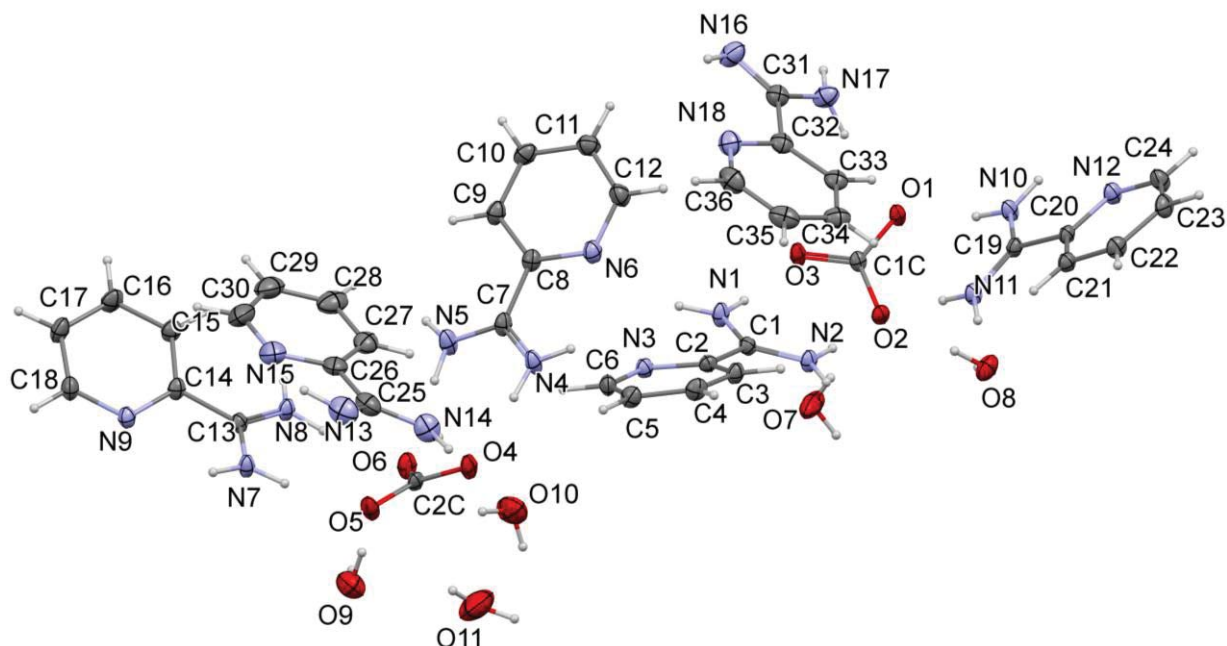


Figure 3.15. The asymmetric unit of **8b** showing the atom-labelling scheme and with hydrogen bonding indicated with dashed lines. Displacement ellipsoids are drawn at 50% probability level and H atoms are shown as small spheres of arbitrary radii.

Table 3.7. Hydrogen Bonds for **8a**

D	H	A	d(D-H)/Å	d(H-A)/Å	d(D-A)/Å	D-H-A/°
O1	H1C	Cl1 ¹	0.829(13)	2.393(13)	3.2163(8)	171.8(16)
O1	H1D	Cl1	0.821(13)	2.381(14)	3.1809(9)	164.8(14)
O2	H2A	O1 ²	0.828(13)	1.953(14)	2.7802(11)	177.4(15)
O2	H2B	Cl1 ³	0.844(13)	2.365(13)	3.2055(9)	174.5(14)
N1	H1A	Cl1	0.860(12)	2.748(13)	3.5889(9)	166.0(13)
N1	H1B	N6 ⁴	0.860(12)	2.281(13)	3.0502(12)	149.0(12)
N2	H2	O2	0.850(12)	2.417(13)	3.0852(12)	136.0(12)
N4	H4A	O2	0.885(12)	2.048(12)	2.9261(11)	171.4(13)
N4	H4B	N3 ⁵	0.887(12)	2.249(12)	3.0301(11)	146.8(11)
N5	H5A	Cl1	0.878(12)	2.469(13)	3.2748(9)	152.9(12)
N5	H5B	N2	0.922(12)	1.809(12)	2.7268(12)	172.9(12)

¹3/2-X,1/2+Y,1/2-Z; ²1-X,1-Y,1-Z; ³1-X,-Y,1-Z; ⁴-1/2+X,1/2-Y,-1/2+Z; ⁵1/2+X,1/2-Y,1/2+Z

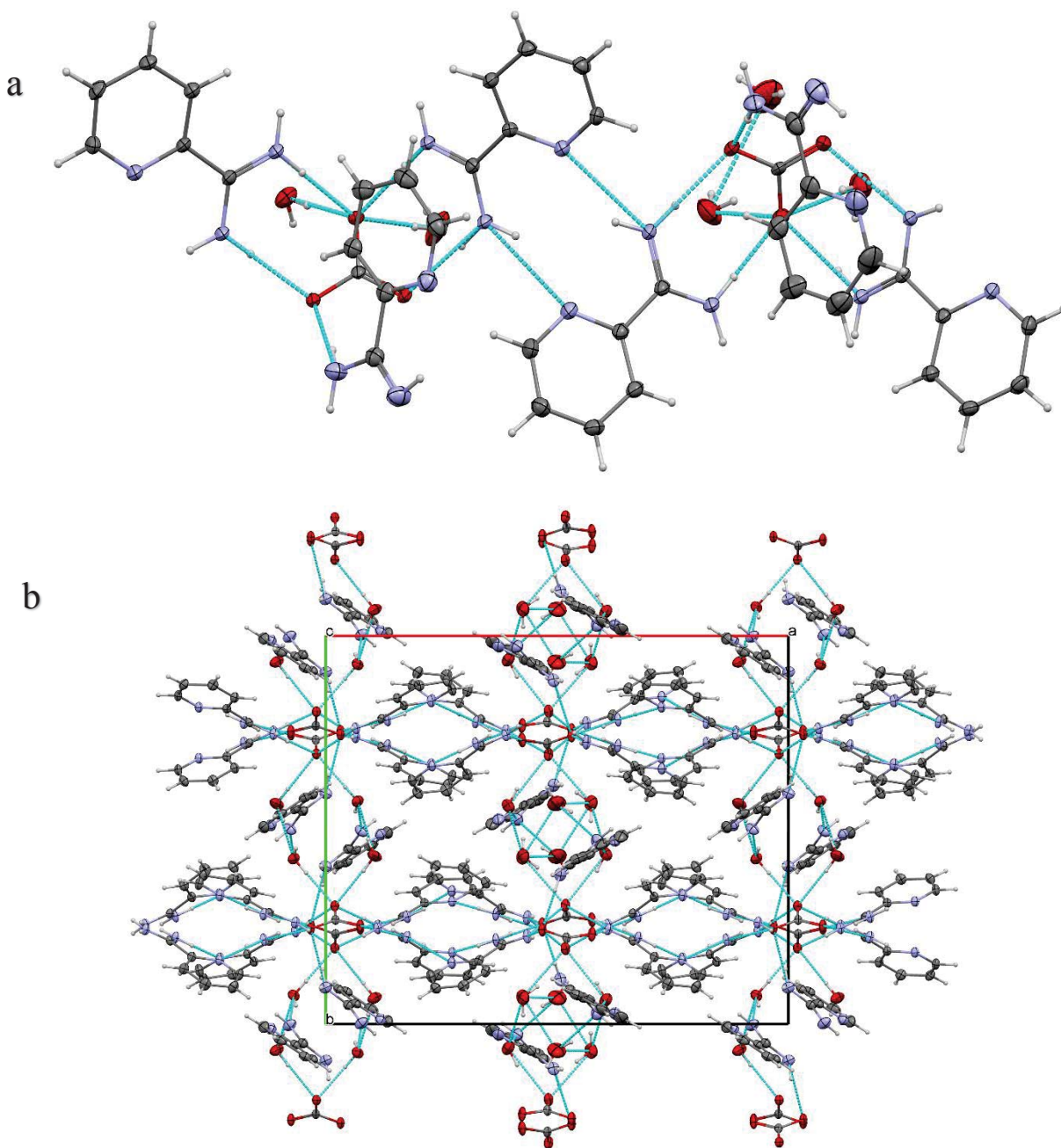


Figure 3.16. The (a) H-bond motif and (b) crystal packing structure of **8b** projected down *c* axis. Displacement ellipsoids drawn at the 50% probability level. Hydrogen bonding is indicated by green dashed lines.

Table 3.8. Hydrogen Bonds for **8b**.

D	H	A	d(D-H)/Å	d(H-A)/Å	d(D-A)/Å	D-H-A/°
O7	H7C	O2	0.848(18)	2.119(19)	2.965(2)	176(4)
O7	H7D	O8 ¹	0.843(18)	2.02(2)	2.852(2)	170(4)
O8	H8C	N16 ²	0.829(17)	2.000(19)	2.805(3)	164(3)
O8	H8D	O2	0.851(17)	1.975(18)	2.824(2)	176(3)
O9	H9A	N13 ³	0.861(18)	1.942(19)	2.792(3)	168(3)
O9	H9B	O6	0.856(18)	2.13(2)	2.952(2)	162(3)
O10	H10C	O6	0.860(18)	2.13(2)	2.907(3)	150(3)
O10	H10C	O11	0.860(18)	2.50(4)	3.02(3)	120(3)
O10	H10D	O9 ⁴	0.839(18)	2.05(2)	2.815(3)	151(4)
O10	H10D	O11 ⁴	0.839(18)	2.38(4)	2.91(3)	121(3)
N1	H1A	O3	0.912(17)	1.867(18)	2.759(2)	165(2)
N1	H1B	N6	0.887(17)	2.23(2)	3.042(2)	152(2)
N2	H2A	O2	0.894(16)	1.894(17)	2.786(2)	176(2)
N2	H2B	O3 ⁵	0.877(17)	1.927(17)	2.793(2)	169(2)
N4	H4A	O4	0.889(17)	1.901(17)	2.786(2)	173(3)
N4	H4B	N3	0.883(17)	2.19(2)	2.949(2)	144(2)
N5	H5A	O4 ³	0.892(17)	1.911(18)	2.787(2)	167(3)
N5	H5B	O6	0.880(17)	1.908(17)	2.788(2)	177(3)
N7	H7A	N12 ⁶	0.869(17)	2.27(2)	3.032(2)	146(2)
N7	H7B	O5	0.884(17)	1.920(17)	2.796(2)	170(2)
N8	H8A	O5 ³	0.880(17)	1.902(17)	2.781(2)	177(3)
N8	H8B	O6	0.889(16)	1.939(17)	2.823(2)	172(2)
C17	H17	O8 ⁷	0.95	2.59	3.443(3)	149.6
N10	H10A	O1	0.902(17)	1.878(18)	2.766(2)	167(2)
N10	H10B	N9 ⁸	0.882(16)	2.19(2)	2.987(2)	149(2)
N11	H11A	O1 ⁵	0.897(17)	1.901(17)	2.787(2)	169(2)
N11	H11B	O2	0.892(17)	1.905(17)	2.796(2)	177(2)
N13	H13	N15	0.921(18)	2.23(3)	2.743(3)	115(2)
N14	H14A	O4	0.896(17)	2.093(18)	2.986(3)	174(3)
N14	H14B	O6 ⁵	0.895(17)	2.51(2)	3.255(3)	141(3)
N14	H14B	O10 ⁵	0.895(17)	2.53(2)	3.327(3)	148(3)
N16	H16A	N18	0.883(17)	2.23(3)	2.731(3)	116(2)
N17	H17A	O8 ³	0.884(17)	2.606(19)	3.461(3)	163(2)
N17	H17B	O1	0.905(17)	2.083(18)	2.982(2)	172(3)

¹-X,2-Y,1-Z; ²-X,1/2+Y,1/2-Z; ³+X,3/2-Y,-1/2+Z; ⁴1-X,2-Y,1-Z; ⁵+X,3/2-Y,1/2+Z; ⁶1+X,+Y,+Z; ⁷1+X,3/2-Y,-1/2+Z; ⁸-1+X,+Y,+Z

3.4 Conclusions

A new alternative procedure was successfully developed for the isolation of 2-amidinopyridine and 2-amidinopyrimidine from their chloride salts in high yields. This achievement will facilitate organic synthesis where the use of high purity 2-amidinopyridine and 2-amidinopyrimidine as synthons is necessary particularly in drug and material design. Specifically, in this thesis, these essential precursors are used in the synthesis of imidoamidines (Chapter 4). It was discovered that the orientation of the amidine or amidinium molecules in the crystal structures and the nature of hydrogen-bonding in the structures based on the potential acceptors in the structure influence the degree of twisting of the amidine or amidinium cation fragments in structure packing. The distinct supramolecular structures via charge-assisted hydrogen bonding observed in the crystal structure analyses of the reported amidines and their derivatives could serve as hints for the application of mixed salts in crystal engineering.

3.5 References

1. Quin, L. D.; Tyrell, J. A., Fundamentals of heterocyclic chemistry: importance in nature and in the synthesis of pharmaceuticals. *John Wiley & Sons* **2010**.
2. Hofmann, K., The Chemistry of Heterocyclic Compounds. *Weissberger. New York: Interscience* **1953**.
3. Zhang, X.; Rueter, J. K.; Chen, Y.; Moorjani, M.; Lanier, M. C.; Lin, E.; Gross, R. S.; Tellew, J. E.; Williams, J. P.; Lechner, S. M., Synthesis of N-pyrimidinyl-2-phenoxyacetamides as adenosine A2A receptor antagonists. *Bioorg. Med. Chem. Lett.* **2008**, *18*, 1778-1783.
4. Karfunkel, H. R.; Wu, Z. J.; Burkhard, A.; Rihs, G.; Sinnreich, D.; Buerger, H. M.; Stanek, J., Crystal packing calculations and Rietveld refinement in elucidating the crystal structures of two modifications of 4-amidinoindanone guanylhydrazone. *Acta Crystallogr., Sect. B* **1996**, *52*, 555-561.
5. Ratera, I.; Veciana, J., Playing with organic radicals as building blocks for functional molecular materials. *Chem. Soc. Rev.* **2012**, *41*, 303-349.
6. Rawson, J. M.; Alberola, A.; Whalley, A., Thiazyl radicals: old materials for new molecular devices. *J. Mater. Chem.* **2006**, *16*, 2560-2575.
7. Norrestam, R.; Mertz, S.; Crossland, I., Structure of acetamidine, C₂H₆N₂, at 108 K. *Acta Crystallogr., Sect. C* **1983**, *39*, 1554-1556.
8. Shriner, R. L.; Neumann, F. W., The Chemistry of the Amidines. *Chem. Rev.* **1944**, *35*, 351-425.
9. Barker, J.; Phillips, P. R.; Wallbridge, M. G. H.; Powell, H. R., Benzamidine. *Acta Crystallogr., Sect. C* **1996**, *52*, 2617-2619.
10. Jokic, M.; Bajic, M.; Zinic, M.; Peric, B.; Kojic-Prodic, B., Benzdiamidine. *Acta Crystallogr., Sect. C* **2001**, *57*, 1354-1355.
11. Yousaf, M.; Yutronkie, N. J.; Castañeda, R.; Klein, J. A.; Brusso, J., Boratriazines: inducing luminescence through boron incorporation into a terpy-type framework. *New J. Chem.* **2017**, *41*, 12218-12224.
12. Chen, Q.; Zhang, H.; Zhang, F.; Liu, F., Pyridine-2-carboximidamide chloride monohydrate. *Acta Crystallogr., Sect. E* **2010**, *66*, o3169.
13. Liu, F.; Zhang, F.; Chen, Q.; Zhang, H., Pyridine-3-carboxamidinium chloride. *Acta Crystallogr., Sect. E* **2011**, *67*, o781.
14. Fan, P.; Wang, L.; Zhang, H., Pyridine-4-carboximidamide chloride. *Acta Crystallogr., Sect. E* **2009**, *65*, o2408.

15. Pinner, A.; Klein, F., Umwandlung der Nitrile in Amide. *Berichte der deutschen chemischen Gesellschaft* **1878**, *11*, 4-11.
16. Kennard, O.; Walker, J., Crystallographic data for certain amidinium carboxylates. *Acta Crystallogr.* **1961**, *14*, 91-92.
17. Hayes, P. J.; Oakley, R. T.; Cordes, A. W.; Pennington, W. T., Preparation and dimerization of 1,2,4,6-thiatriazinyl radicals - crystal and molecular-structure of bis(3,5-diphenyl-1,2,4,6-thiatriazine). *J. Am. Chem. Soc.* **1985**, *107*, 1346-1351.
18. Kamei, K.; Maeda, N.; Katsuragi-Ogino, R.; Koyama, M.; Nakajima, M.; Tatsuoka, T.; Ohno, T.; Inoue, T., New piperidiny- and 1,2,3,6-tetrahydropyridinyl-pyrimidine derivatives as selective 5-HT_{1A} receptor agonists with highly potent anti-ischemic effects. *Bioorg. Med. Chem. Lett.* **2005**, *15*, 2990-2993.
19. Boeré, R. T.; Oakley, R. T.; Reed, R. W., Preparation of N,N,N'-tris(trimethylsilyl)amidines; a convenient route to unsubstituted amidines. *J. Organomet. Chem.* **1987**, *331*, 161-167.
20. Boeré, R. T.; French, C. L.; Oakley, R. T.; Cordes, A. W.; James Privett, J. A.; Craig, S. L.; Graham, J. B., Preparation and interconversion of dithiatriazine derivatives: Crystal, molecular, and electronic structure of bis(5-phenyl-1,3,2,4,6-dithiatriazine) (PhCN₃S₂)₂. *J. Am. Chem. Soc.* **1985**, *107*, 7710-7717.
21. Sanger, A. R., Reactions of benzonitrile with lithium amides. *Inorg. Nucl. Chem. Lett.* **1973**, *9*, 351-354.
22. Safin, D. A.; Tumanov, N. A.; Leitch, A. A.; Brusso, J. L.; Filinchuk, Y.; Murugesu, M., Elucidating the elusive crystal structure of 2,4,6-tris(2-pyrimidyl)-1,3,5-triazine. *Cryst. Eng. Comm.* **2015**, *17*, 2190-2195.
23. Leitch, A. A.; Korobkov, I.; Assoud, A.; Brusso, J. L., Non-innocent pyridyl nitrogens: unprecedented interconversion of N-bridgehead-thiadiazolium salts and thiatriazine in the generation of thiatriazinyl. *Chem. Commun.* **2014**, *50*, 4934-4936.
24. Krygowski TM, W. K., Patai S, Rappoport, Z., The chemistry of amidines and imidates. *Wiley & Sons Ltd., New York* **1991**, 2:142.
25. Dunn, P. J., Amidines and N-substituted amidines. *Chem. Inform.* **1995**, *27*, 741-782.
26. Chen, D.; Kim, S. H.; Hodges, B.; Li, G., The cinnamate-based aminohalogenation provides an easy access to anti methyl 3-aryl-N-p-tosyl-and N-o-nosyl-aziridine-2-carboxylates. *ARKIVOC* **2003**, *12*, 56-63.
27. Kumar, T.; Verma, D.; Menna-Barreto, R. F. S.; Valença, W. O.; da Silva Júnior, E. N.; Namboothiri, I. N. N., Synthesis of imidazoles via cascade reaction of nitroallylic acetates with amidines and studies on their trypanocidal activity. *Org. Biomol. Chem.* **2015**, *13*, 1996-2000.

28. Boéré, R. T.; Roemmele, T. L.; Yu, X., Unsymmetrical 1λ3-1,2,4,6-thiatriazinyls with aryl and trifluoromethyl substituents: Synthesis, crystal structures, EPR spectroscopy, and voltammetry. *Inorg. Chem.* **2011**, *50*, 5123-5136.
29. Blumhoff, J.; Beckert, R.; Rau, S.; Losse, S.; Matschke, M.; Günther, W.; Görls, H., Synthesis of ligands based on 4H-imidazoles and pyridine subunits: Selective complexation and bathochromically absorbing complexes. *Eur. J. Inorg. Chem.* **2009**, *2009*, 2162-2169.
30. Schaefer, F. C.; Krapcho, A. P., Preparation of amidine salts by reaction of nitriles with ammonium salts in the presence of ammonia. *J. Org. Chem.* **1962**, *27*, 1255-1258.
31. Lewis, C. A.; Wolfenden, R., The nonenzymatic decomposition of guanidines and amidines. *J. Am. Chem. Soc.* **2014**, *136*, 130-136.
32. Norrestam, R., Structure of bis(acetamidinium) carbonate monohydrate, $2(\text{C}_2\text{H}_7\text{N}_2^+).\text{CO}_3^{2-}.\text{H}_2\text{O}$, at 108 K. *Acta Crystallogr., Sect. C* **1984**, *40*, 297-299.
33. Portalone, G., Supramolecular association in proton-transfer adducts containing benzamidinium cations. I. Four molecular salts with uracil derivatives. *Acta Crystallogr., Sect. C* **2010**, *66*, 295-301.
34. Li, X.; He, X.; Wang, B.; Merz Jr, K., Conformational variability of benzamidinium-based inhibitors. *J. Am. Chem. Soc.* **2009**, *131*, 7742-7754.
35. Irrera, S.; Portalone, G., 4-Methoxybenzamidinium chloride monohydrate. *Acta Crystallogr., Sect. E* **2012**, *68*, 3083.

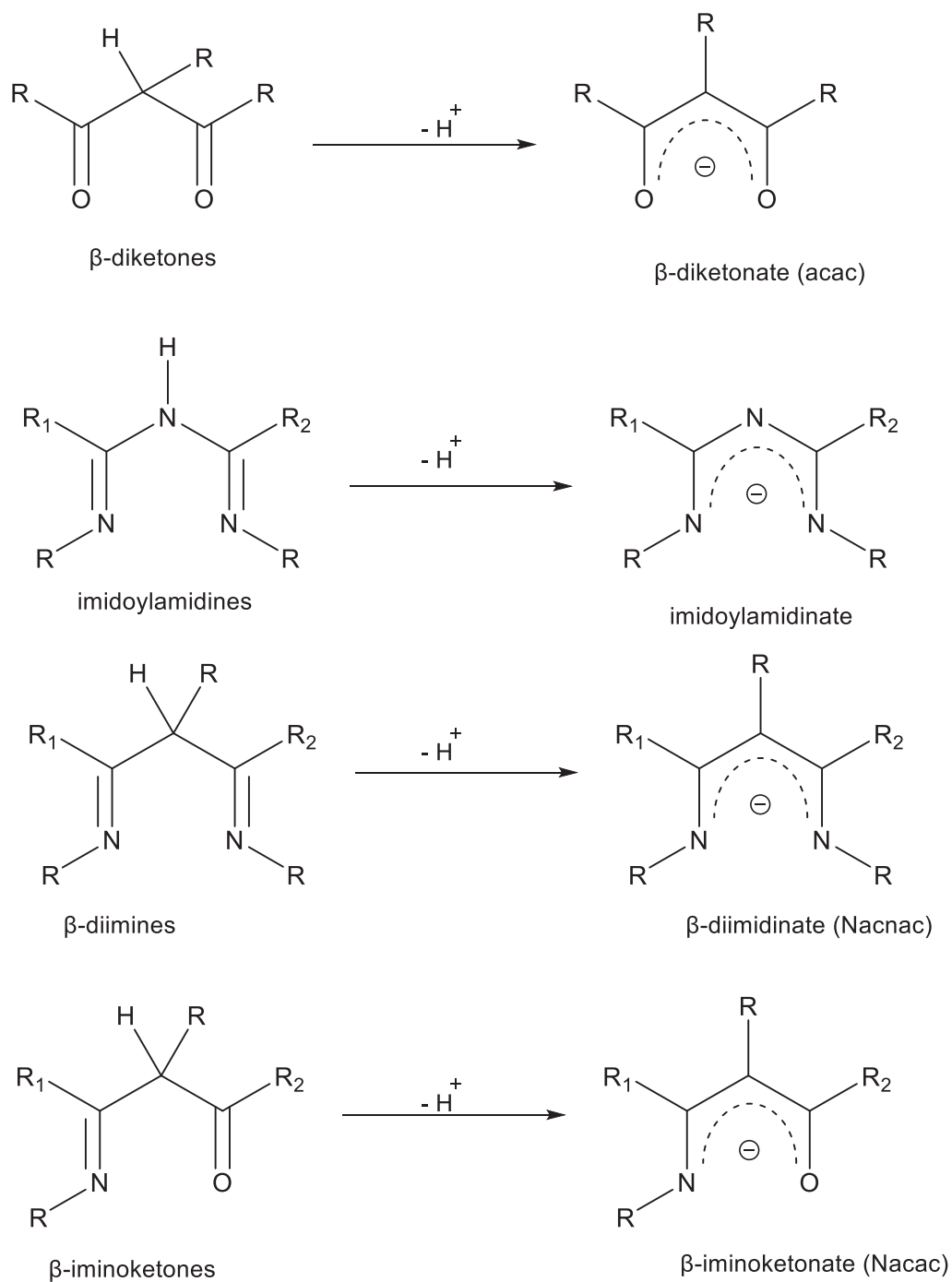
Chapter 4 Preparation of functionalized imidoamidines

This part of the thesis addresses the synthesis of *N'*-(2,2,2-trichloroethanimido)pyrid-2-yl-carboximidamide (**11**) and *N'*-(2,2,2-trichloroethanimido)pyrimid-2-yl-carboximidamide (**13**), and their hydrochloride salts, as precursors for the synthesis of thiaziazines (Chapter 5).

4.1 Introduction

Imidoamidines, also called 1,3,5-triazapenta-1,3-dienes, are well-known multifunctional tri-nitrogen chelating compounds with distinct physical, chemical, and electronic properties.¹ They are isoelectronic to the well-known β -diketones (acac), β -diimines (nacnac) and β -iminoketones (nacac) with the character of two amidine functional groups fused together, and have a high degree of unsaturation with delocalization in the N=C–N=C–N unit (Scheme 4.1). This system has received a lot of attention in recent years, and various species with variation of the R groups to generate derivatives including alkyls, aryls, CX₃, silyl and hydrogen have led to the isolation of many symmetric (where R₁ = R₂) molecules. However, less work has been done on the asymmetric (where R₁ \neq R₂) architecture. Their unique reactivity has found them to be potential synthons for various organic molecules in diverse areas of application, and they also display efficacy as building blocks in supramolecular engineering.²

Like β -diketones, β -diimines and β -iminoketones in Scheme 4.1, imidoamidines could be deprotonated to their corresponding monoanions leading to delocalization of a negative charge throughout the system, in which form they are strongly chelating monanionic ligands (Scheme 4.1, r.h.s.). In addition, the central nitrogen atom (at position 3) makes a considerable change to the electronic structure even in its neutral form.³ This essential characteristic makes imidoamidines demonstrate rich coordination chemistry like acac, nacnac and nacac.



R = H, alkyl, aryl, heterocycles, silyl.

Scheme 4.1. Structure of imidoylamidines and analogous unsaturated chelates

The multiple nitrogen content also allow them to coordinate in mono-, di- or tridentate mode to metals in which the central N atom is also a prospective binding site.³⁻⁵ Imidoamidines typically undergo tautomerization, which has been established in the solid-state⁶ and in solution.⁷⁻⁸ As shown in Scheme 4.2, the two main tautomers are the amino-imino (tautomer **I**) with one of the terminal nitrogen atoms having two protons and the imino-imino (tautomer **II**) with one of the protons located on the central nitrogen atom. Tautomer **I** and tautomer **II** could potentially transform to conformers **IA** and **IIA** respectively based on the bulkiness of the R groups with consequent rotation of the N=C–N=C–N due to allylic strain. The conformers **IA** and **IIA** are rare and only exist for extremely sterically hindered imidoamidines.⁹⁻¹¹ Moreover, the stability of all the isomers have been recognized with computational studies¹² with observations of the U-shaped (tautomer **I** and **II**)¹³⁻¹⁶ and the W-shaped (conformer **IA** and **IIA**)^{11, 17}. The U-shaped tautomer has been demonstrated to be more stable, and it is the most reported in all the isomers due to strong internal resonance-assisted hydrogen bond (RAHB)¹⁸ as shown in the center of Scheme 4.2. Among the U-shaped conformers, tautomer **II** is the main conformation in coordination chemistry.

In line with the hydrogen content on the nitrogen atoms, imidoamidines are classified into primary with three nitrogen hydrogens; secondary with only two nitrogen hydrogens; tertiary with one nitrogen hydrogen; and quaternary with no nitrogen hydrogens (Scheme 4.2). The tertiary derivatives are the most reported in the literature because they are easily generated *in situ* in a one-pot synthesis via metal-assisted reaction from their precursors to produce important organometallic complexes with distinguish electronic, magnetic, catalytic and redox properties.¹⁹⁻²¹ They are usually considered for this process because the bulky groups at the terminal N atoms help to stabilize the coordination environment and minimize unwanted reactions at the two terminal nitrogen atoms.²² This discovery led to the development of many substituted imidoamidines as

building blocks for metal complexes and clusters with a broad range of applications from catalysis to molecular magnets.^{10, 23-31} The first and second row transition metal complexes are the most investigated, and some studies have also focused on the third row transition metals of the periodic table.^{3, 10, 13, 24, 26-27, 32-41} Recent work by Rad'kova et al.⁴² has also considered rare-earth metal complexes. For instance, rhodium^{III}-imidoylamidine complex were prepared by coupling substituted nitriles in the rhodium (Rh) complexes, [(^tbpy)₂Rh(NCR)₂][OTf]₃ (where R = Me/Ph; ^tbpy = 4,4'-di-*tert*-butyl-2,2'-bipyridine; OTf = CF₃SO₃⁻) with R-substituted anilines.⁴³ Double coupling of a substituted platinum(Pt)-coordinated nitrile with 2,3-diphenylmaleimidine has also resulted in the generation of a phosphorescent Pt complex featuring two fused imidoylamidine units.⁴⁴ Kajiwara and coworkers⁴ have also synthesized different ferromagnetic supramolecular complexes of Fe, Ni and Cu using 2,4-bis(2-pyridyl)-1,3,5-triazapentadiene as a bridging ligand with $\kappa^1\text{N}:\kappa^2\text{N}$ (i.e. the central N and the two terminal N atoms) coordination mode as shown in Figure 4.1. This group had also prepared $\kappa^3\text{N}:\kappa^2\text{N}$ (i.e. the central N with two N atoms of ligand and the two terminal N atoms) bridged complexes from the decomposition of 1,3,5-tris(2-pyridyl)-2,4,6-triazine in the presence of the metal ion.⁵

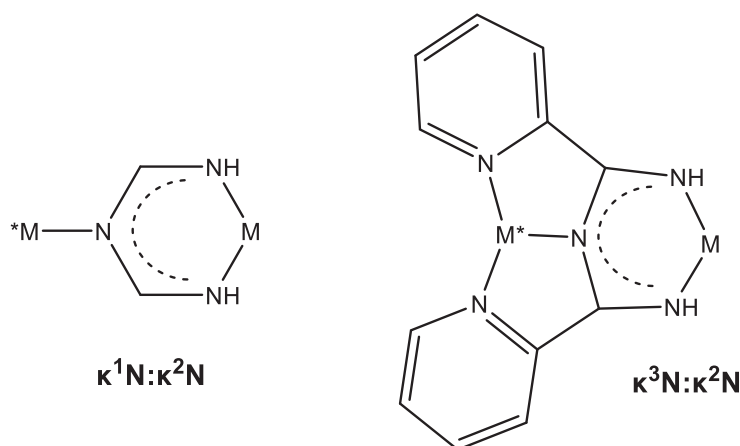
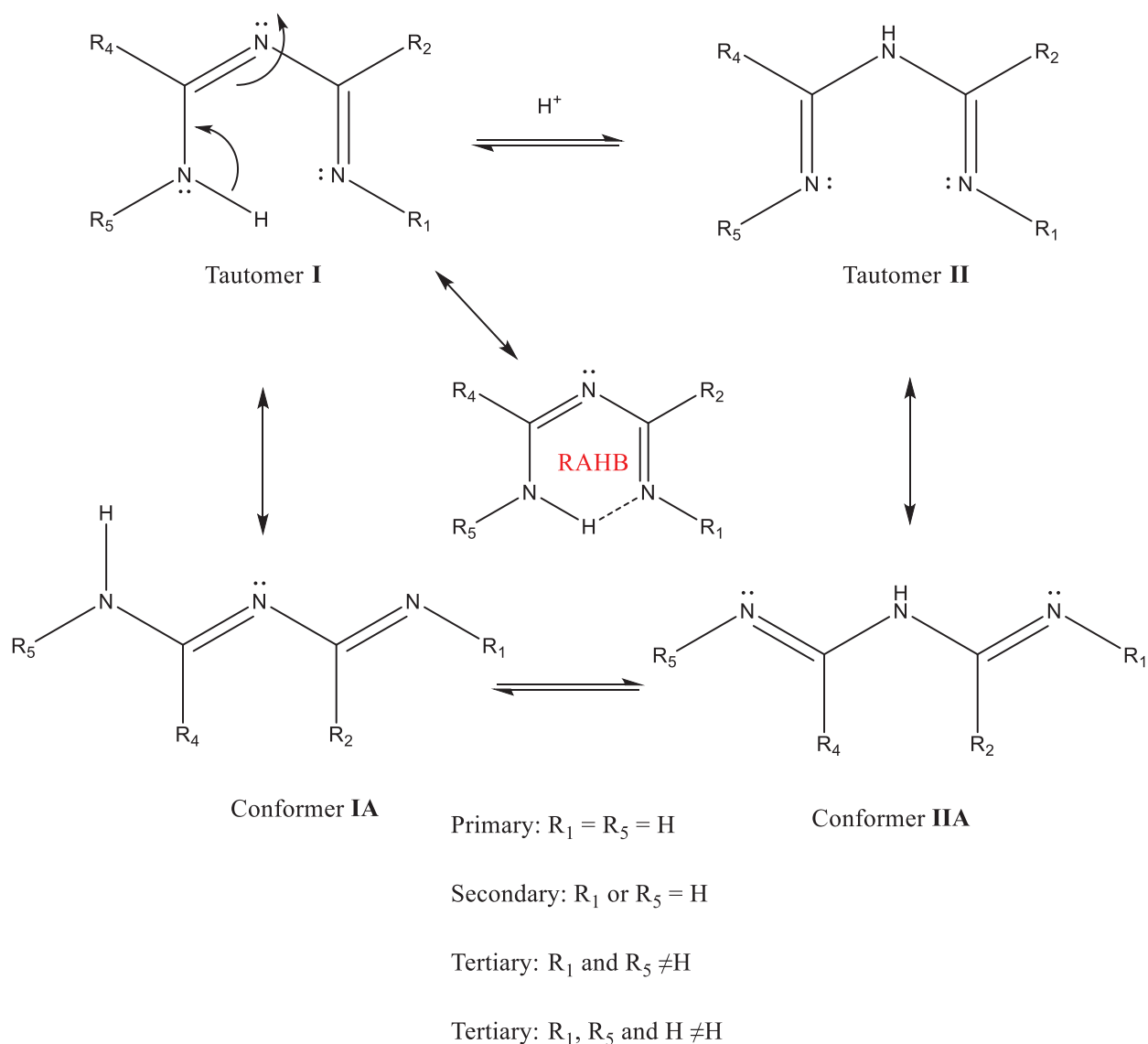


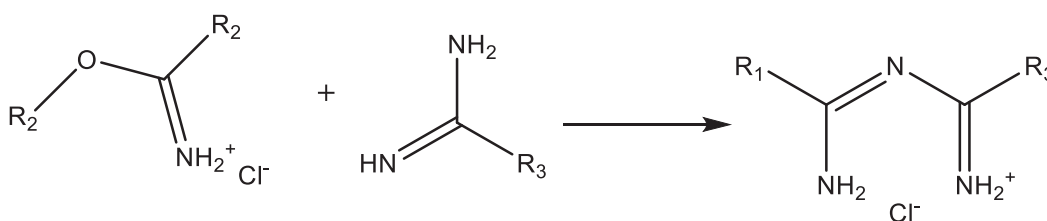
Figure 4.1. Coordination mode of bridged complexes of imidoylamidines.



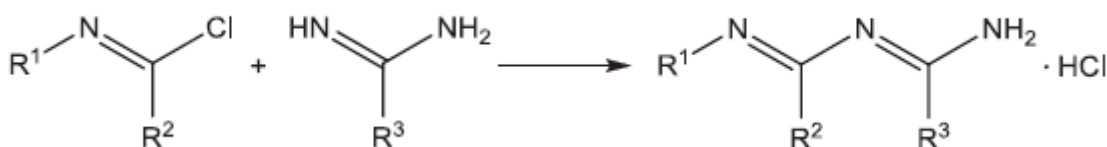
Scheme 4.2. Tautomers and conformers of imidoamidine

Compared to the metal-assisted imidoamide condensation reactions, there are limited existing methods for the synthesis of uncoordinated imidoamidines. The Pinner method (Chapter 3) could be extended to imidoamidine synthesis (Scheme 4.3).⁴⁵⁻⁴⁶ This route, and Ley and Muller's method⁴⁷ (Scheme 4.4) are the earliest ways to imidoamidines. Both reactions are suitable for the preparation of the secondary, tertiary, and quaternary imidoamidines, while the primary analogues could only be obtained by Pinner's reaction.

The Pinner synthesis typically involves the generation of an imidoamidinium hydrochloride salt from the reaction of imino-ester hydrochloride salt with amidine. However, low yields limit its application in the preparation of imidoamidiniums. On the other hand, the Ley and Muller method involves the reaction of imido chloride with amidine to generate the imidoamidinium hydrochlorides which is usually subjected to a hot-water wash workup to give good yield of the product.⁴⁸ The replacement of amidine with amine has been found to give same similar results.⁴⁹



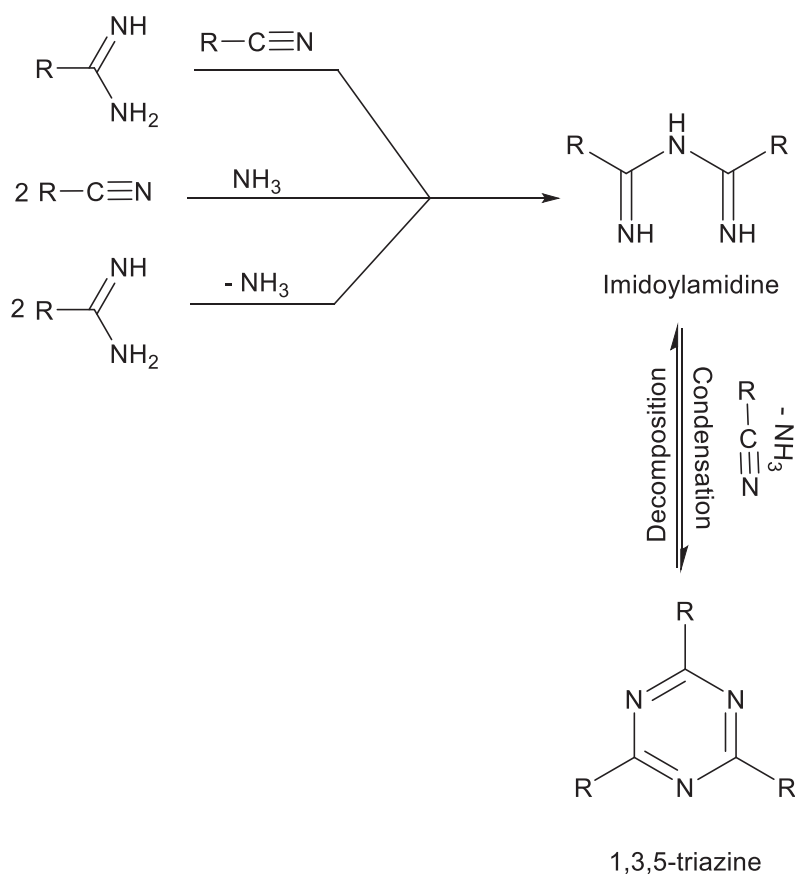
Scheme 4.3. Pinner method



Scheme 4.4. Ley and Muller method

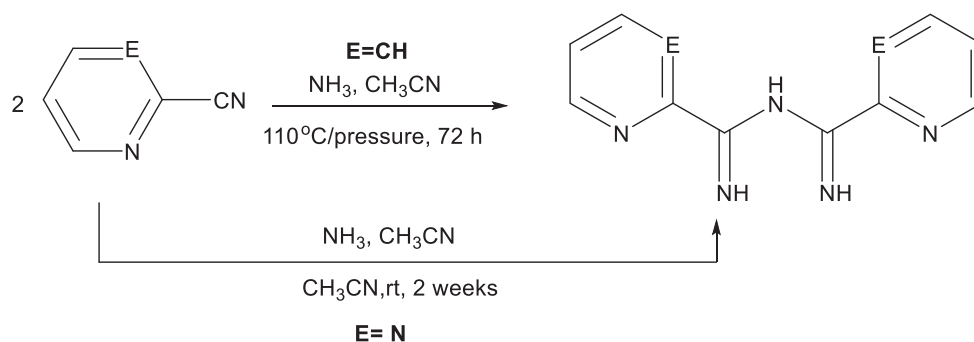
There are limited methods known in the literature for robust preparation of primary imidoamidiniums which is the main focus of this study. Primary imidoamidiniums may be synthesized by condensation of nitrile with ammonia through nucleophilic attack on two activated nitriles,^{16, 50} an amidine attack on an activated nitrile⁵⁰ or condensation or coupling of two amidine molecules with the elimination of ammonia (Scheme 4.5).⁵¹ These methods are only applicable to electron withdrawing substituents such as perhalogenatedalkyl,⁵² aryl^{6, 53-54} and heterocycles (pyridine).^{21, 34, 55} Under thermal conditions, symmetric imidoamidiniums transform into the corresponding 1,3,5-triazines due to their high reactivity.^{50, 56-57} Using the condensation of amidine

with nitrile route, Boeré and coworkers have synthesized many asymmetric aryl- and trihalomethyl-substituted ($-CCX_3$, $X = F, Cl$) primary imidoamidines.⁶



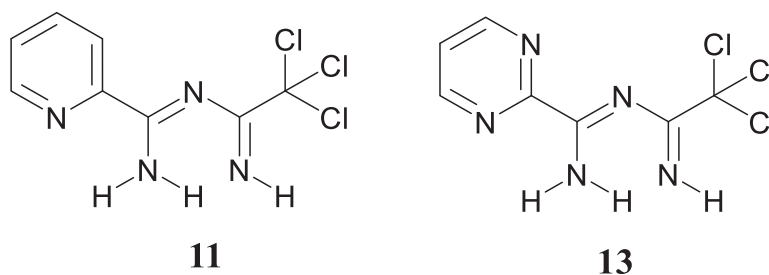
Scheme 4.5. Primary imidoamidine synthesis from nitriles and amidines.

Brusso and coworkers recently developed symmetric-substituted primary imidoamidines of pyridine and pyrimidine in good yields via the nitrile condensation with ammonia reaction with slight modifications (Scheme 4.6).⁷⁻⁸ Using commercially available nitriles of the corresponding heterocycles, the *N*-2-pyridylimido-2-pyridylamidine (Py_2ImAm) and *N*-2-pyrimidylimido-2-pyrimidylamidine (Pm_2ImAm) were prepared by amination of the activated nitrile. The Py_2ImAm reaction was carried out at elevated temperature ($110^\circ C$) and pressure while Pm_2ImAm was generated at room temperature in two weeks.



Scheme 4.6. Synthesis of symmetric pyridine/pyrimidine-substituted primary imidoamidines.

The primary imidoamidines have attracted rising interest in the last two decades with regards to their interesting electronic, structural, and chemical properties. The coordination chemistry of the system has been exploited in the development of numerous metal–organic frameworks. However, the asymmetric imidoamidines have received less attention. Therefore, it is worthwhile to dig into and understand the chemistry of asymmetric **11** and **13** in comparison to the already existing symmetric analogues.



4.2 Results and discussion

4.2.1 Synthesis of PyCCl₃Imidoamidine and PmCCl₃Imidoamidine and the HCl salts

Adapting the amidine attack on the activated nitrile method,^{6, 58} asymmetric *N'*-(2,2,2-trichloro-ethanimidoyl)pyrid-2-yl-carboximidamide(**11**) and *N'*-(2,2,2-trichloroethanimidoyl)pyrimid-2-yl-carboximidamide (**13**) as well as their corresponding hydrochloride salts (**12** and **14**) were prepared and isolated. On refluxing one equivalents of trichloroacetonitrile and the

corresponding amidine in acetonitrile for 30 mins, **11** and **13** were formed (Figure 4.2). **11** and **13** crystallized from acetonitrile at -18°C . Room temperature ^1H NMR (300 MHz) experiments in CDCl_3 referenced against TMS indicate successful isolation of the compounds in high purity. As illustrated in Figure 4.3, only tautomer **I** of imidoamidinium is exhibited by **11** with an internal resonance-assisted hydrogen bond (RAHB)¹⁸ associated with peak **B**. Moreover, proton **B** is sandwiched between two electronegative terminal N atoms which leads to high polarization of electron from the proton with consequent deshielding effect on its chemical shift (δ 10.43). All the N–H proton peaks are a bit broadened demonstrating a slow proton exchange process. In addition, the obtained N–H chemical shifts (δ 10.43, 9.47 and 8.48) are in agreement with the average order of those reported for the aryl- CF_3 Imidoamidinium (δ 11.0, 9.0 and 6.8) analogs.⁶ The aromatic proton peaks have similar patterns to the corresponding amidines, but the signals are slight shifted to higher frequency compared to them (Table 4.1). The N–H proton peak **C** overlaps with that of the pyridine *ortho* C-H (Figure 4.3).

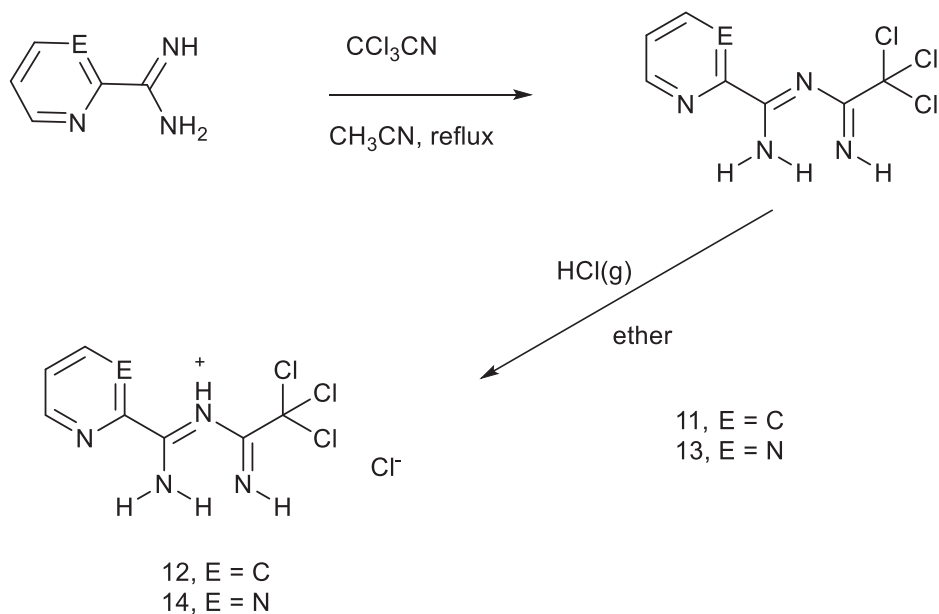


Figure 4.2. The synthetic routes to **11**, **12**, **13**, and **14**.

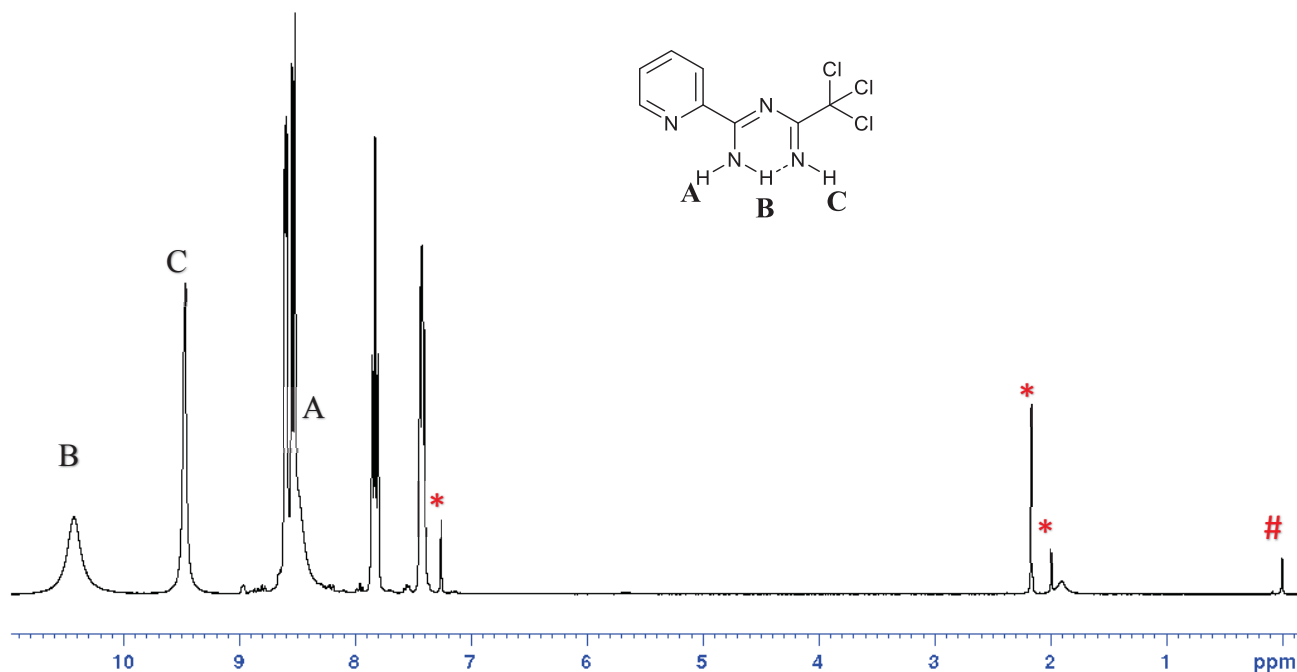


Figure 4.3. ^1H NMR spectrum of **11** (* are solvent peaks and # is TMS).

However, in the ^1H NMR spectrum of **13** (Figure 4.4), both tautomer **I** and tautomer **II** presumably exist in solution in equilibrium with tautomer **I** being the dominant species which is approximately 87% composition in accordance with integration of the proton peaks.⁸ Tautomer **I** N – H proton signals have similar shape and chemical shifts order observed for **11** (Figure 4.4), but they are lying above those of **13** by 102 Hz. Like **11**, the aromatic proton peaks of the **13** are shifted to higher frequencies relative to its corresponding amidine (Table 4.1). The N – H protons chemical shifts A, B, and C of tautomer **II** are shifted to higher frequencies (9.85, 11.60, and 10.10 ppm) compared to tautomer **I** (8.51, 10.77 and 9.68 ppm). The aromatic proton peaks are also shifted to higher frequencies against the corresponding amidine.

The HCl salts of both **11** and **13** (i.e., **12** and **14**) were generated by bubbling HCl gas directly into the suspension of the corresponding imidoylamidine in ether to get a white precipitate in pure form.

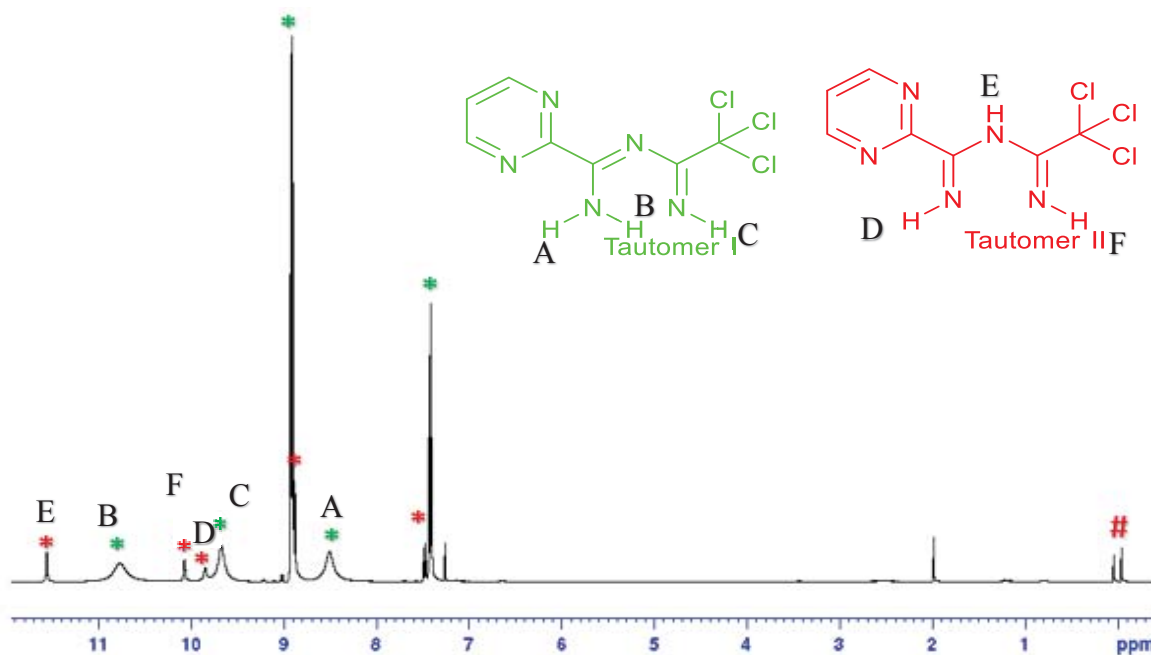
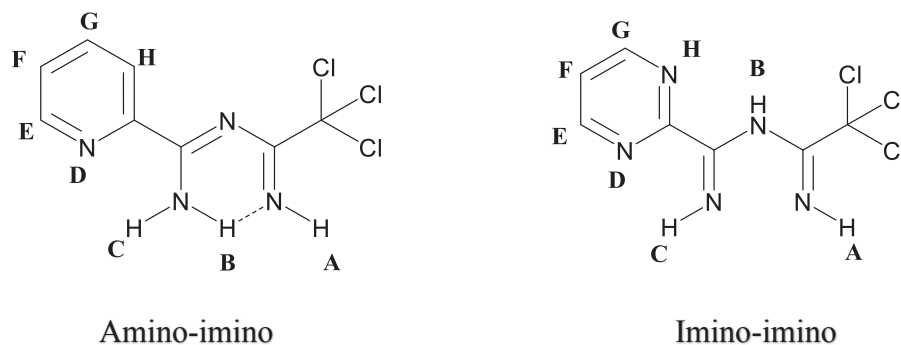


Figure 4.4. ^1H NMR spectrum of **13** (* are tautomer peaks and # is TMS and silicone grease).

Table 4.1. ^1H NMR chemical shift comparison of **11** and **13** with corresponding amidines



Compound	A (ppm)	B (ppm)	C (ppm)	E (ppm)	F (ppm)	G (ppm)	H (ppm)
8 (amidine)	N/A	N/A	N/A	8.58	7.38	7.80	8.13
9 (amidine)	N/A	N/A	N/A	8.81	7.36	8.81	N/A
11	8.48	10.43	9.47	8.61	7.44	7.85	8.55
13 ^a	8.51 ^a	10.77 ^a	9.68 ^a	8.91 ^a	7.42 ^a	8.91 ^a	N/A
13 ^b	9.85 ^b	11.60 ^b	10.10 ^b	8.88 ^b	7.48 ^b	8.88 ^b	N/A

N/A: Not applicable; ^aAmino-imino tautomer; ^bImino-imino tautomer.

4.3 Crystal structures

To understand the solid-state structures of **11** and **13** as well as the ambiguity observed in the NMR spectroscopy, single crystal X-ray diffraction was attempted on both compounds. No X-ray data is reported for salts **12** and **14** because several attempts to grow crystals were not successful. The crystal structures obtained on **11** and **13** are isomorphous. Both crystalize in $P\bar{1}$ with unit cells (\AA) 6.6005(2) 6.9738(3) 12.6419(4) 87.921(3) 85.709(3) 64.337(4) and 6.73775(18) 6.77818(17) 12.5793(3) 87.921(3) 85.709(3) 64.337(4) respectively. Figures 4.5a and b show the asymmetric units of both structures with the atomic numbering schemes of the single independent crystallographic molecule in each. Comparing the molecular geometries in relation to selected bond distances and angles of the compounds, there is no significant difference between **11** and **13**. No obvious discrepancy in the N–C=N–C=N group of the two compounds, and the parameters are comparable to the average values reported for the ArylCCl₃ imidoamidines analogs (Table 4.2).⁵⁸ The N–C=N–C=N fragments show characteristic similar/averaged C–N bond distances, suggesting a level of electron delocalization. The structures are also similar to that of guanidine such as N,N',N''-tris(2,6-Di-isopropylphenyl)guanidine (with CSD reference code XICQEF)⁵⁹ and 2-(4-Amidino-1-indanylideneamino)guanidine (with CSD reference code HIJFIP01)⁶⁰, and other primary imidoamidines like N'-(2,2,2-Trichloroethanimido)benzene-1-carboximidamide (with CSD reference code AWIDUG)⁵⁸ and N-[amino(pyridin-2-yl)methylidene]pyridine-2-carboximidamide (with CSD reference code SEMQEJ)⁷. Overall, the molecules are perfectly planar with an approximately 180° angle around C2 and C3 of the N–C=N–C=N fragment. More importantly, both **11** and **13** display intramolecular resonance-assisted hydrogen bonding (RAHB). The strong intramolecular RAHB N–H...N observed in **11** and **13** with donor-acceptor (D–A) distances [2.635 (3) \AA] and [2.633 (2) \AA] are identical to those of related structures of aryl-

trichloromethylimidoylamidines [2.66 (2)Å] and aryl-trifluoromethylimidoylamidines [2.616 (2)–2.657 (4)Å].⁵⁸

Table 4.2. Selected bond lengths (Å) and angles (°) of **11** and **13** in comparison with the average parameters of the aryl analogs

Compound	11	13	ArylCCl ₃ Imidoylamidines ⁵⁸
C2 – N1	1.278(3)	1.281(3)	1.278(3)
C2 – N2	1.375(3)	1.372(2)	1.370(3)
C3 – N2	1.320(3)	1.315(3)	1.323(7)
C3 – N3	1.327(3)	1.327(3)	1.327(5)
C1 – C2	1.560(3)	1.555(3)	1.552(7)
C3 – C4	1.497(3)	1.508(2)	1.488(5)
N1– C2– N2	127.0(2)	127.7(2)	127.3(3)
N1– C2– C1	122.9(2)	122.3(2)	122.7(4)
N2– C2– C1	110.0(2)	110.0(2)	110.0(4)
C2– N2– C3	119.4(2)	119.2(2)	120.1(2)
N3– C3– N2	127.0(2)	127.0(2)	125.6(2)
N3– C3– C4	115.4(2)	115.2(2)	117.8(4)
N2– C3– C4	117.6(2)	117.7(2)	116.7(3)

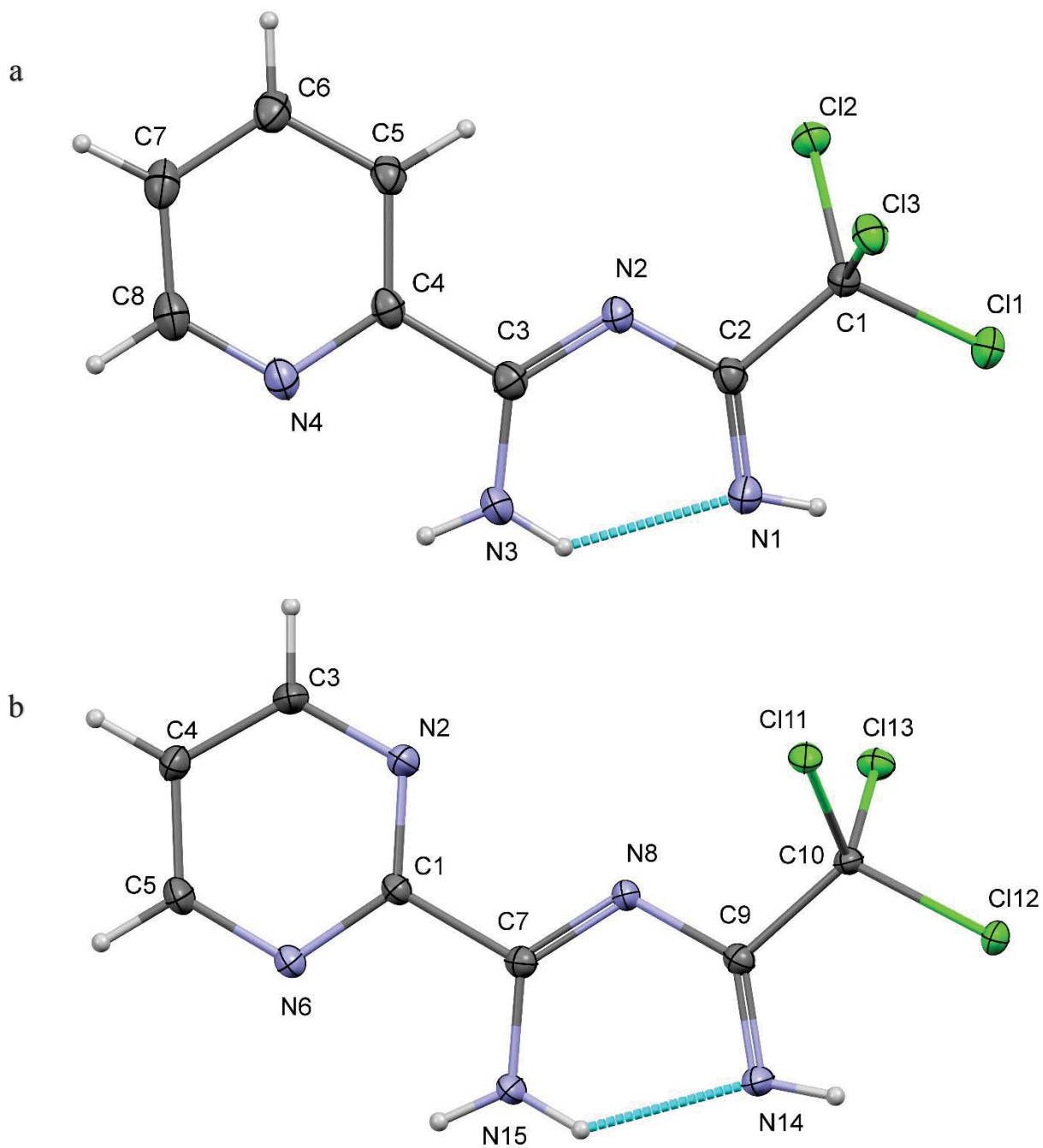


Figure 4.5. Displacement ellipsoid plots of (a) **11** and (b) **13** drawn at the 50% probability level showing the atom-labelling scheme and intramolecular hydrogen bonding (indicated with dashed lines). The H atoms are shown as small spheres of arbitrary radii.

It is also worth mentioning the intermolecular hydrogen bonding. The asymmetric units of **11** (Figure 4.6) is linked to another molecule via a discrete N–H...H. hydrogen bonds involving N atom of the heterocyclic ring to form a dimer. This resulted in formation of graph set motif $R_2^2(10)$ which is extended to 2D by N–H...Cl to form a chain. A similar hydrogen bonding pattern is observed in **13** (Figure 4.7). The extended intermolecular hydrogen bonding in **11** involves one N–H...N and three N–H...Cl moderate electrostatic hydrogen bonds (Table 4.3), which aggregate the molecules in a continuous 1D chain running along the crystallographic *b* axis forming a twofold helix structure and further to a 2D net along the *a* axis (Figure A.30, appendix).

Table 4.3. Hydrogen bonds of **11**

D	H	A	d(D-H)/Å	d(H-A)/Å	d(D-A)/Å	D-H-A/°	H-Bond Type
N3	H3A	N4 ¹	0.81(3)	2.70(3)	3.313(3)	134(2)	Inter
N3	H3B	Cl2 ²	0.83(3)	3.00(3)	3.733(2)	148(3)	Inter
N3	H3B	N1	0.83(3)	2.00(3)	2.635(3)	132(3)	Intra RAHB
N1	H1	Cl1	0.78(3)	2.45(3)	2.9779(19)	127(3)	Inter
N1	H1	Cl3 ³	0.78(3)	3.45(3)	4.1486(19)	151(3)	Inter

¹2-X,2-Y,1-Z; ²+X,1+Y,+Z; ³1-X,2-Y,-Z

Table 4.4. Hydrogen bonds of **13**

D	H	A	d(D-H)/Å	d(H-A)/Å	d(D-A)/Å	D-H-A/°	H-Bond Type
N1	H1	Cl12	0.84(3)	2.39(3)	2.9644(16)	126(2)	Inter
N3	H3B	N3 ¹	0.84(3)	3.51(3)	4.342(3)	171(2)	Inter
N3	H3B	N4 ¹	0.84(3)	2.52(3)	3.201(2)	139(2)	Inter
N3	H3A	Cl11 ²	0.85(3)	3.12(3)	3.8019(16)	138.9(2)	Inter
N3	H3A	Cl13 ³	0.85(3)	3.03(2)	3.6251(17)	129.0(2)	Inter
N3	H3A	N1	0.85(3)	1.96(2)	2.633(2)	135(2)	Intra RAHB

¹2-X,2-Y,1-Z; ²1+X,+Y,+Z; ³+X,1+Y,+Z

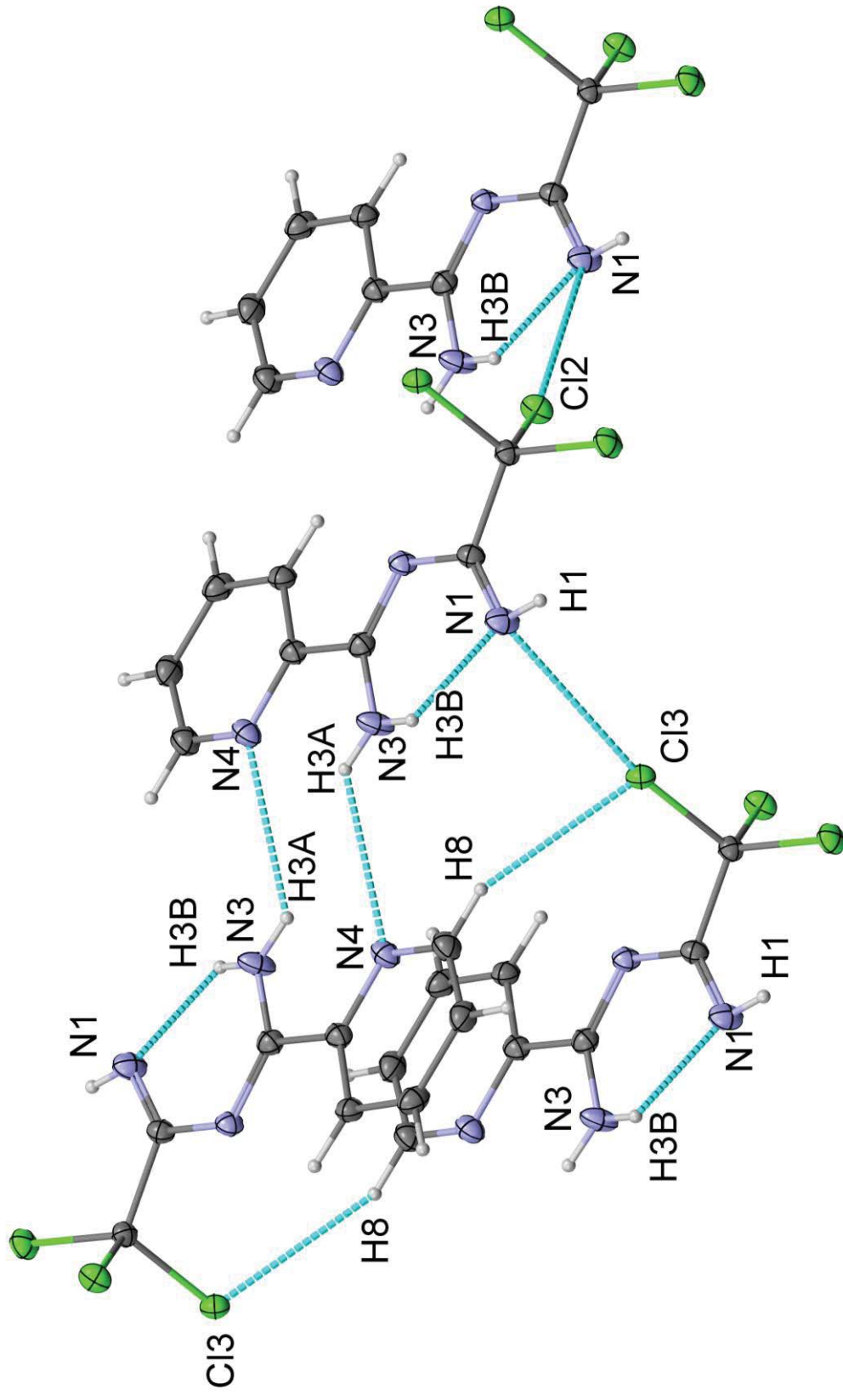


Figure 4.6. Structure of **11** showing hydrogen bonding (indicated by dashed lines). Displacement ellipsoids drawn at the 50% probability level. Key atoms involved in H-bonding are labelled.

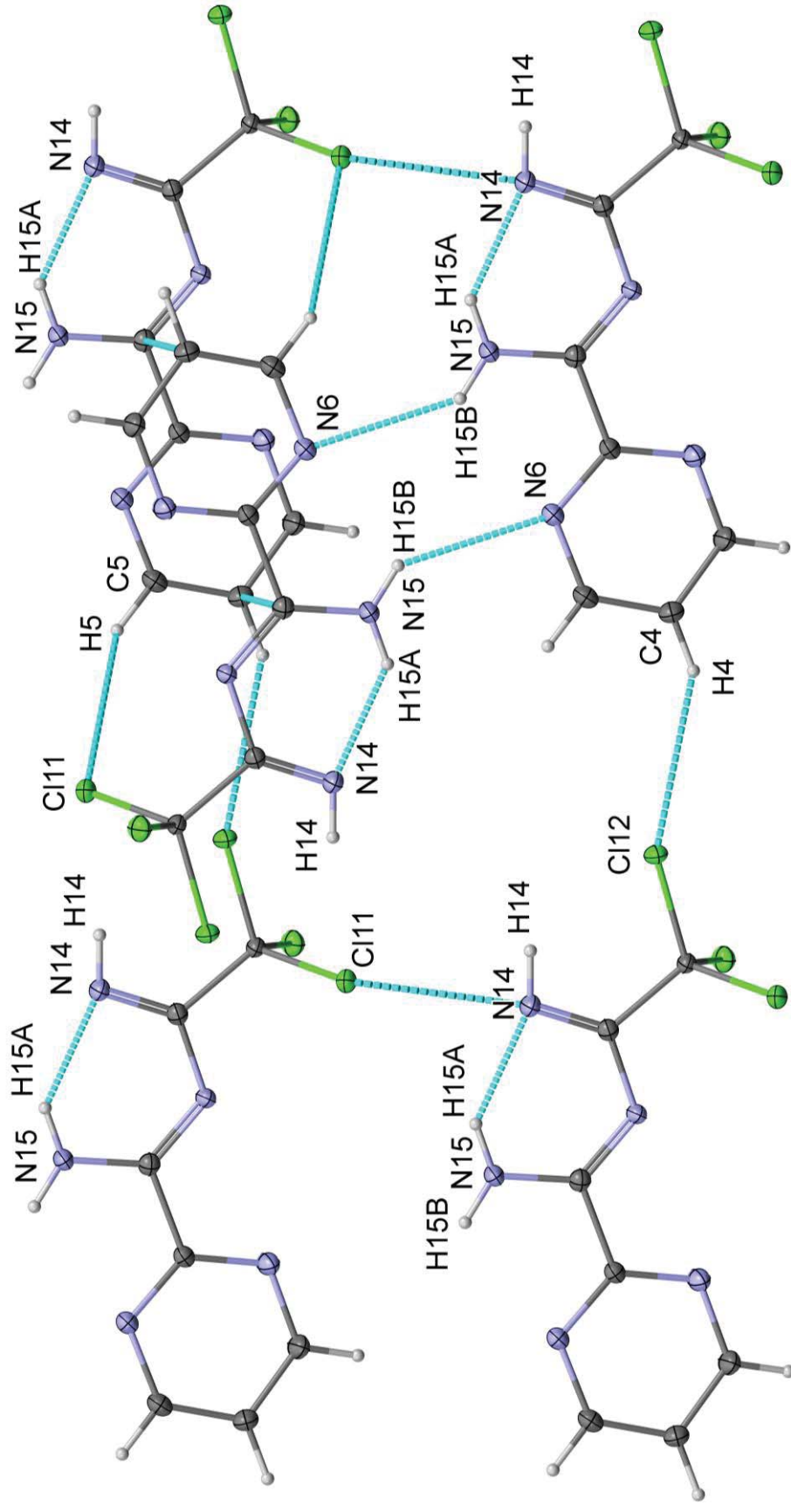


Figure 4.7. Structure of **13** showing hydrogen bonding (indicated by dashed lines). Displacement ellipsoids drawn at the 50% probability level. Key atoms involved in H-bonding are labelled.

An identical intermolecular hydrogen bonding network is observed in **13** with a total of five moderate electrostatic hydrogen bonds (Table 4.4) involving two N–H...N and three N–H...Cl forming 2D framework (Figure A.31, appendix). The unique N1–H1...Cl2 hydrogen bond in both structures helps to restrain the Cl2 which is almost co-planar to the N–C=N–C=N moiety.

4.4 Conclusions

The asymmetric imidoamidines **11** and **13** were successfully prepared and characterized. The structures of the compounds display unexpected remarkable properties in the solid-state and in solution. It is expected that the isolated **11** and **13** would be potent ligands with a rich coordination chemistry in addition to existing complexes of imidoamidines in the literature. More so, they are also ideal precursor candidates for the synthesis of valuable organic compounds including thiatriazines which is the eventual goal of this research work and other nitrogen-rich compounds in industrial and manufacturing applications.

4.5 References

1. Bourget-Merle, L.; Lappert, M. F.; Severn, J. R., The chemistry of β -diketiminatometal complexes. *Chem. Rev.* **2002**, *102*, 3031-3065.
2. Xiao, J.; Ren, S.; Liu, Q., Atom-efficient synthesis of 2,4,6-trisubstituted 1,3,5-triazines via Fe-catalyzed cyclization of aldehydes with NH_4I as the sole nitrogen source. *RSC Adv.* **2020**, *10*, 22230-22233.
3. Clodt, J. I.; Wigbers, C.; Reiermann, R.; Froehlich, R.; Wuerthwein, E.-U., Synthesis and aggregation properties of two- and three-armed nitrogen-rich chelate ligands: novel bis(N-acylamidines), tris(N-acylamidines) and bis(triazapentadienes) with flexible or rigid spacers. *Eur. J. Org. Chem.* **2011**, *2011*, 3197-3209.
4. Kajiwara, T.; Ito, T., 1,3,5-Triazapentadiene, a novel tridentate ligand that bridges two metal ions in a $\kappa_1\text{N}:\kappa_2\text{N}$ bridging mode with C2 symmetry. *Eur. J. Inorg. Chem.* **2004**, 3084-3088.
5. Kajiwara, T.; Kamiyama, A.; Ito, T., Complexed bridging ligand, $(\text{Cu}(\text{bptap})_2)$, as a ferromagnetic coupler. *Chem. Commun.* **2002**, *2*, 1256-1257.
6. Boeré, R. T.; Roemmele, T. L.; Yu, X., Unsymmetrical 1 λ 3-1,2,4,6-thiatriazinyls with aryl and trifluoromethyl substituents: Synthesis, crystal structures, EPR spectroscopy, and voltammetry. *Inorg. Chem.* **2011**, *50*, 5123-5136.
7. Castañeda, R.; Hollingshead, A.; Gabidullin, B.; Brusso, J. L., Probing the coordination chemistry of N-2-pyridylimidoyl-2-pyridylamidine: A versatile ligand with multiple coordination sites. *Cryst. Growth Des.* **2017**, *17*, 6572-6578.
8. Yousaf, M.; Yutronkie, N. J.; Castañeda, R.; Klein, J. A.; Brusso, J., Boratriazines: inducing luminescence through boron incorporation into a terpy-type framework. *New J. Chem.* **2017**, *41*, 12218-12224.
9. Dias, H. V. R.; Singh, S., Copper(I) complexes of fluorinated triazapentadienyl ligands: Synthesis and characterization of $[\text{N}\{(\text{C}_3\text{F}_7)\text{C}(\text{DiPP})\text{N}\}_2]\text{CuL}$ (where L = NCCCH_3 , CNBut , CO ; DiPP = 2,6-diisopropylphenyl). *Inorg. Chem.* **2004**, *43*, 5786-5788.
10. Kulkarni, N. V.; Das, A.; Ridlen, S. G.; Maxfield, E.; Adiraju, V. A. K.; Yousufuddin, M.; Dias, H. V. R., Fluorinated triazapentadienyl ligand supported ethyl zinc(ii) complexes: Reaction with dioxygen and catalytic applications in the Tishchenko reaction. *Dalton Trans.* **2016**, *45*, 4896-4906.
11. Dias, H. V. R.; Singh, S.; Cundari, T. R., Monomeric thallium(I) complexes of fluorinated triazapentadienyl ligands. *Angew. Chem., Int. Ed.* **2005**, *44*, 4907-4910.
12. Wigbers, C.; Prigge, J.; Mu, Z.; Fröhlich, R.; Chi, L.; Würthwein, E. U., Synthesis, structures, and aggregation properties of N-acylamidines. Wiley Online Library: 2011.

13. Gushchin, P. V.; Tyan, M. R.; Bokach, N. A.; Revenco, M. D.; Haukka, M.; Wang, M. J.; Lai, C. H.; Chou, P. T.; Kukushkin, V. Y., Novel tailoring reaction for two adjacent coordinated nitriles giving platinum 1,3,5-triazapentadiene complexes. *Inorg. Chem.* **2008**, *47*, 11487-11500.
14. Heße, N.; Fröhlich, R.; Humelnicu, I.; Würthwein, E. U., 1,3,5-Triazapentadienes as chelating ligands: 1,2,4-triphenyl-1,3,5-triazapentadiene complexes of cobalt(II), nickel(II), palladium(II), copper(II) and zinc(II). *Eur. J. Inorg. Chem.* **2005**, 2189-2197.
15. Kopylovich, M. N.; Kirillov, A. M.; Tronova, E. A.; Haukka, M.; Kukushkin, V. Y.; Pombeiro, A. J. L., 1,3,5-Triazapentadiene nickel(ii) complexes derived from a ketoxime-mediated single-pot transformation of nitriles. *Eur. J. Inorg. Chem.* **2010**, 2425-2432.
16. Kopylovich, M. N.; Pombeiro, A. J. L., Coordination chemistry of 1,3,5-triazapentadienes. *Coord. Chem. Rev.* **2011**, *255*, 339-355.
17. Dias, H. V. R.; Flores, J. A.; Pellei, M.; Morresi, B.; Lobbia, G. G.; Singh, S.; Kobayashi, Y.; Yousufuddin, M.; Santini, C., Silver(I) and copper(I) complexes supported by fully fluorinated 1,3,5-triazapentadienyl ligands. *Dalton Trans.* **2011**, *40*, 8569-8580.
18. Mahmudov, K. T.; Pombeiro, A. J. L., Resonance-assisted hydrogen bonding as a driving force in synthesis and a synthon in the design of materials. *Chem. - Eur. J.* **2016**, *22*, 16356-16398.
19. Gilli, P.; Bertolasi, V.; Pretto, L.; Antonov, L.; Gilli, G., Variable-temperature X-ray crystallographic and DFT computational study of the N-H center dot center dot center dot O/N center dot center dot center dot H-O tautomeric competition in 1-(arylo)-2-naphthols. Outline of a transition-state hydrogen-bond theory. *J. Am. Chem. Soc.* **2005**, *127*, 4943-4953.
20. Mahmudov, K. T.; Maharramov, A. M.; Aliyeva, R. A.; Chyragov, F. M.; Askerov, R. K.; Hasanov, P. Q.; Kopylovich, M. N.; Pombeiro, A. J. L., Tautomeric equilibria of para-bromophenyl substituted arylhydrazones of beta-diketones. *J. Mol. Struct.* **2011**, *1006*, 576-579.
21. Kopylovich, M. N.; Lasri, J.; Da Silva, M. F. C. G.; Pombeiro, A. J. L., Single-pot template transformations of cyanopyridines on a PdII centre: Syntheses of ketoimine and 2,4-dipyridyl-1,3,5-triazapentadiene palladium(II) complexes and their catalytic activity for microwave-assisted Suzuki-Miyaura and Heck reactions. *Dalton Trans.* **2009**, 3074-3084.
22. Marihart, E. A.; Greving, J. B.; Fröhlich, R.; Würthwein, E. U., (5-Imino-4,5-dihydro-3H-pyrrol-2-yl)amines as sterically restrained 1,3,5-triazapenta-1,3-dienes: Useful building blocks for the synthesis of oligonitriles. *Eur. J. Org. Chem.* **2007**, 5071-5081.
23. Nesterova, O. V.; Kopylovich, M. N.; Nesterov, D. S., A comparative study of the catalytic behaviour of alkoxy-1,3,5-triazapentadiene copper(II) complexes in cyclohexane oxidation. *Inorg.* **2019**, *7*.

24. Figiel, P. J.; Kopylovich, M. N.; Lasri, J.; Da Silva, M. F. C. G.; Da Silva, J. J. R. F.; Pombeiro, A. J. L., Solvent-free microwave-assisted peroxidative oxidation of secondary alcohols to the corresponding ketones catalyzed by copper(II) 2,4-alkoxy-1,3,5-triazapentadienato complexes. *Chem. Commun.* **2010**, *46*, 2766-2768.
25. Flores, J. A.; Badarinarayana, V.; Singh, S.; Lovely, C. J.; Dias, H. V. R., Synthesis and catalytic activity of an electron-deficient copper-ethylene triazapentadienyl complex. *Dalton Trans.* **2009**, 7648-7652.
26. Kopylovich, M. N.; Karabach, Y. Y.; Guedes Da Silva, M. F. C.; Figiel, P. J.; Lasri, J.; Pombeiro, A. J. L., Alkoxy-1,3,5-triazapentadien copper(II) complexes: Template formation and applications for the preparation of pyrimidines and as catalysts for oxidation of alcohols to carbonyl products. *Chem. - Eur. J.* **2012**, *18*, 899-914.
27. Ribeiro, A. P. C.; Karabach, Y. Y.; Martins, L. M. D. R. S.; Mahmoud, A. G.; Fátima Guedes da Silva, M. C.; Pombeiro, A. J. L., Nickel(II)-2-amino-4-alkoxy-1,3,5-triazapentadienate complexes as catalysts for Heck and Henry reactions†. *RSC Adv.* **2016**, *6*, 29159-29163.
28. Shixaliyev, N. Q.; Gurbanov, A. V.; Maharramov, A. M.; Mahmudov, K. T.; Kopylovich, M. N.; Martins, L. M. D. R. S.; Muzalevskiy, V. M.; Nenajdenko, V. G.; Pombeiro, A. J. L., Halogen-bonded tris(2,4-bis(trichloromethyl)-1,3,5-triazapentadienato)-M(III) [M = Mn, Fe, Co] complexes and their catalytic activity in the peroxidative oxidation of 1-phenylethanol to acetophenone. *New J. Chem.* **2014**, *38*, 4807-4815.
29. Shixaliyev, N. Q.; Maharramov, A. M.; Gurbanov, A. V.; Nenajdenko, V. G.; Muzalevskiy, V. M.; Mahmudov, K. T.; Kopylovich, M. N., Zinc(II)-1,3,5-triazapentadienate complex as effective catalyst in Henry reaction. *Catal. Today* **2013**, *217*, 76-79.
30. Tian, D.; Xie, Q.; Yan, L.; Tong, H.; Zhou, M., Zinc and aluminum complexes derived from 2, 4-N, N'-disubstituted 1, 3, 5-triazapentadienyl ligands: Synthesis, characterization and catalysis of the ring-opening polymerization of rac-lactide. *Inorg. Chem. Commun.* **2015**, *58*, 35-38.
31. Starikova, A. A.; Minkin, V. I., Magnetic properties of adducts of trinuclear heterometallic complexes with acetonitrile: Quantum chemical study. *Russ. J. Coord. Chem.* **2018**, *44*, 483-488.
32. Siedle, A. R.; Webb, R. J.; Behr, F. E.; Newmark, R. A.; Weil, D. A.; Erickson, K.; Naujok, R.; Brostrom, M.; Mueller, M.; Chou, S. H.; Young Jr, V. G., Perfluoroalkyl-substituted triazapentadienes and their metal complexes. *Inorg. Chem.* **2003**, *42*, 932-934.
33. Cooper, F. C.; Partridge, M. W.; Short, W. F., 88. Diamidides. Part I. Derivatives of triazapentadiene and tetra-azaheptatriene. *J. Chem. Soc. (Res.)* **1951**, 391-404.
34. Eliseev, I. I.; Gushchin, P. V.; Chen, Y. A.; Chou, P. T.; Haukka, M.; Starova, G. L.; Kukushkin, V. Y., Phosphorescent Pt(II) systems featuring both 2,2'-dipyridylamine and 1,3,5-triazapentadiene ligands. *Eur. J. Inorg. Chem.* **2014**, *2014*, 4101-4108.

35. Elvidge, J. A.; Barot, N. R., Imidines and diamidides (1,3,5-triazapentadienes). In *Supplement A The Chemistry of Double-Bonded Functional Groups*, 2010; pp 1167-1249.
36. Flores, J. A.; Rasika Dias, H. V., Gold(I) ethylene and copper(I) ethylene complexes supported by a polyhalogenated triazapentadienyl ligand. *Inorg. Chem.* **2008**, *47*, 4448-4450.
37. Flores, J. A.; Kobayashi, Y.; Dias, H. V. R., Synthesis and characterization of silver(I) adducts supported solely by 1,3,5-triazapentadienyl ligands or by triazapentadienyl and other N-donors. *Dalton Trans.* **2011**, *40*, 10351-10359.
38. Guo, J. P.; Wong, W. K.; Wong, W. Y., The template effect of palladium(II): Synthesis, characterization, and crystal structures of 2,4-substituted 1,3,5-triazapentadienatopalladium(II) complexes. *Eur. J. Inorg. Chem.* **2006**, 3634-3640.
39. Häger, I.; Fröhlich, R.; Würthwein, E. U., Synthesis of secondary, tertiary and quaternary 1,3,5-triazapenta-1,3- dienes and their Co(II), Zn(II), Pd(II), Cu(II) and BF₂ coordination compounds. *Eur. J. Inorg. Chem.* **2009**, 2415-2428.
40. Kalutarage, L. C.; Heeg, M. J.; Martin, P. D.; Saly, M. J.; Kuiper, D. S.; Winter, C. H., Volatility and high thermal stability in mid-to-late first-row transition-metal complexes containing 1,2,5-triazapentadienyl ligands. *Inorg. Chem.* **2013**, *52*, 1182-1184.
41. Pernik, I.; Maitland, B. J.; Stasch, A.; Jones, C., Synthesis and attempted reductions of bulky 1,3,5-triazapentadienyl groups 2 and 13 halide complexes. *Can. J. Chem.* **2018**, *96*, 513-521.
42. Rad'kova, N. Y.; Kovylyna, T. A.; Cherkasov, A. V.; Lyssenko, K. A.; Ob'edkov, A. M.; Trifonov, A. A., Coordination features of the 1,3,5-triazapentadienyl ligand in alkyl complexes of rare-earth metals. *Eur. J. Inorg. Chem.* **2021**.
43. Bolaño, T.; Brent Gunnoe, T.; Sabat, M., Direct coupling of nitriles and aniline to form the triazapentadiene species Rh(III){NH=C(R)N(Ph)C(R)=NH}. *Dalton Trans.* **2013**, *42*, 347-350.
44. Ivanov, D. M.; Gushchin, P. V.; Novikov, A. S.; Avdontceva, M. S.; Zolotarev, A. A.; Starova, G. L.; Chen, Y.-T.; Liu, S.-H.; Chou, P.-T.; Kukushkin, V. Y., Platinum(II)-mediated double coupling of 2,3-diphenylmaleimidine with nitrile functionalities to give annulated pentaazanotetraenate (PANT) systems. *Eur. J. Inorg. Chem.* **2016**, *2016*, 1480-1487.
45. Pinner, A., Ueber das sog. Dibenzimidin. *Berichte der deutschen chemischen Gesellschaft* **1892**, *25*, 1624-1627.
46. Peak, D. A., Diamidides. Part II. 2:4-Diaryltriazapentadienes. *J. Chem. Soc. (Res.)* **1952**, 215-226.

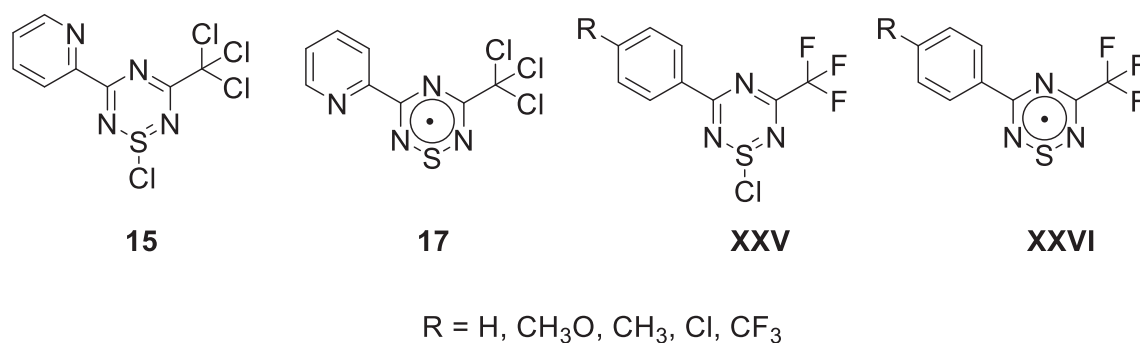
47. Ley, H.; Müller, F., Über zwei neue Klassen Metallsalze bildender Imidbasen. Beitrag zur Theorie der inneren Metallkomplexsalze. *Berichte der deutschen chemischen Gesellschaft* **1907**, *40*, 2950-2958.
48. Heße, N.; Fröhlich, R.; Wibbeling, B.; Würthwein, E. U., 1,3,5-Triazapenta-1,3-dienes: Useful building blocks for the synthesis of 1,2-dihydro-1,3,5-triazines and oligonitriles. *Eur. J. Org. Chem.* **2006**, 3923-3937.
49. Masuda, J. D.; Stephan, D. W., Neutral and cationic aluminium complexes of a sterically demanding N-imidoamidate ligand. *Dalton Trans.* **2006**, 2089-2097.
50. Zhang, J.-P.; Lin, Y.-Y.; Huang, X.-C.; Chen, X.-M., Copper(I) 1,2,4-triazolates and related complexes: Studies of the solvothermal ligand reactions, network topologies, and photoluminescence properties. *J. Am. Chem. Soc.* **2005**, *127*, 5495-5506.
51. Kopylovich, M. N.; Pombeiro, A. J. L.; Fischer, A.; Kloo, L.; Kukushkin, V. Y., Facile Ni(II)/ketoxime-mediated conversion of organonitriles into imidoamidate ligands. Synthesis of imidoamidates and acetyl amides. *Inorg. Chem.* **2003**, *42*, 7239-7248.
52. Subbarayan, V.; Ruppel, J. V.; Zhu, S.; Perman, J. A.; Zhang, X. P., Highly asymmetric cobalt-catalyzed aziridination of alkenes with trichloroethoxysulfonyl azide (TcesN(3)). *Chem. Commun.* **2009**, 4266-4268.
53. Prashanth, B.; Singh, S.; Verma, A., Co(II), Ni(II) and Cu(II) complexes of sterically encumbered N-arylimidoamidate based [N,N'] chelating ligands. *Polyhedron* **2015**, *99*, 17-25.
54. Wikstrom, J. P.; Filatov, A. S.; Rybak-Akimova, E. V., Condensation of nitriles with amides promoted by coordinatively unsaturated bis-nickel(ii)-hydroxy complex: A new route to alkyl- and aryl-imidoamidates. *Chem. Commun.* **2010**, *46*, 424-426.
55. Guo, J.; Wong, W. K.; Wong, W. Y., Syntheses and Crystal Structures of Tetrakis(arylamidate)nickel(II) Chloride and Bis[2,4-dipyridyl-1,3,5-triazapentadienato]nickel(II). *Eur. J. Inorg. Chem.* **2004**, 267-275.
56. Schaefer, F. C.; Hechenbleikner, I.; Peters, G. A.; Wystrach, V. P., Synthesis of the sym-triazine system. Trimerization and cotrimerization of amidines. *J. Am. Chem. Soc.* **1959**, *81*, 1466-1470.
57. Schaefer, F. C.; Krapcho, A. P., Preparation of amidine salts by reaction of nitriles with ammonium salts in the presence of ammonia. *J. Org. Chem.* **1962**, *27*, 1255-1258.
58. Boere, R. T.; Roemmele, T. L.; Kondage, S. S.; Zhou, J.; Parvez, M., Five related N'-(2,2,2-trichloroethanimido)benzene-1-carboximidamides. *Acta Crystallogr., Sect. C: Cryst. Struct. Commun.* **2011**, *67*, O273-O277.

59. Boéré, R. E.; Boéré, R. T.; Masuda, J.; Wolmershäuser, G., Preparation, X-ray structure, and dynamic solution behaviour of N,N',N'-tris(2,6-diisopropylphenyl)-guanidine, and its reaction with molybdenum carbonyl. *Can. J. Chem.* **2000**, *78*, 1613-1619.
60. Karfunkel, H. R.; Wu, Z. J.; Burkhard, A.; Rihs, G.; Sinnreich, D.; Buerger, H. M.; Stanek, J., Crystal packing calculations and Rietveld refinement in elucidating the crystal structures of two modifications of 4-amidinoindanone guanylhydrazone. *Acta Crystallogr., Sect. B* **1996**, *52*, 555-561.

Chapter 5 Progress towards the preparation of asymmetric 3-trichloromethyl-5-(2-pyridyl)-1-thia-2,4,6-triazinyl

This chapter describes the achievements to date in the synthesis of asymmetric 1-chloro-3-trichloromethyl-5-(2-pyridyl)-1-thia-2,4,6-triazine (**15**) and the associated thiatriazinyl radical (**17**) (Chart 5.1). The radical is intended to be used as a chelating ligand for transition metals complexes with interesting magnetic properties.

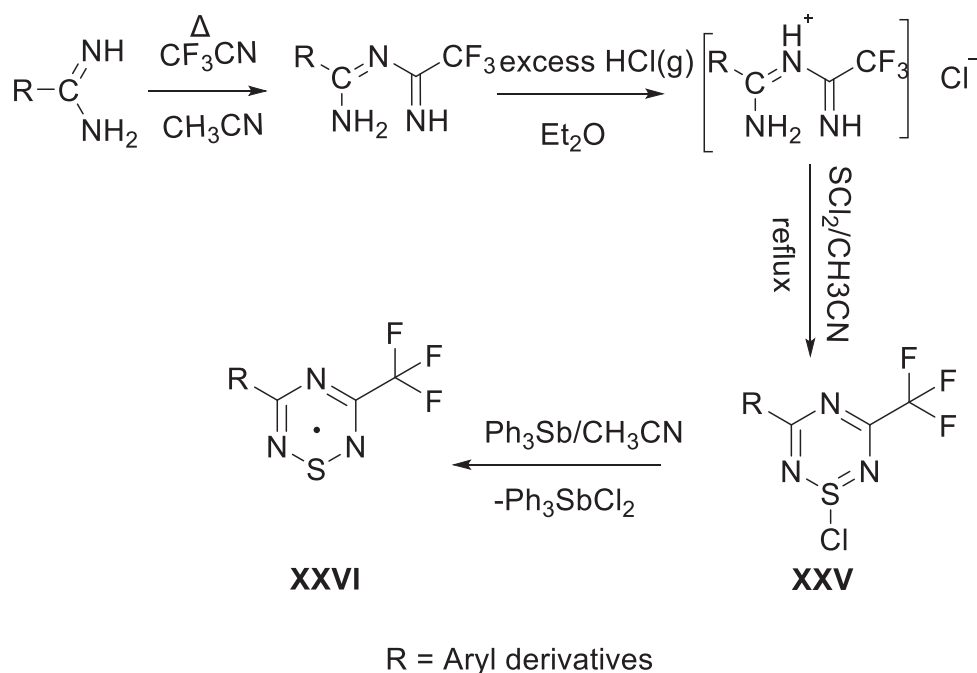
Chart 5.1



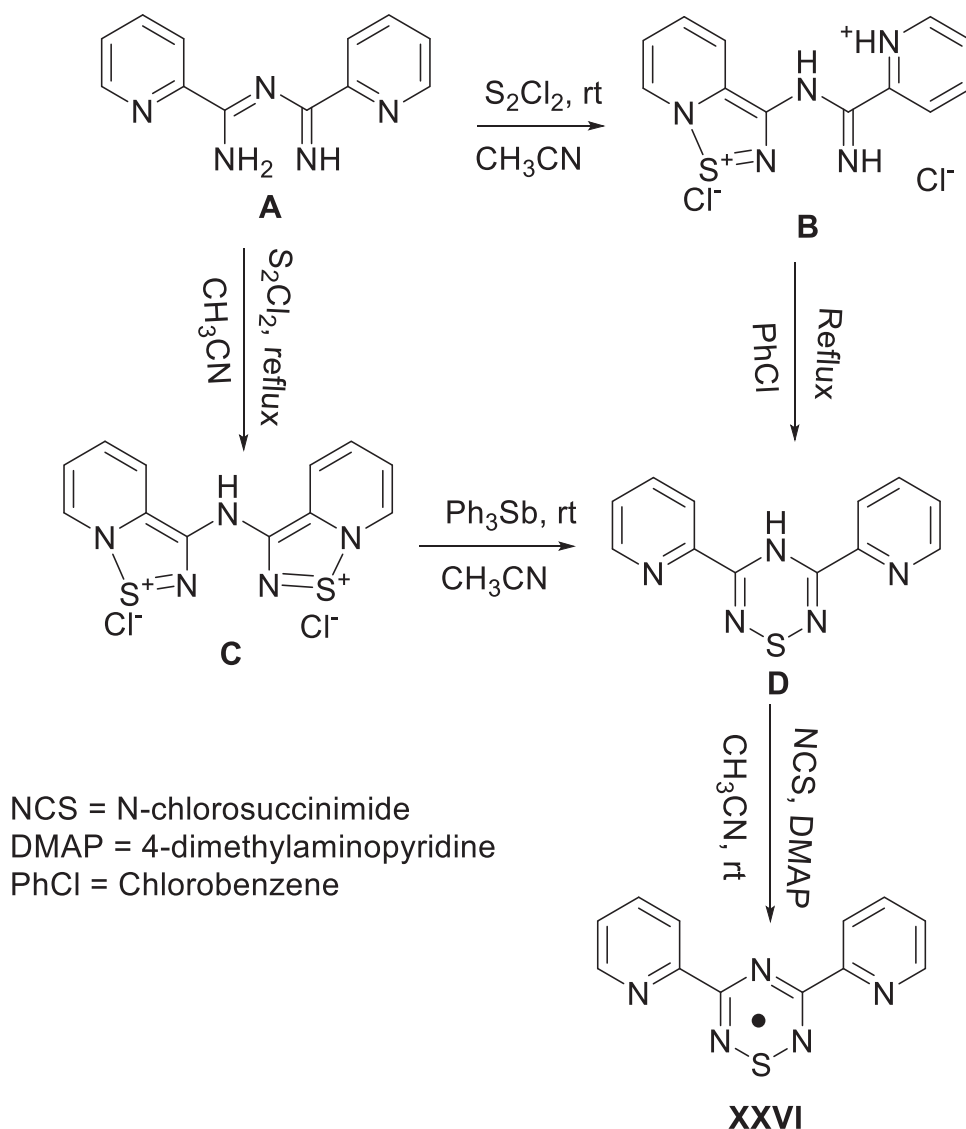
5.1 Introduction

Detailed background on thiatriazinyl radicals (TTA[•]) has been covered in Chapter 1. The radicals generally exist as diamagnetic cofacial dimers in the solid-state with short S \cdots S contacts (Section 1.4).¹⁻³ The reaction of sulfur dichloride (SCl₂) with *N*-imidoylamidines, passivated with anhydrous hydrogen chloride to their corresponding hydrochlorides, under reflux in acetonitrile (CH₃CN) has been found effective for the synthesis of asymmetric 1-chloro-3-trifluoromethyl-5-aryl-1,2,4,6-thiatriazines (RCF₃TTACl, **XXV**) from which their radicals (RCF₃TTA[•], **XXVI**) were generated in high yields by one electron reduction by Ph₃Sb in CH₃CN (Scheme 5.1).⁴ The method has also been used successfully for the synthesis of most symmetric aryl¹⁻² and halogenated³ TTA's. Using non-passivated imidoylamidines typically results in unwanted product that hinders

the formation of the TTACl ring. For instance, Brusso and coworkers⁵ went through a complex synthetic pathway to generate the first symmetric heterocyclic-substituted TTA*, 3,5-bis(2-pyridyl)-1,2,4,6-thiatriazinyl (Py₂TTA*, **XXVI**, Section 1.4.1). As shown in Scheme 5.2, they discovered that the condensation of N-2-pyridylimidoyl-2-pyridylamidine (Py₂ImAm, **A**) with sulfur monochloride (S₂Cl₂) in CH₃CN at room temperature and under reflux led to the formation of bridgehead cation salt (**B**) and bridgehead dication chloride (**C**) salts respectively. Two electron reduction of the latter with Ph₃Sb led to the isolation of 8 electron closed-shell 3,5-bis(2-pyridyl)-4-hydro-1,2,4,6-thiatriazine (Py₂TTAH, **D**) which was then oxidized to open-shell 7π electron Py₂TTA* with N-chlorosuccinimide (NCS) in the presence of 4-dimethylaminopyridine (DMAP).



Scheme 5.1. Asymmetric TTACl and TTA radical synthesis route.



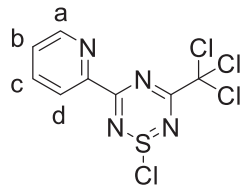
Scheme 5.2. Synthesis of **XXIV** using S_2Cl_2 .

5.2 Preparation of 1-chloro-3-trichloromethyl-5-(2-pyridyl)-1-thia-2,4,6-triazine via S_2Cl_2 condensation reaction

The synthesis of the asymmetric 1-chloro-3-trichloromethyl-5-(2-pyridyl)-1-thia-2,4,6-triazine (**15**) and 3-trichloromethyl-5-(2-pyridyl)-1-thia-2,4,6-triazinyl radical (**17**) was undertaken following established condensation procedures in the literature (Scheme 5.1). In this work S_2Cl_2 is however considered instead of SCl_2 , because the latter is not commercially available

anymore. As shown in Scheme 5.3, preparation of **15** was attempted through the condensation reaction of the 2-pyridylimidoamidinium hydrochloride, **14** (see Chapter 4) with excess S_2Cl_2 under reflux to ensure reaction completion. The TTACl ring was successfully formed with no evidence of bridge-head formation as previously mentioned by Brusso and coworkers.⁵ This indicates that the passivation of imidoamidiniums (with HCl) is important to tailor the condensation reaction mechanism towards formation of TTACl. However, isolation of **15** is quite difficult due to protonation of the nitrogen atom of the pyridyl substituent which is associated with the basic nature of the ring to form **15**.HCl. More importantly, it seems that mixed salts like **15**–**15**.HCl salt (Scheme 5.3) can form, as confirmed by an X-ray structural analysis of yellow blocks that grew from solution of the condensation reaction (prepared by refluxing for 16 h) after staying in a freezer at $-35^\circ C$ for two weeks. Optimization of this method for effective isolation of either **15** or high purity **15**.HCl were conducted, but various complications ensued from the trials. For instance, an attempt to isolate **15**.HCl for subsequent treatment to generate the free TTACl (**15**) by reducing reaction time to around 1–2 h was not successful because **15** was still co-generated. Besides, a large amount of sulfur ascribed to S_2Cl_2 disproportionation is a significant by-product that hinders further workup. An attempt to extract cogenerated component **15** from the oil (**15**–**15**.HCl) using carbon disulfide (CS_2) resulted in the hydrolysis of **15** to the corresponding 1-oxo-3-trichloromethyl-5-(2-pyridyl)-1-thia-2,4,6-triazine, (**16**) due to high reactivity of the S–Cl bond towards moisture and oxygen.⁶⁻⁷ 1H NMR data substantiate the formation of the TTACl ring (Table 5.1) since only pyridyl signals were observed with no peaks associated with the imidoamidinium N–H protons.

Table 5.1. ^1H NMR data of **15–15.HCl** and **16**.

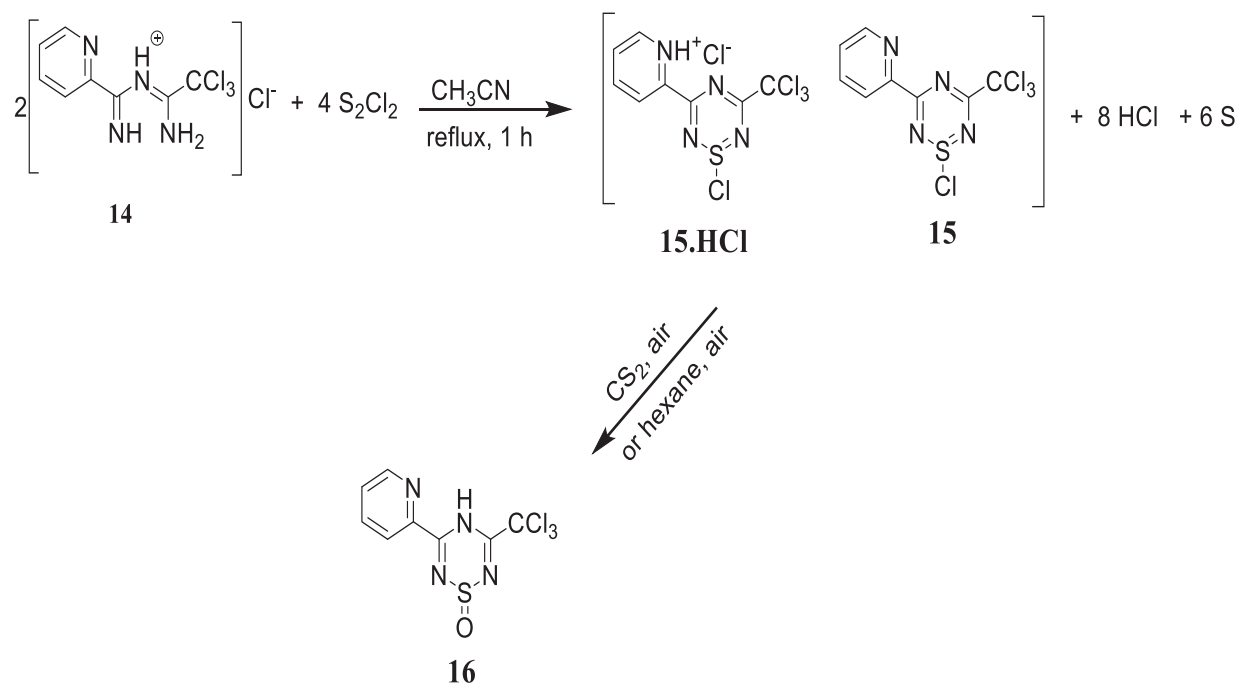


Compound	a (δ , ppm)	b (δ , ppm)	c (δ , ppm)	d (δ , ppm)
15 Py ₂ TTACl	9.31	8.27	7.89	8.82
Py ₂ TTA=O, 16	8.71	8.00	7.63	8.48
16	8.71	7.99	7.63	8.48

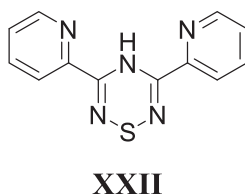
The ^1H NMR spectrum does not fully interpret the composition of **15–15.HCl** as only part of the material, **15** is soluble in CDCl_3 while the **15.HCl** portion is insoluble. The ^1H NMR spectra of the CDCl_3 extract revealed sets of minor and major peaks. The minor signals are assigned to **16** due to partial hydrolysis as confirmed by ^1H NMR spectroscopy on a pure sample of **16** obtained from intentional hydrolysis of **15**. The major component is assigned to **15** and it is quite soluble in chlorinated solvents being a halogenated organic molecule.⁸⁻⁹

The signals of *ortho* protons in both **16** and assumed **15** are shifted to low frequency relative to Py₂ImAm (**11**) whilst the two *meta* and *para* peaks shift to higher frequency. The ^1H NMR peaks of **15** are strongly influenced with 0.52 ppm of H *meta* next to N atom, 0.42 ppm of the second *meta* H and 0.45 ppm of *para* H deviating from those of **11** whereas the signals of **16** are less affected with shifts of 0.10 ppm, 0.14 ppm and 0.19 ppm respectively from corresponding signals in **11**. The *ortho* H next to the TTA ring experiences a significant shift in **15** (0.27 ppm) compared to **16** (0.07 ppm) against **11**. A similar pattern of proton NMR signal variation has been observed in the formation of TTA rings in the synthesis of 3,5-di(pyridin-2-yl)-4H-1,2,4,6-

thiatriazine (**XXII**).⁵ Due to high susceptibility of **15** to hydrolysis in air, a ¹³C NMR experiment was not conducted.

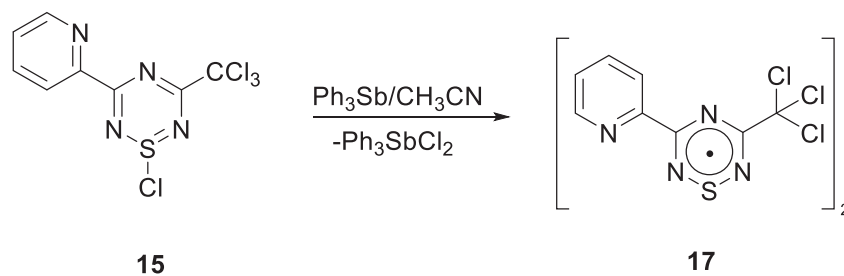


Scheme 5.3. Synthesis of **15** by S_2Cl_2 condensation



In furthering the modification of experimental conditions to generate **15**, thermolysis to decompose **15–15.HCl** to **15** and HCl (g) was attempted. A dark colored sticky oil was obtained in this step which did not permit product crystallization, however, reduction of a solution of this material in (3X) freeze-pump-thawed CH_3CN using triphenyl antimony (Ph_3Sb) as illustrated in Scheme 5.4 using the setup in Figure 5.1 led to the thiatriazinyl radical (**17**) dimer with distinctive deep, purple-colored microcrystals in low yield (~14 %).

Since condensation of **11** to **15** using S_2Cl_2 is prone to high sulfur production, SCl_2 was thus considered because it has been proved to be viable for TTACl synthesis with insignificant side reactions.^{2, 6, 10-12} On repeating the reaction with SCl_2 , the sulfur production was drastically reduced, but formation of **15**-**15**.HCl (an oily product) still remains a major challenge. Despite the formation of **15**-**15**.HCl, crystals of **15**.HCl were found in the oil. An extraction workup on the oil with hot hexane produced a leftover solid assumed to be the insoluble **15**.HCl which accounts for over 80–90 % of the oil. The thermal decomposition of the solid residue, however, gave a reddish melt that failed to produce dimer **17** with the formation of a deep red solution. This implies that complete thermolysis of the protonated Py_2TTACl (**15**.HCl) is not feasible due to strong basicity of the pyridyl group of the molecule.



Scheme 5.4. Reduction of **15** to corresponding radical dimer **17**

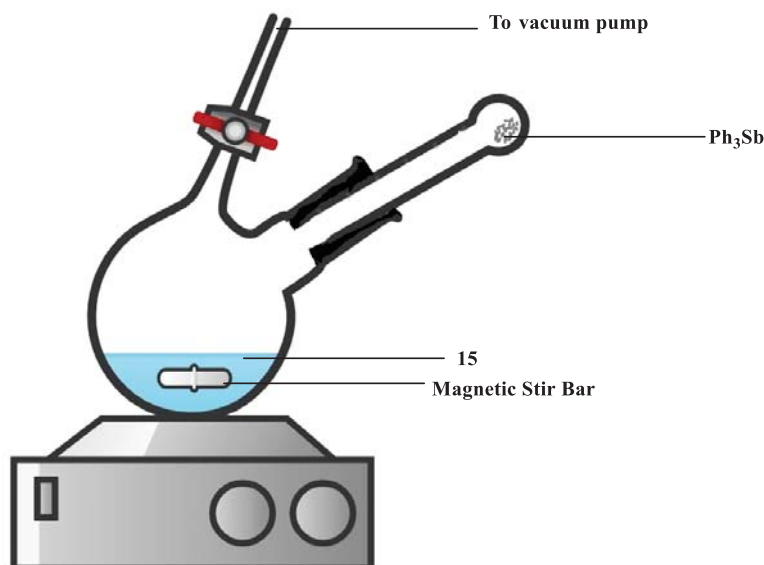


Figure 5.1. Setup for reduction of **15** to corresponding radical dimer **17**.

5.3 Crystallographic analysis of structures

Crystallographic experimental and refinement data are summarized in Table 6.1 (Chapter 6). A total of five crystal structures were determined at 100 K. All the structures obtained confirm the formation of the TTA ring with the S–Cl in **15–15.HCl** (Figure 5.2) and **15.HCl** (Figure 5.3) as well as the S=O bonds in two polymorphs **a** and **b** of **16** that were obtained from different solvents (Figure 5.4). Both S–Cl and S=O bonds are almost perpendicular to the ring plane which is an intrinsic characteristic of TTA system.^{2, 13-16} The compounds **15–15.HCl**, **16b** and **17** crystallize in the triclinic space group $P\bar{1}$ with two formula units in their unit cells while **16a** and **15.HCl** both crystallize in the monoclinic space group $P2_1/c$ with four formula units in their unit cells (Chapter 6). All C–N and S–N bonds except for the structures for **16a** and **16b** are not significantly different indicating a delocalized electronic structure of the TTA rings.

both structures. In all, the average C–N bond lengths recorded are within the range of 1.329(2)–1.341(2) Å for the asymmetric **XXV**⁴ analogues and 1.332(5) – 1.375(4) Å for symmetric thiatriazines.^{1-2, 12}

Table 5.2. Selected bond distances (Å) and bond angles (°) of thiatriazines and the thiatriazinyl dimer

Compound	15–15.HCl		15.HCl	16a	16b	17
	15.HCl	15				
S1-Cl1/O1	2.1713(6)	2.3394(5)	2.160(3)	1.473(3)	1.471(2)	—
N1-C1	1.311(2)	1.310(2)	1.32(1)	1.274(5)	1.279(3)	1.29(2)
S1-N1	1.626(1)	1.627(1)	1.609(7)	1.703(4)	1.707(2)	1.65(2)
N2-S1	1.597(1)	1.595(1)	1.612(7)	1.690(3)	1.688(2)	1.63(2)
C2-N2	1.335(2)	1.337(2)	1.34(1)	1.282(5)	1.287(3)	1.31(2)
N3-C2	1.339(2)	1.334(2)	1.33(1)	1.371(6)	1.368(3)	1.35(2)
C1-N3	1.341(2)	1.338(2)	1.34(1)	1.368(4)	1.364(3)	1.38(3)
S1-N2-C2	117.3(1)	117.5(1)	116.2(6)	119.1(3)	119.2(2)	119(1)
N2-C2-N3	128.2(1)	127.8(1)	129.3(8)	125.3(4)	125.1(2)	127(2)
C2-N3-C1	117.1(1)	117.1(1)	117.1(7)	121.0(3)	121.6(2)	118(2)
N3-C1-N1	130.3(1)	130.2(1)	128.6(8)	126.3(4)	126.3(2)	128(2)
C1-N1-S1	116.0(1)	115.8(1)	116.8(6)	118.2(3)	117.8(2)	118(2)
N1-S1-N2	110.42(6)	110.25(6)	109.3(3)	104.2(2)	104.3(1)	108.4(9)

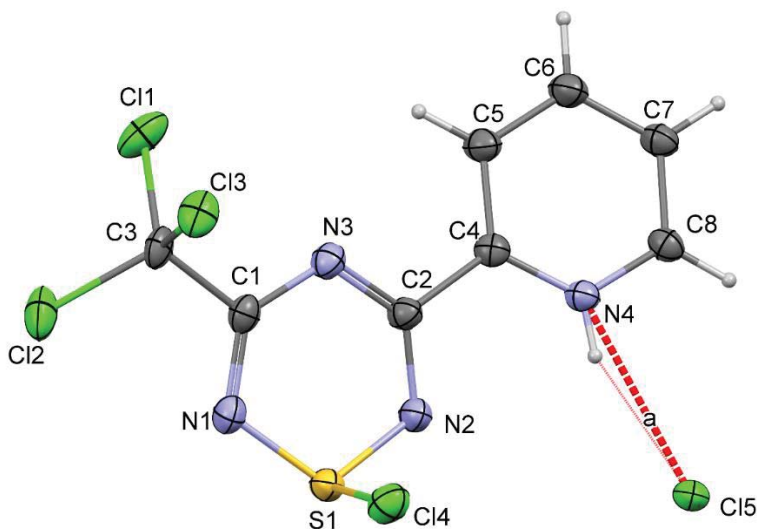


Figure 5.2. Displacement ellipsoid plot of **15.HCl** drawn at the 50% probability level showing the atom-labelling scheme and with short contacts indicated with dashed lines. The H atoms are shown as small spheres of arbitrary radii.

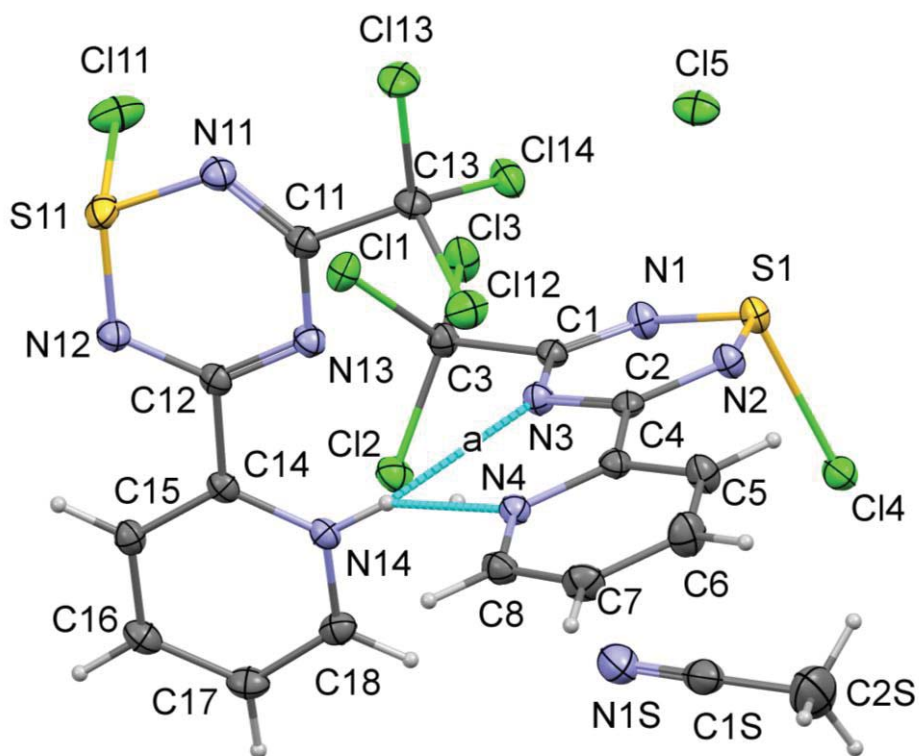


Figure 5.3. Displacement ellipsoid plot of **15-15.HCl** solvated with CH_3CN drawn at the 50% probability level showing the atom-labelling scheme with short contacts indicated with dashed lines. The H atoms are shown as small spheres of arbitrary radii. The two H^+ atoms have half occupancy each.

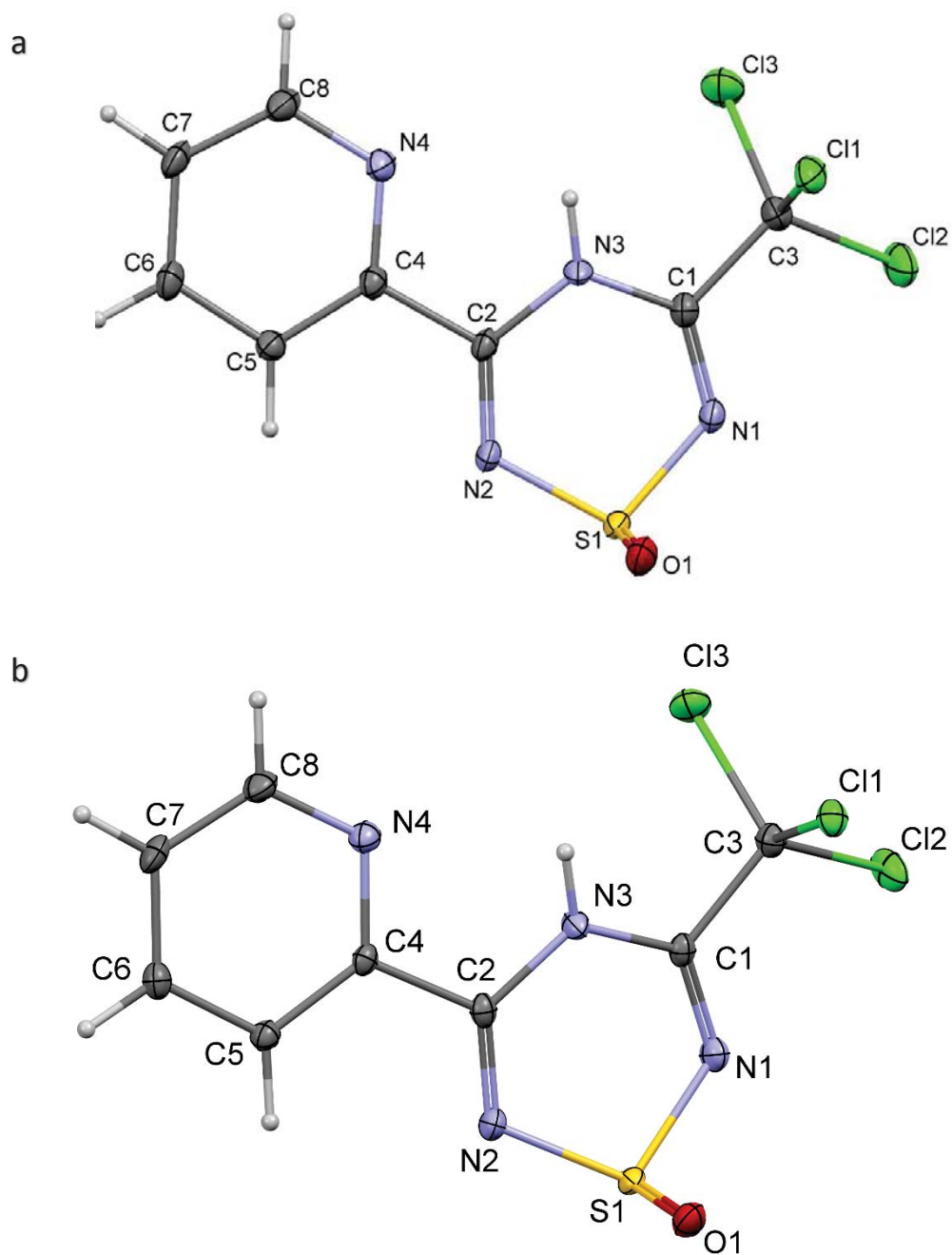


Figure 5.4. Displacement ellipsoid plot of (a) **16a** (space group $P2_1/c$) and (b) **16b** (space group $P\bar{1}$ with minor disorder O component omitted for clarity) drawn at the 50% probability level showing the atom-labelling schemes and with short contacts indicated with dashed lines. The H atoms are shown as small spheres of arbitrary radii.

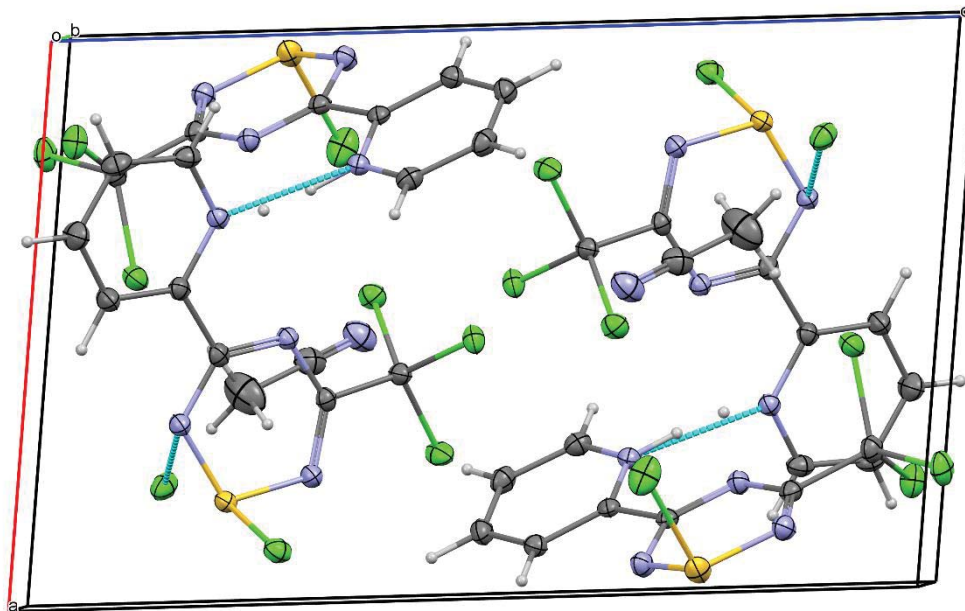


Figure 5.5. A crystal packing diagram of **15–15.HCl** projected almost down the *b* axis. Displacement ellipsoids are drawn at the 50% probability level. Hydrogen bonding and short contacts are indicated by green dashed lines.

Table 5.3. Hydrogen bonds of **15.HCl**

D	H	A	d(D-H)/Å	d(H-A)/Å	d(D-A)/Å	D-H-A/°
N4	H4	Cl5	0.80(10)	2.22(10)	2.977(7)	157(9)

Table 5.4. Hydrogen bonds of **15–15.HCl**

D	H	A	d(D-H)/Å	d(H-A)/Å	d(D-A)/Å	D-H-A/°
N14	H14	N4	0.901(19)	1.84(3)	2.6708(16)	152(4)
N4	H4	N14	0.89(2)	1.82(3)	2.6708(16)	158(5)

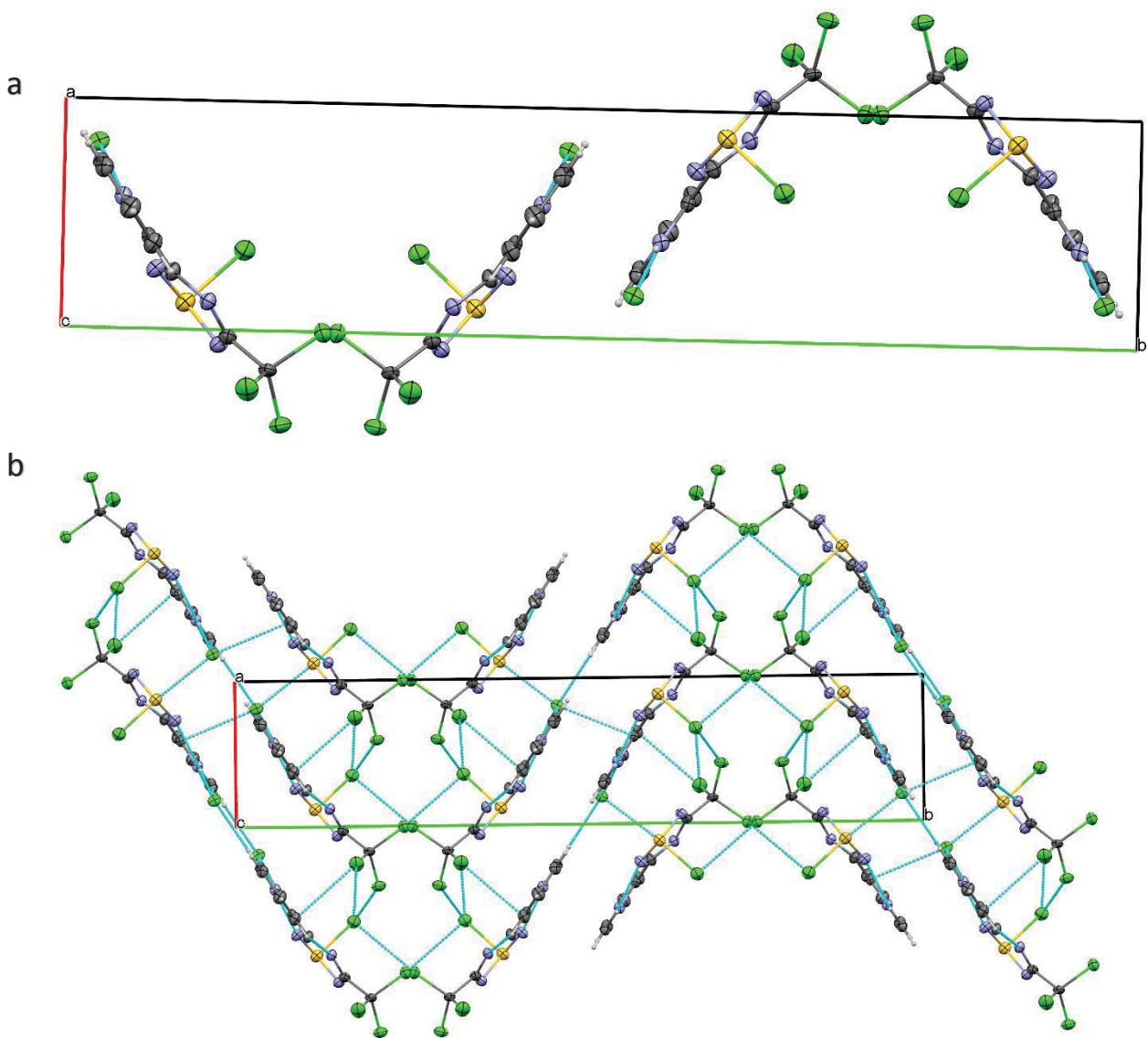


Figure 5.6. The crystal packing structure of **15.HCl** projected down the *c* axis (a) without and (b) with short contacts. Displacement ellipsoids are drawn at the 50% probability level. Hydrogen bonding and short contacts are indicated by green dashed lines.

5.3.2 Structure of **16**

The structure of **16** expresses two distinctive packing arrangements when crystallized from different solvents. Structure **16a** was obtained from CS₂ and **16b** from hexanes (Figure 5.4 a and b). The two structures are similar in geometry but different in their packing arrangements leading to the two distinguishing space groups observed. A second oxygen atom of 4% occupancy is found in the structure of **16b** which is omitted in Figure 5.4b, solvent interaction is a likely cause of the structure crystallizing in a different space group than **16a**. Both structures have puckered heterocyclic rings, with sulfur atoms lying at 0.372 Å and 0.396 Å in **16a** and **16b** above the mean N–C–N–C–N planes. The analysis of the bond distances and angles shows that the two structures are highly similar. The geometric parameters are comparable with those of previously reported structures of symmetric Ph₂TTA=O (FOMTIK)⁶ and Py₂TTA=O¹⁸ (Table 5.5) in CSD. The packing structure of **16a** (Figure 5.7a) and **16b** (Figure 5.8a) display two molecules that are related by an inversion center and both of them show interesting short contacts with **16a** reflecting a 3D channel network (Figure 5.7b) and **16b** exhibiting a layered arrangement (Figure 5.8b) via N–H···S and N–H···O bonds (Table 5.6) to form an infinite chain that aligns along the *a* axis.

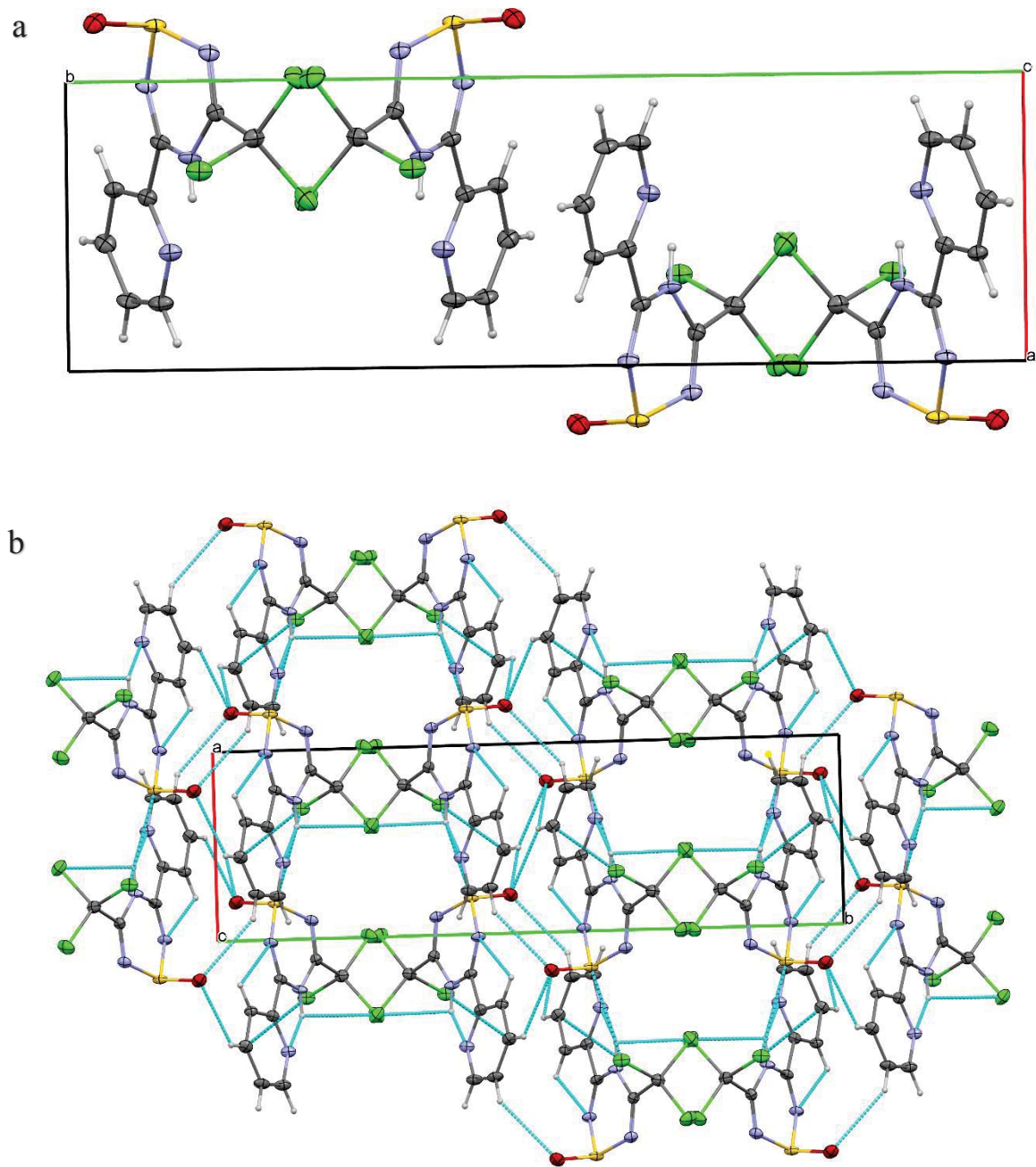


Figure 5.7. A crystal packing diagram of **16a** projected down *c* axis (a) without and (b) with short contacts. Displacement ellipsoids are drawn at the 50% probability level. Short contacts are indicated by blue dashed lines.

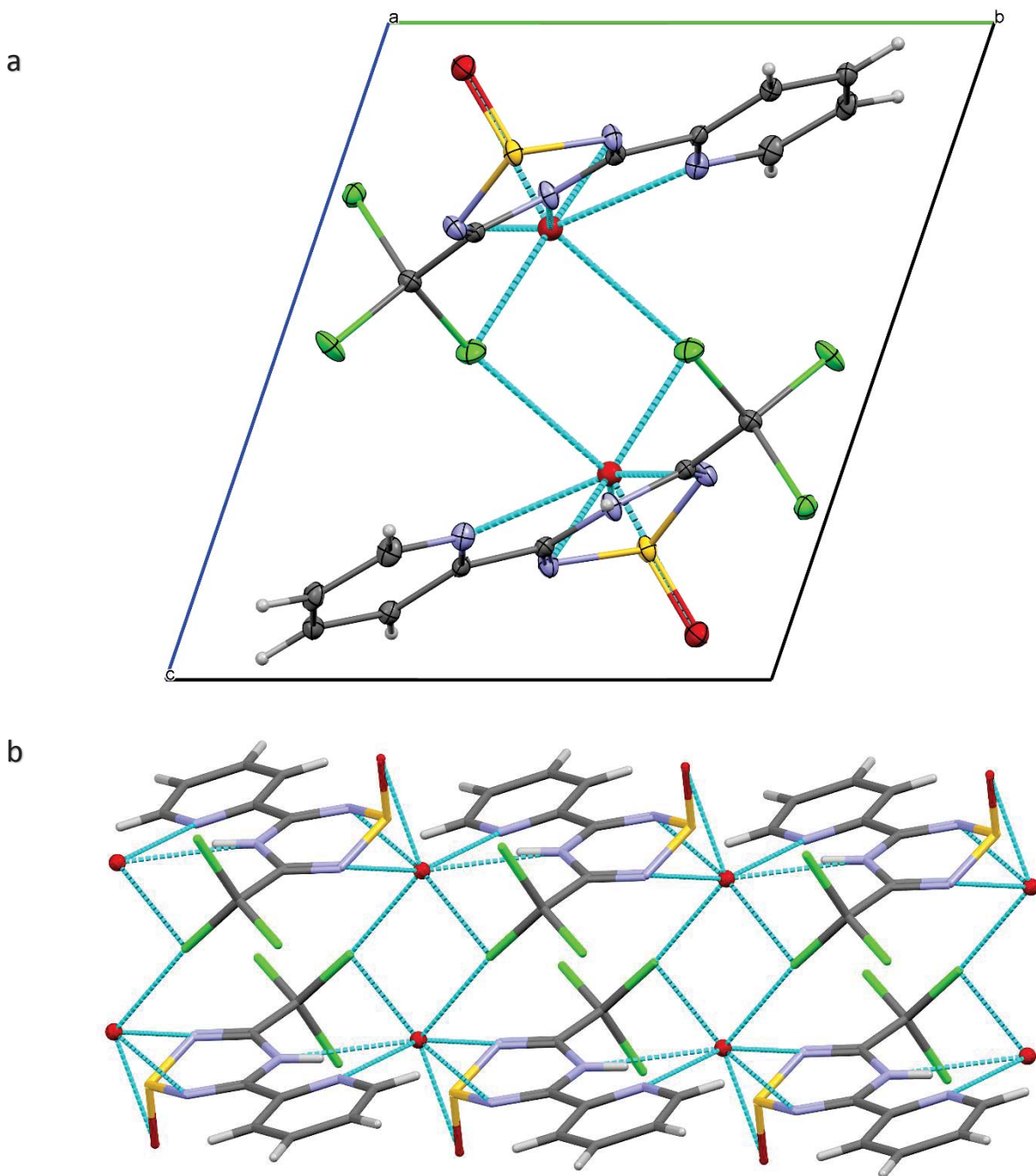


Figure 5.8. A crystal packing diagram of **16b** (a) projected down the *a* axis with displacement ellipsoids drawn at the 50% probability level. Hydrogen bonding is indicated by green dashed lines (b) capped sticks projected almost down the *b* axis, short contacts are indicated by green dashed lines. O is red; S is yellow; N is purple; C is ash; and H is grey.

Table 5.5. Comparison of bond distances and angles of 16 with previously reported analogs.

Bond	16a	FOMTIK¹⁴	KOMZUJ01¹⁸
S1-O1 (Å)	1.473(3)	1.476(4)	1.459(4)
N1-C1 (Å)	1.274(5)	1.281(7)	1.283(4)
S1-N1 (Å)	1.703(4)	1.677(5)	1.681(3)
N2-S1 (Å)	1.690(3)	1.674(4)	1.687(3)
C2-N2 (Å)	1.282(5)	1.281(7)	1.285(4)
N3-C2 (Å)	1.371(6)	1.378(7)	1.367(4)
C1-N3 (Å)	1.368(4)	1.411(7)	1.373(4)
S1-N2-C2 (°)	119.1(3)	118.6(4)	118.7(2)
N2-C2-N3 (°)	125.3(4)	124.7(5)	125.5(3)
C2-N3-C1 (°)	121.0(3)	120.3(4)	121.7(3)
N3-C1-N1 (°)	126.3(4)	123.0(5)	124.9(3)
C1-N1-S1 (°)	118.2(3)	119.1(2)	119.1(2)
N1-S1-N2 (°)	104.2(2)	103.2(2)	105.1(1)

Table 5.6. Hydrogen bonds of 16b

D	H	A	d(D-H)/Å	d(H-A)/Å	d(D-A)/Å	D-H-A/°
N3	H3	S1 ¹	0.88	3.04	3.8766(18)	158.7
N3	H3	O1A ¹	0.88	2.18	3.05(4)	168.4

¹-1+X,+Y,+Z

5.3.3 Crystal structure of **17**

It is worth mentioning that the current crystal structure of radical dimer **17** is derived from a microcrystal that did not permit a complete dataset. The quality of the current structural data is still of sufficient quality to discuss the molecular architecture of the radical dimer (**17**). The displacement ellipsoids drawing of the structure of **17** is depicted in Figure 5.9 with the atom numbering scheme. Comparing the thiazyl core ring statistically with that of the **15** in **15–15.HCl** (Table 5.1), there is a slight difference between the C–N and S–N bond lengths as expected reflecting the radical character of **17**. It is expected that the geometry of **17** should be different from **15**, because the single electron is occupying an antibonding SOMO orbital which has been shown in past work with distinctive difference between the cation, neutral and anion TTA.³ Moreover, slight differences are observed in some of the angles within the ring including S1–N2–C2 and C1–N1–S1 that increase by 1.5(1)° and 2.2(2)° as well as N3–C1–N1 that reduces by 2.2(2)° relative to **15**. Similar behavior has been observed in other thiatriazinyl derivatives.^{1, 3, 12, 19-20} In analysing the crystal packing of **17** (Figure 5.10a and b), each dimer of **17** is made up of two molecules that are closely packed and strangely arranged in an unprecedented head-to-tail manner with the Cl₃ groups rotated 180° to each other contrary to the head-to-head S⋯S pancake (cofacial) dimer arrangement largely reported for the diverse existing thiatriazinyls in the CSD. The two halves of the dimer are strongly held together by two 2.92(2) Å S(δ⁺)⋯N(δ⁻) dispersive electrostatic short contacts (Figure 5.10a). Each of the dimers are linked together via S⋯N short contacts resulting into an infinite chain network in which the dimers are laying edge-to-edge to one another.

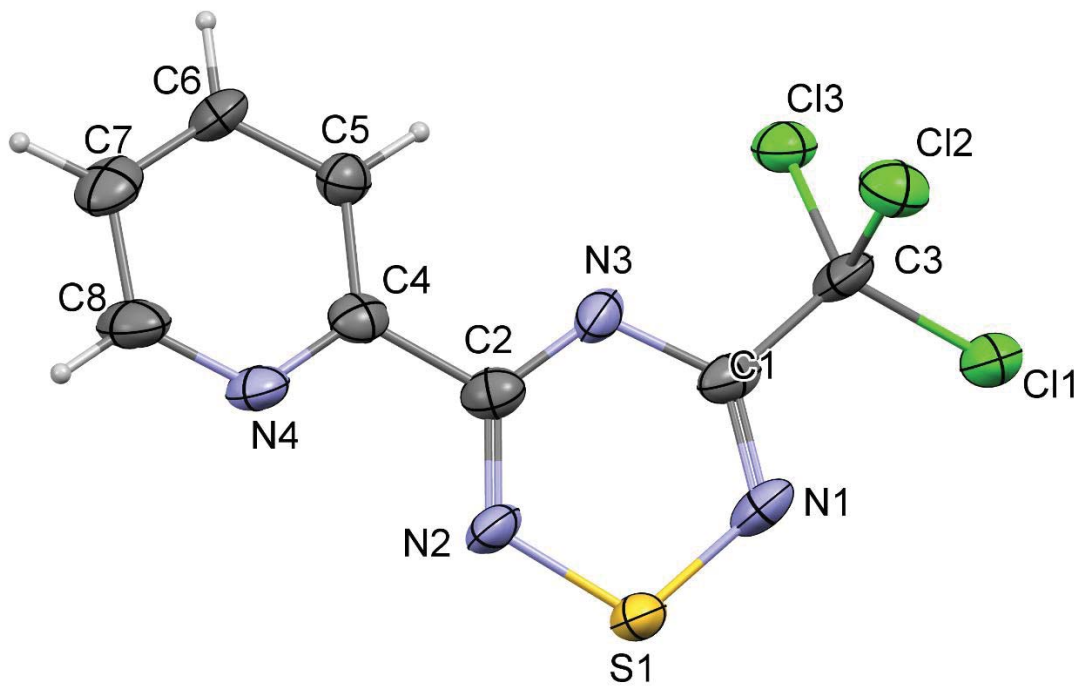


Figure 5.9. Displacement ellipsoid plot of the monomer which is the asymmetric unit of **17** (the true structure is the dimer) drawn at the 50% probability level showing the atom-labelling scheme. The H atoms are shown as small spheres of arbitrary radii.

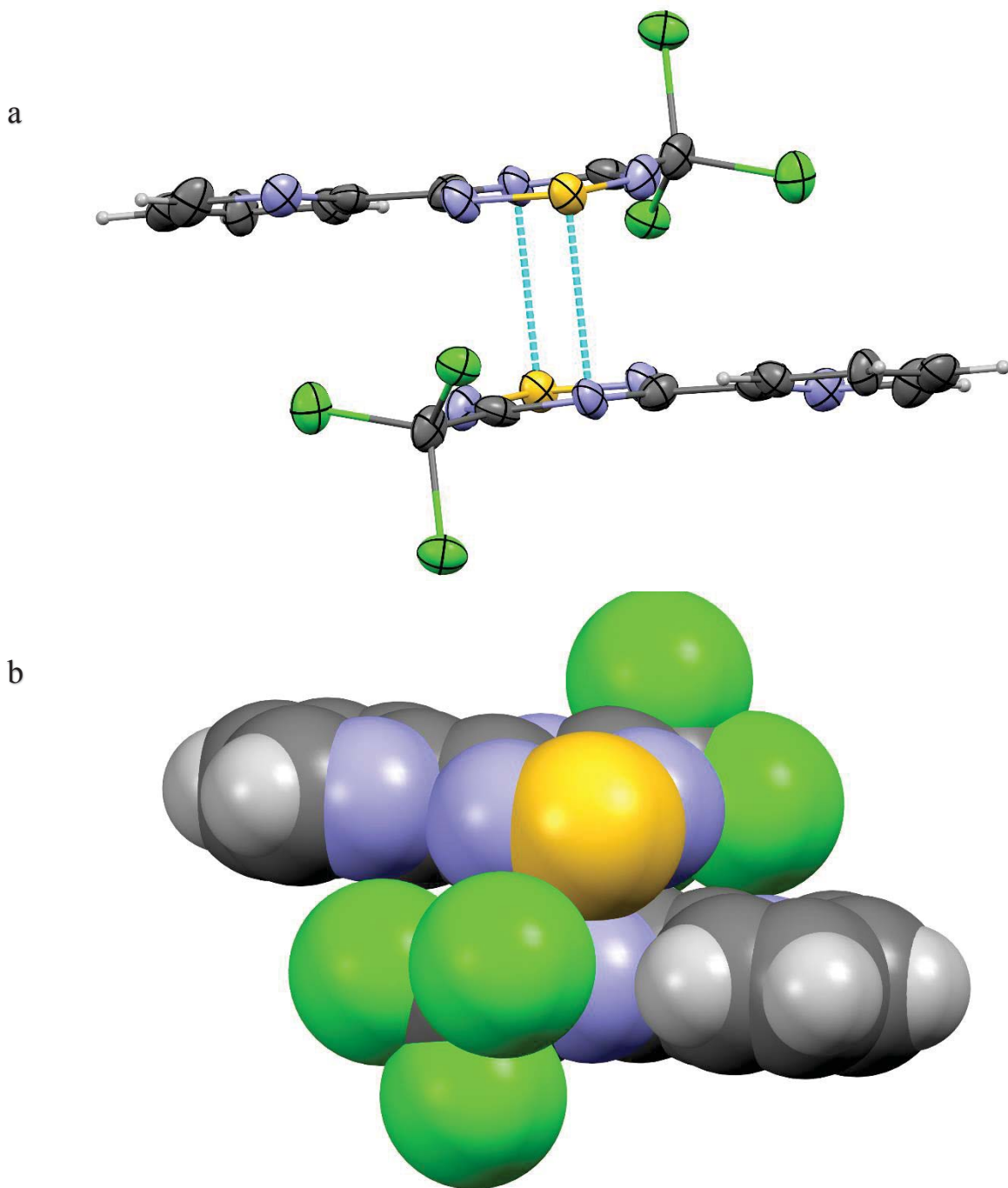


Figure 5.10. (a) The crystal packing displacement ellipsoid plot drawn at the 50% probability level. Short contacts are indicated by green dashed lines. (b) Space filling structure of **17**. Cl is green; S is yellow; N is purple; C is charcoal; and H is grey.

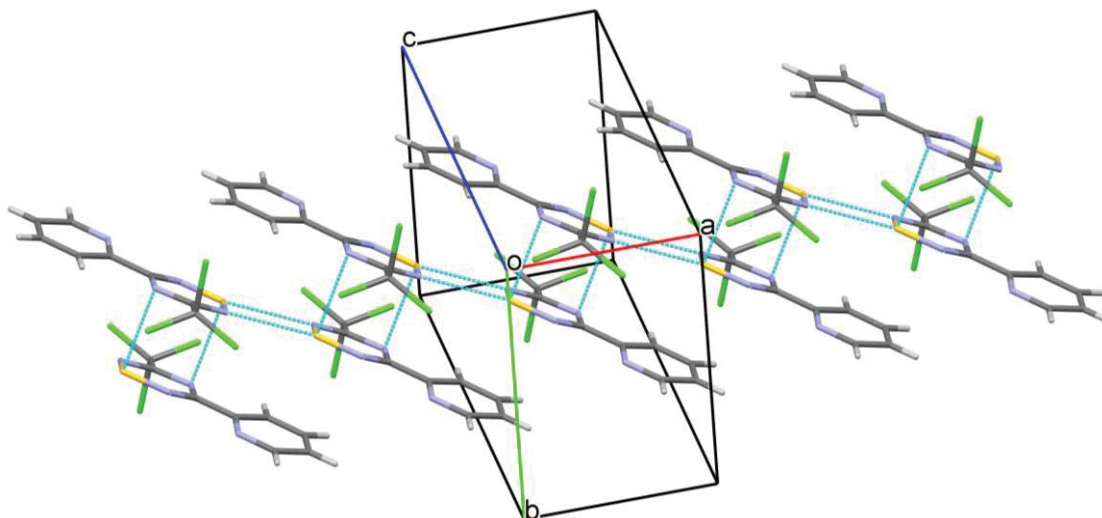


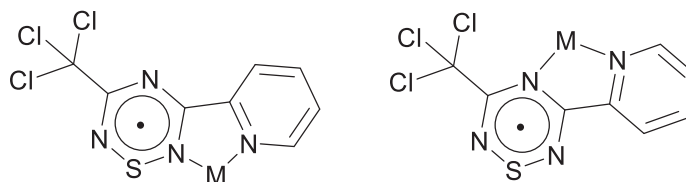
Figure 5.11. The crystal packing structure of **17** shown as capped sticks. Short contacts are indicated by green dashed lines with a chain running along *a* axis. Cl is green; S is yellow; N is blue; C is ash; and H is grey.

5.4 Conclusions

The synthesis of unsymmetrical 5-(2-pyridyl)-3-trichloromethyl-substituted thiatriazines (PyCCl₃TTACl) and subsequent thiatriazinyls (PyCCl₃TTA') was investigated as a potential building block for molecular magnet development through condensation of imidoamidine hydrochloride with sulfur chlorides. The route which has been found to work excellently for 5-aryl-3-trifluoro thiatriazinyl preparation has proven very challenging in the case of the 2-pyridyl derivative due to protonation of its nitrogen atom with hydrochloride proton which is the major by-product of the reaction process. The TTA ring appears to be successfully formed, but the problematic protonation significantly hinders the isolation of the intended product. The results of various optimizations of the synthesis up to this moment are supported with spectroscopic data from NMR as well as reliable structural examinations using X-ray diffraction. All structural data evidently corroborate the NMR results. In all, the results obtained so far give positive hope for efficient generation of the 3-trichloromethyl-5-(2-pyridyl)-1-thia-2,4,6-triazinyl that the current

structure at hand shows possible geometries for bidentate chelate coordination to transition metals for conceivable application as a molecular magnet (Chart 5.2).

Chart 5.2



XXVII

5.5 Future work

Optimization of the current achievement on this project in getting the free TTACl and subsequent generation of the stable radical for the next line of studies in reasonable yield is ongoing. Two concepts are under investigation to combat the current difficulties. The first option is to painstakingly neutralize the moisture sensitive **15–15**.HCl using a suitable organic or inorganic base in an appropriate solvent. An alternative is to switch to utilizing a persilylated imidoamidate to avoid the HCl by-product present in the current method. Here the leaving group will be the relatively unreactive $(\text{CH}_3)_3\text{SiCl}$.

The synthesis of the 2-pyrimidyl (Pm) substituted thiatriazinyl analog is in progress as well. These studies which I plan to finalize in a PhD program in future will provide me further information on the unique chemistry of the asymmetric Py- and Pm- substituted thiatriazinyl.

5.6 References

1. Hayes, P. J.; Oakley, R. T.; Cordes, A. W.; Pennington, W. T., Preparation and dimerization of 1,2,4,6-thiatriazinyl radicals - crystal and molecular-structure of bis(3,5-diphenyl-1,2,4,6-thiatriazine). *J. Am. Chem. Soc.* **1985**, *107*, 1346-1351.
2. Cordes, A. W.; Hayes, P. J.; Josephy, P. D.; Koenig, H.; Oakley, R. T.; Pennington, W. T., Preparation and molecular-structure of 1-chloro-3,5-diphenyl-1,2,4,6-thiatriazine - reduction of $\text{Ph}_2\text{C}_2\text{N}_3\text{SCl}$ and the electron-spin-resonance spectrum of the $\text{Ph}_2\text{C}_2\text{N}_3\text{S}$). *J. Chem. Soc., Chem. Commun.* **1984**, 1021-1022.
3. Boere, R. T.; Oakley, R. T.; Reed, R. W.; Westwood, N. P., Ultraviolet photoelectron and ESR studies of 1, 2, 4, 6-thiatriazinyl and 1, 2, 3, 5-dithiadiazolyl radicals. *J. Am. Chem. Soc.* **1989**, *111*, 1180-1185.
4. Boeré, R. T.; Roemmele, T. L.; Yu, X., Unsymmetrical 1,3-1,2,4,6-thiatriazinyls with aryl and trifluoromethyl substituents: Synthesis, crystal structures, EPR spectroscopy, and voltammetry. *Inorg. Chem.* **2011**, *50*, 5123-5136.
5. Leitch, A. A.; Korobkov, I.; Assoud, A.; Brusso, J. L., Non-innocent pyridyl nitrogens: unprecedented interconversion of N-bridgehead-thiadiazolium salts and thiatriazine in the generation of thiatriazinyl. *Chem. Commun.* **2014**, *50*, 4934-4936.
6. Cordes, A. W.; Oakley, R. T., Structure of 3,5-Diphenyl-4h-1,2,4,6-Thiatriazine 1-Oxide. *Acta Crystallogr., Sect. C: Cryst. Struct. Commun.* **1987**, *43*, 1645-1646.
7. Kong, Y. C.; Kim, K.; Ja Park, Y., Reactions of (aryl)(chloro)methyl p-tolyl sulfoxides with tetrasulfur tetranitride (S_4N_4): Formation and characterization of 3,5-diaryl-1,2,4,6-thiatriazine 1-oxides. *Tetrahedron* **2000**, *56*, 7153-7161.
8. Shixaliyev, N. Q.; Gurbanov, A. V.; Maharramov, A. M.; Mahmudov, K. T.; Kopylovich, M. N.; Martins, L. M. D. R. S.; Muzalevskiy, V. M.; Nenajdenko, V. G.; Pombeiro, A. J. L., Halogen-bonded tris(2,4-bis(trichloromethyl)-1,3,5-triazapentadienato)-M(III) [M = Mn, Fe, Co] complexes and their catalytic activity in the peroxidative oxidation of 1-phenylethanol to acetophenone. *New J. Chem.* **2014**, *38*, 4807-4815.
9. Shixaliyev, N. Q.; Maharramov, A. M.; Gurbanov, A. V.; Gurbanova, N. V.; Nenajdenko, V. G.; Muzalevskiy, V. M.; Mahmudov, K. T.; Kopylovich, M. N., Structure and supramolecular arrangement of bis(2,4-bis(trichloromethyl)-1, 3,5-triazapenta-dienato)-M(II) [M = Ni(II), Cu(II) and Pd(II)] complexes. *J. Mol. Struct.* **2013**, *1041*, 213-218.
10. Boeré, R. T.; Cordes, A. W.; Oakley, R. T., Synthesis and interconversion of 5-phenyl-1,3,2,4,6-dithiatriazine derivatives; Crystal and molecular structure of the bicyclic molecule PhCN_5S_3 . *J. Chem. Soc., Chem. Commun.* **1985**, 929-930.
11. Farrar, J. M.; Patel, M. K.; Kaszynski, P.; Young Jr, V. G., A new thiatriazine isomer: Synthesis, tautomerism, and molecular structure of 3,6-diphenyl-4H-1,2,4,5-thiatriazine as a precursor to the 1,2,4,5-thiatriazinyl radical. *J. Org. Chem.* **2000**, *65*, 931-940.

12. Boere, R. T.; Cordes, A. W.; Hayes, P. J.; Oakley, R. T.; Reed, R. W.; Pennington, W. T., Redox chemistry of 1,2,4,6-thiatriazinyls - preparation and crystal-structures of "3,5-diphenyl-1,2,4,6-thiatriazinium hexafluorophosphate, $\text{Ph}_2\text{C}_2\text{N}_3\text{S} + \text{PF}_6^-$, and 3,5-diphenyl-4-hydro-1,2,4,6-thiatriazine, $\text{Ph}_2\text{C}_2\text{N}_3\text{SH}$. *Inorg. Chem.* **1986**, *25*, 2445-2450.
13. Chen, S. J.; Mews, R.; Behrens, U.; Fischer, E.; Pauer, F.; Sheldrick, G. M.; Stalke, D.; Stohrer, W. D., Chlorthiatriazine. *Chem. Ber.* **1993**, *126*, 2601-2607.
14. Cordes, A. W.; Oakley, R. T., Structure of 3,5- diphenyl- 4H- 1,2,4,6- thiatriazine 1-oxide. *Acta Crystallogr., Sect. C: Cryst. Struct. Commun.* **1987**, *43*, 1645-1646.
15. Hayes, P. J.; Oakley, R. T.; Cordes, A. W.; Pennington, W. T., Preparation and dimerization of 1, 2, 4, 6-thiatriazinyl radicals; crystal and molecular structure of bis (3, 5-diphenyl-1, 2, 4, 6-thiatriazine). *J. Am. Chem. Soc.* **1985**, *107*, 1346-1351.
16. Ramakrishna, T. V. V.; Elias, A. J.; Vij, A., Dealkylation reactions of trialkylamines with 1,3,5-trichloro-1,2,4,6-cyclothiatriazine: A novel route to regioselective dialkylamino substitution on cyclocarbathiazines. *Inorg. Chem.* **1999**, *38*, 3022-3026.
17. Jeffrey, G. A.; Jeffrey, G. A., *An introduction to hydrogen bonding*. Oxford university press New York: 1997; Vol. 12.
18. Yutronkie, N. J.; Leitch, A. A.; Korobkov, I.; Brusso, J. L., 1,2,4,6-Thiatriazinyl radicals and dimers: Structural and electronic tuning through heteroaromatic substituent modification. *Cryst. Growth Des.* **2015**, *15*, 2524-2532.
19. Ang, C. Y.; Boéré, R. T.; Goh, L. Y.; Koh, L. L.; Kuan, S. L.; Tan, G. K.; Yu, X., η^1 and η^2 complexes of λ^3 -1,2,4,6-thiatriazinyls with $\text{CpCr}(\text{CO})_x$. *Chem. Commun.* **2006**, 4735-4737.
20. Boere, R. T.; Roemmele, T. L., 1,2,4,6-Thiatriazinyls: Stable free radicals with well-defined EPR spectra. *Phosphorus Sulfur and Silicon and the Related Elements* **2004**, *179*, 875-882.

Chapter 6 Experimental procedures

This chapter presents the experimental details and characterization data for all results reported in the thesis.

6.1 General procedures

All reagents including copper(I) chloride (CuCl, Sigma-Aldrich), copper(I) bromide (CuBr, Sigma-Aldrich), 2-pyridinecarbonitrile (PyCN, Aldrich), 2-pyrimidinecarbonitrile (PmCN, Aldrich), trichloroacetonitrile (CCl₃CN, Aldrich), (calcium chloride (CaCl₂, EMD, USA), carbon disulfide (CS₂, EMD, USA), ammonium chloride (NH₄Cl, EMD, USA), magnesium sulfate (MgSO₄, Fisher) are commercial grade and were used as received except solvents for moisture-sensitive reactions that required drying. Acetonitrile (CH₃CN, Fisher) was distilled over P₂O₅ and stored over CaH₂ from which it was freshly distilled before use, while chloroform (CHCl₃, BDH) was purified by distillation over P₂O₅. Acetonitrile and chloroform were degassed by three freeze-pump-thaw cycles and stored under nitrogen prior to use. Heptane (Fisher Chemicals, USA), ethanol (Greenfield Global, Canada), methanol (Fisher Chemicals, USA), and isopropanol (Fisher Chemicals, USA) were used as received. Ether and dichloromethane were collected from a Solvent Purification System (SPS, MBraun). The experiments were conducted under an inert nitrogen gas stream using standard Schlenk techniques or glove box unless otherwise stated. Deuterated chloroform (CDCl₃) used as solvent for NMR spectroscopy was dried over 4 Å molecular sieves. The ligands (PPh_{3-n}(dipp)_n, dipp = 2,6-Diisopropylphenyl) were prepared and purified as previously reported.¹ NMR (¹H, ¹³C and ³¹P) were recorded at ambient temperature (22°C) on a 300 MHz Bruker Avance II liquids spectrometer or on a 700 MHz Bruker Avance III HD liquids and solids with sample changer spectrometer (Bruker, Germany). Spectra are referenced with respect to TMS as internal standard at 0.0 ppm or the solvent peak (CHCl₃ in case of CDCl₃, 7.26

ppm for ^1H and 77.0 ppm for ^{13}C) or against 85% H_3PO_4 external standard for ^{31}P at 0.0 ppm. The NMR coupling constants are reported in Hertz with abbreviations such as d = doublet, t = triplet, Br = broad, Sh = sharp and m = multiplet, while the chemical shifts are in ppm. ^1H - ^1H COSY, ^1H - ^{13}C HSQC and ^1H - ^{13}C HMBC experiments were undertaken for resonance assignments. Melting points were determined in open tubes on a Barnstead Electrothermal Digital Mel-Temp 3.0. Infrared (IR) spectra were collected using Bruker Tensor 37 Fourier Transform Infrared Spectrophotometer with ATR (attenuated total reflectance) and diffuse reflectance accessories. Elemental compositions of compounds were evaluated using an Elementar CHNS analyzer Vario Micro Cube (solvent amounts are included in isolated solvates parameters).*

6.2 Synthetic procedures

6.2.1 $[\text{CuCl}(\text{DippPh}_2\text{P})]_2$ (1)

DippPh₂P (70 mg, 0.202 mmol) was added to a suspension of CuCl (20 mg, 0.202 mmol) in 2.5 mL of CHCl_3 . The mixture was stirred for 30 min. The solution was filtered through glass wool, and pure colorless crystals were grown overnight by carefully layering heptane onto the chloroform solution of the copper complex in a narrow tube. Yield: 78.6% (70.7 mg, MP = 228 – 231°C). Calculated, % (Analysis found, %) for $\text{C}_{48}\text{H}_{54}\text{P}_2\text{Cu}_2\text{Cl}_2$: C- 64.71 (C- 64.71); H- 6.11 (H- 6.22). ^1H NMR (300 MHz, CDCl_3): δ 7.52 – 7.45 (m, Ph_{meta}, 8H; t, $J_{\text{HH}}=7.8$ Hz, dipp_{para}, 2H); δ 7.37 – 7.35 (m, Ph_{para}, 4H; m, Ph_{ortho}, 8H), δ 7.25 – 7.22 (d of d, $J_{\text{HH}}=7.8$ Hz dipp_{meta} 4H); δ 3.72 (sept, $J_{\text{HH}} = 6.5$ Hz, $J_{\text{PH}} = < 1$ Hz, dipp-H, 4H); δ 0.90 (d, $J_{\text{HH}}=6.6$ Hz, 24H, dipp-Me). ^{13}C NMR (300 MHz, CDCl_3): δ 155.4 (Br s, dipp-iPr ipso-C), δ 132.9 (d, Ph_{meta}, $J_{\text{PC}} = 42$ Hz), δ 132.3 and δ 132.1 (Ph ipso), δ 131.9 (s, dipp_{para}), δ 129.7 (Ph_{para}), δ 128.8 (Br, Ph_{ortho}), δ 125.2 (Br s, dipp_{meta}), δ 125.0 (Br s, dipp ipso), δ 33.0 (d, dipp iPr, $J_{\text{PC}} = 42$ Hz), δ 24.6 (s, dipp-Me). ^{31}P NMR (300 MHz, CDCl_3): δ -14.66. FTIR (diamond anvil ATR, cm^{-1}): 3050w, 2968w, 2955w, 2924w, 2866w,

2369w, 2338w, 1583w, 1568w, 1478w, 1454w, 1434s, 1383w, 1361w, 1340w, 1329w, 1306w, 1242w, 1226w, 1180w, 1159w, 1122w, 1095m, 1070w, 1060w, 1047m, 1027m, 997w, 973w, 960w, 926w, 894w, 852w, 800m, 751m, 741vs, 694vs, 625w, 617w, 585w, 531vs, 522s, 485vs, 466vs, 445s.

6.2.2 [CuBr(DippPh₂P)]₂ (2)

Preparation of **2** was achieved following the procedure for complex **1** with the replacement of CuCl with CuBr. Colorless crystals were also achieved by slow cooling of a CHCl₃ saturated solution of the product. Yield: 74% (73 mg, MP = 206 – 208°C). Calculated, % (Analysis found, %) for C₅₀H₅₆P₂Cu₂Br₂: C- 62.75 (62.03); H- 5.61 (5.42). ¹H NMR (300 MHz, CDCl₃): δ 7.57 – 7.43 (m, Ph_{meta}, 8H; t, J_{HH}=7.8 Hz, dipp_{para}, 2H); δ 7.39 – 7.32 (m, Ph_{para}, 4H; m, Ph_{ortho}, 8H), δ 7.28 – 7.20 (d of d, J_{HH}=7.8 Hz, J_{PH}=3.1 Hz dipp_{meta} 4H); δ 3.74 (sept of d, J_{HH} = 6.6 Hz, J_{PH} = 4.2 Hz dipp-H, 4H); δ 0.88 (d, J_{HH}=6.6 Hz, 24H, dipp-Me). ¹³C NMR (300 MHz, CDCl₃): δ 155.6 (dipp-iPr ipso-C, J_{PC} = 42 Hz), δ 132.9 (d, Ph_{meta}, J_{PC} = 57.4 Hz), δ 132.3 (Ph ipso, J_{PC} = 15.4 Hz) and δ 132.1 (Br s, Ph ipso), δ 132 (s, dipp_{para}), δ 129.6 (Ph_{para}), δ 128.8 (d, Ph_{ortho}, J_{PC} = 37.8 Hz), δ 125.4 (d, dipp_{meta}, J_{PC} = 28.7 Hz), δ 125.2 (d, dipp ipso, J_{PC} = 25.9 Hz), δ 33.1 (d, dipp iPr, J_{PC} = 60.2 Hz), δ 24.7 (s, dipp-Me). ³¹P NMR (300 MHz, CDCl₃): δ -16.68. FTIR (Diamond Anvil ATR, cm⁻¹): 3056w, 2962w, 2953w, 2924w, 2865w, 1584w, 1569w, 1477w, 1461w, 1434m, 1381w, 1361w, 1337w, 1305w, 1240w, 1213m, 1178w, 1157w, 1124w, 1096m, 1057w, 1044w, 1027w, 999w, 925w, 912w, 842w, 805m, 758vs, 743vs, 694vs, 670, 624, 586w, 528s, 486s, 465s, 439m, 426w.

6.2.3 [CuCl(Dipp₂PhP)]₂ (3)

The CuCl (10 mg, 0.101 mmol) and Dipp₂PhP (43.5 mg, 0.101 mmol) were introduced into a Schlenk flask under a N₂ atmosphere. About 1.8 mL of CHCl₃ was then introduced and the

suspension was stirred for 30 min to complete the reaction. The resulting solution was filtered through tissue/glass wool bed into a narrow tube, and pure colorless crystals were grown overnight by carefully layering heptane over the chloroform. Yield: 67.3% (36 mg, MP = 215 – 218°C). Calculated, % (Analysis found, %) for $C_{60}H_{78}P_2Cu_2Cl_2$: C- 68.04 (68.04); H- 7.42 (7.45). 1H NMR (300 MHz, $CDCl_3$): δ 7.56 – 7.7035 (m, Ph_{meta} , 8H; t, $J_{HH}=7.6$ Hz, $dipp_{para}$, 2H); δ 7.26 – 7.19 (m, Ph_{para} , 4H; m, Ph_{ortho} , 4H; d of d, $J_{HH}=7.1$ Hz, $J_{PH}=3.3$ Hz $dipp_{meta}$ 4H); δ 3.51 (sept of d, $J_{HH} = 6.3$ Hz, $J_{PH} = 3.7$ Hz, $dipp-H$, 4H); δ 1.01 (d, $J_{HH}=6.6$ Hz, 12H, $dipp-Me$); δ 0.87 (d, $J_{HH} = 6.6$ Hz, 12H, $dipp-Me$). ^{13}C NMR (300 MHz, $CDCl_3$): δ 152.7 ($dipp-iPr$ ipso-C, $J_{PC} = 42$ Hz), δ 137.3 (Br, Ph_{para}), δ 131.7 (d, Ph ipso, $J_{PC} = 175$ Hz), δ 131.5 (s, $dipp_{para}$), δ 131.2 (s, Ph_{meta}), δ 129.3 (d, Ph_{ortho} , $J_{PC} = 49$ Hz), δ 127.1 (d, $dipp$ ipso, $J_{PC} = 175$ Hz), δ 126 (d, $dipp_{meta}$, $J_{PC} = 28$ Hz), δ 32.6 (d, $dipp$ iPr , $J_{PC} = 55.3$ Hz), δ 24.8 (s, $dipp-Me$), δ 24.2 (s, $dipp-Me$). ^{31}P NMR (300 MHz, $CDCl_3$): δ -17.42. FTIR (Diamond Anvil ATR, cm^{-1}): 3049w, 2997w, 2958m, 2924w, 2864w, 1586w, 1571w, 1483w, 1460m, 1435m, 1385w, 1362w, 1342w, 1312w, 1242w, 1227w, 1182w, 1161w, 1126w, 1103w, 1087w, 1048w, 1028w, 1000w, 922w, 846w, 806vs, 744s, 700s, 688w, 618w, 586w, 527w, 514s, 480s, 462vs, 441m, 426w, 406w.

6.2.4 [CuBr(Dipp₂PhP)]₂ (4)

This was obtained in the same way as complex **3** with the replacement of CuCl with CuBr (14.5 mg, 0.101 mmol). The CuBr suspension in 1.8 mL $CHCl_3$ was reacted with one equivalent of Dipp₂PhP by stirring for 30 min. Colorless crystals suitable for X-ray crystallographic analysis were recovered overnight from heptane layering over the $CHCl_3$ solution. Yield: 65.5% (38 mg, MP = 222 – 226°C). Calculated, % (Analysis found, %) for $C_{62}H_{80}P_2Cu_2Br_2$: C- 63.42 (63.53); H- 6.87 (6.76). 1H NMR (300 MHz, $CDCl_3$): δ 7.51 – 7.37 (m, Ph_{meta} , 8H; t, $J_{HH}=7.8$, $dipp_{para}$, 2H); δ 7.26 – 7.16 (m, Ph_{para} , 4H; m, Ph_{ortho} , 4H; d of d, $J_{HH}=7.8$ Hz, $J_{PH}=3.2$ Hz $dipp_{meta}$ 4H); δ 3.52 (d

of sept, $J_{\text{HH}} = 6.5$ Hz, $J_{\text{PH}} = 3.9$ Hz, dipp-H, 4H); δ 1.01 (d, $J_{\text{HH}} = 6.60$ Hz, 12H, dipp-Me) ; δ 0.87 (d, $J_{\text{HH}} = 6.60$ Hz, 12H, dipp-Me). ^{13}C NMR (300 MHz, CDCl_3): δ 152.7 (dipp-iPr ipso-C, $J_{\text{PC}} = 42$ Hz), δ 137.3 (Br, Ph_{para}), δ 131.8 (d, Ph ipso, $J_{\text{PC}} = 153.3$ Hz), δ 131.5 (s, dipp $_{\text{para}}$), δ 131.2 (s, Ph_{meta}), δ 129.3 (d, Ph_{ortho} , $J_{\text{PC}} = 44.1$ Hz), δ 127.2 (d, dipp ipso, $J_{\text{PC}} = 170.8$ Hz), δ 126 (d, dipp $_{\text{meta}}$, $J_{\text{PC}} = 29.4$ Hz), δ 32.6 (d, dipp iPr, $J_{\text{PC}} = 56$ Hz), δ 24.8 (s, dipp-Me), δ 24.3 (s, dipp-Me). ^{31}P NMR (300 MHz, CDCl_3): δ -17.5. FTIR (Diamond Anvil ATR, cm^{-1}): 3002w, 2955w, 2925w, 2865w, 1586w, 1570w, 1482w, 1462m, 1447m, 1435m, 1383m, 1362m, 1345w, 1312w, 1270w, 1228w, 1203w, 1185w, 1161w, 1125w, 1101w, 1088w, 1048w, 922w, 904w, 852w, 810m, 801m, 765s, 751vs, 742vs, 704s, 690m, 666m, 586w, 528s, 514m, 479w, 461s, 442w, 431w.

6.2.5 [CuCl(DippPh₂P)₂] (5)

The solution of CuCl (20 mg, 0.202 mmol) prepared by dissolving CuCl in 5 mL CH_3CN under stirring for 5 min was reacted with DippPh₂P (70 mg, 0.202 mmol) added into the dried solution. The mixture while stirring led to the formation of pure colorless microcrystals of [CuCl(DippPh₂P)₂] (1) containing some crystals that diffracted excellently for X-ray crystallography, while a bigger sized crystal suitable for crystallography analysis was grown in CHCl_3 by slow cooling. Yield: 95.3% (76.2 mg, MP = 204 – 207°C). Calculated, % (Analysis found, %) for $\text{C}_{48}\text{H}_{54}\text{P}_2\text{CuCl}$: C- 72.80 (73.09); H- 6.87 (6.78). ^1H NMR (300 MHz, CDCl_3): δ 7.48 – 7.42 (m, Ph_{meta} , 8H; m, dipp $_{\text{para}}$, 2H); δ 7.29 – 7.25 (m, Ph_{para} , 4H; m, Ph_{ortho} , 4H); δ 7.24 – 7.20 (d of d, $J_{\text{HH}}=7.8$ $J_{\text{PH}}=2.3$ Hz, dipp $_{\text{meta}}$ 4H); δ 3.63 (sept of d, $J_{\text{HH}} = 6.3$ Hz, $J_{\text{PH}} = 5.4$ Hz, dipp-H, 4H); δ 0.83 (d, $J_{\text{HH}} = 6.90$ Hz, 24H, dipp-Me). ^{13}C NMR (300 MHz, CDCl_3): δ 155.8 (dipp-iPr ipso-C), δ 133.6 (Br s, Ph ipso), δ 132.5 (d, Ph_{meta} , $J_{\text{PC}} = 60.2$ Hz), δ 131.7 (s, dipp $_{\text{para}}$), δ 128.9 (Ph_{para}), δ 128.5 (Ph_{ortho} $J_{\text{PC}} = 31.5$ Hz), δ 127.0 (Br s, dipp ipso), δ 125.0 (d, dipp $_{\text{meta}}$ $J_{\text{PC}} = 22.4$ Hz), δ 33.2 (d, dipp iPr, $J_{\text{PC}} = 63$ Hz), δ 24.5 (s, dipp-Me). ^{31}P NMR (300 MHz, CDCl_3): δ -17.96.

FTIR (Diamond Anvil ATR, cm^{-1}): 3050w, 2975w, 2957w, 2923w, 2864w, 2846w, 1581w, 1566w, 1483w, 1462m, 1435m, 1382w, 1360w, 1333w, 1304w, 1278w, 1260m, 1238w, 1180m, 1160m, 1147m, 1094s, 1047s, 1026s, 921m, 806vs, 742vs, 694vs, 624m, 616m, 583m, 521vs, 494s, 482vs, 465vs, 441s, 418s.

6.2.6 [CuBr(DippPh₂P)₂] (6)

This complex was prepared in a manner similar to complex **5** with the replacement of CuCl by CuBr (29 mg, 0.202 mmol) using two equivalent DippPh₂P. Colorless crystals were also generated by slow cooling of CHCl₃ saturated solution of the product. Yield: 91.1% (77 mg, MP = 209 – 211°C). Calculated, % (Analysis found, %) for C₄₈H₅₄P₂CuBr: C- 68.93 (69.07); H- 6.51 (6.71). ¹H NMR (300 MHz, CDCl₃): δ 7.51 – 7.41 (m, Ph_{meta}, 8H; t, J_{HH}=7.8, dipp_{para}, 2H); δ 7.32 – 7.24 (m, Ph_{para}, 4H; m, Ph_{ortho}, 8H); δ 7.23 – 7.19 (d of d, dipp_{meta} J_{HH}=7.8 J_{PH}=2.6 4H); δ 3.64 (sept, J_{HH} = 6.6Hz, J_{PH} = 6.1 Hz, dipp-H, 4H); δ 0.83 (d, J_{HH}=6.6 Hz, 24H, dipp-Me). ¹³C NMR (300 MHz, CDCl₃): δ 155.9 (dipp-iPr ipso-C), δ 133.6 (Br s, Ph ipso), δ 132.5 (d, Ph_{meta}, J_{PC} = 67.2 Hz), δ 131.7 (s, dipp_{para}), δ 128.9 (Ph_{para}), δ 128.6 (Ph_{ortho} J_{PC} = 31.5 Hz), δ 127.1 (Br s, dipp ipso), δ 125.0 (d, dipp_{meta} J_{PC} = 24.4 Hz), δ 33.3 (d, dipp iPr, J_{PC} = 65 Hz), δ 24.6 (s, dipp-Me). ³¹P NMR (300 MHz, CDCl₃): δ -18.65. FTIR (Diamond Anvil ATR, cm^{-1}): 3051w, 2975w, 2954w, 2926w, 2863w, 2844w, 1582w, 1566w, 1483w, 1462w, 1435m, 1382w, 1361w, 1333w, 1304w, 1278w, 1263w, 1237w, 1219w, 1180w, 1160w, 1147w, 1122w, 1095w, 1048w, 1027w, 999w, 989w, 967w, 952w, 921w, 879w, 842w, 806m, 742vs, 696vs, 624w, 616w, 583w, 522vs, 495m, 483m, 4645m, 442m, 418w.

6.2.7 Synthesis of 2-amidinopyridine hydrochloride (7)

2-Amidinopyridine hydrochloride was prepared in high yield as described in the literature with slight modification.² In summary, 2-pyridinecarbonitrile (10 g, 96.1 mmol) was dissolved in

100 mL of MeOH using a 500 mL round bottom flask equipped with a magnetic stir bar. Sodium methoxide, MeONa (1.08 g, 20 mmol) was then added, and the solution stirred at room temperature for 12 h. Ammonium chloride, NH₄Cl (5.14 g, 96.1 mmol) was added, and the slurry refluxed for 5 h. The unreacted NH₄Cl was filtered off under gravity and the filtrate concentrated to ¼ of the solution. Pure **7** was precipitated from the concentrated solution by adding 150 mL ether to yield 12.85 g (85.1%) solid; MP = 149-151°C. Anhydrous crystals of **7** suitable for X-ray analysis were recovered by slow cooling of isopropanol solution while the hydrated crystals were formed by either solid state recrystallization of the anhydrous crystals on exposure to air or slow evaporation of ethanol solution in air. ¹H NMR (300 MHz, CDCl₃): δ 9.45 (Br s, N-H, 4H); δ 8.92 (d, J_{HH} = 8.1 Hz, pyridyl_{meta}, 1H); δ 8.72 (d, J_{HH} = 4.5 Hz, pyridyl_{ortho}, 1H); δ 8.06 (d of d of d, J_{HH} = 7.8 Hz, pyridyl_{meta}, 1H); δ 7.63 (d of d, J_{HH} = 12.3 Hz, J_{HH} = 4.65 Hz, pyridyl_{para}, 1H). FTIR (Diamond Anvil ATR, cm⁻¹): 3396w, 3052w, 2753w, 1691w, 1657w, 1642w, 1592s, 1536m, 1521m, 1489m, 1458s, 1405w, 1345s, 1328s, 1292vs, 1232s, 1175m, 1137m, 1102m, 1090m, 1077m, 1041m, 1010m, 974w, 900w, 787vs, 748s, 701m, 675s, 652s, 627s, 591s, 564s, 526vs, 484s, 461vs, 439vs, 426vs, 406vs.

6.2.8 Preparation of 2-amidinopyridine (**8**)

7 (12.26 g) was suspended in 15 mL MeOH in a 500 mL round bottom flask. While stirring, 1.5 equivalent KOH suspended in 15 mL MeOH was added and stirred for 3 min. DCM (150 mL) was immediately added to extract the liberated PyA. The KCl formed was filtered under gravity using a large glass funnel, and MgSO₄ (3 g) was added to the filtrate to remove moisture. The MgSO₄ was then filtered, and the solvent removed under reduced pressure. Light brown sticky material obtained was further dried at high vacuum to remove traces of MeOH. The material was re-dissolved in 150 mL DCM and the suspended solid (MeOH soluble KCl) filtered. The solution

was evaporated to dryness, and the final product was vacuum-dried to give crystalline off-white solid **8** with 83.14 % (7.83 g) yield, MP = 50 – 54°C. Single crystals of **8** suitable for X-ray diffraction analysis was grown from MeOH/DCM. Calculated, % (Analysis found, %) for C₆H₇N₃: C- 59.49 (C- 59.41); H- 5.82 (H- 5.85); N- 34.69 (N- 34.49). ¹H NMR (300 MHz, CDCl₃): δ 8.58 (d, J_{HH} = 4.2 Hz, pyridyl_{meta}, 1H); δ 8.13 (d, J_{HH} = 7.8 Hz, pyridyl_{ortho}, 1H); δ 7.80 (d of d of d, J_{HH} = 7.8 Hz, J_{HH} = 1.5 Hz, pyridyl_{meta}, 1H); δ 7.38 (d of d of d, J_{HH} = 12.4 Hz, J_{HH} = 4.8 Hz, J_{HH} = 1.2 Hz, pyridyl_{para}, 1H); δ 6.0 (Br s, N-H, 3H). FTIR (Diamond Anvil ATR, cm⁻¹): 3462w, 3443w, 3342w, 3266w, 3230w, 3064w, 3051 w, 3005w, 2732w, 1706w, 1617s, 1587s, 1563s, 1477vs, 1453vs, 1415vs, 1373m, 1310w, 1289m, 1254m, 1199s, 1148s, 1090m, 1043m, 997s, 964w, 890m, 847s, 804s, 773m, 742s, 688m, 655s, 629s, 607s, 470vs, 450vs.

6.2.9 Synthesis of 2-amidinopyrimidine hydrochloride (**9**)

This was prepared in a manner analogous to **7** utilizing 14.63 g (0.14 mol) 2-pyrimidine carbonitrile (PmCN, 1.58 g, 29.25 mmol) MeONa and 7.46 g (0.14 mol) of NH₄Cl. A brown mixture was obtained after refluxing for 3 h in 150 mL of MeOH. The solvent was removed and the recovered solid suspended in 150 mL EtOH and refluxed for 1 h. The unreacted NH₄Cl was filtered using a gravity setup and the filtrate concentrated to ¼ of the initial volume. About 50 mL of ether was added, and pure colorless plate crystals of 2-amidinopyrimidine hydrochloride **9** precipitated out of solution within 12 h from which suitable single crystal were obtained to collect X-ray data for structural determination, yield: 17.27 g (78.22%); MP = 190–192 °C. FTIR (Diamond Anvil ATR, cm⁻¹): 3277w, 3079w, 3040w, 1691m, 1566m, 1540m, 1477w, 1435w, 1391vs, 1285w, 1274w, 1230w, 1194w, 1093m, 1052m, 999m, 901w, 842m, 812m, 785m, 710s, 662s, 634vs, 588s, 506s.

6.2.10 Preparation of 2-amidinopyrimidine (10)

This is a known compound with CAS Registry number [45695-56-5].³ It was synthesized in a manner similar to **8** using 1.5 equivalents of KOH. After neutralization of PmA.HCl in 50 mL MeOH in 5 min, 200 mL DCM was used to extract the free **10**. Excess KOH and KCl which was formed was filtered off and the filtrate was dried with MgSO₄. The solution was evaporated to dryness, and the solid recrystallized from 1:5 methanol:DCM to afford pure colorless block crystals of **10** (yield: 11.5 g, 86.14%) which are of excellent qualities for X-ray analysis; MP = 162 – 164 °C [lit. 159 – 163 °C]³. Calculated, % (Analysis found, %) for C₅H₆N₄: C- 49.17 (C- 49.02); H- 4.95 (H- 4.99); N- 45.88 (N- 45.49). ¹H NMR (300 MHz, CDCl₃) [300 MHz, DMSO-*d*₆]³: δ 8.81 [8.95] (d, J_{HH} = 4.8 Hz, pyrimidyl_{meta}, 2H); δ 7.36 [7.63] (t, J_{HH} = 4.8 Hz, pyrimidyl_{para}, 1H); δ 6.69 [7.12] (br s, N-H, 3H). ¹³C NMR (300 MHz, CDCl₃) [300 MHz, DMSO-*d*₆]³: δ 160.5 [159.6] (s, N–C =N_{ipso} C), δ 157.4 [157.5] (s, pyrimidyl_{meta}, 2C), δ 156.6 [156.2] (pyrimidyl_{ipso}), δ 121.7 [121.8] (s, pyrimidyl_{para}). FTIR (Diamond Anvil ATR, cm⁻¹): 3404w, 3286w, 3106w, 3057w, 1652m, 1594w, 1562m, 1471w, 1443w, 1399s, 1284m, 1250s, 1158s, 1104m, 996m, 897w, 857m, 818s, 784s, 702s, 663s, 630vs, 548s, 509s, 423s.

6.2.11 Synthesis of trichloromethyl-2-pyridylimidoamidide (11)

Following a literature procedure,⁴ to PyA (4.5 g, 37.15 mmol) dissolved in 25 mL dried and degassed acetonitrile in a 100 mL Schlenk flask placed in an ice bath was added 3.81 mL of CCl₃CN (37.15 mmol) dropwise through a syringe over a period of 3 min under an inert atmosphere. The resulting mixture was allowed to warm to room temperature and heated to reflux for 1 h. The colorless solution obtained was cooled to ambient temperature wherein no crystals were formed. Pure colorless crystals (needles) of PyCCl₃ImAm grew out of solution by slow cooling to –35 °C in the freezer, yield: 9.56 g (97%); MP = 80 – 83 °C. Calculated, % (Analysis

found, %) for $C_8H_7N_4Cl_3$: C- 36.19 (C- 36.37); H- 2.66 (H- 2.67); N- 21.10 (N- 20.79). 1H NMR (300 MHz, $CDCl_3$): δ 10.43 (Br s, amino N-H, 1H); δ 9.47 (Br s, amino N-H, 1H); δ 8.61 (d, $J_{HH} = 4.0$ Hz, pyridyl_{meta}, 1H); δ 8.55 (d, $J_{HH} = 7.9$ Hz, pyridyl_{ortho}, 1H); δ 8.48 (Br s, imino N-H, 1H); δ 7.85 (d of d of d, $J_{HH} = 7.8$ Hz, $J_{HH} = 1.7$ Hz, pyridyl_{meta}, 1H); δ 7.44 (d of d of d, $J_{HH} = 12.3$ Hz, $J_{HH} = 4.8$ Hz, $J_{HH} = 1.2$ Hz pyridyl_{para}, 1H). ^{13}C NMR (300 MHz, $CDCl_3$): δ 168.2 (s, imino ipso – C), δ 161.2 (s, amino ipso – C), δ 150.6 (s, pyridyl_{ipso} C), δ 148.5 (s, pyridyl_{para}), δ 137.4 (pyridyl_{meta}), δ 126.4 (s, pyridyl_{para}), δ 122.9 (s, pyridyl_{ortho}), δ 97.9 (s, CCl_3 -C). FTIR (Diamond Anvil ATR, cm^{-1}): 3379w, 3310w, 3188w, 3152w, 3131w, 1722w, 1611m, 1582m, 1563s, 1529m, 1498s, 1455s, 1428m, 1368m, 1322s, 1256m, 1173m, 1141s, 1092m, 1048s, 1032m, 998m, 966w, 933m, 903w, 853m, 839s, 809vs, 792s, 757s, 746s, 724s, 673vs, 646s, 627s, 564vs, 498vs, 458s, 414s.

6.2.12 Generation of trichloromethyl-2-pyridylimidoamidinium hydrochloride (12)

A solution of $PyCCl_3ImAm$ (4 g, mmol) in 120 mL ether placed in a three-necked flask equipped with a gas inlet through which HCl gas was bubbled through the solution and a Liebig condenser with attached drying tube. Upon bubbling HCl gas into the solution for 1 min under N_2 flow, the slurry formed was stirred for 3 h for efficient $PyCCl_3ImAm.HCl$ salt formation. The precipitate was collected on Büchner funnel, rinse with ether, and dried in vacuo to afford 7.15 g (99.72%) yield; MP = 160 – 164 °C. FTIR (Diamond Anvil ATR, cm^{-1}): 3259w, 3090m, 2978m, 1660s, 1603s, 1579s, 1517m, 1503m, 1462m, 1437m, 1406s, 1371s, 1325s, 1260m, 1226m, 1175w, 1158w, 1120m, 1092m, 1042m, 996s, 930w, 912w, 842s, 808vs, 776vs, 741vs, 673vs, 620s, 584vs, 519s, 435s, 406vs.

6.2.13 Synthesis of trichloromethyl-2-pyrimidylimidoylamidine (13)

This was prepared by same method reported for **11**. Using PmA (6.5 g, 53.02 mmol) and 5.5 mL (53.74 mmol), 12.03 g (85.14 %) of PmCCl₃ImAm was obtained; MP = 131 – 133 °C. Calculated, % (Analysis found, %) for C₇H₆N₅Cl₃: C- 31.55 (C- 31.65); H- 2.27 (H- 2.09); N- 26.28 (N- 26.23). ¹H NMR (300 MHz, CDCl₃): Amino-Imino tautomer: δ 10.77 (Br s, amino N-H, 1H); δ 9.68 (Br s, imino N-H, 1H); δ 8.91 (d, J_{HH} = 4.8 Hz, pyrimidyl_{meta}, 2H); δ 8.51 (Br s, amino N-H, 1H); δ 7.42 (t, J_{HH} = 4.8 Hz, pyrimidyl_{para}, 1H). ¹³C NMR (300 MHz, CDCl₃): δ 168.8 (s, imino ipso – C), δ 160.2 (s, amino ipso – C), δ 158.9 (s, pyrimidyl_{ipso} C), δ 157.9 (pyrimidyl_{meta}, 2C), δ 122.4 (s, pyrimidyl_{para}), δ 97.4 (s, CCl₃–C); Imino-Imino tautomer: δ 11.6 (Sh s, amino N-H, 1H); δ 10.1 (Sh s, imino N-H, 1H); δ 9.85 (Sh s, imino N-H, 1H); δ 8.88 (d, J_{HH} = 4.8 Hz, pyrimidyl_{meta}, 2H); δ 7.48 (t, J_{HH} = 4.8 Hz, pyrimidyl_{para}, 1H). ¹³C NMR (300 MHz, CDCl₃): δ 157.8 (pyrimidyl_{meta}, 2C), δ 157.4 (s, imino ipso – C), δ 154.5 (s, amino ipso – C), δ 154.21 (s, pyrimidyl_{ipso} C), δ 122.6 (s, pyrimidyl_{para}), δ 94.8 (s, CCl₃–C). FTIR (Diamond Anvil ATR, cm⁻¹): 3374w, 3305w, 3136w, 3118w, 3036w, 1613m, 1555s, 1495m, 1446w, 1405m, 1322s, 1279m, 1263w, 1213m, 1182m, 1145m, 1102w, 1035m, 996w, 973w, 931w, 844m, 827s, 816s, 801s, 759s, 735s, 694m, 669s, 636s, 592vs, 503s, 463s, 424m, 414m.

6.2.14 Generation of trichloromethyl-2-pyrimidylimidoylamidinehydrochloride (14)

Similar method for **12** was adopted using 8.6 g (37.97 mmol) PmCCl₃ImAm and 150 mL ether to give 99.7% yield; MP = 143 – 145 °C. FTIR (Diamond Anvil ATR, cm⁻¹): 3247w, 3063w, 2911w, 1681s, 1626s, 1564vs, 1472w, 1452w, 1410m, 1379m, 1226w, 1169w, 1148w, 1105w, 1030m, 1005w, 976w, 936w, 910w, 837vs, 805m, 691s, 632s, 583s, 522vs.

6.2.15 Synthesis of asymmetric 1-chloro-3-trichloromethyl-5-(2-pyridyl)-1-thia-2,4,6-triazine, PyCCl₃TTACl (15)

This was carried out using S₂Cl₂ for the condensation reaction to generate the intended asymmetric TTACl in acetonitrile (MeCN). However, the outcome of the reaction resulted in the isolation of the hydrochloride hemi-salt of PyCCl₃TTACl. In summary, PyCCl₃ImAm.HCl (1 g, 3.31 mmol) was suspended in 40 mL MeCN, and 6 equivalents of S₂Cl₂ (1.63 mL, 19.87 mmol) in 10 mL MeCN were added dropwise via a dropping funnel within 5 min under an inert atmosphere. The flask containing the mixture was then equipped with a water condenser having an attached drying tube, and the resulting yellow slurry refluxed for 10 h. The mixture was filtered hot and slowly cooled to room temperature wherein colorless crystals of sulfur formed. The yellow block crystals of PyCCl₃TTACl [PyCCl₃TTACl.HCl] crystallized out of solution after spending three weeks in the freezer ; MP = 148 – 151 °C. ¹H NMR (300 MHz, CDCl₃): PyCCl₃TTACl (Major): δ 9.13 (d, J_{HH} = 4.9 Hz, pyridyl_{meta}, 1H); δ 8.82 (d, J_{HH} = 7.9 Hz, pyridyl_{ortho}, 1H); δ 8.27 (d of d of d, J_{HH} = 7.9 Hz, J_{HH} = 1.6 Hz, pyridyl_{meta}, 1H); δ 7.89 (d of d of d, J_{HH} = 7.5 Hz, J_{HH} = 4.8 Hz, J_{HH} = 0.9 Hz pyridyl_{para}, 1H); PyCCl₃TTA=O (Minor): δ 8.71 (d, J_{HH} = 4.9 Hz, pyridyl_{meta}, 1H); δ 8.48 (d, J_{HH} = 7.9 Hz, pyridyl_{ortho}, 1H); δ 8.00 (d of d of d, J_{HH} = 7.9 Hz, J_{HH} = 1.6 Hz, pyridyl_{meta}, 1H); δ 7.63 (d of d of d, J_{HH} = 7.5 Hz, J_{HH} = 4.8 Hz, J_{HH} = 0.9 Hz pyridyl_{para}, 1H). FTIR (Diamond Anvil ATR, cm⁻¹): 3134w, 3038w, 2331w, 2115w, 2087w, 1710m, 1688s, 1681s, 1649m, 1643m, 1602m, 1581m, 1572m, 1548m, 1526s, 1502s, 1460s, 1453s, 1406vs, 1331s, 1301s, 1260s, 1214s, 1551s, 1112s, 1090s, 1042s, 1016s, 997s, 928s, 842vs, 805vs, 742vs, 711vs, 698vs, 674vs, 642vs, 617vs, 586s, 554s, 529vs, 491s, 467s.

6.2.16 Preparation of asymmetric 1-oxo-3-trichloromethyl-2-pyridyl thiatriazine,

PyCCl₃TTA=O (16) from the hydrolysis of PyCCl₃TTACl

Following the same method for **15** using PyCCl₃ImAm.HCl (1 g, 3.31 mmol in 40 mL MeCN) and 4 equivalents of S₂Cl₂ (1.00 mL, 13.24 mmol in 10 mL MeCN), the resulting slurry was heated under reflux for 1.5 h, cooled to room temperature, and filtered under N₂ atmosphere. The solvent of the filtrate was removed in vacuo to give 1.10 g of oily crude product. The oil was then extracted with 5 mL of CS₂ to afford 0.81 g (74.3%) brownish-orange oil. Colorless crystals of PyCCl₃TTA=O suitable for X-ray analysis were generated by slow evaporation of the CS₂ solution; MP = 128 – 130 °C. Calculated, % (Analysis found, %) for C₈H₄N₄Cl₃SO: C- 30.84 (C- 30.77); H- 1.62 (H- 2.02); N- 17.98 (N- 18.21); S- 10.29 (N- 10.29). ¹H NMR (300 MHz, CDCl₃): δ 8.71 (d, J_{HH} = 4.8 Hz, pyridyl_{meta}, 1H); δ 8.48 (d, J_{HH} = 7.8 Hz, pyridyl_{ortho}, 1H); δ 7.99 (d of d of d, J_{HH} = 7.8 Hz, J_{HH} = 1.5 Hz, pyridyl_{meta}, 1H); δ 7.63 (d of d of d, J_{HH} = 7.5 Hz, J_{HH} = 4.8 Hz, J_{HH} = 0.9 Hz pyridyl_{para}, 1H). ¹³C NMR (300 MHz, CDCl₃): δ 149.2 (s, pyridyl_{para}), δ 146.4 (s, pyridyl_{ipso} C), δ 138.6 (pyridyl_{meta}), δ 128.6 (s, pyridyl_{para}), δ 123.3 (s, pyridyl_{ortho}), δ 97.9 (s, CCl₃-C). FTIR (Diamond Anvil ATR, cm⁻¹): 3227w, 3064w, 1646m, 1584w, 1562m, 1452s, 1415s, 1326w, 1291w, 1256w, 1157w, 1115vs, 1091m, 1040w, 1020s, 998m, 972w, 925m, 843m, 801vs, 771m, 751s, 692vs, 674vs, 635s, 553s, 469m, 422s.

6.2.17 Synthesis of 3-trichloromethyl-5-(2-pyridyl)-1-thia-2,4,6-triazinyl, PyCCl₃TTA• (17)

An oily hemi-salt, PyCCl₃TTACl [PyCCl₃TTACl.HCl] (3.53 g) obtained through S₂Cl₂ condensation was pyrolyzed under vacuum at 85 °C. The resulting brown oil (2.12 g) was then reduced chemically in 20 mL three cycle freeze-pump-thaw degassed acetonitrile with Ph₃Sb (1.16 g, 3.29 mmol) added under vacuum with a pear-shaped solids addition vessel under vacuum, with stirring. This resulted in a deep purple precipitate of PyCCl₃TTA radical dimer which was stirred

for 15 min under vacuum and for another 30 min under N₂. The precipitate was then filtered and thoroughly dried under vacuum to give 0.26 g, 13.8% yield; MP = 91 – 93 °C. Calculated, % (Analysis found, %) for C₈H₄N₄Cl₃S: C- 32.62 (C- 32.76); H- 1.37 (H- 1.35); N- 19.02 (N- 17.58); S- 10.89 (N- 15.21). The precipitate contains uniform-shaped microcrystals suitable for X-ray analysis, which were not homogeneous under microscope observation.

6.2.18 X-ray crystal structure data collection and refinement

The selected crystals were coated in Paratone™ oil, mounted on a MiTeGen loop on a goniometer head and cooled to 100 (±1) K except where otherwise stated. High resolution data was collected on a Rigaku-Oxford Diffraction SuperNova/Pilatus200K using Mo K α radiation (λ = 0.71073 Å) for well diffracting crystals and Cu K α radiation (λ = 1.54184 Å) for low diffracting crystals from micro-focus sealed tubes. The data collection and processing were done on the Rigaku CrysAlisPro 171.40_64.53 software and with multi-scan absorption correction. The structures were solved using SHELXT and refined using SHELXL-2014 on $|F|^2$ by full least squares methods within the Olex2 software package. All non-H atoms were refined anisotropically with proper restrains on their ADP for structures that are not suitable for quantum refinement. The H atoms connected to carbon (C) and nitrogen were revealed through a fine-focus Fourier map. The H attached to aromatic C were refined as riding with $U_{iso} = 1.2U_{eq}(C)$ while those of terminal N as free with $U_{iso} = 1.5U_{eq}(N)$. Structures with exceptional data quality were refined by NoSphereA2 in Olex2 to account for precise positions of H atoms on accurate determination of their electron density by quantum calculation while others with moderate quality data H atoms were refined using the traditional independent atom model (IAM). The full crystal parameters including interatomic distances and angles are compiled in the appendix. Geometric properties and structural visualization were undertaken using Mercury v.4.2.0 and the electronic structural data

will be deposited in Cambridge Crystallographic Data Centre (CCDC). Table 6.1 presents the details of crystal and structural refinement.

6.2.19 Computational studies

Theoretical studies of some compounds were undertaken to supplement experimental spectroscopic characterizations and explain fundamental properties of individual molecules. All calculations were undertaken with the Gaussian W16⁵ program package and structures generated using Gaussview 06 software. The electronic energies and frequency calculations of the phosphine complexes, their monomers, and the free phosphine were computed by density function theory (DFT) using B3LYP level of theory and 6-31+G (d, p) basis set, and the Cartesian coordinates obtained from the crystal structures as starting points.

Table 6.1. X-ray crystal structure and refinement data of compounds

Compound	1	1a	2a
Formula	C ₂₄ H ₂₇ ClCuP	C ₂₆ H ₂₉ Cl ₇ CuP	C ₂₅ H ₂₈ BrCl ₃ CuP
Formula weight (FW, g/mol)	445.41	684.15	609.24
Crystal size (mm ³)	0.30 × 0.13 × 0.04	0.23 × 0.04 × 0.04	0.15 × 0.09 × 0.04
Crystal system	triclinic	triclinic	triclinic
Space group	P-1	P-1	P-1
Temperature (K)	99.98(10)	100.01(10)	99.99(10)
a (Å)	8.6758(3)	9.2137(4)	9.0378(3)
b (Å)	9.1950(4)	12.8322(7)	9.3098(3)
c (Å)	14.8249(5)	13.6549(9)	16.2183(5)
α (°)	80.012(3)	89.620(5)	105.130(3)
β (°)	80.290(3)	70.898(5)	97.167(2)
γ (°)	67.876(4)	80.413(4)	100.203(3)
Volume (Å ³)	1072.02(8)	1502.26(15)	1275.30(7)
Z	2	2	2
ρ _{calc} (g Cm ⁻³)	1.380	1.512	1.587
μ (mm ⁻¹)	1.224	1.418	2.812
F(000)	464.0	696.0	616.0
Reflections collected	23132	14737	27984
Independent reflections	5327	14737	6331
Parameters	5327/0/248	14737/256/321	6331/0/284
R1, wR2 [all data]	0.0508, 0.1152	0.0978, 0.1556	0.0529, 0.0850
R1, wR2[I ≥ 2σ (I)]	0.0423, 0.1106	0.0583, 0.1373	0.0384, 0.0813

Table 6.1, continued. X-ray crystal structure and refinement data of compounds

Compound	3	3a	4a
Formula	C ₃₀ H ₃₉ ClCuP	C ₃₁ H ₄₀ Cl ₄ CuP	C ₃₁ H ₄₀ BrCl ₃ CuP
Formula weight (FW, g/mol)	529.57	648.94	693.40
Crystal size (mm ³)	0.29 × 0.23 × 0.03	0.36 × 0.28 × 0.20	0.10 × 0.09 × 0.06
Crystal system	monoclinic	monoclinic	monoclinic
Space group	P2 ₁ /n	P2 ₁ /n	P2 ₁ /n
Temperature (K)	99.98(10)	100.01(10)	100.00(10)
a (Å)	10.2678(9)	10.2615(3)	10.2618(2)
b (Å)	10.0641(8)	14.7387(4)	14.7775(2)
c (Å)	27.414(3)	21.4025(7)	21.4776(3)
α (°)	90	90	90
β (°)	96.050(9)	103.602(3)	103.756(2)
γ (°)	90	90	90
Volume (Å ³)	2817.1(4)	3146.15(17)	3163.52(9)
Z	4	4	4
ρ _{calc} (g Cm ⁻³)	1.249	1.370	1.456
μ (mm ⁻¹)	0.942	1.104	2.277
F(000)	1120.0	1352.0	1424.0
Reflections collected	16842	43002	96508
Independent reflections	6517	8634	8577
Parameters	6517/0/306	8634/0/342	8577/0/342
R1, wR2 [all data]	0.0956, 0.1790	0.0431, 0.0844	0.0280, 0.0577
R1, wR2[I>=2σ(I)]	0.0749, 0.1720	0.0332, 0.0810	0.0229, 0.0564

Table 6.1, continued. X-ray crystal structure and refinement data of compounds

Compound	4b	5	6
Formula	C ₉₂ H ₁₂₀ Br ₃ Cu ₃ NP ₃	C ₄₈ H ₅₄ ClCuP ₂	C ₄₈ H ₅₄ BrCuP ₂
Formula weight (FW, g/mol)	1763.14	791.84	836.30
Crystal size (mm ³)	0.23 × 0.15 × 0.10	0.29 × 0.19 × 0.18	0.21 × 0.18 × 0.08
Crystal system	orthorhombic	monoclinic	monoclinic
Space group	Pbca	I2/a	C2/c
Temperature (K)	99.98(10)	100.00(10)	99.98(11)
a (Å)	15.4399(2)	18.7280(8)	20.8129(10)
b (Å)	20.3485(3)	11.5421(3)	11.5674(4)
c (Å)	55.0355(12)	22.0844(9)	18.9686(10)
α (°)	90	90	90
β (°)	90	119.367(5)	112.976(6)
γ (°)	90	90	90
Volume (Å ³)	17291.0(5)	4160.3(3)	4204.4(4)
Z	8	4	4
ρ _{calc} (g Cm ⁻³)	1.355	1.264	1.321
μ (mm ⁻¹)	3.330	0.698	1.578
F(000)	7328.0	1672.0	1744.0
Reflections collected	48800	24064	14360
Independent reflections	17095	5261	4854
Parameters	17095/833/958	5261/0/240	4854/0/240
R1, wR2 [all data]	0.1246, 0.3133	0.0299, 0.0705	0.0332, 0.0702
R1, wR2 [I ≥ 2σ (I)]	0.1104, 0.3037	0.0275, 0.0694	0.0265, 0.0684

Table 6.1, continued. X-ray crystal structure and refinement data of compounds

Compound	7	8	9
Formula	C ₆ H ₈ ClN ₃	C ₆ H ₇ N ₃	C ₅ H ₇ ClN ₄
Formula weight (FW, g/mol)	157.60	121.15	158.60
Crystal size (mm ³)	0.50 × 0.02 × 0.02	0.21 × 0.12 × 0.04	0.10 × 0.08 × 0.02
Crystal system	orthorhombic	monoclinic	monoclinic
Space group	Fdd2	I2/a	C2
Temperature (K)	100.0(5)	99.9(4)	99.9(4)
a (Å)	38.3355(14)	22.5590(14)	18.6130(3)
b (Å)	18.4105(6)	8.2344(4)	7.44760(10)
c (Å)	4.0811(2)	21.2914(11)	10.2778(2)
α (°)	90	90	90
β (°)	90	110.267(7)	93.978(2)
γ (°)	90	90	90
Volume (Å ³)	2880.3(2)	3710.2(4)	1421.30(4)
Z	16	24	8
ρ _{calc} (g Cm ⁻³)	1.454	1.301	1.482
μ (mm ⁻¹)	4.057	0.085	4.157
F(000)	1312.0	1536.0	656.0
Reflections collected	3390	12060	13569
Independent reflections	1232	4124	2893
Parameters	1232/1/104	4124/9/280	2893/1/206
R1, wR2 [all data]	0.0439, 0.1203	0.0445, 0.0927	0.0246, 0.0680
R1, wR2[I >= 2σ (I)]	0.0434, 0.1199	0.0352, 0.0882	0.0244, 0.0679

Table 6.1, continued. X-ray crystal structure and refinement data of compounds

Compound	9.H₂O	10	8a
Formula	C ₅ H ₉ ClN ₄ O	C ₅ H ₆ N ₄	C ₁₂ H ₁₉ ClN ₆ O ₂
Formula weight (FW, g/mol)	176.61	122.14	314.78
Crystal size (mm ³)	0.33 × 0.33 × 0.23	0.30 × 0.23 × 0.11	0.42 × 0.11 × 0.06
Crystal system	monoclinic	triclinic	monoclinic
Space group	P2 ₁ /n	P-1	P2 ₁ /n
Temperature (K)	99.9(4)	100.0(3)	99.9(3)
a (Å)	10.0168(5)	5.47045(15)	14.0348(4)
b (Å)	5.5161(2)	7.1234(2)	7.4311(2)
c (Å)	15.8244(8)	7.65746(18)	15.0277(5)
α (°)	90	85.577(2)	90
β (°)	107.616(5)	72.697(2)	101.247(3)
γ (°)	90	81.189(2)	90
Volume (Å ³)	833.35(7)	281.374(14)	1537.20(8)
Z	4	2	4
ρ _{calc} (g Cm ⁻³)	1.408	1.442	1.360
μ (mm ⁻¹)	0.409	0.814	0.263
F(000)	368.0	128.0	664.0
Reflections collected	22154	5401	13727
Independent reflections	4293	1139	4170
Parameters	4293/0/118	1139/0/92	4170/11/223
R1, wR2 [all data]	0.0472, 0.0926	0.0323, 0.0859	0.0338, 0.0819
R1, wR2 [I ≥ 2σ (I)]	0.0363, 0.0877	0.0315, 0.0854	0.0286, 0.0794

Table 6.1, continued. X-ray crystal structure and refinement data of compounds

Compound	8b	11	12
Formula	C ₁₉ H _{27.1} N ₉ O _{5.05}	C ₈ H ₇ Cl ₃ N ₄	C ₇ H ₆ Cl ₃ N ₅
Formula weight (FW, g/mol)	462.40	265.53	266.52
Crystal size (mm ³)	0.56 × 0.26 × 0.08	0.45 × 0.19 × 0.10	0.41 × 0.14 × 0.13
Crystal system	monoclinic	triclinic	triclinic
Space group	P2 ₁ /c	P-1	P-1
Temperature (K)	99.9(2)	100.0(3)	99.9(4)
a (Å)	20.8250(6)	6.6005(2)	6.73775(18)
b (Å)	17.4470(6)	6.9738(3)	6.77818(17)
c (Å)	12.3681(5)	12.6419(4)	12.5793(3)
α (°)	90	87.921(3)	84.8855(19)
β (°)	90.217(3)	85.709(3)	89.9656(19)
γ (°)	90	64.337(4)	62.141(3)
Volume (Å ³)	4493.7(3)	523.04(4)	505.34(2)
Z	8	2	2
ρ _{calc} (g Cm ⁻³)	1.367	1.686	1.752
μ (mm ⁻¹)	0.103	0.845	8.002
F(000)	1956.0	268.0	268.0
Reflections collected	37552	2841	9348
Independent reflections	11476	2841	2033
Parameters	11476/432/697	2841/0/148	2033/0/148
R1, wR2 [all data]	0.0829, 0.1506	0.0341, 0.1164	0.0282, 0.0729
R1, wR2 [I ≥ 2σ (I)]	0.0580, 0.1400	0.0318, 0.1067	0.0281, 0.0728

Table 6.1, continued. X-ray Crystal structure and refinement data of compounds

Compound	15.HCl	15.HCl-15	16a
Formula	C ₈ H ₅ Cl ₅ N ₄ S	C ₁₈ H ₁₂ Cl ₉ N ₉ S ₂	C ₈ H ₅ Cl ₃ N ₄ OS
Formula weight (FW, g/mol)	366.47	737.54	311.57
Crystal size (mm ³)	0.14 × 0.12 × 0.09	0.18 × 0.16 × 0.13	0.31 × 0.25 × 0.22
Crystal system	monoclinic	triclinic	monoclinic
Space group	P2 ₁ /c	P-1	P2 ₁ /c
Temperature (K)	100(1)	100.0(3)	100.0(3)
a (Å)	6.0844(3)	9.5720(2)	6.4664(5)
b (Å)	28.4409(10)	9.8187(2)	20.2370(12)
c (Å)	8.0799(3)	15.4407(2)	9.3660(7)
α (°)	90	98.1480(10)	90
β (°)	96.234(4)	95.7200(10)	109.093(8)
γ (°)	90	90.9010(10)	90
Volume (Å ³)	1389.93(9)	1428.73(5)	1158.22(15)
Z	4	2	4
ρ _{calc} (g Cm ⁻³)	1.751	1.714	1.787
μ (mm ⁻¹)	10.816	9.699	0.957
F(000)	728.0	736.0	624.0
Reflections collected	8057	26632	4649
Independent reflections	2769	5732	4649
Parameters	2769/126/166	5732/2/351	4649/0/155
R1, wR2 [all data]	0.0946, 0.2372	0.0216, 0.0523	0.0570, 0.1539
R1, wR2 [I>=2σ (I)]	0.0878, 0.2341	0.0206, 0.0517	0.0544, 0.1523

Table 6.1, continued. X-ray crystal structure and refinement data of compounds

Compound	16b	17
Formula	C ₈ H ₅ Cl ₃ N ₄ OS	C ₈ H ₄ Cl ₃ N ₄ S
Formula weight (FW, g/mol)	311.57	294.56
Crystal size (mm ³)	0.35 × 0.30 × 0.27	0.08 × 0.03 × 0.01
Crystal system	triclinic	triclinic
Space group	P-1	P-1
Temperature (K)	100.4(9)	100.2(8)
a (Å)	6.5992(3)	6.3516(11)
b (Å)	9.5331(4)	9.3967(14)
c (Å)	10.4858(5)	10.018(2)
α (°)	103.154(4)	107.881(16)
β (°)	101.587(4)	104.877(16)
γ (°)	109.914(4)	98.235(13)
Volume (Å ³)	575.36(5)	533.69(17)
Z	2	2
ρ _{calc} (g Cm ⁻³)	1.798	1.833
μ (mm ⁻¹)	8.832	9.408
F(000)	312.0	294.0
Reflections collected	10459	3242
Independent reflections	2308	1601
Parameters	2308/1/159	1601/0/145
R1, wR2	0.0313, 0.0775	0.1695, 0.4369
[all data]		
R1, wR2	0.0307, 0.0773	0.1482, 0.4258
[I>=2σ (I)]		

Acknowledgement

* I thank Dylan Webb of Prof. Hayes' lab for carrying out the elemental analyses of all the isolated compounds in this project.

6.3 References

1. Bullock, J. P.; Bond, A. M.; Boéré, R. T.; Gietz, T. M.; Roemmele, T. L.; Seagrave, S. D.; Masuda, J. D.; Parvez, M., Synthesis, characterization, and electrochemical studies of PPh₃-n(dipp)_n (dipp = 2,6-diisopropylphenyl): Steric and electronic effects on the chemical and electrochemical oxidation of a homologous series of triarylphosphines and the reactivities of the corresponding phosphoniumyl radical cations. *J. Am. Chem. Soc.* **2013**, *135*, 11205-11215.
2. Blumhoff, J.; Beckert, R.; Rau, S.; Losse, S.; Matschke, M.; Günther, W.; Görls, H., Synthesis of ligands based on 4H-imidazoles and pyridine subunits: Selective complexation and bathochromically absorbing complexes. *Eur. J. Inorg. Chem.* **2009**, *2009*, 2162-2169.
3. Safin, D. A.; Tumanov, N. A.; Leitch, A. A.; Brusso, J. L.; Filinchuk, Y.; Murugesu, M., Elucidating the elusive crystal structure of 2,4,6-tris(2-pyrimidyl)-1,3,5-triazine. *Cryst. Eng. Comm.* **2015**, *17*, 2190-2195.
4. Boéré, R. T.; Roemmele, T. L.; Yu, X., Unsymmetrical 1λ3-1,2,4,6-thiatriazinyls with aryl and trifluoromethyl substituents: Synthesis, crystal structures, EPR spectroscopy, and voltammetry. *Inorg. Chem.* **2011**, *50*, 5123-5136.
5. Frisch, M. J.; Trucks, G. W.; Schlegel, H. B.; Scuseria, G. E.; Robb, M. A.; Cheeseman, J. R.; Scalmani, G.; Barone, V.; Petersson, G. A.; Nakatsuji, H.; Li, X.; Caricato, M.; Marenich, A. V.; Bloino, J.; Janesko, B. G.; Gomperts, R.; Mennucci, B.; Hratchian, H. P.; Ortiz, J. V.; Izmaylov, A. F.; Sonnenberg, J. L.; Williams; Ding, F.; Lipparini, F.; Egidi, F.; Goings, J.; Peng, B.; Petrone, A.; Henderson, T.; Ranasinghe, D.; Zakrzewski, V. G.; Gao, J.; Rega, N.; Zheng, G.; Liang, W.; Hada, M.; Ehara, M.; Toyota, K.; Fukuda, R.; Hasegawa, J.; Ishida, M.; Nakajima, T.; Honda, Y.; Kitao, O.; Nakai, H.; Vreven, T.; Throssell, K.; Montgomery Jr., J. A.; Peralta, J. E.; Ogliaro, F.; Bearpark, M. J.; Heyd, J. J.; Brothers, E. N.; Kudin, K. N.; Staroverov, V. N.; Keith, T. A.; Kobayashi, R.; Normand, J.; Raghavachari, K.; Rendell, A. P.; Burant, J. C.; Iyengar, S. S.; Tomasi, J.; Cossi, M.; Millam, J. M.; Klene, M.; Adamo, C.; Cammi, R.; Ochterski, J. W.; Martin, R. L.; Morokuma, K.; Farkas, O.; Foresman, J. B.; Fox, D. J. *Gaussian 16 Rev. C.01*, Wallingford, CT, 2016.

Appendix

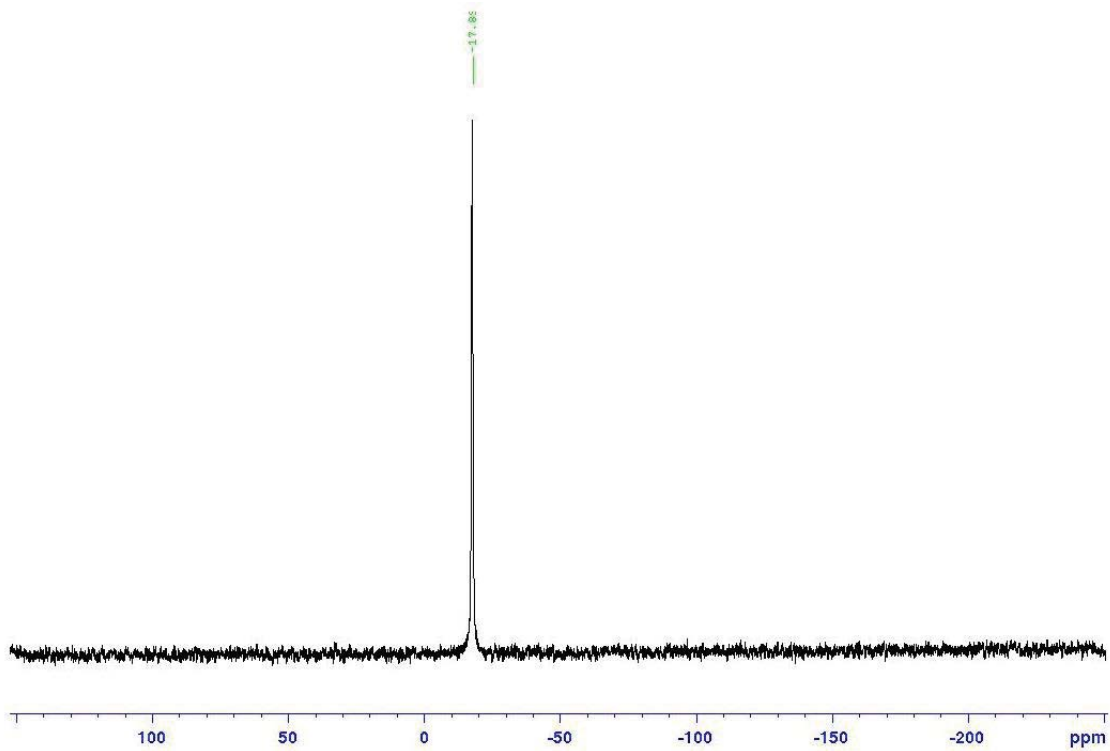


Figure A. 1. ^{31}P NMR spectrum of **5** in CDCl_3 (300 MHz).

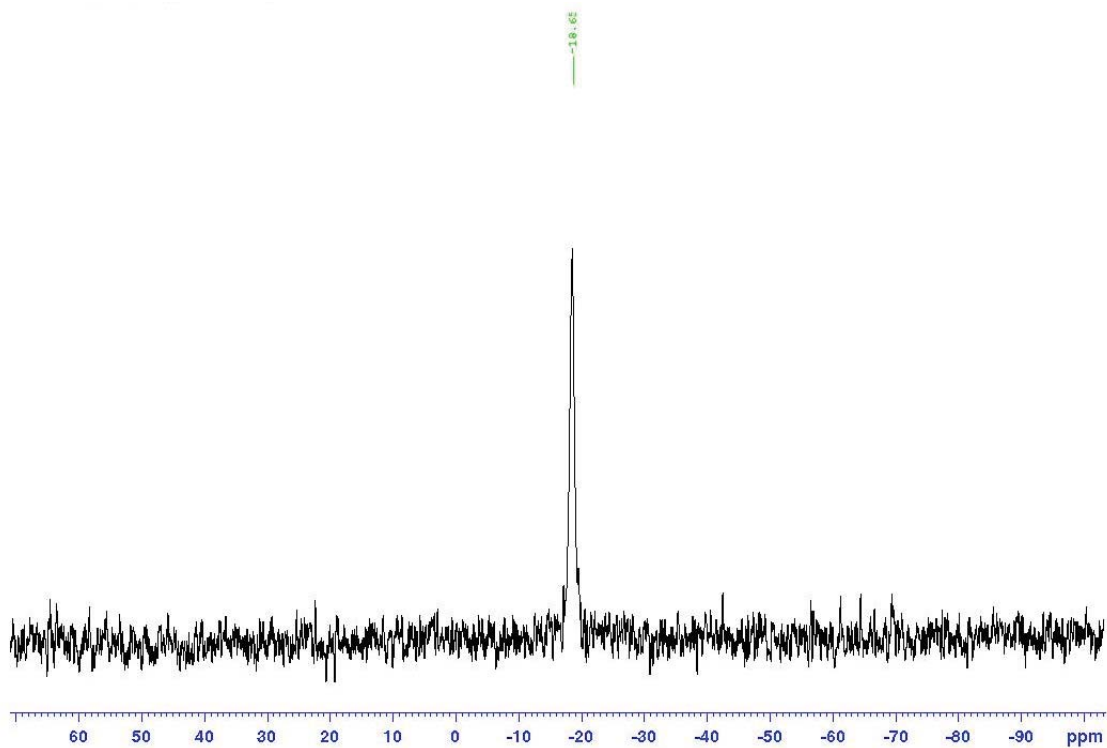


Figure A. 2. ^{31}P NMR spectrum of **6** in CDCl_3 (300 MHz).

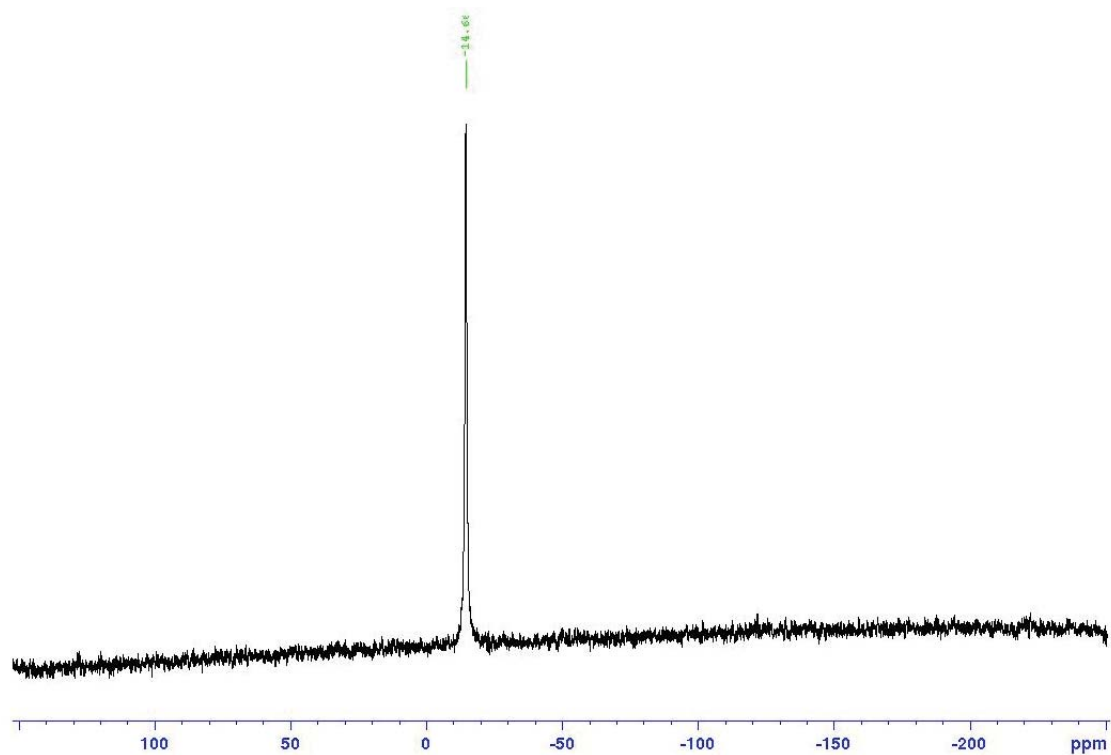


Figure A. 3. ^{31}P NMR spectrum of **1** in CDCl_3 (300 MHz).

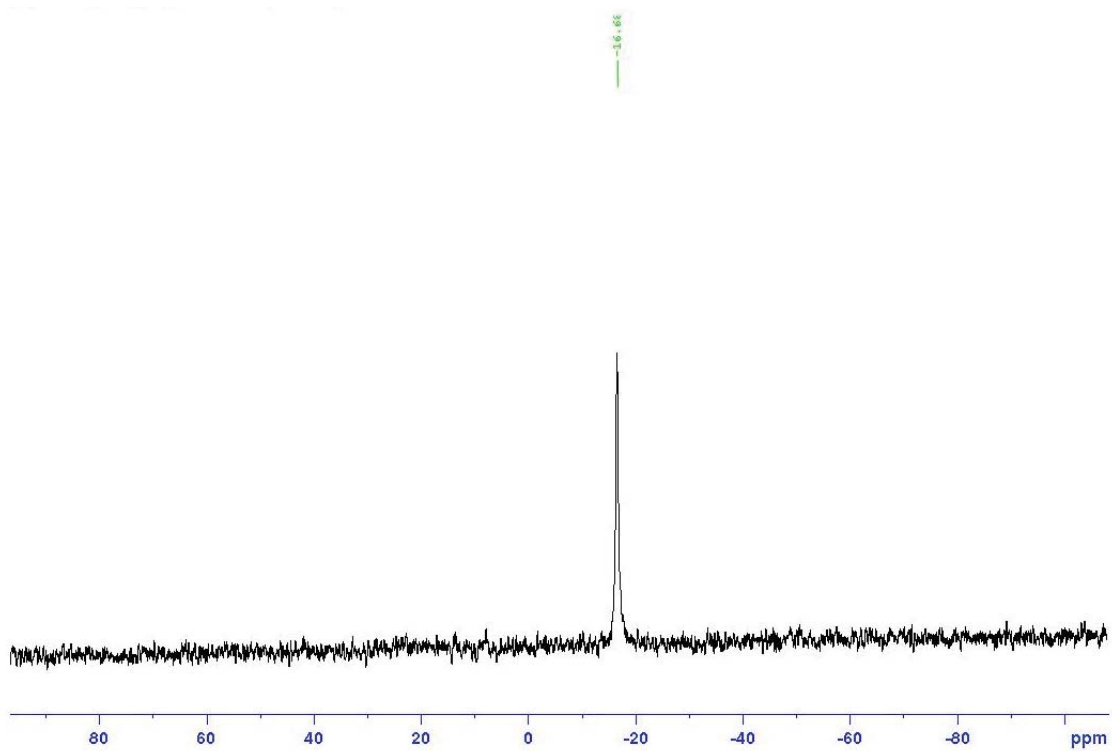


Figure A. 4. ^{31}P NMR spectrum of **2** in CDCl_3 (300 MHz).

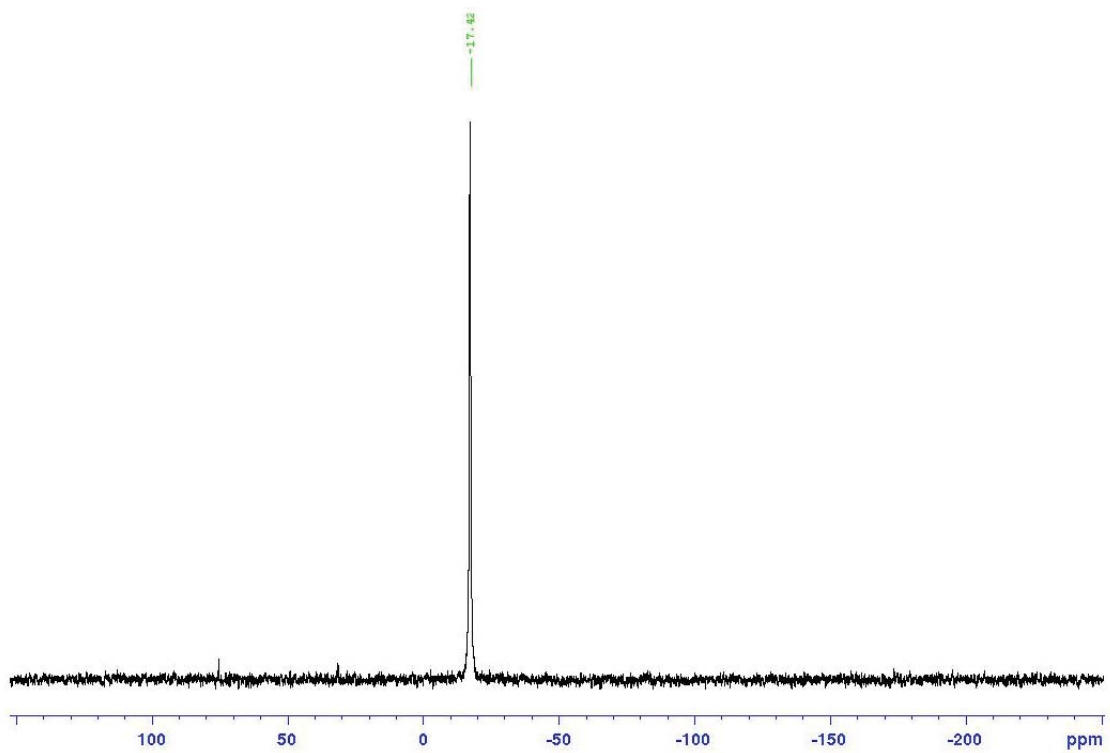


Figure A. 5. ^{31}P NMR spectrum of **3** in CDCl_3 (300 MHz).

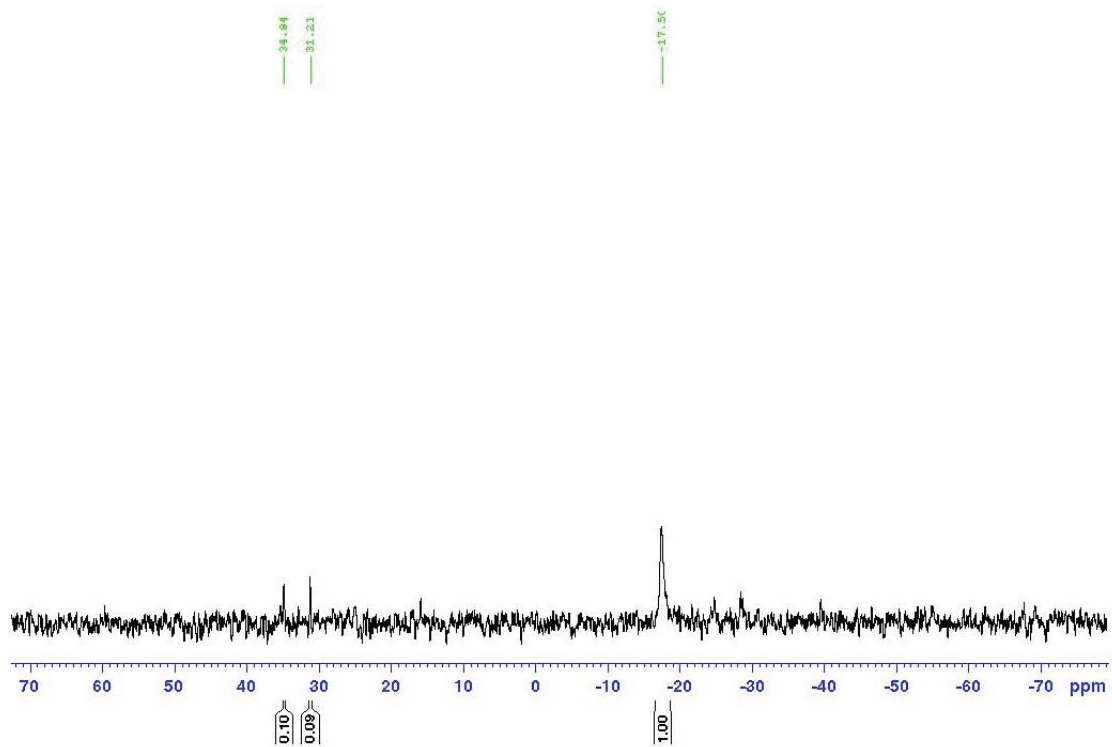


Figure A. 6. ^{31}P NMR spectrum of 4 in CDCl_3 (300 MHz).

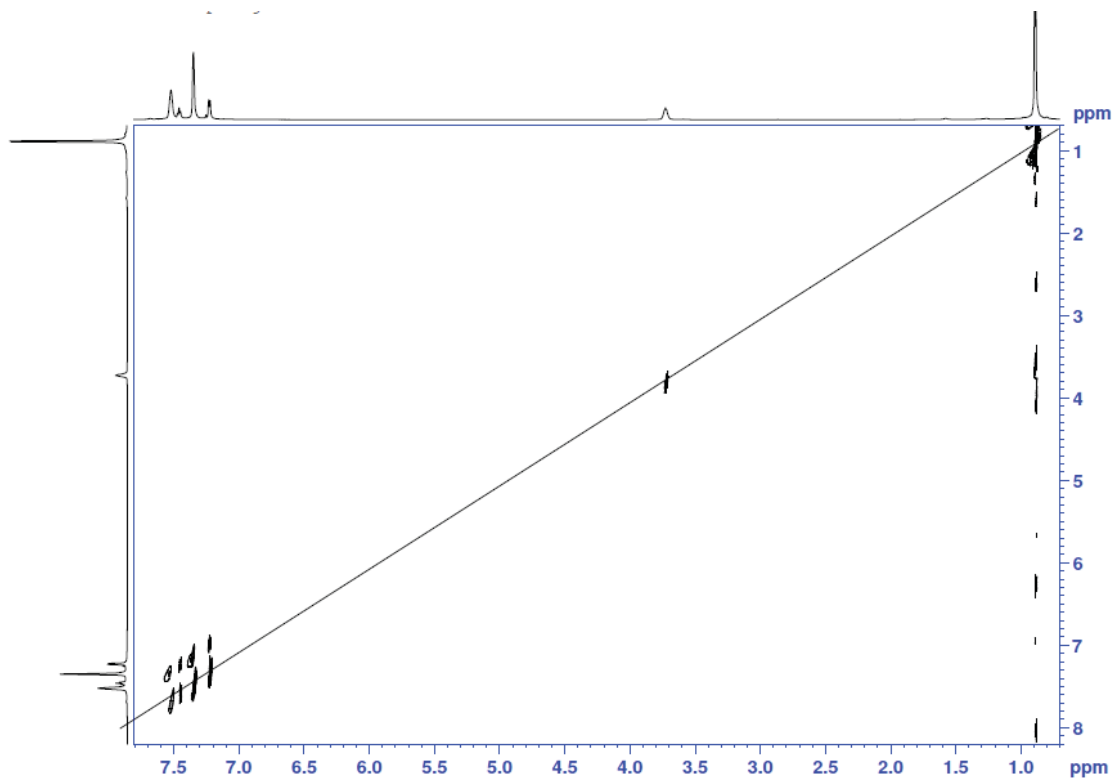


Figure A. 7. 2D COSY NMR spectrum of **1** in CDCl₃ (700 MHz).

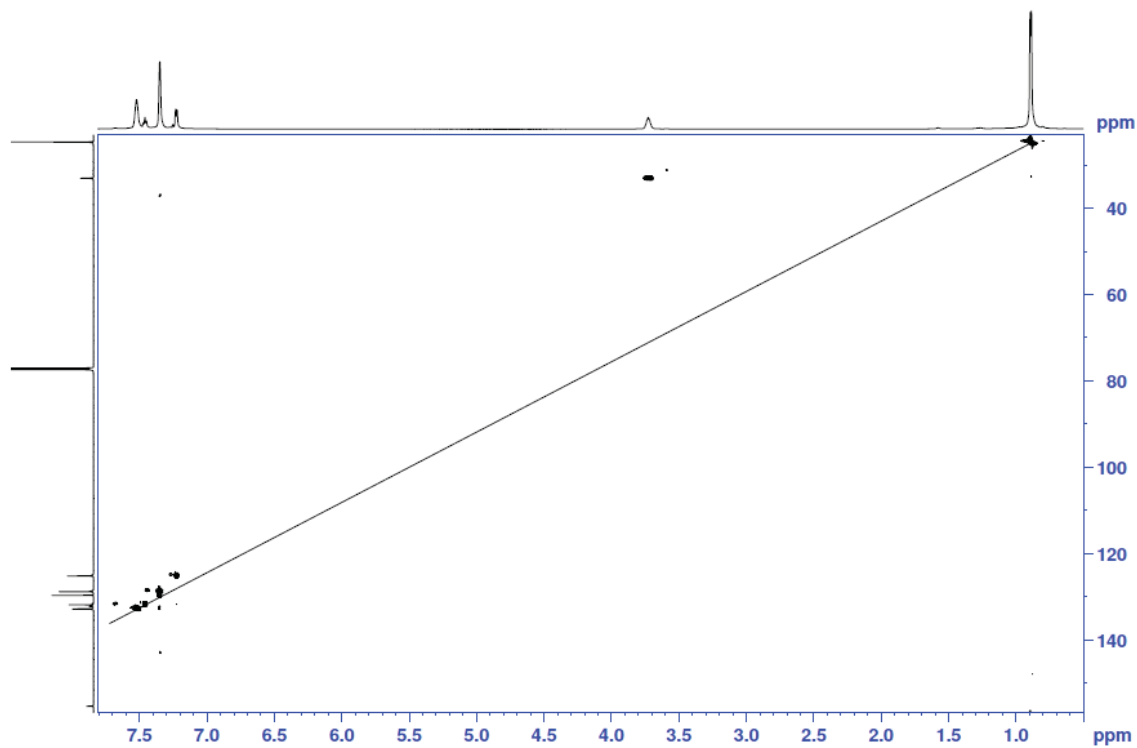


Figure A. 8. 2D HSQC NMR spectrum of **1** in CDCl₃ (700 MHz).

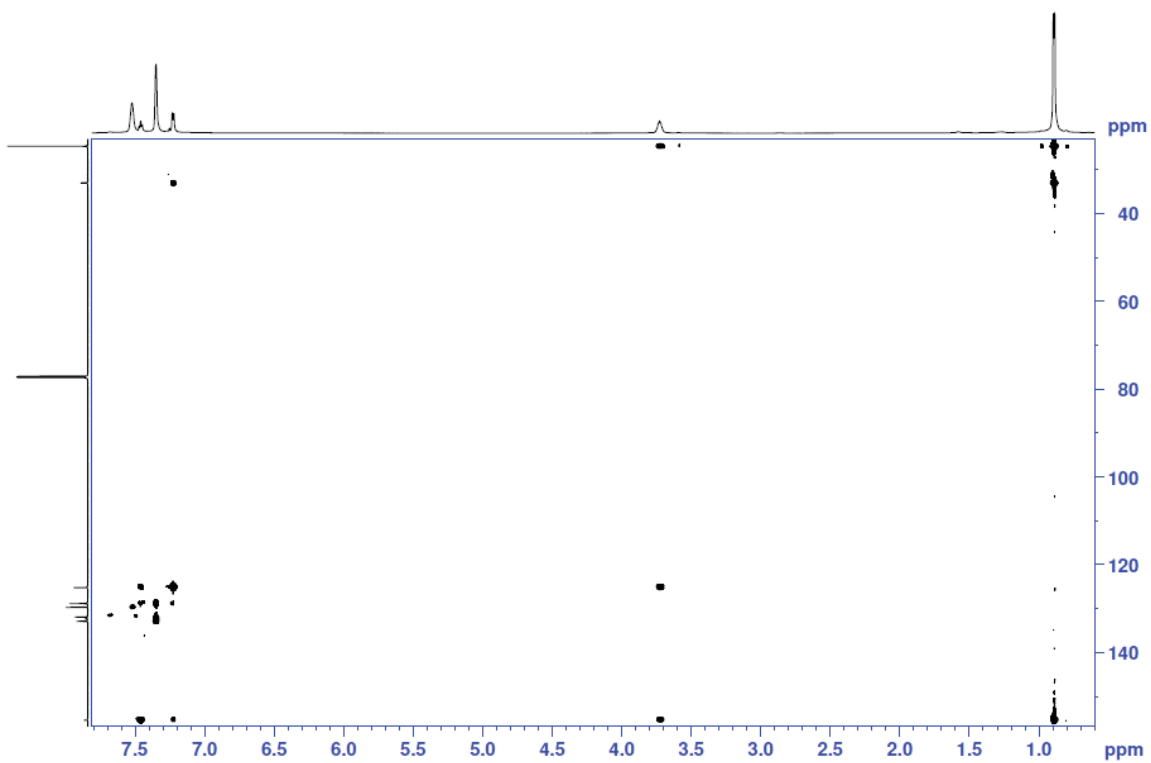


Figure A. 9. 2D HSQC NMR spectrum of **1** in CDCl₃ (700 MHz).

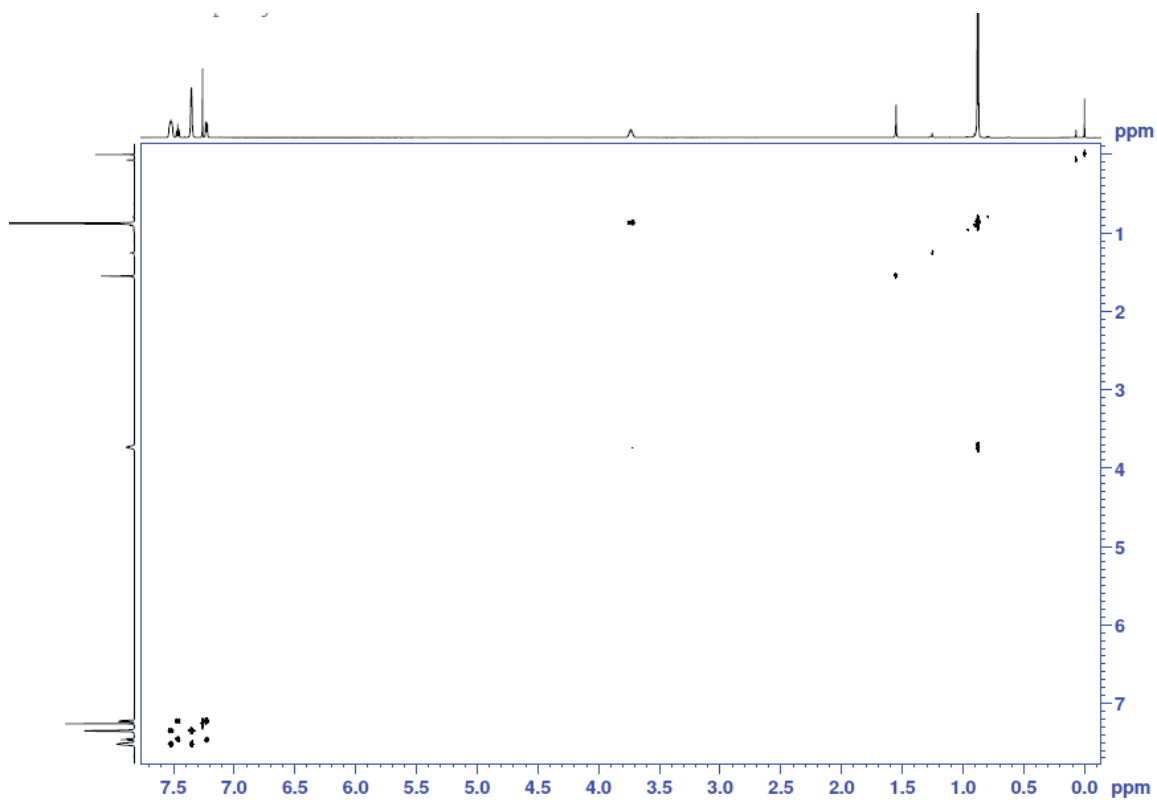


Figure A. 10. 2D COSY NMR spectrum of **2** in CDCl₃ (700 MHz).

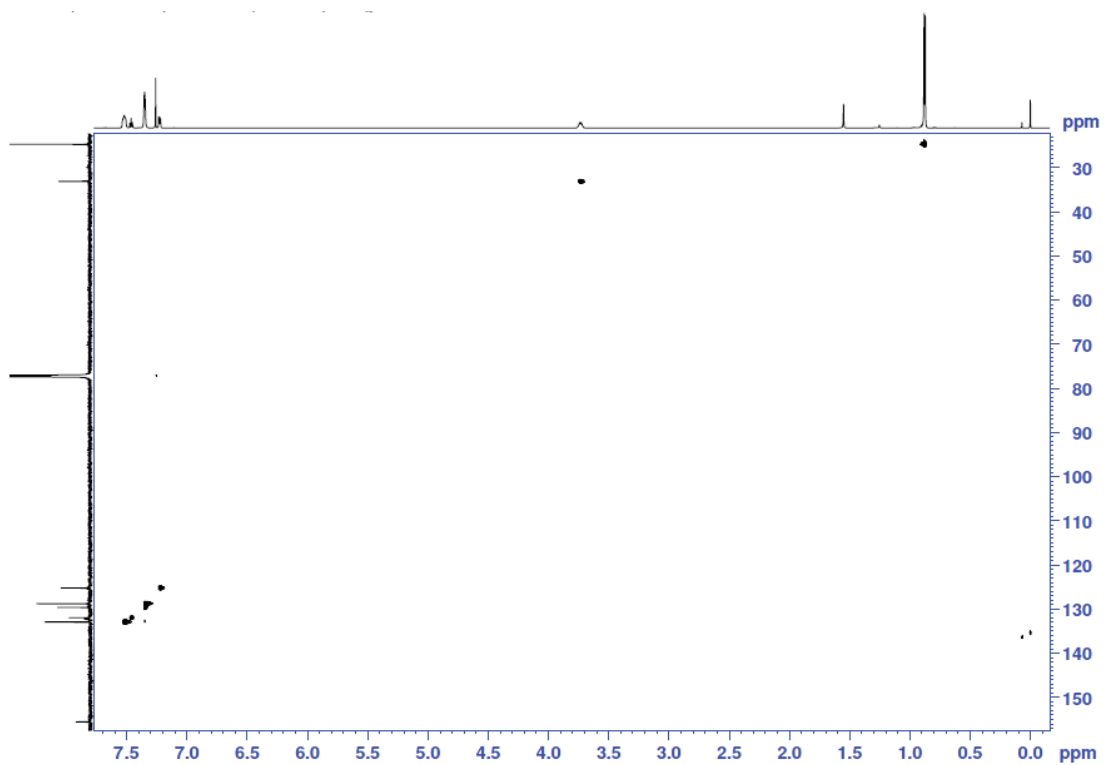


Figure A. 11. 2D HSQC NMR spectrum of **2** in CDCl_3 (700 MHz).

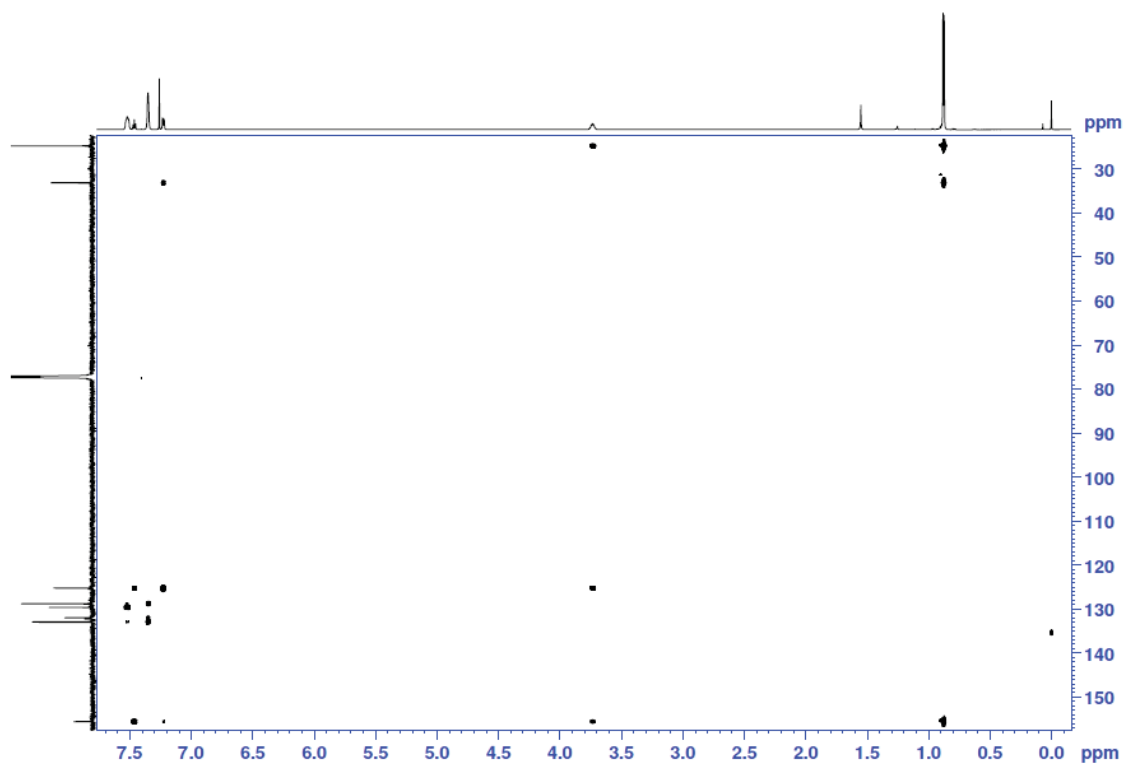


Figure A. 12. 2D HMBC NMR spectrum of **2** in CDCl_3 (700 MHz).

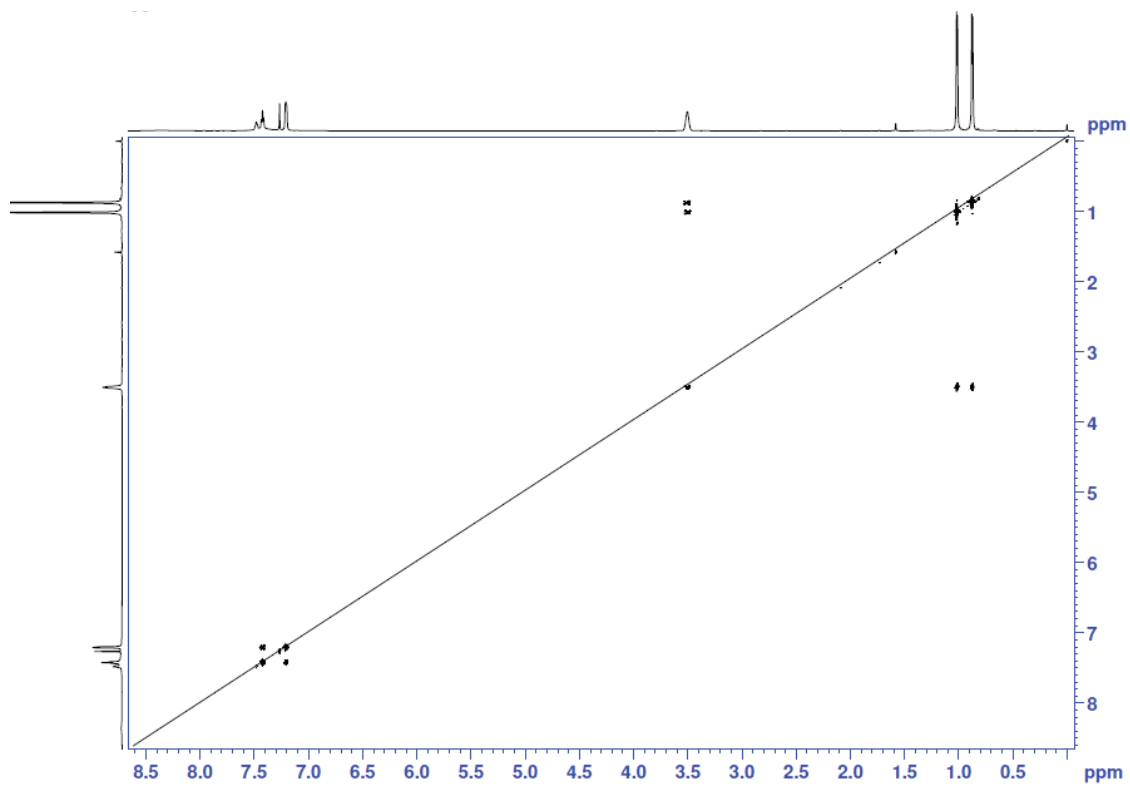


Figure A. 13. 2D COSY NMR spectrum of **3** in CDCl_3 (700 MHz).

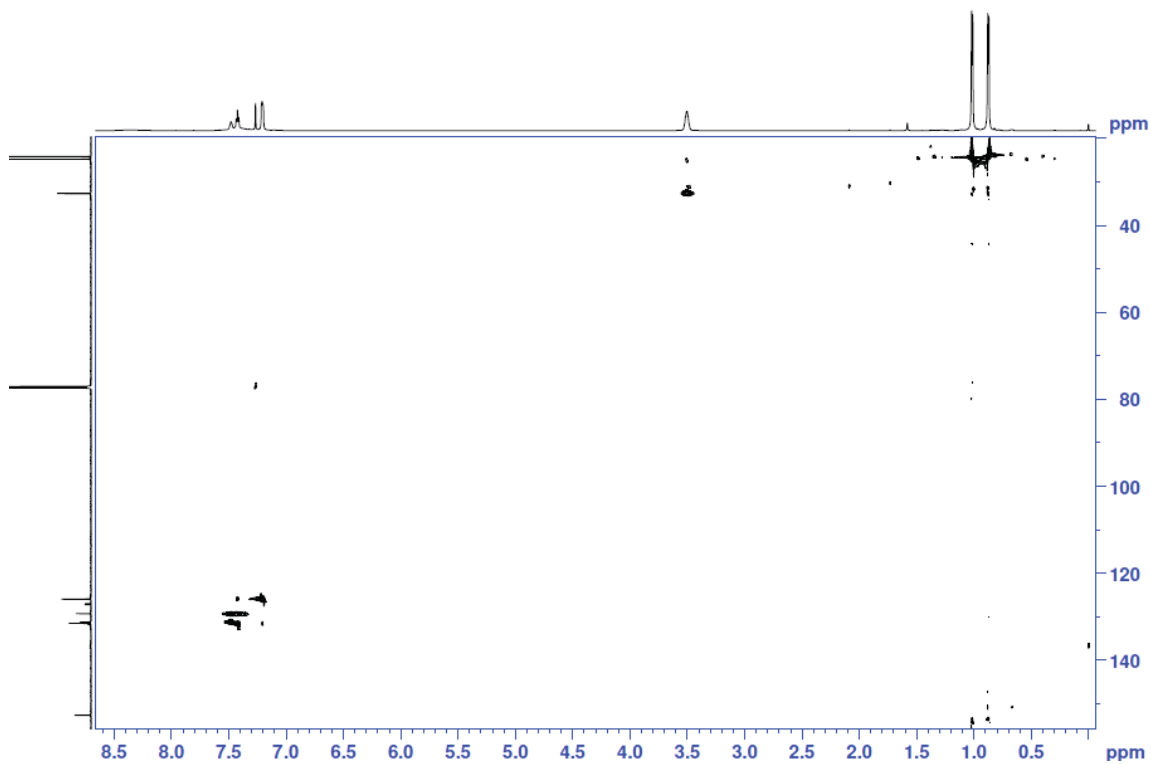


Figure A. 14. 2D HSQC NMR spectrum of **3** in CDCl_3 (700 MHz).

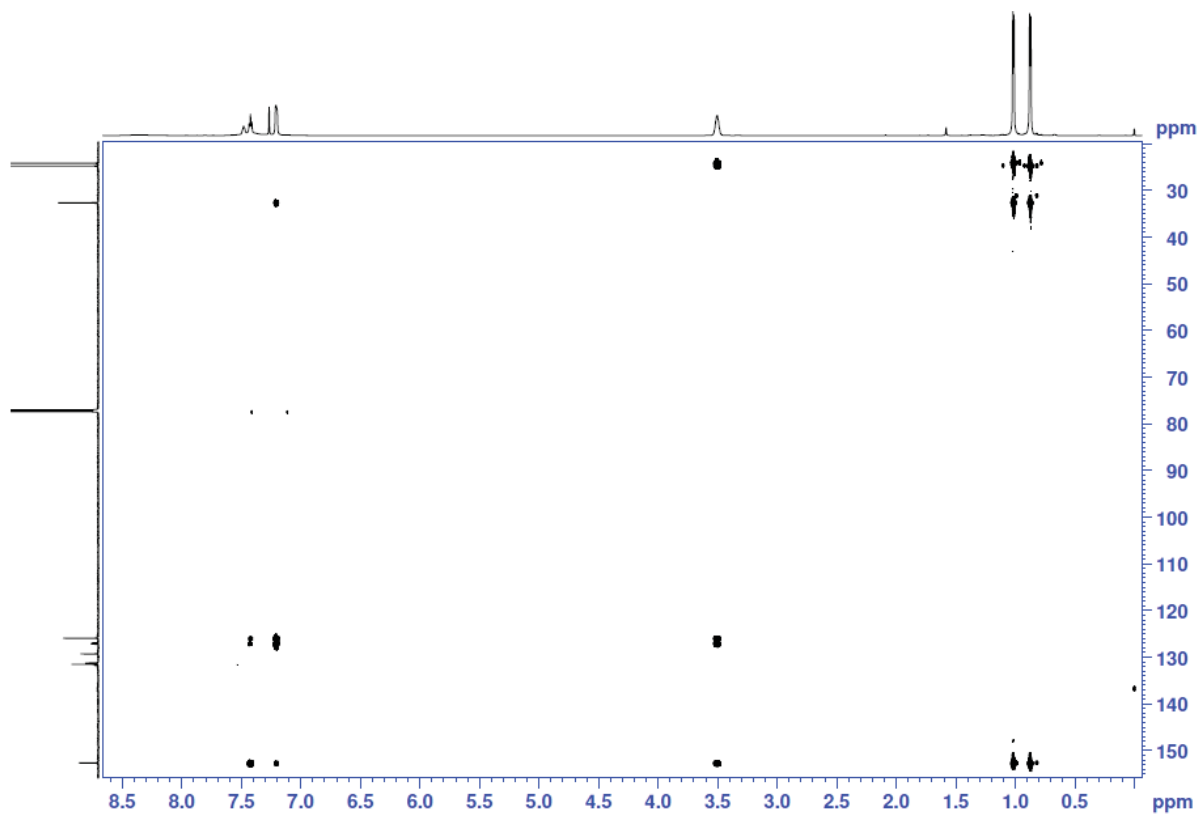


Figure A. 15. 2D HMBC NMR spectrum of **3** in CDCl_3 (700 MHz).

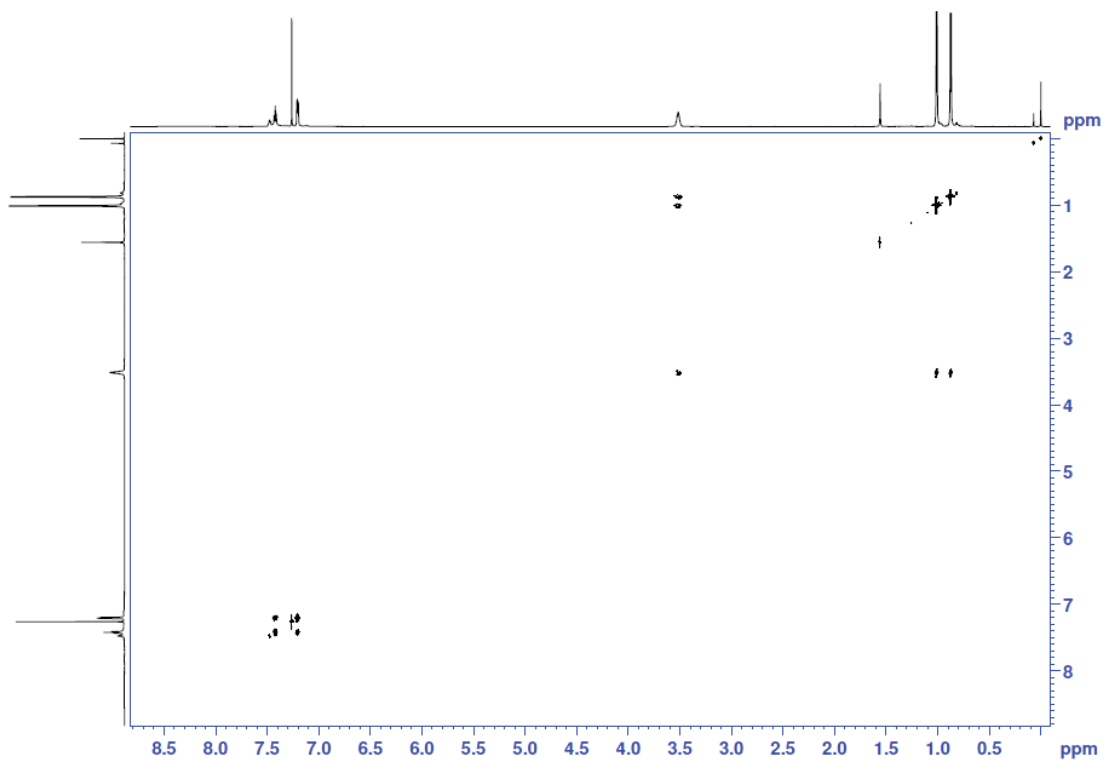


Figure A. 16. 2D COSY NMR spectrum of **4** in CDCl_3 (700 MHz).

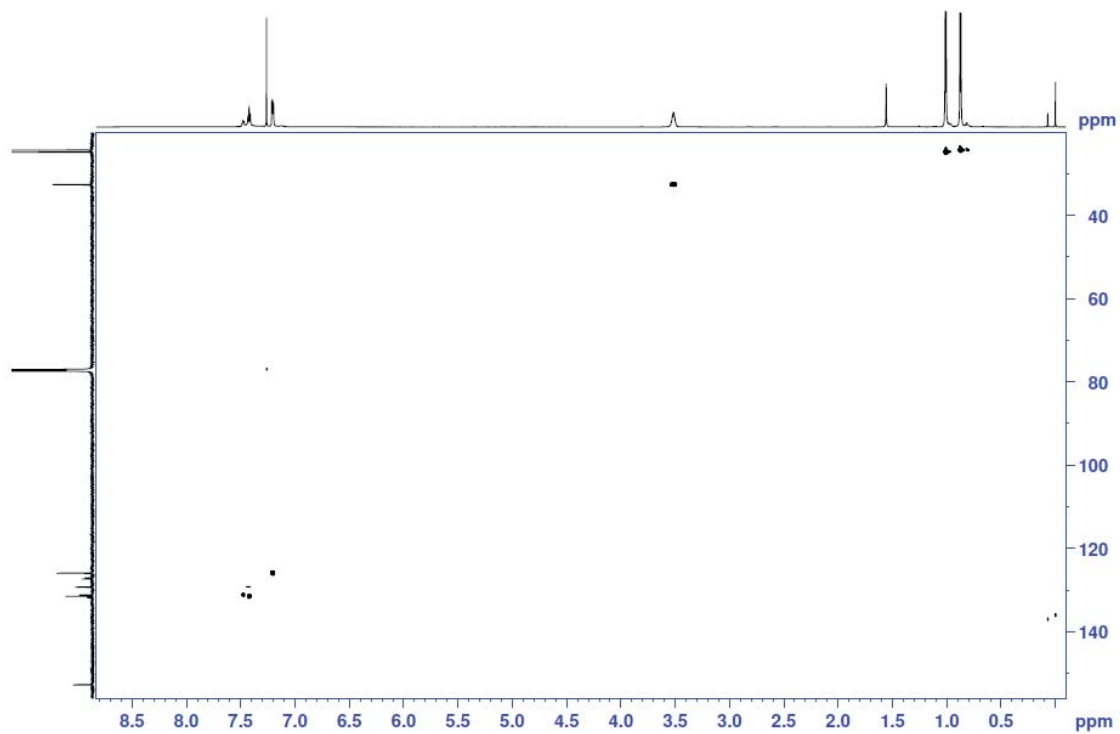


Figure A. 17. 2D HSQC NMR spectrum of **4** in CDCl_3 (700 MHz).

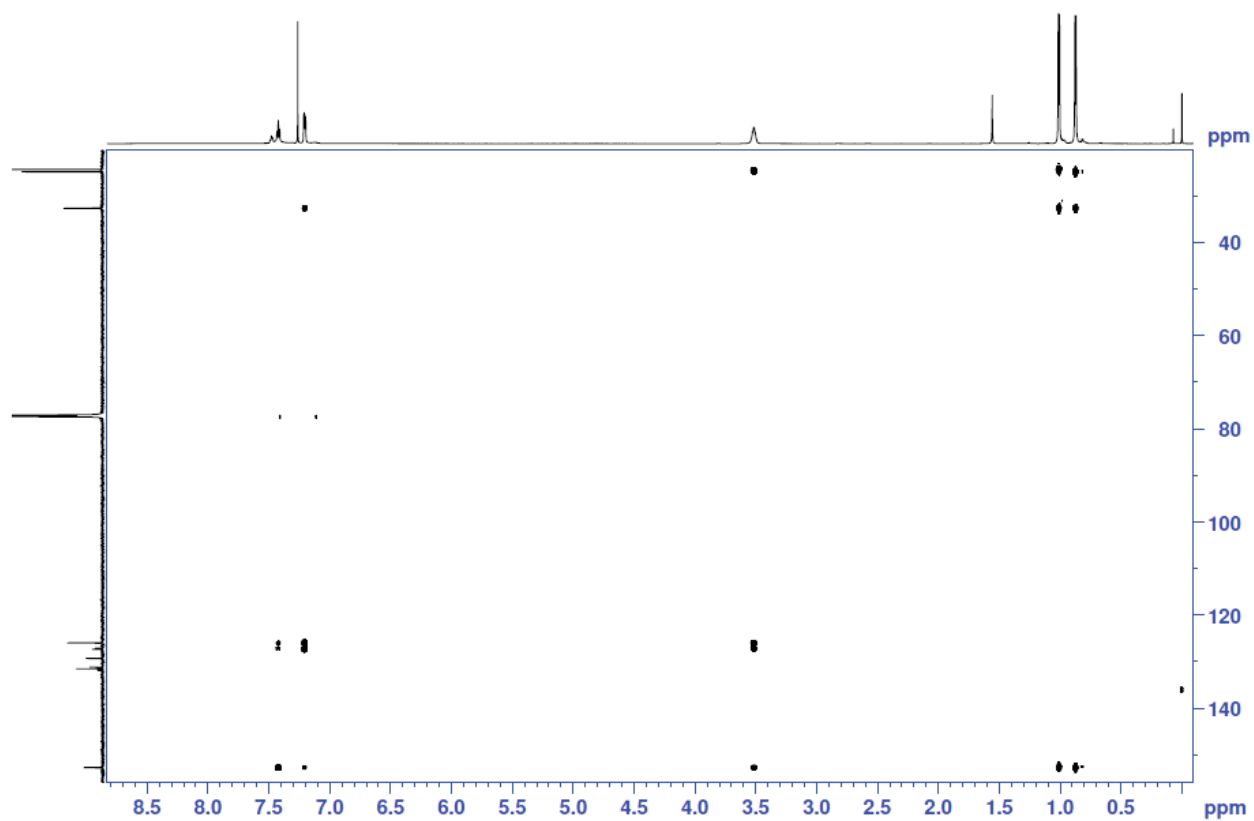


Figure A. 18. 2D HMBC NMR spectrum of **4** in CDCl_3 (700 MHz).

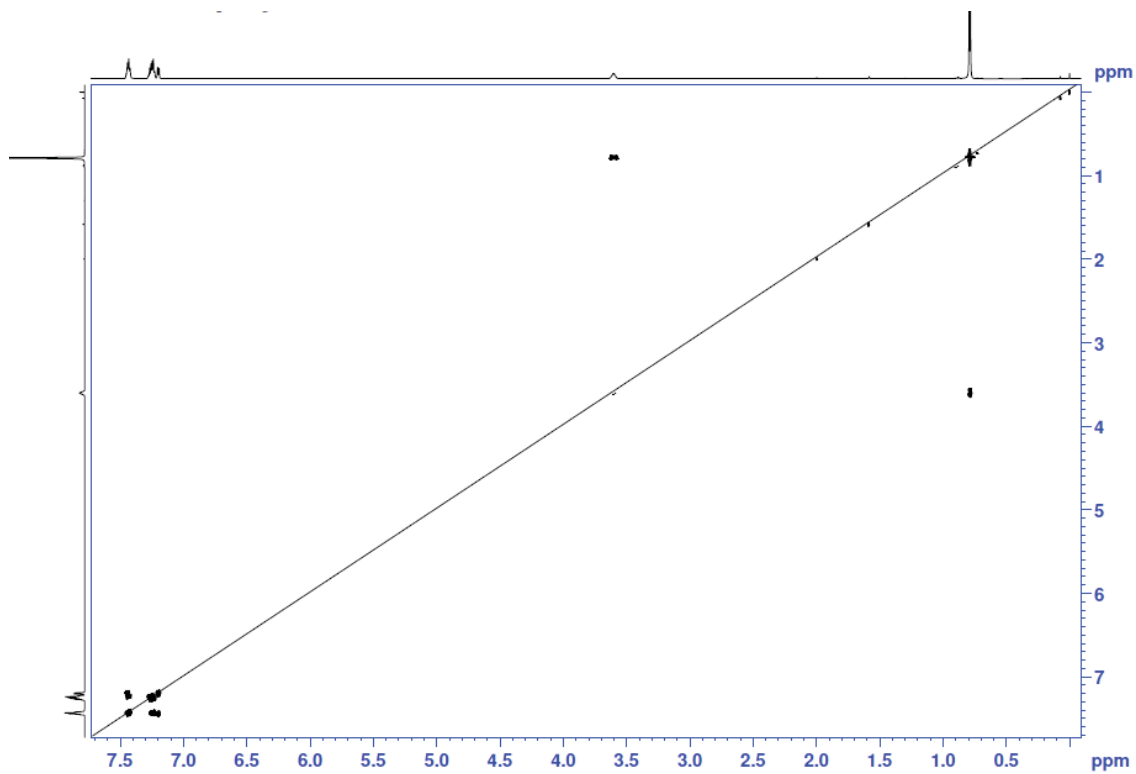


Figure A. 19. 2D COSY NMR spectrum of **5** and **6** in CDCl_3 (700 MHz).

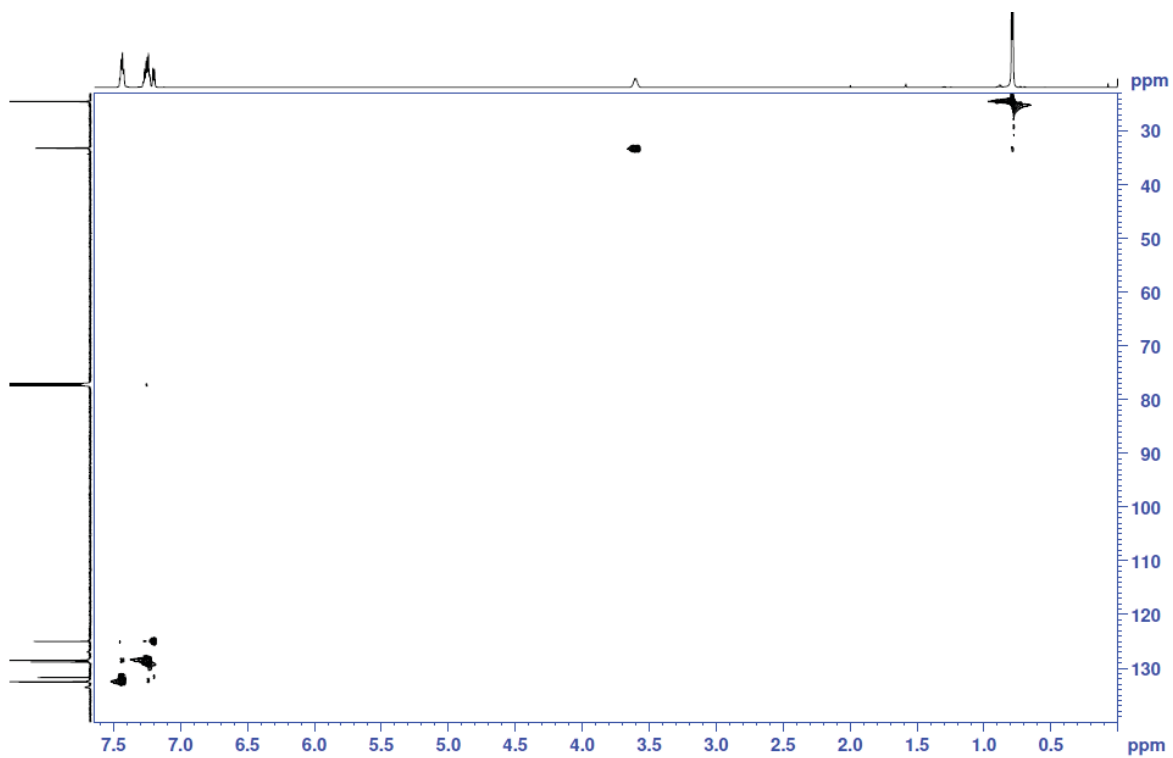


Figure A. 20. 2D HSQC NMR spectrum of **5** and **6** in CDCl_3 (700 MHz).

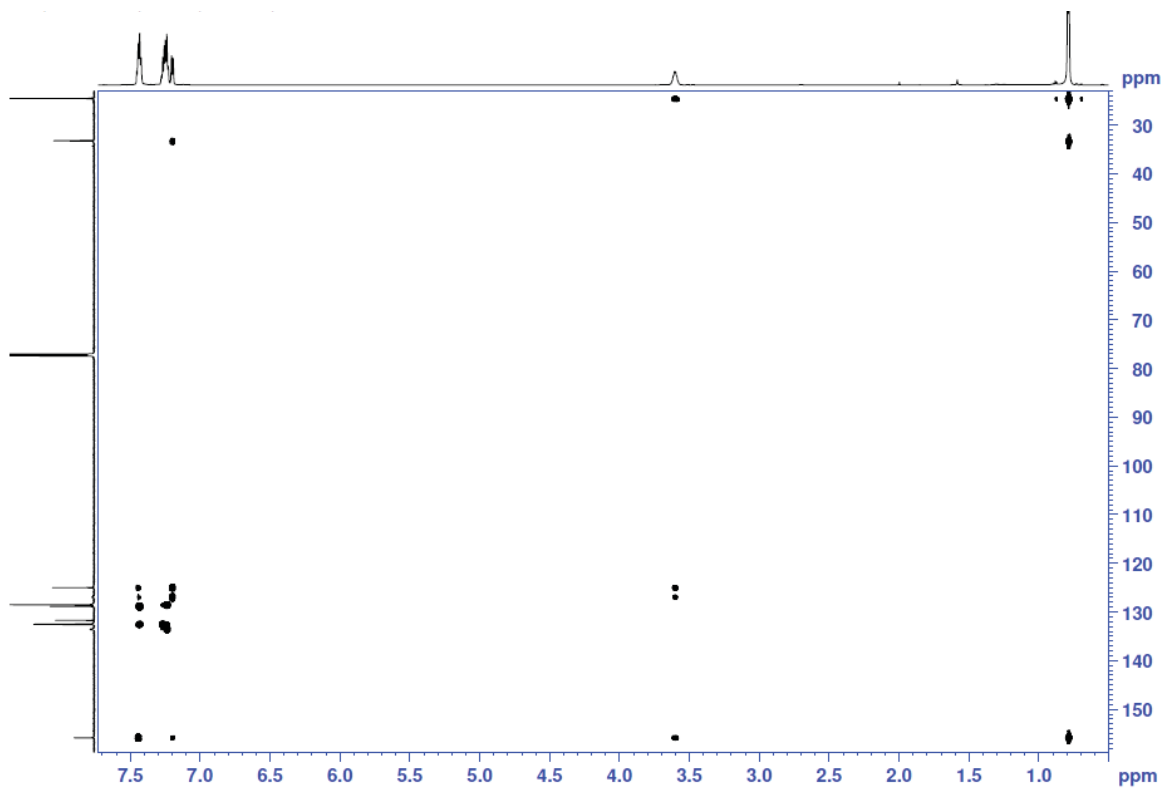


Figure A. 21. 2D HMBC NMR spectrum of **5** and **6** in CDCl_3 (700 MHz).

Table A.1. The change in free energy of copper-phosphine complexes

Molecule	Free Energy, G (kJ/mol)	$\Delta_r G$ (kJ/mol): (product-reactant)
[(DippPh ₂) ₂ CuCl], [5]	-12193709.86	48.25405715
[a] + [c]	-12193758.12	
½ [1] + [a]	-12193709.86	54.45154895
[5]	-12193764.32	
[(DippPh ₂) ₂ PCuBr], [6]	-17737584.7	15.33291766
[a] + [d]	-17737600.03	
½ [2] + [a]	-17737584.7	41.71918864
[6]	-17737626.42	
½ [DippPh ₂ PCuCl] ₂ , [1]	-8854516.395	-6.197491804
[c]	-8854510.198	
½ [DippPh ₂ PCuBr] ₂ , [2]	-14398378.5	-26.38627098
[d]	-14398352.11	
½ [Dipp ₂ PhPCuCl] ₂ , [3]	-9473397.012	4.371456834
[e]	-9473401.383	
½ [Dipp ₂ PhPCuBr] ₂ , [4]	-15017274.96	-23.36169544
[f]	-15017251.6	

[a] = DippPh₂P, [b] = Dipp₂PhP, [c] = DippPh₂PCuCl, [d] = DippPh₂PCuBr,
[e] = Dipp₂PhPCuCl, [f] = Dipp₂PhPCuBr

Table A. 2. Selected short contacts in the complexes

Complex	Atom1	Atom2	Length(Å)	Length-VdW(Å)
1	Cu1	H7	2.429	-0.171
1a	Cu1	H7	2.098	-0.502
2a	Cu1	H7	2.354	-0.246
3	Cu1	H19	2.456	-0.144
	Cl1	H19	2.844	-0.106
3a	Cu1	H19	2.564	-0.036
4a	Cu1	H7	2.545	-0.055
4b	Cu1	H7	2.438	-0.162
4b'	Cu2	H37	2.367	-0.233
	Cu3	H67	2.341	-0.259
5	Cu1	H7	2.298	-0.302
6	Cu1	H7	2.271	-0.329

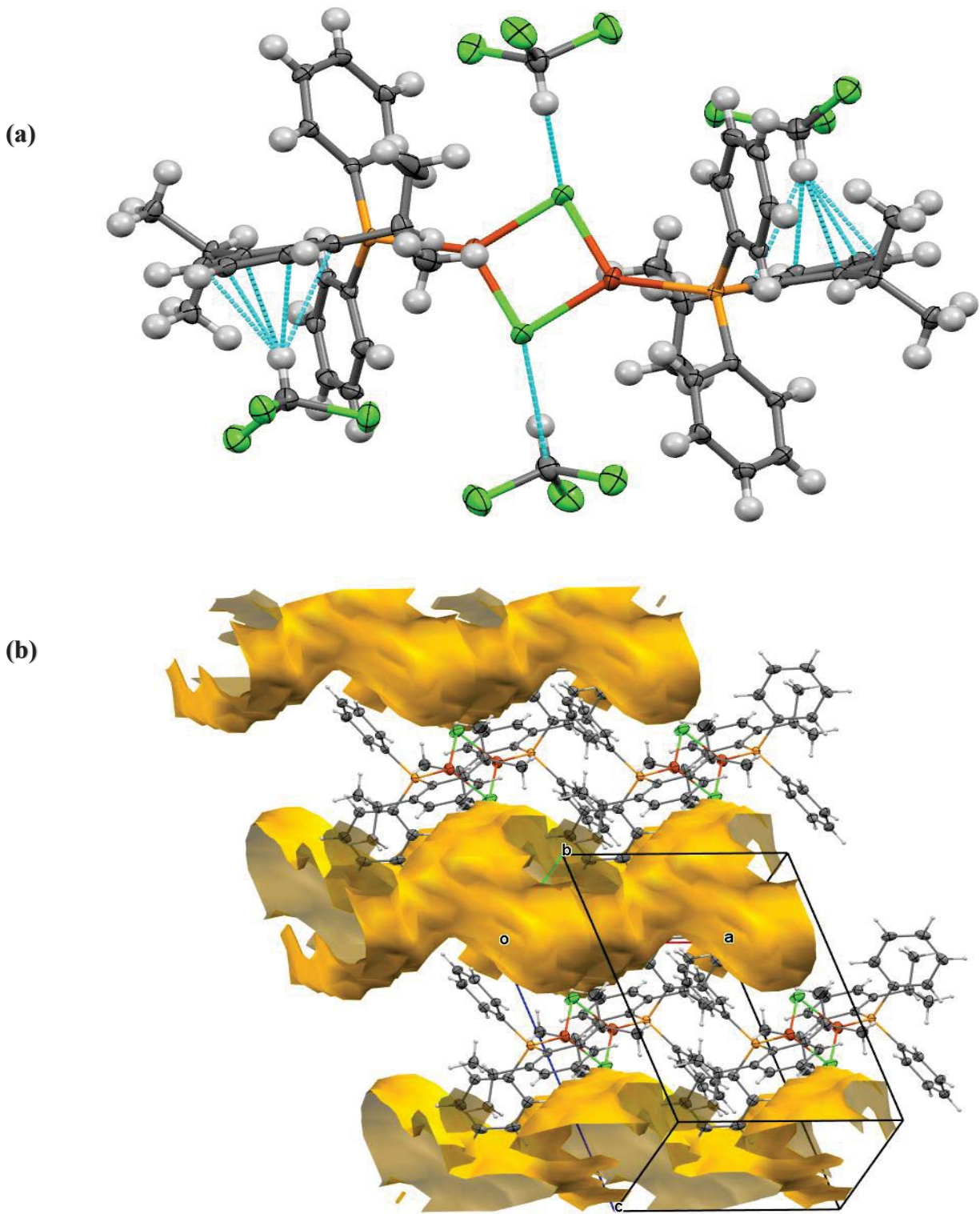


Figure A. 22. Displacement ellipsoid plots (50%) showing the (a) intermolecular interaction and (b) packing diagram with solvent contact surface voids in **1a** after removing the solvent molecules.

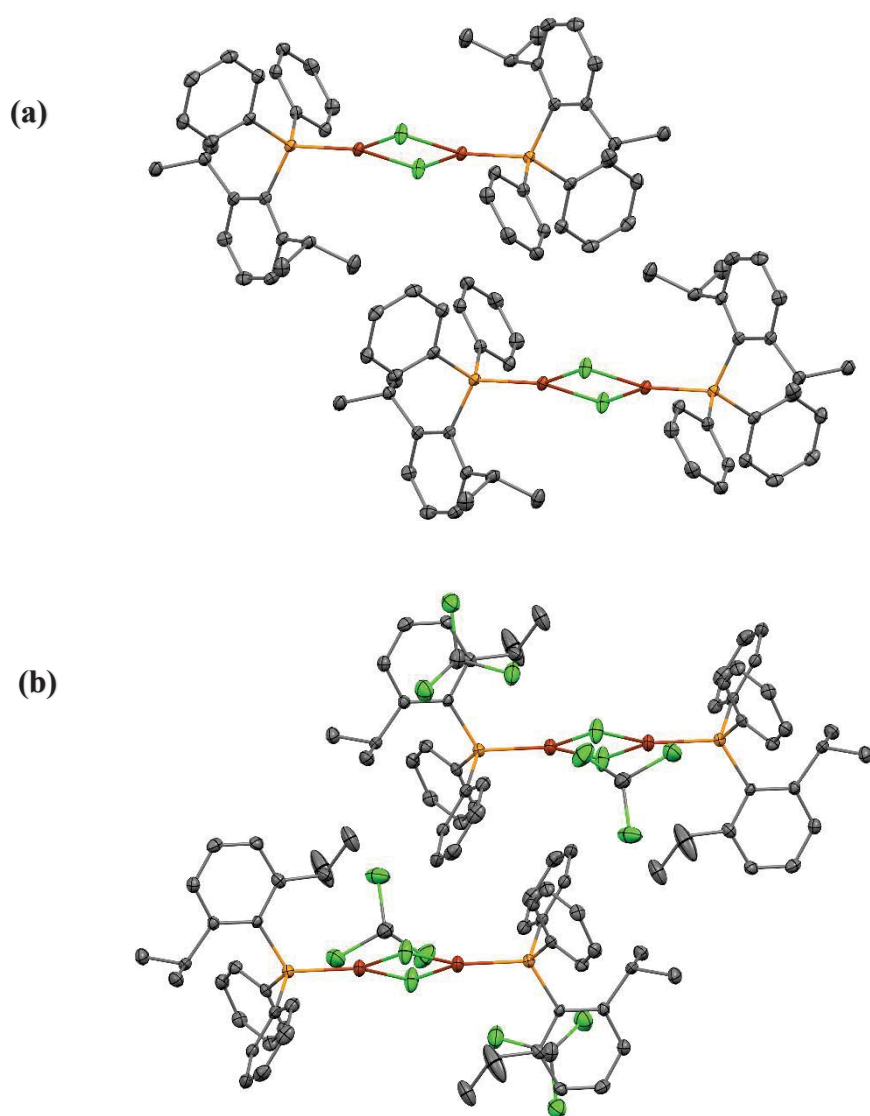


Figure A. 23. Crystal structure packing diagrams (ellipsoids drawn at 50% probability) of (a) **1** and (b) **1a**.

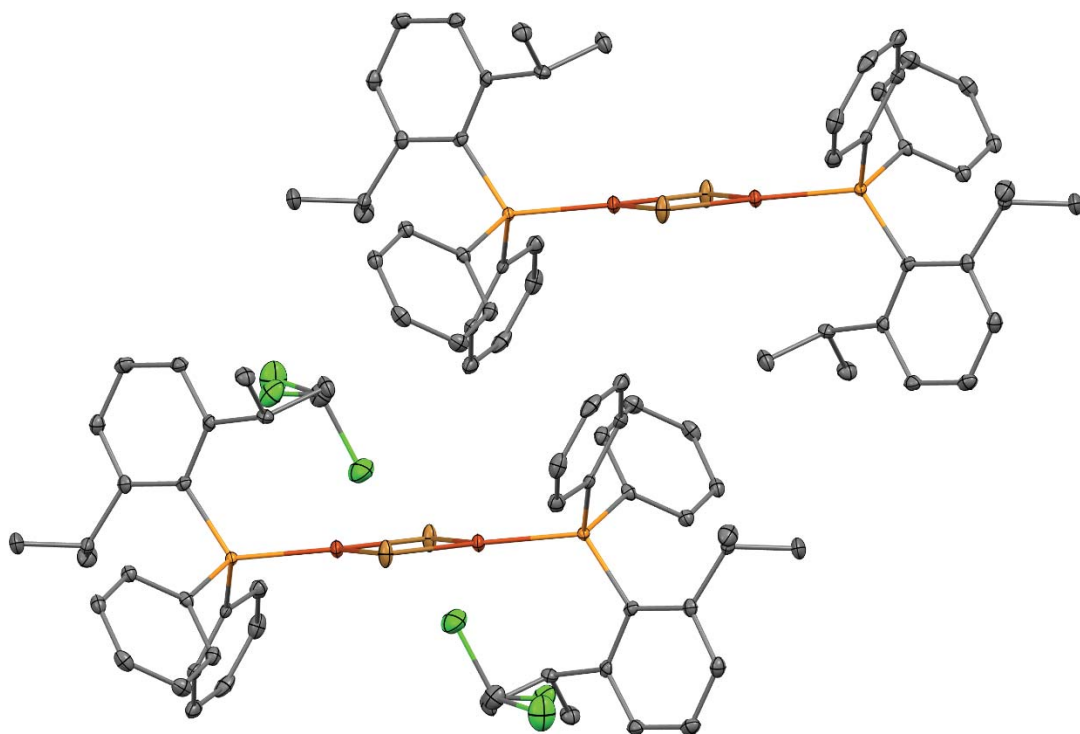


Figure A. 24. Crystal structure packing diagrams (ellipsoids drawn at 50% probability) of **2a**.

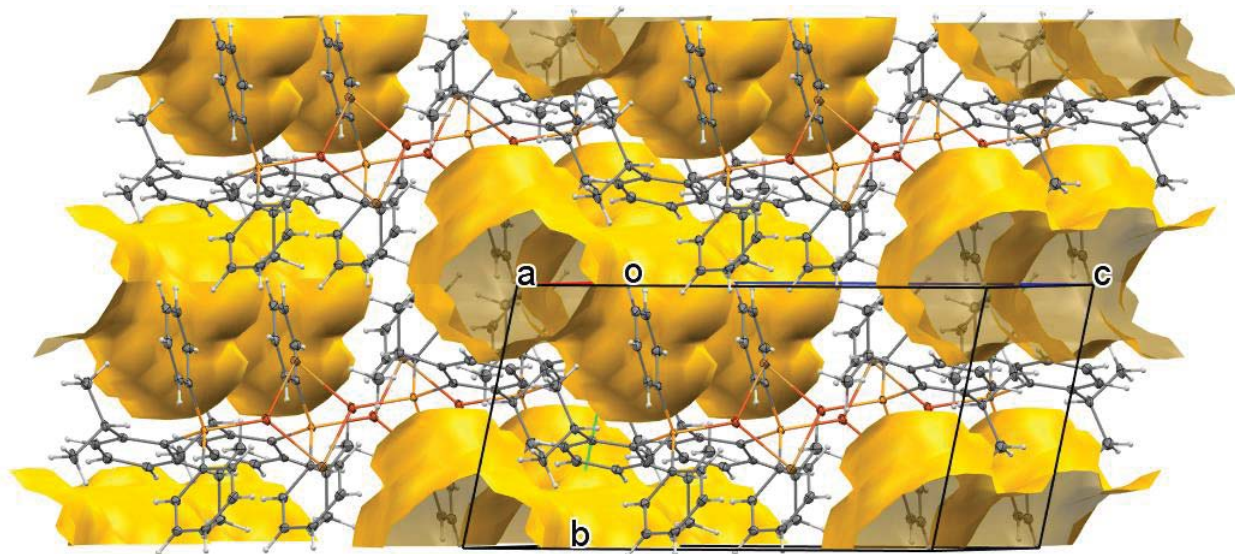


Figure A. 25. Displacement ellipsoid plots (50%) showing the structure packing diagram with solvent contact surface voids in **2a** after removing the solvent molecules.

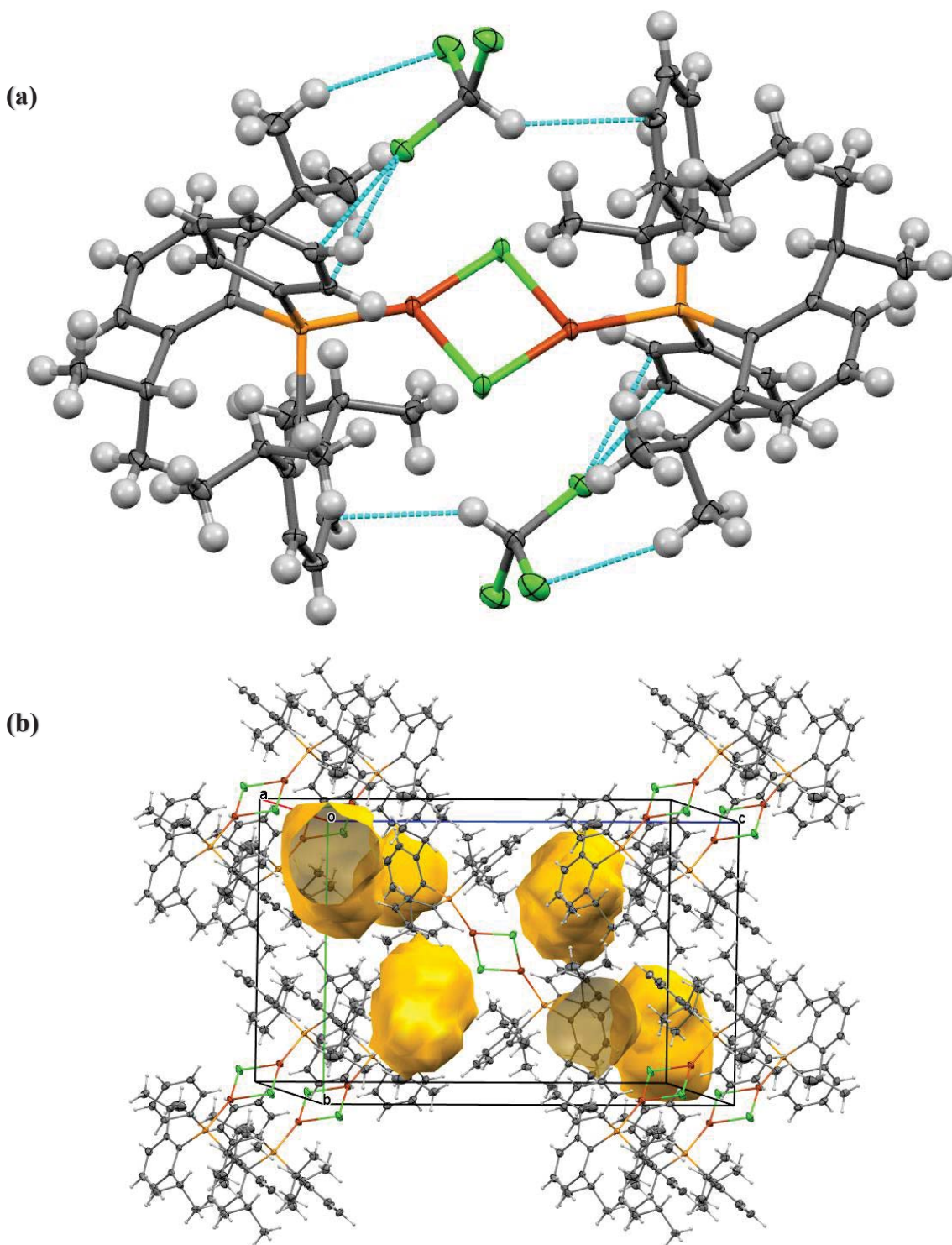


Figure A. 26. Displacement ellipsoid plots (50%) showing the (a) intermolecular interaction and (b) packing diagram with solvent contact surface voids in **3a** after removing the solvent molecules.

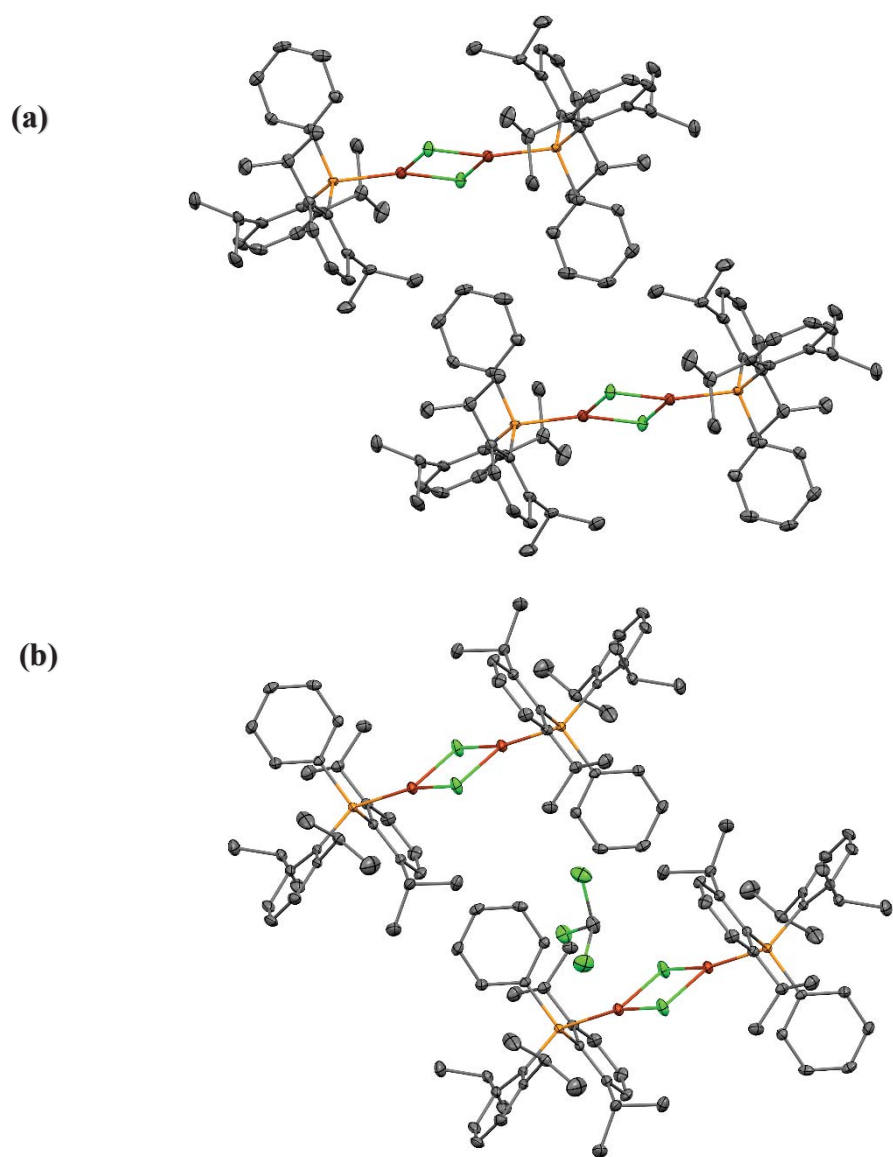


Figure A. 27. Crystal structure packing diagrams (ellipsoids drawn at 50% probability) of (a) **3** and (b) **3a**.

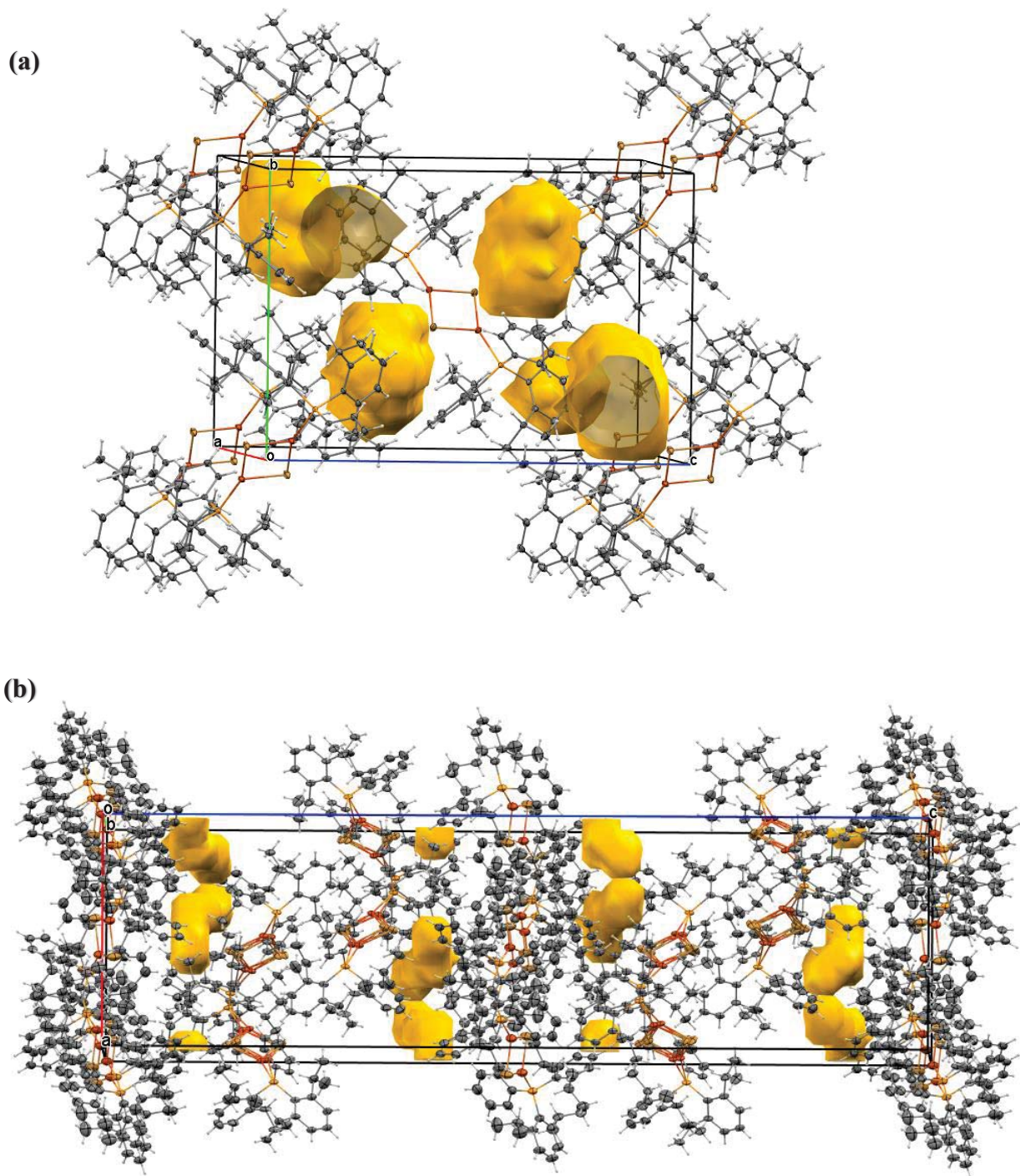


Figure A. 28. Crystal structure packing diagrams view of the solvent voids of (a) **4a** and (b) **4b** after removing the solvent molecules.

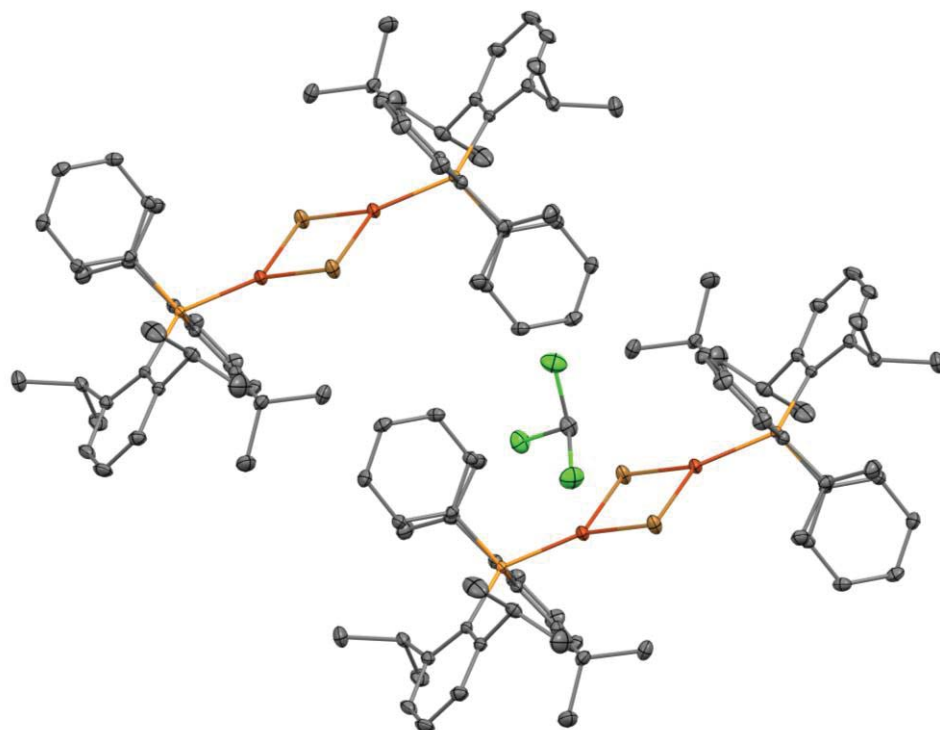


Figure A. 29. Crystal structure packing diagrams (ellipsoids drawn at 50% probability) of **4a**.

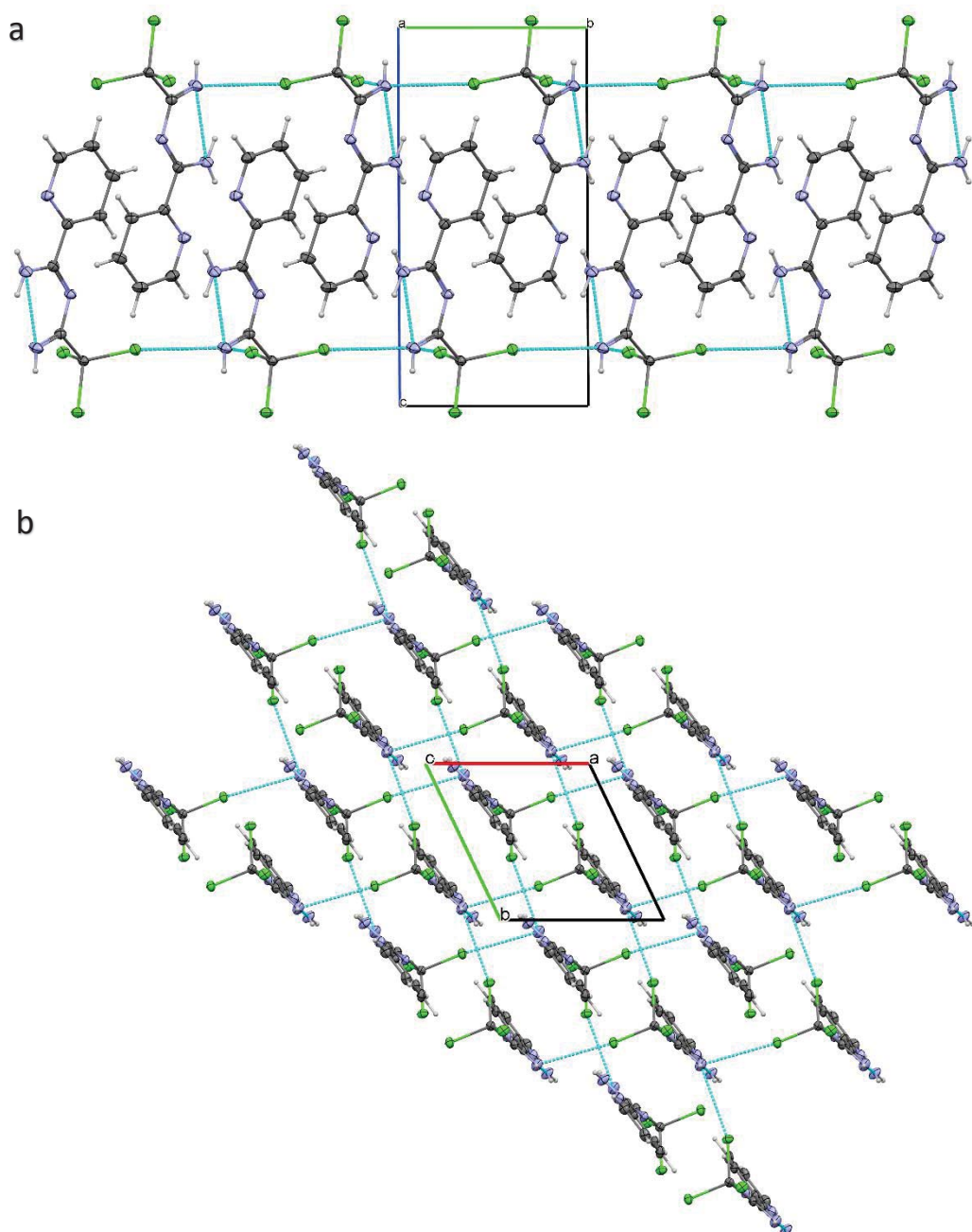


Figure A. 30. The crystal packing structure of **11** projected down (a) *a* axis and (b) *c* axis. Displacement ellipsoids drawn at the 50% probability level. Hydrogen bonding is indicated by green dashed lines.

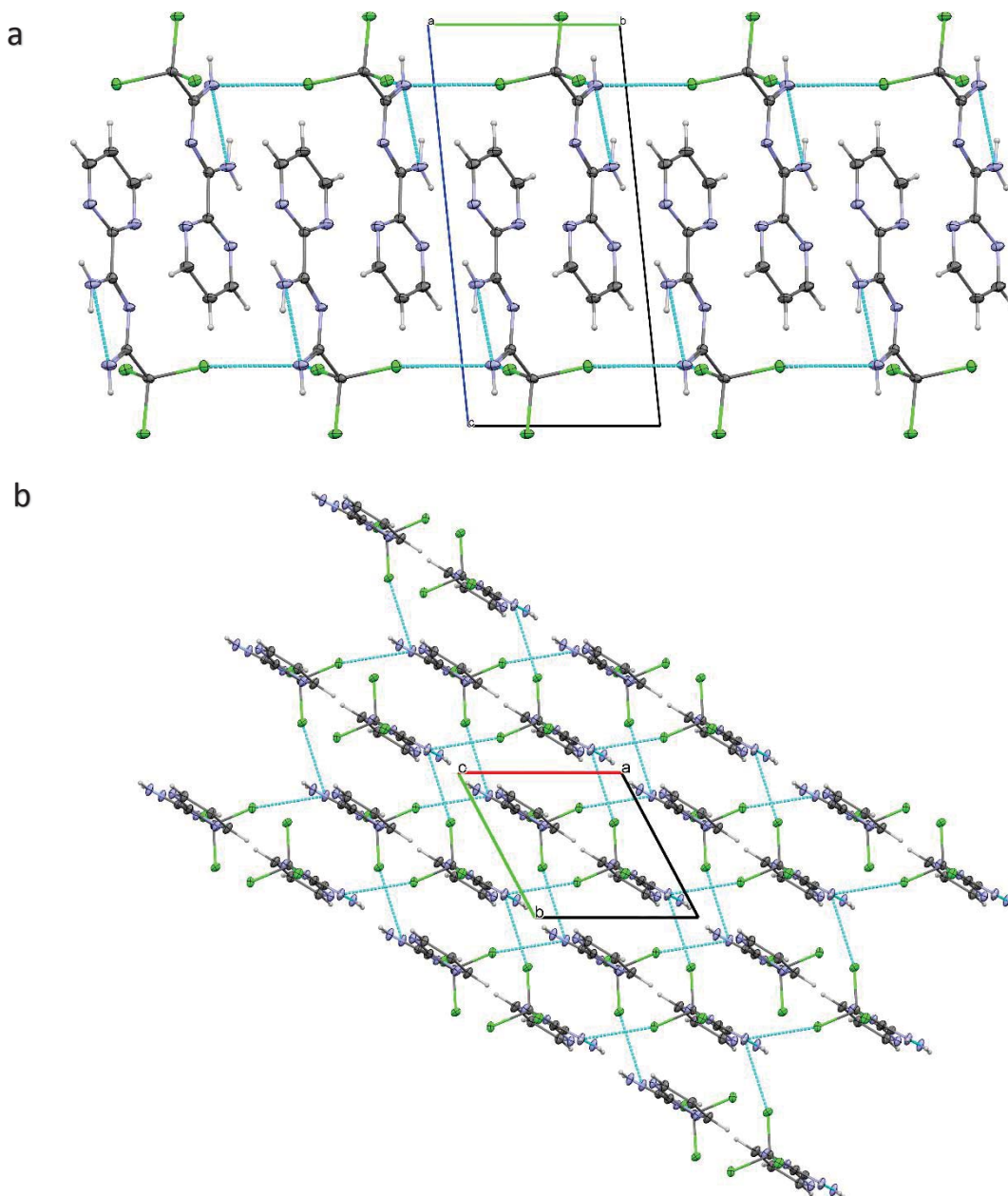


Figure A. 31. The crystal packing structure of **13** projected down (a) a axis and (b) c axis. Displacement ellipsoids drawn at the 50% probability level. Hydrogen bonding is indicated by blue dashed lines.

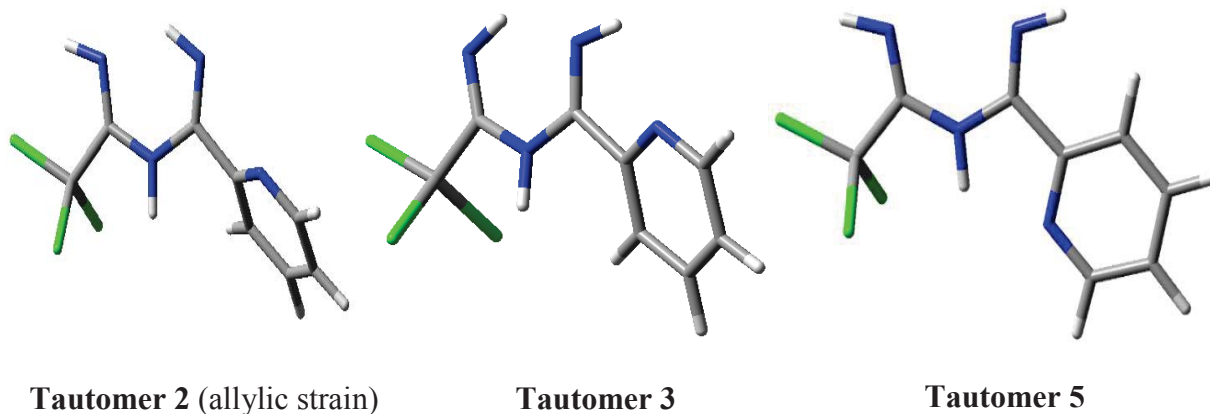


Figure A. 32. The geometries of other likely tautomers and conformers of **11** considered for only gas phase calculation.

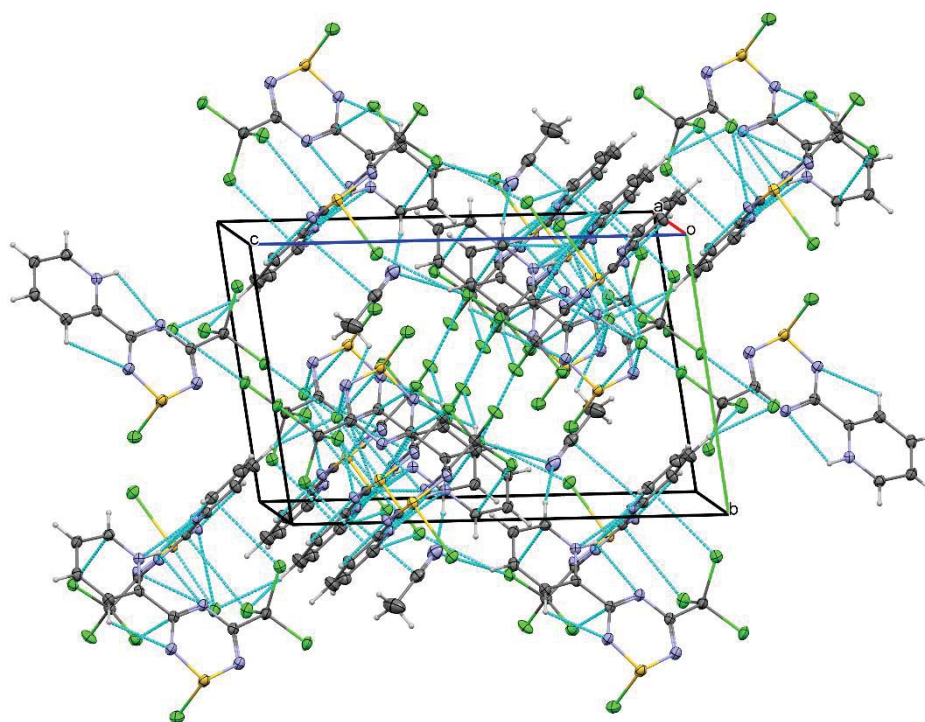


Figure A. 33. The crystal packing structure of **15–15.HCl** projected almost down *a* axis showing intermolecular contacts. Displacement ellipsoids drawn at the 50% probability level.

Table A. 3. Statistical analysis comparison of **16a** and Py2TTA=O (FOMTIK).

Bond	16a (A)	FOMTIK(B)	A	B	Δ	s.u.	s.u.	s.u.A ²	s.u.B ²	s.u.A ² - s.u.B ²	$\Delta/(s.u.A^2 - s.u.B^2)$
S1-O1	1.473(3)	1.476(4)	1.473	1.476	-0.003	0.003	0.004	0.000009	0.000016	0.005	-0.6
N1-C1	1.274(5)	1.281(7)	1.274	1.281	-0.007	0.005	0.007	0.000025	0.000049	0.008602	-0.81373
S1-N1	1.703(4)	1.677(5)	1.703	1.677	0.026	0.004	0.005	0.000016	0.000025	0.006403	4.060518
N2-S1	1.690(3)	1.674(4)	1.69	1.674	0.016	0.003	0.004	0.000009	0.000016	0.005	3.2
C2-N2	1.282(5)	1.281(7)	1.282	1.281	0.001	0.005	0.007	0.000025	0.000049	0.008602	0.116248
N3-C2	1.371(6)	1.378(7)	1.371	1.378	-0.007	0.006	0.007	0.000036	0.000049	0.00922	-0.75926
C1-N3	1.368(4)	1.411(7)	1.368	1.411	-0.043	0.004	0.007	0.000016	0.000049	0.008062	-5.33349
S1-N2-C2	119.1(3)	118.6(4)	119.1	118.6	0.5	0.3	0.4	0.09	0.16	0.5	1
N2-C2-N3	125.3(4)	124.7(5)	125.3	124.7	0.6	0.4	0.5	0.16	0.25	0.640312	0.937043
C2-N3-C1	121.0(3)	120.3(4)	121	120.3	0.7	0.3	0.4	0.09	0.16	0.5	1.4
N3-C1-N1	126.3(4)	123.0(5)	126.3	123	3.3	0.4	0.5	0.16	0.25	0.640312	5.153734
C1-N1-S1	118.2(3)	119.0(4)	118.2	119	-0.8	0.3	0.4	0.09	0.16	0.5	-1.6
N1-S1-N2	104.2(2)	103.2(2)	104.2	103.2	1	0.2	0.2	0.04	0.04	0.282843	3.535534

Table A. 4. Statistical analysis comparison of **16b** and Py2TTA=O (FOMTIK).

Bond	16a (A)	FOMTIK(B)	A	B	Δ	s.u.A	s.u.B	s.u.A²	s.u.B²	s.u.A²-s.u.B²	$\Delta/(s.u.A^2-s.u.B^2)$
S1-O1	1.471(2)	1.476(4)	1.471	1.476	-0.005	0.002	0.004	0.000004	0.000016	0.004472	-1.11803
N1-C1	1.279(3)	1.281(7)	1.279	1.281	-0.002	0.003	0.007	0.000009	0.000049	0.007616	-0.26261
S1-N1	1.707(2)	1.677(5)	1.707	1.677	0.03	0.002	0.005	0.000004	0.000025	0.005385	5.57086
N2-S1	1.688(2)	1.674(4)	1.688	1.674	0.014	0.002	0.004	0.000004	0.000016	0.004472	3.130495
C2-N2	1.287(3)	1.281(7)	1.287	1.281	0.006	0.003	0.007	0.000009	0.000049	0.007616	0.787839
N3-C2	1.368(3)	1.378(7)	1.368	1.378	-0.01	0.003	0.007	0.000009	0.000049	0.007616	-1.31306
C1-N3	1.364(3)	1.411(7)	1.364	1.411	-0.047	0.003	0.007	0.000009	0.000049	0.007616	-6.1714
S1-N2-C2	119.2(2)	118.6(4)	119.2	118.6	0.6	0.2	0.4	0.04	0.16	0.447214	1.341641
N2-C2-N3	125.1(2)	124.7(5)	125.1	124.7	0.4	0.2	0.5	0.04	0.25	0.538516	0.742781
C2-N3-C1	121.6(2)	120.3(4)	121.6	120.3	1.3	0.2	0.4	0.04	0.16	0.447214	2.906888
N3-C1-N1	126.3(2)	123.0(5)	126.3	123	3.3	0.2	0.5	0.04	0.25	0.538516	6.127946
C1-N1-S1	117.8(2)	119.0(4)	117.8	119	-1.2	0.2	0.4	0.04	0.16	0.447214	-2.68328
N1-S1-N2	104.3(1)	103.2(2)	104.3	103.2	1.1	0.1	0.2	0.01	0.04	0.223607	4.91935